

Molecular Workstation Roadmap II:

Survey of Single-Atom Tips (SATs) for Diamondoid Mechanosynthesis

This document internally DECLASSIFIED in 2025

HISTORICAL NOTE: This document was **completed and privately circulated in 2010**. It was a part of **the first known effort to comprehensively describe one possible experimental technology development pathway that could directly lead to the first working nanofactory** capable of atomically precise manufacturing of products in macroscale quantities. The timescale for nanofactory development was originally estimated to require about 20 years of dedicated and intensive research effort. Elements of this initial proposal were later substantially simplified on the basis of subsequent research.

This document internally DECLASSIFIED in 2025

© 2010, 2025. Robert A. Freitas Jr. All Rights Reserved.

Cite as: Freitas RA Jr. Molecular Workstation Roadmap II: Survey of Single-Atom Tips (SATs) for Diamondoid Mechanosynthesis. IMM Report No. 60, 2010/2025;
<http://www.imm.org/Reports/rep060.pdf>.

Table of Contents

1. Introduction.....	4
2. 2008 Preliminary Survey of Ultrasharp SPM Tips.....	8
3. Nonuniform Atomically-Imprecise Ultrasharp Tip Fabrication.....	20
3.1 Current Sharp-Probe Technique.....	20
3.2 Asperity and Nanotube Tips	22
3.3 Nanowire Tips	24
3.4 Hut Structures.....	32
3.5 Metal Surface Faceting.....	36
3.6 Graphene-on-Metal Dome Structures.....	51
3.7 Pyramidal Cavity Templating.....	52
3.8 EBID Fabrication of SPM Tips.....	56
3.9 Molecular Beam Epitaxy (MBE) and CVD-Based Nanopyramids	60
3.10 Field-Assisted Tip Sharpening.....	71
3.11 Tip Sharpening by Oxygen Annealing	76
3.12 Electrochemical Etching and Annealing.....	78
3.13 Other Ways of Making Sharp Tips	90
4. Patterned Atomic Layer Epitaxy (ALE).....	93
4.1 ALE-Coated Single-Atom SPM Tips.....	94
4.2. Atomically-Precise Single-Atom Tips from PALE.....	95
5. Single-Atom Tips (SATs).....	104
5.1 Field-Assisted Tungsten SATs	105
5.2 Palladium-Coated Tungsten SATs	118
5.3 Other Noble-Metal-On-Tungsten SATs.....	124
5.4 Other Metal-On-Metal SATs	135
5.5 Pure Noble Metal Wire SATs	137
5.6 Metal Cluster SATs.....	142
5.7 Accreted Metal-Atom SATs	143
5.8 Cleaved Si, NiO, and Be Crystallite SATs	144
5.9 Other Studies of SATs	149
5.9.1 Diamond SAT Theory Studies.....	149
5.9.2 Single-Atom Metal Carbide Tips.....	150
5.9.3 Single-Atom Aluminum Tips	154
5.9.4 Metal-Atom Doped-Coating SATs.....	157
6. Single-Atom Tip Systems	158
6.1 qPlus-Based AFM Tip System	158

6.2 Iridium qPlus Tip System.....	170
6.2.1 Brief EBID Primer.....	171
6.2.2 Step 1: Attach Iridium Nanowire to Quartz Fork	183
6.2.3 Step 2: Surface Cleaning and Annealing	193
6.2.4 Step 3: Formation of Pyramidal SAT at the Apex	196
6.2.5 Step 4: Formation of Electrical Contacts	196
6.3 Tungsten-Iridium qPlus Tip System	198
6.3.1 Step 1: Attach Tungsten Nanowire to Quartz Fork	198
6.3.1.1 Which Tungsten Surfaces are Facetogenic?.....	200
6.3.1.2 Crystal Structure of Beam-Deposited Tungsten	203
6.3.1.3 Beam-Deposited Tungsten-Silicon Exchange.....	208
6.3.2 Step 2: Formation of Pyramidal Iridium SAT at the Apex	211
6.3.3 Step 3: Formation of Electrical Contacts	211
6.4 EBID/Field-Sharpener qPlus System.....	212
6.5 MEMS-Based qPlus Tip System.....	212
6.5.1 Conventional Unitary Lithographic Fabrication.....	212
6.5.2 Two-Component Lithographic Fabrication with Microassembly.....	212
Appendix A. Directory of Quartz Crystal & Crystal Oscillator Manufacturers...	214

Accompanying documents include:

Freitas RA Jr., Merkle RC. A Nanofactory Roadmap: Research Proposal for a Comprehensive Diamondoid Nanofactory Development Program. IMM Report No. 58, 2008/2025; <http://www.imm.org/Reports/rep058.pdf>.

and

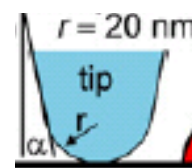
Freitas RA Jr. Molecular Workstation Roadmap I: Survey of Key Technologies Needed to Perform Positionally Controlled Diamondoid Mechanosynthesis using a Molecular Workstation. IMM Report No. 59, 2009/2025; <http://www.imm.org/Reports/rep059.pdf>.

1. Introduction

The completion of the Minimal Toolset paper¹ provided a first cut at the required operations that a DMS molecular manufacturing system must perform. Further analysis of alternative tooltips and stratagems to be employed in the bootstrap development sequence leading to a full diamondoid manufacturing system will result in an elucidation of the system specifications for the first molecular workstation. These specifications will define the number of tooltips and surfaces needed, the number of DOFs needed for each tooltip and for the workpiece surface, the ranges of motion and forces required to perform the specified DMS operations, the precision of motion for each DOF of each tooltip or surface, and so forth. With these specifications in hand, we can then proceed to a comprehensive molecular workstation design effort. An extensive survey² of technologies relevant to the design and construction of a molecular workstation for DMS has identified atomically sharp tooltips as a major technology driver for this project.

To perform atomically precise DMS operations, we need tooltips that are as sharp as possible, in order to reduce the positional and orientational uncertainty of the reactive sites at the tip as these tips are brought together, recharged, or applied to a workpiece with sub-Angstrom positional accuracy. The sharpest possible material tip terminates in a single atom. At minimum, a useful DMS tip must: (1) be mechanically and thermodynamically stable, (2) exhibit satisfactory reaction energetics for the full range of essential DMS reactions, including avoidance of all pathological intermediates, and (3) allow mechanical force transmission of a magnitude sufficient for successful DMS operations without destabilizing the tip structure.

A fourth related but less well-defined requirement is that the tips must have the highest possible “aspect ratio” (the ratio of length/width) to maximize steric accessibility of tips to other tips and to workpieces. (Aspect ratio is sometimes alternatively described³ in terms of the “flank angle” of a tip, as indicated by α in the drawing at right.)



However, an excessively high aspect ratio can also produce thermally-driven larger-amplitude lateral mechanical vibrations at the apex of a very long lever arm, reducing positional certainty at the tip and thus decreasing reaction reliability. A simple continuum model⁴ using Bernoulli-Euler

¹ Robert A. Freitas Jr., Ralph C. Merkle, “A Minimal Toolset for Positional Diamond Mechanosynthesis,” *J. Comput. Theor. Nanosci.* 5(May 2008):760-861; <http://www.molecularassembler.com/Papers/MinToolset.pdf>.

² Freitas RA Jr. Molecular Workstation Roadmap I: Survey of Key Technologies Needed to Perform Positionally Controlled Diamondoid Mechanosynthesis using a Molecular Workstation. IMM Report No. 59, 2009/2025; <http://www.imm.org/Reports/rep059.pdf>.

³ P. Colombi, I. Alessandri, P. Bergese, S. Federici, L.E. Depero, “Self-assembled polystyrene nanospheres for the evaluation of atomic force microscopy tip curvature radius,” *Meas. Sci. Technol.* 20(2009):084015.

⁴ Dong Qian, Gregory J. Wagner, Wing Kam Liu, Min-Feng Yu, Rodney S. Ruoff, “Mechanics of Carbon Nanotubes,” in: William A. Goddard III, Donald W. Brenner, Sergey Edward Lyshevski, Gerald J. Iafrate,

beam theory⁵ – with the extended tooltip crudely modeled as a clamped-free cylindrical beam of length $L = 100$ nm, equivalent circular cross-sectional radius $R = 5$ nm, Young's modulus E ($E_{\text{diam}} = 1.05 \times 10^{12}$ N/m² for diamond, $E_{\text{tung}} = 3.4 \times 10^{11}$ N/m² for tungsten metal), density ρ ($\rho_{\text{diam}} = 3510$ kg/m³ for diamond, $\rho_{\text{tung}} = 19,350$ kg/m³ for tungsten metal), frequency mode constant $\beta_1 \sim 1.875$ for the lowest vibrational frequency mode ($i = 1$), and second moment of area $I = \pi R^4 / 4$ at temperature T (kelvins) with Boltzmann's constant $k_B = 1.381 \times 10^{-23}$ J/K – gives the lowest natural resonant frequency as $\nu_1 = (\beta_1^2 / 4\pi) (R / L^2) (E / \rho)^{1/2} \sim 2.4$ GHz with classical amplitude $\sigma = (16 k_B T L^3 / \pi E \beta_1^4 R^4)^{1/2} \sim 26$ pm (80 K) or 51 pm (300 K) for a diamond rod, or $\nu_1 = 0.6$ GHz and $\sigma = 46$ pm (80 K) or 90 pm (300 K) for a tungsten metal rod. These vibrational amplitudes are roughly of the same magnitude as the representative 20-50 pm tolerances for positional uncertainty in DMS operations, so there exists a significant design tradeoff between aspect ratio and tip positional uncertainty in DMS.

Still longer lever arms also mechanically resonate at frequencies that could be relevant on the timescale of megahertz DMS operations – e.g., ~ 10 MHz for a 2-micron long, 20-nm-wide, diamond rod, or ~ 1 MHz as measured experimentally⁶ for pure boron nanowires ~ 50 nm in diameter and ~ 7 microns in length. In general, as tips get very long and narrow the amplitude of their lateral vibrations increases, injecting more uncertainty into the apex position; but as tips get shorter, their aspect ratio declines which increases the risk of handle collision during close proximation. The optimum technical tradeoff must be determined in order to select the best tips for the workstation development efforts.

A fifth desirable characteristic of atomically sharp tips for DMS is that they should be capable of being fabricated in a manner compatible with current scanning probe practice. For example, AFM best practice today involves the qPlus sensor. Hence the most desirable DMS tip would be one that could be fabricated directly onto a qPlus sensor fork, ideally integrally as a unitary structure with a high degree of repeatability and quality control.

A sixth desirable characteristic of a DMS tip is structural atomic precision. It should be noted that an atomically sharp tip is one that terminates in a single atom, whereas an atomically precise tip is one in which the position and bonding pattern of every atom in the tip is exactly known. Tips with a single atom at the apex of an atomically-imprecise handle structure have been used in the mechanosynthesis experiments of the Custance group.⁷ Fully atomically precise tooltips are

eds., Handbook of Nanoscience, Engineering, and Technology, CRC Press, Boca Raton, FL, 2003, pp. 19-8, 19-22.

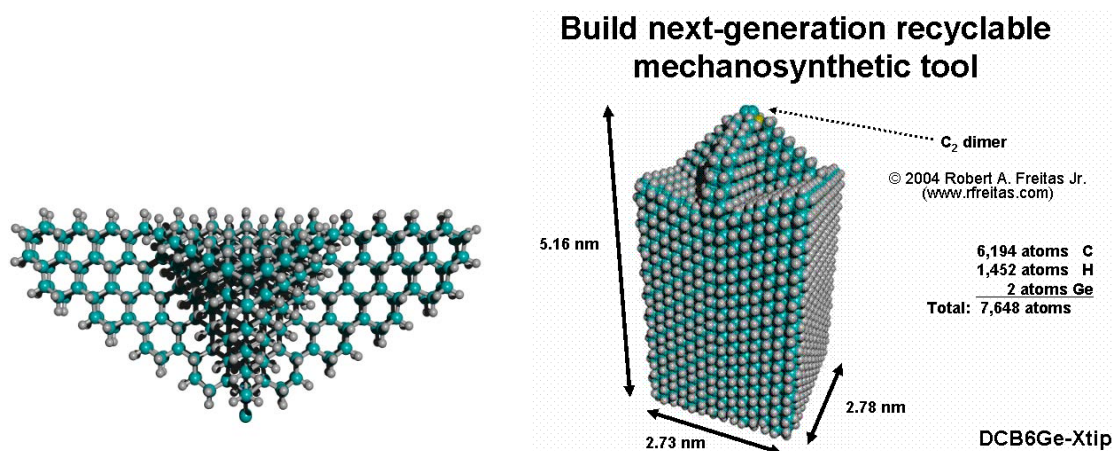
⁵ L. Meirovich, Elements of Vibration Analysis, McGraw-Hill, NY, 1975, p. 212.

⁶ 6 Weiqiang Ding, Lorenzo Calabri, Xinqi Chen, Kevin M. Kohlhaas, Rodney S. Ruoff, "Mechanics of crystalline boron nanowires," Composites Science and Technology 66(2006):1109-1121; http://bimat.princeton.edu/assets/pdf/nw_06_66ding.pdf.

⁷ Yoshiaki Sugimoto, Pablo Pou, Oscar Custance, Pavel Jelinek, Masayuki Abe, Ruben Perez, Seizo Morita, "Complex Patterning by Vertical Interchange Atom Manipulation Using Atomic Force Microscopy," **Science** 322(17 October 2008):413-417; <http://www.sciencemag.org/cgi/content/full/322/5900/413>.

not strictly required to undertake the initial workstation development effort, as the DMS manufacturing development pathway can be bootstrapped using a tip having imprecisely-known atomic structure but possessing atomic sharpness, good stability, and a good aspect ratio. In this case the initial DMS bootstrap system must be capable of fabricating a second generation of high-aspect atomically-sharp tooltips that are also atomically precise. Indeed, the single most important function of an initial molecular workstation using atomically-imprecise tips is the fabrication of atomically precise tips – better tips that can be employed in later generations of the workstation design in order to improve the overall precision, speed, and reliability of the system. Atomically-precise diamondoid pyramidal tooltip geometries (e.g., [Figure 1-1](#)) – that will almost certainly require atomically precise molecular manufacturing to fabricate – would allow the close tip-surface and tip-tip proximations that are required for multi-tip reactions in DMS.

Figure 1-1. Recyclable DCB6Ge tooltip (carbon dimer placement tool) with “Xtip” crossbar handle motif⁸ ([left](#)), which is then inverted and mounted on a massive diamond rod handle structure ([right](#)).



So while we would prefer to have fully atomically precise tips from the start, we don't absolutely require fully atomically precise tips to bootstrap the first instantiation of the workstation, as long as we're sure that once we have the first operational workstation, we'll be able to use it to build fully atomically precise tips that are also atomically sharp and high aspect. However, we would strongly prefer that the first molecular workstation uses atomically-precise, atomically-sharp, high-aspect tips – if we can get this.

Following a brief general survey of currently available “ultrasharp” SPM tips ([Section 2](#)), we summarize current methods for making atomically-imprecise tooltips ([Section 3](#)) and examine

⁸ Jingping Peng, Robert A. Freitas Jr., Ralph C. Merkle, James R. Von Ehr, John N. Randall, George D. Skidmore, “Theoretical Analysis of Diamond Mechanosynthesis. Part III. Positional C_2 Deposition on Diamond C(110) Surface using Si/Ge/Sn-based Dimer Placement Tools,” J. Comput. Theor. Nanosci. 3(February 2006):28-41; <http://www.MolecularAssembler.com/Papers/JCTNPengFeb06.pdf>.

proposed future methods for fabricating atomically sharp tips via atomic layer epitaxy ([Section 4](#)). We then review the current status of single-atom tips (SATs) which are predominantly single-atom metallic SPM tips ([Section 5](#)). We conclude with a discussion of several possible complete AFM single-atom tip systems ([Section 6](#)) that seem to be viable candidates for use in the molecular workstation.

2. 2008 Preliminary Survey of Ultrasharp SPM Tips

Ultrasharp, and preferably atomically sharp, scanning probe tips are needed to reliably perform positionally controlled mechanosynthetic reactions. But current scanning probe tips with a sub-nanometer radius of curvature might still allow 2-tip operations in free space and possibly even multi-tip operations near surfaces, albeit with great difficulty and low reliability. A preliminary 2008 survey (Table 2-1) of commonly available “ultrasharp” tips – generally defined as having a radius of curvature of 10-20 nm (~50-100 carbon atoms) or less – revealed that sub-nanometer (<10 Å) tips are already available in many materials, including diamond and CNTs.

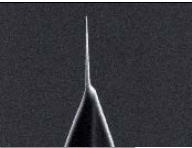
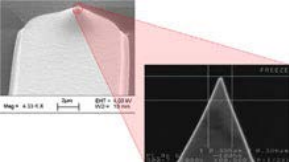
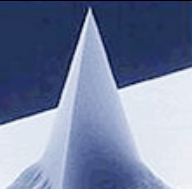
As mentioned in the introduction, another important consideration is that these early tips (the ultrasharps) must also have an adequate aspect ratio – that is, they need to be sufficiently long and pointed. A good range of “high aspect ratio” tips are commercially available, with some providing ratios as high as 20:1 (especially the nanotube-based tips). For example, Ahner et al.⁹ used ultrasharp tungsten tips¹⁰ to place four independent probes on the facet faces of selected single Ge nanodots, and on various assemblies of dots, with a positional accuracy of better than 5 nm. Olbrich et al.¹¹ have fabricated high aspect ratio (7:1) diamond tips using focused ion beam methods, although the tip radius is rather large (~30 nm) and milling of the tip left a 10-20 nm thick nonconducting amorphous carbon layer that had to be etched away by pure HNO₃ to expose the diamond surface. Others have fabricated conical silicon tips having nanoscale sharpness using localized laser irradiation.¹²

⁹ Joachim Ahner, Olivier Guise, Hubertus Marbach, Jeremy Levy, Jr. Yates, “The Nanoworkbench: Electron transport on Ge/Silicon Surfaces. First Results,” [N14.005] Session N14 - Microscopic Techniques. ORAL session, Wednesday morning, March 05, Room 8C, Austin Convention Center, APS Meeting March 2003, <http://flux.aps.org/meetings/YR03/MAR03/baps/abs/S4940.html>.

¹⁰ Olivier L. Guise, Joachim W. Ahner, Moon-Chul Jung, Peter C. Goughnour, John T. Yates Jr., “Reproducible Electrochemical Etching of Tungsten Probe Tips,” Nano Letters 2(2002):191-193; <http://pubs.acs.org/cgi-bin/abstract.cgi/nalefd/2002/2/i03/abs/nl010094q.html>.

¹¹ A. Olbrich, B. Ebersberger, C. Boit, Ph. Niedermann, W. Hänni, J. Vancea, H. Hoffmann, “High aspect ratio all diamond tips formed by focused ion beam for conducting atomic force microscopy,” J. Vac. Sci. Tech. B 17(July 1999):1570-1574; <http://link.aip.org/link/?JVTBD9/17/1570/1>.

¹² Joseph P. Moening, Daniel G. Georgiev, “Formation of conical silicon tips with nanoscale sharpness by localized laser irradiation,” J. Appl. Phys. 107(2010):014307

Table 2-1. Experimentally Attainable or Commercially Available Ultrasharp Probe Tips for Scanning Probe Microscopy			
Probe Tip Manufacturer or Experimentalist Group	Probe Tip Product	Probe Tip Radius	Image of Tip
Silicon			
Tao et al. ¹³	experimental tip	< 20 nm	
Park Systems ¹⁴	HART0-#-05	10 nm	
Nanochip ¹⁵	data storage cantilever tips	10 nm	
Park et al. ¹⁶	experimental tip	< 10 nm	
Nanosensors ¹⁷	Pointprobe® Silicon-SPM-Sensors	< 10 nm	

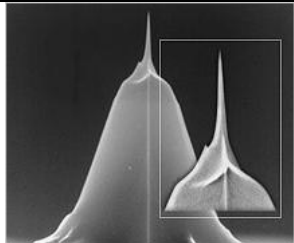
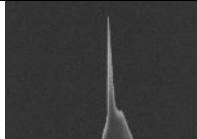
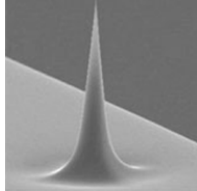

¹³ Y. Tao, R. J. Fasching, F. B. Prinz, "Ultra-sharp High-aspect-ratio Probe Array for SECM and AFM Analysis," 2003, <http://www-rpl.stanford.edu/goto-publication/138>; Ye Tao, Rainer J. Fasching, Fritz B. Prinz, "Ultrasharp high-aspect-ratio probe array for SECM and AFM Analysis," Proceedings of SPIE, Vol. 5389, Smart Structures and Materials 2004: Smart Electronics, MEMS, BioMEMS, and Nanotechnology, Vijay K. Varadan, ed., July 2004, pp. 431-442.

¹⁴ Park Systems (<http://www.parkafm.com/>) SPM Tool Box; HART0-#-05, <http://www.psiastore.com/product.sc?categoryId=11&productId=98>.

¹⁵ Kevin Bullis, "Higher-Capacity Memory: A new type of memory could soon be available to device makers," Technology Review, 12 February 2008; <http://www.technologyreview.com/Nanotech/20192/>. See also Nanochip website: <http://www.nanochipinc.com/>.

¹⁶ Jaehong Park, Kidong Park, Byoungdoo Choi, Kyo-In Koo, Seung-Joon Paik, Sangjun Park, Jongpal Kim, Dong-Il Dan Cho, "A novel fabrication process for ultra-sharp, high-aspect ratio nano tips using (111) single crystalline silicon," 12th International Conference on Transducers, Solid-State Sensors, Actuators and Microsystems, 2003, Vol. 2, 8-12 June 2003, pp. 1144-1145.

¹⁷ Nanosensors™ Probes, Pointprobe® Silicon-SPM-Sensors http://www.nano-tools.com/php/cantilever.php?g_id=2&t_id=18.

Innovative Solutions ¹⁸	ISB-BudgetSensors	< 10 nm	
NanoWorld® ¹⁹	AR5-NCHR Cantilevers	< 10 nm	
ASM ²⁰	various tips	< 10 nm	
Applied NanoStructures ²¹	HART0-1	< 10 nm	
Veeco ²²	Super Cone Probes	< 10 nm	
Park Systems ²³	FORTA-10	5-6 nm	

¹⁸ [Innovative Solutions Bulgaria](http://www.budgetsensors.com/) (ISB-BudgetSensors) Sofia, Bulgaria; <http://www.budgetsensors.com/>.

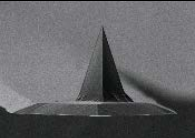
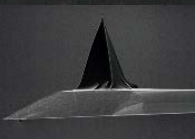
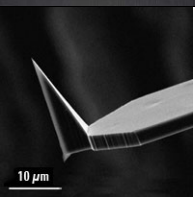


¹⁹ NanoWorld® POINTPROBE® sensors, <https://ssl.jpk.com/cantilevers/images/ar5.jpg>; Type AR5-NCHR Cantilevers, [https://ssl.jpk.com/cantilevers/csc_article_details.php?nPos=0&saArticle\[ID\]=29&VID=NyVAykQ2RMEgcnrx](https://ssl.jpk.com/cantilevers/csc_article_details.php?nPos=0&saArticle[ID]=29&VID=NyVAykQ2RMEgcnrx).

²⁰ [Advanced Surface Microscopy](http://www.asmicro.com/), Inc. (ASM) Indianapolis, IN; <http://www.asmicro.com/>.

²¹ Applied NanoStructures, high aspect ratio probe tips, HART0-1; http://www.2spi.com/catalog/spec_prep/high-aspect-ratio-AFM-probe-tips.shtml.

²² IBMSC – Super Cone Probes; https://www.veecoprobes.com/probe_detail.asp?ClassID=28.

²³ Park Systems (<http://www.parkafm.com/>) SPM Tool Box; FORTA-10, <http://www.psiastore.com/product.sc?categoryId=7&productId=95>.

Park Systems ²⁴	SICONA-10	5-6 nm		
Park Systems ²⁵	ACLA-10	5-6 nm		
MikroMasch ²⁶	GP AFM probe STING probe (DP14)	5-10 nm		
Park Systems ²⁷	ACTA-10	5-6 nm		
Park Systems ²⁸	NCHR (610-#051)	2-5 nm		
Veeco ²⁹	TESP-SS - ESP Series Probes - Super Sharp Tip	2-5 nm		

²⁴ Park Systems (<http://www.parkafm.com/>) SPM Tool Box; SICONA-10, <http://www.psiastore.com/product.sc?categoryId=6&productId=94>.

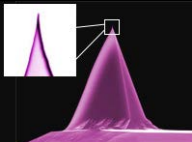
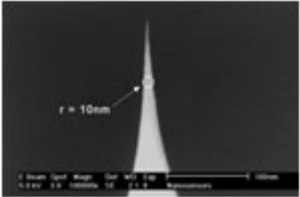
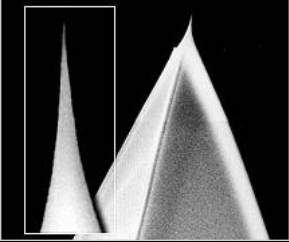
²⁵ Park Systems (<http://www.parkafm.com/>) SPM Tool Box; ACLA-10, <http://www.psiastore.com/product.sc?categoryId=4&productId=92>.

²⁶ MikroMasch <http://www.spmtips.com/>, GP AFM probe <http://www.spmtips.com/products/cantilevers/datasheets/gp>, DP14/GP series <http://www.spmtips.com/dp140/gp>.

²⁷ Park Systems (<http://www.parkafm.com/>) SPM Tool Box; ACTA-10, <http://www.psiastore.com/product.sc?categoryId=4&productId=93>.

²⁸ Park Systems (<http://www.parkafm.com/>) SPM Tool Box; NCHR (610-#051), <http://www.psiastore.com/product.sc?categoryId=4&productId=102>.

²⁹ TESP-SS - ESP Series Probes - Super Sharp Tip; https://www.veecoprobes.com/probe_detail.asp?ClassID=111.

NanoScience Instruments ³⁰	ACL-SS Super Sharp Dynamic Mode AFM Probes	2-3 nm	
Nanosensors ³¹	SuperSharpSilicon™	< 2 nm	
NanoWorld® ³²	SSS-NCH Cantilevers	< 2 nm	
Marcus et al. ³³	experimental tip	~1 nm	
Ding et al. ³⁴	field emission tip	~0.75 nm	
Tungsten			
Fujita et al. ³⁵	experimental tip	5 nm	

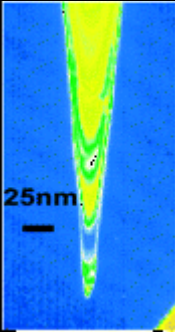
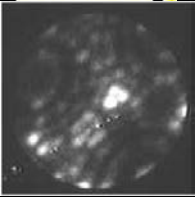
³⁰ NanoScience Instruments, “ACL-SS Super Sharp Dynamic Mode AFM Probes” AC / tapping mode - 225 micron Long cantilever - Super Sharp tip;
<http://store.nanoscience.com/store/pc/viewCategories.asp?idCategory=83>.

³¹ Nanosensors <http://www.nanosensors.com/> ;
http://www.nanosensors.com/products_overview.html SuperSharpSilicon™
http://www.nanosensors.com/products_overview.html#SSS (Image)
 Writeup on SSS is at: <http://www.nanosensors.com/SuperSharpSilicon.pdf>.

³² NanoWorld®, Tip shape: Super Sharp, <https://ssl.jpk.com/cantilevers/images/sss.jpg>
 Type SSS-NCH Cantilevers
[https://ssl.jpk.com/cantilevers/csc_article_details.php?nPos=0&saArticle\[ID\]=45&VID=NyVAykQ2RMEgcnrx](https://ssl.jpk.com/cantilevers/csc_article_details.php?nPos=0&saArticle[ID]=45&VID=NyVAykQ2RMEgcnrx).

³³ R.B. Marcus, T.S. Ravi, T. Gmitter, K. Chin, D. Liu, W.J. Orvis, D.R. Ciarlo, C.E. Hunt, J. Trujillo, “Formation Of Silicon Tips with < 1 nm Radius,” Appl. Phys. Lett. 56(15 January 1990):236-238;
http://www.ece.ucdavis.edu/HuntGroup/Publications/APL_Marcus_AtomSharp.pdf. See also: Yongxia Zhang, Yanwei Zhang, T.S. Sriram, R.B. Marcus, “Formation of single tips of oxidation-sharpened Si,” Appl. Phys. Lett. 69(30 December 1996):4260.

³⁴ Ding Meng, Sha Guobin, A.I. Akinwande, “Silicon field emission arrays with atomically sharp tips: turn-on voltage and the effect of tip radius distribution,” IEEE Transactions on Electron Devices 49(December 2002):2333-2342.

Guise et al. ³⁶	electrochemical etch	5 nm	
Lucier ³⁷	three-atom apex W(111) tip	< 0.6 nm	
Chen, ³⁸ Binh ³⁹	single-atom “Teton tip”	~0.3 nm (single-atom tip)	

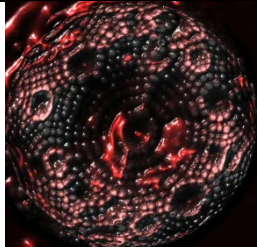
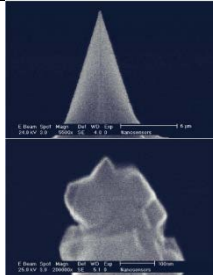

³⁵ Jun-ichi Fujita, Yuta Ikeda, Satoshi Okada, Kodai Higashi, Shotaro Nakazawa, Masahiko Ishida, Shinji Matsui, “In-situ Visualization of Local Field Enhancement in an Ultra Sharp Tungsten Emitter under a Low Voltage Scanning Transmission Electron Microscope,” Japanese Journal of Applied Physics 46(2007):L498-L501; <http://jjap.ipap.jp/link?JJAP/46/L498/>.

³⁶ Olivier L. Guise, Joachim W. Ahner, Moon-Chul Jung, Peter C. Goughnour, John T. Yates Jr., “Reproducible Electrochemical Etching of Tungsten Probe Tips,” Nano Letters 2(2002):191-193; <http://pubs.acs.org/cgi-bin/abstract.cgi/nalefd/2002/2/i03/abs/nl010094q.html>.

³⁷ 37. Anne-Sophie Lucier, “Preparation and Characterization of Tungsten Tips Suitable for Molecular Electronics Studies,” M.S. Thesis, Center for the Physics of Materials, Department of Physics, McGill University, Montreal, Quebec, Canada, February 2004; <http://www.physics.mcgill.ca/~peter/theses/lucier.pdf>. See also: Anne-Sophie Lucier, Henrik Mortensen, Yan Sun, and Peter Grütter, “Determination of the atomic structure of scanning probe microscopy tungsten tips by field ion microscopy,” Phys. Rev. B 72, 235420 (2005).

³⁸ C.J. Chen, Introduction to Scanning Tunneling Microscopy, Oxford University Press, 1993.

³⁹ V.T. Binh, J. Marien, “Characterization of microtips for scanning tunneling microscopy,” Surf. Sci. 202(1 August 1988):L539-L549. V.T. Binh, “In Situ Fabrication and Regeneration of Microtips for Scanning Tunnelling Microscopy,” J. Microsc. 152(November 1988):355-361.

Rezeq et al. ⁴⁰	single-atom tip (FIM image)	~0.3 nm (inside centermost ring)		
Diamond/DLC				
Wang et al. ⁴¹	solid diamond	< 50 nm		
Olbrich et al. ⁴²	FIB diamond	~30 nm		
Nanosensors ⁴³	diamond-coated silicon	10 nm		
Nanotools ⁴⁴	T-EAR M* 8-40 (high dense carbon over silicon nitride)	~10 nm		

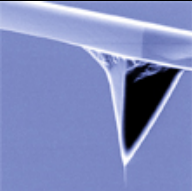
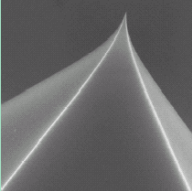
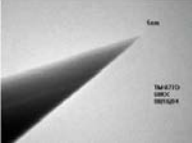
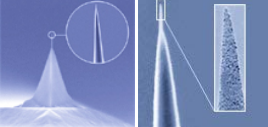

⁴⁰ Moh'd Rezeq, Jason Pitters, Robert Wolkow, "Tungsten nanotip fabrication by spatially controlled field-assisted reaction with nitrogen," J. Chem. Phys. 124(28 May 2006):204716, <http://www.aip.org/png/2006/264.htm> (image), <http://www.phys.ualberta.ca/~wolkow> (movie); see also: "University of Alberta Nanotechnology Researchers Create Sharpest Tip Ever Known," 11 July 2006, University of Alberta press release, <http://www.azonano.com/news.asp?newsID=2606>.

⁴¹ Zongli Wang, Changzhi Gu, Junjie Li, Zheng Cui, "A novel method for making high aspect ratio solid diamond tips," Microelectronic Engineering 78-79(March 2005):353-358.

⁴² A. Olbrich, B. Ebersberger, C. Boit, Ph. Niedermann, W. Hänni, J. Vancea, H. Hoffmann, "High aspect ratio all diamond tips formed by focused ion beam for conducting atomic force microscopy," J. Vac. Sci. Tech. B 17(July 1999):1570-1574; <http://link.aip.org/link/?JVTBD9/17/1570/1>.

⁴³ Nanosensors: Diamond Coated Silicon-SPM-Sensors Pointprobe®; <http://www.nanosensors.com/Diamond.pdf>.

⁴⁴ Nanotools Scanning Probes, "Supersharpe Probes," <http://www.nano-tools.com/>.

Nanotools ⁴⁵	Universal Type U3 (high dense carbon over silicon nitride)	~10 nm		
Advanced Diamond Technologies, Inc. ⁴⁶	NaDiaProbe™ (ultrananocrystalline (~5 nm) diamond)	7-12 nm		
Mesa & Magonov ⁴⁷	solid diamond experimental tips	5 nm		
Nanotools ⁴⁸	Supersharps (high density carbon over silicon nitride)	2-3 nm		
Veeco ⁴⁹	Diamond-Like Carbon Spike Probe	1 nm (asperity) 5 nm (tip)		


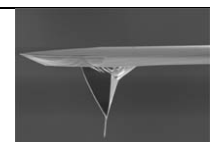
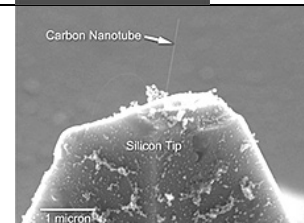
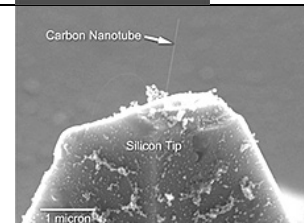
⁴⁵ Nanotools Scanning Probes, “Supersharps Probes,” <http://www.nano-tools.com/>.

⁴⁶ Advanced Diamond Technologies, Inc., “NaDiaProbe™ – Monolithic Diamond AFM Probes,” accessed March 2008; <http://www.thindiamond.com/downloads/NaDiaProbe.pdf>.

⁴⁷ Bernard Mesa, Sergei Magonov, “Novel diamond/sapphire probes for scanning probe microscopy applications,” Journal of Physics: Conference Series 61(2007):770-774;
<http://www.microstartech.com/index/mesa-magonov.pdf>.

⁴⁸ Nanotools Scanning Probes, “Supersharps Probes,” <http://www.nano-tools.com/>.

⁴⁹ “Diamond-Like Carbon Spike Probes,” https://www.veecoprobes.com/probe_detail.asp?ClassID=12.

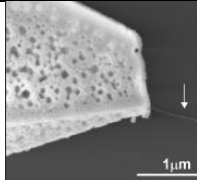
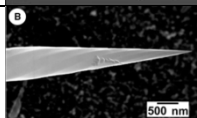
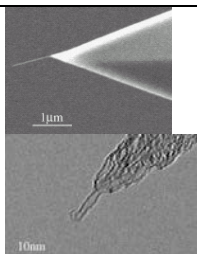
NT-MDT ⁵⁰	Super sharp Diamond-Like Carbon (DLC) tips	≤ 1 nm	
Carbon Nanotube Tips			
Dai et al. ⁵¹	MWCNT	5-20 nm	
NanoScience Instruments ⁵²	Carbon Nanotube AFM Tips	5-15 nm	
Xidex ⁵³	MWCNT	~10 nm	

⁵⁰ NT-MDT (Molecular Devices and Tools for Nanotechnology, Moscow, Russia, <http://www.ntmdt.com>), "Super sharp Diamond-Like Carbon (DLC) tips," from their "SPM Probe and Accessories" catalog, 2008; http://www.ntmdt.com/download/accessories_catalog.pdf.

⁵¹ Hongjie Dai, Jason H. Hafner, Andrew G. Rinzler, Daniel T. Colbert, Richard E. Smalley, "Nanotubes as Nanoprobes in Scanning Probe Microscopy," Nature 384(1996):147-151; http://web.archive.org/web/20020609154706/http://cnst.rice.edu/TIPS_rev.htm.

⁵² NanoScience Instruments, "Carbon Nanotube AFM Tips," CNTek™ AFM Probes; http://www.nanoscience.com/products/carbon_nanotube_probes.html.

⁵³ "AMRC Research Leads to Promising Nanotechnology Application for Chip Industry," (23 February, 2005), Advanced Materials Research Center, SEMATECH; <http://www.amrcctx.org/news/20050223.htm>.

Cheung et al. ⁵⁴	MWCNT	3-8 nm	
Zhang et al. ⁵⁵	tubular graphite cones	2-10 nm	
Lieber et al. ⁵⁶	MWCNT	3-5 nm	
Martinez et al. ⁵⁷	MWCNT sharpened to SWCNT radius	~0.9 nm	
Nguyen et al. ⁵⁸	SWCNT	0.7 nm	

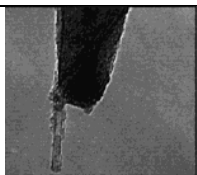
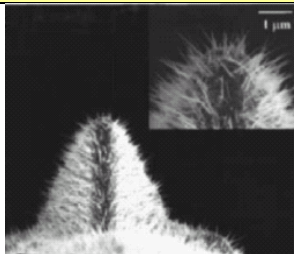

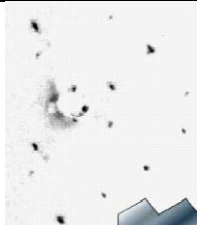
⁵⁴ Chin Li Cheung, Jason H. Hafner, Charles M. Lieber, "Carbon nanotube atomic force microscopy tips: Direct growth by chemical vapor deposition and application to high-resolution imaging," Proc. Natl. Acad. Sci. USA 97(11 April 2000):3809-3813;
<http://www.pubmedcentral.nih.gov/articlerender.fcgi?artid=18098>.

⁵⁵ Guangyu Zhang, Xin Jiang, Enge Wang, "Tubular Graphite Cones," Science 300(18 April 2003):472-474; <http://www.scienceonline.org/cgi/content/full/300/5618/472>.

⁵⁶ Charles M. Lieber, Adam T. Woolley, Jong-in Hahm, David Housman, "Direct haplotyping using carbon nanotube probes," United States Patent 20020146714, 10/10/2002,
<http://freepatentsonline.com/20020146714.html>; see also (WO/2002/022889) Direct Haplotyping Using Carbon Nanotube Probes, <http://www.wipo.int/pctdb/en/wo.jsp?IA=US2001042138&DISPLAY=DESC>.

⁵⁷ J. Martinez, T.D. Yuzvinsky, A.M. Fennimore, A. Zettl, R. Garcia, C. Bustamante, "Length control and sharpening of atomic force microscope carbon nanotube tips assisted by an electron beam," Nanotechnology 16(2005):2493-2496;
<http://socrates.berkeley.edu/~tyuz/pub/nanotechnology16.pdf>.

⁵⁸ Cattien V. Nguyen, Kuo-Jen Chao, Ramsey M.D. Stevens, Lance Delzeit, Alan Cassell, Jie Han, M. Meyyappan, "Carbon nanotube tip probes: stability and lateral resolution in scanning probe microscopy and application to surface science in semiconductors," Nanotechnology 12(September 2001):363-367;
<http://www.iop.org/EJ/abstract/0957-4484/12/3/326/>.

Hafner et al. ⁵⁹	SWCNT	0.5-1.4 nm		
Other				
Zhu et al. ⁶⁰	Fe ₂ O ₃ nanoflakes	12-22 nm		
Lee et al. ⁶¹	ZnO piezo tip	< 15 nm		
Asylum Research ⁶²	aluminum tip	< 15 nm		
Libioulle et al. ⁶³	platinum tip	~5 nm		
Ermanoski et al. ⁶⁴	faceted clean iridium	~0.3 nm (single-atom tip; schematic at lower right)		

⁵⁹ J.H. Hafner, C.L. Cheung, T.H. Oosterkamp, C.M. Lieber, "High-Yield Assembly of Individual Single-Walled Carbon Nanotube Tips for Scanning Probe Microscopies," J. Phys. Chem. B. 105(2001):743-746; http://cmliris.harvard.edu/publications/2000s/2001/jPCB105_743.pdf.


⁶⁰ Y.W. Zhu, T.Yu, C.H. Sow, Y.J. Liu, A.T.S. Wee, X.J. Xu, C.T. Lim, J.T.L. Thong, "Efficient field emission from -Fe₂O₃ nanoflakes on an atomic force microscope tip," Appl. Phys. Lett. 87(2005):023103; http://www.ntu.edu.sg/home/yuting/papers/APL_Fe2O3%20on%20AFM%20tip.pdf.

⁶¹ S.H. Lee, S.S. Lee, J.-J. Choi, J.U. Jeon, K. Ro, "Fabrication of a ZnO piezoelectric micro cantilever with a high-aspect-ratio nano tip," Microsystem Technologies 11(June 2005):416-423.

⁶² Asylum Research, AC160BN, High Aspect Ratio, AC Mode; <http://www.asylumresearch.com/Products/Levers/AC160BN.shtml>.

⁶³ L. Libioulle, Y. Houbion, J.-M. Gilles, "Very sharp platinum tips for scanning tunneling microscopy," Rev. Sci. Instrum. 66(January 1995):97.

⁶⁴ Ivan Ermanoski, Kalman Pelhos, Wenhua Chen, Jamie S. Quinton, Theodore E. Madey, "Oxygen-induced nano-faceting of Ir(210)," Surf. Sci. 549(10 January 2004):1-23.

Fu et al., ⁶⁵ Madey et al., ⁶⁶ Kuo et al., ⁶⁷ Itagaki et al. ⁶⁸	Pd-coated tungsten	~0.3 nm (single-atom tip)	
---	--------------------	------------------------------	---

⁶⁵ T.-Y. Fu, L.C. Cheng, C.H. Nien, T.T. Tsong, "Method of creating a Pd-covered single-atom sharp W pyramidal tip: Mechanism and energetics of its formation," Phys. Rev. B 64(15 September 2001):113401; <http://www.phys.sinica.edu.tw/~nano/publication/223.pdf>.

⁶⁶ Theodore E. Madey, Kalman Pelhos, Qifei Wu, Robin Barnes, Ivan Ermanoski, Wenhua Chen, Jacek J. Kolodziej, John E. Rowe, "Nanoscale surface chemistry," Proc. Nat. Acad. Sci. USA 99(2002):6503-6508; http://www.physics.rutgers.edu/~wchen/Madey_page/Full_Publications/PDF/madey_PNAS_2002.pdf.

⁶⁷ H.S. Kuo, I.S. Hwang, T.-Y. Fu, J.Y. Wu, C.C. Chang, T.T. Tsong, "Preparation and characterization of single-atom tips," Nano Lett. 4(December 2004):2379-2382; http://aao.sinica.edu.tw/download/publication_e/Year2005/math04.pdf , http://dns.ntu-ccms.ntu.edu.tw/references/NANO_LETT-4-2379-2004.pdf.

⁶⁸ T. Itagaki, E. Rokuta, H.-S. Kuo, K. Nomura, T. Ishikawa, B.-L. Cho, I.-S. Hwang, T.T. Tsong, C. Oshima, "Stabilities in field electron emissions from noble-metal covered W nano-tips: apex structure dependence," Surface and Interface Analysis 39(2006):299-303..

3. Nonuniform Atomically-Imprecise Ultrasharp Tip Fabrication

In the last 20 years there have been great strides in producing sharper and sharper SPM probe tips for use in atomic-scale scanning and related applications (e.g., see [Table 2-1](#)). Conventionally, sharp tips have been prepared by various polishing methods, e.g., by electrochemical polishing as described in U.S. Pat. No. 6,249,965, yielding tips that are nearly hemi-spherical in shape (also called an equilibrium tip shape) with radii from 0.05-50 microns. However, most of these tips are sub-optimal for “production” use in a DMS-based molecular manufacturing system for two reasons: First, they are not atomically sharp, and second, their apex is not atomically precise (in fabrication *or* characterization) either at the start of use, or after significant use, in the lab.

In this Section, we review some of these methods as background for later discussions.

3.1 Current Sharp-Probe Technique

Experimentalists pursuing ultrahigh vacuum (UHV) scanning probe microscopy frequently spend many (often fruitless) hours trying to coerce a commercially-obtained SPM probe into a structure that yields, retains, and accurately reproduces atomic resolution images, notes Philip Moriarty.⁶⁹ Collectively, vast numbers of researcher person-months in the scanning probe and nanoscience research communities are currently wasted in conditioning STM and AFM tips (during the scanning process) via voltage pulsing, field emission, high bandwidth scanning, high (or low) feedback loop gains, and other “tricks of the trade”.⁷⁰ A number of techniques are used to form atomically sharp tips for state-of-the-art SPM imaging under UHV conditions but the acquisition of stable and high resolution images remains something of a “black art”.⁷¹ For example, following preparation of a probe using electrochemical etching, sometimes with subsequent heating to remove oxides and other contamination, it can still take many hours of a researcher’s time to optimize the apex of the probe’s structure. The operator in general adopts a poorly-defined approach to optimize the tip during scanning by altering various parameters such as voltage, current, scan speed, etc. This time-consuming procedure is required in order to modify the atomic scale/nanoscale structure of the tip, as opposed to the microscale and macroscale modifications resulting from etching and annealing.⁷² In some cases, experimentalists are forced

⁶⁹ Philip Moriarty, Natalio Krasnogor, Richard Woolley, “Automated Optimisation of Scanning Probes: Accelerating Nanoscience,” University of Nottingham, U.K., funding proposal, 2009. Philip Moriarty, personal communication to Robert A. Freitas Jr., 11 June 2009 and 26 June 2009.

⁷⁰ Philip Moriarty, Natalio Krasnogor, Richard Woolley, “Automated Optimisation of Scanning Probes: Accelerating Nanoscience,” University of Nottingham, U.K., funding proposal, 2009.

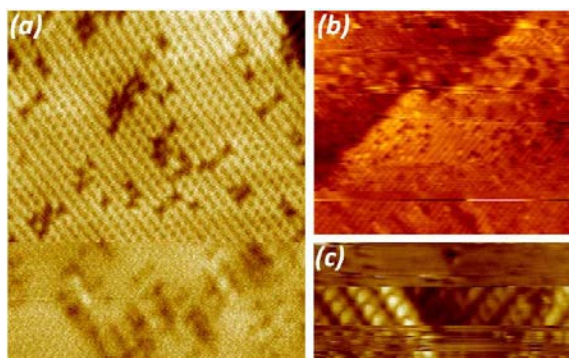
⁷¹ Peter Siepmann, Christopher P. Martin, Ioan Vancea, Philip J. Moriarty, Natalio Krasnogor, “A Genetic Algorithm Approach to Probing the Evolution of Self-Organized Nanostructured Systems,” *Nano Lett.* 7(2007):1985-1990.

⁷² Philip Moriarty, Natalio Krasnogor, Richard Woolley, “Automated Optimisation of Scanning Probes: Accelerating Nanoscience,” University of Nottingham, U.K., funding proposal, 2009.

to “gently crash the tip into the surface deliberately (i.e., turn the feedback loop off and push the tip a few nanometers towards the surface) to get a tip capable of atomic resolution”⁷³ presumably by accreting a small silicon cluster onto the tip.

Figure 3-1a and **Figure 3-1b** show the dramatic changes in STM image quality that occur during an optimization process of this type.⁷⁴ The change from a very poorly resolved image, with no evidence of atomic-scale features, to the acquisition of high resolution data following a voltage or “height” (i.e., Δz) pulse will be familiar to practically every UHV scanning probe microscopist. **Figure 3-1c** shows similar tip changes that occur during qPlus AFM imaging of Si(100) but, in this case, the changes are spontaneous (i.e., not induced by an operator-initiated change in scan parameters). In NC-AFM experiments (including those using the qPlus technique as well as those of others involving the more widely used cantilever approach) there can be many tip changes, due to strong surface-tip interactions and the associated dynamics of cantilever motion, before the tip settles down into a stable imaging mode. During this “settle” time, the operator needs to continually adjust the scan parameters (including the XY position of the tip) in order to ensure that, following a tip change, the highest quality image is obtained.

Figure 3-1. Role of the tip structure in SPM imaging. (a) STM imaging of Si(100)-(2x1) where, prior to a voltage pulse (lower third of image), atomic resolution is not observed but defects in the dimer row structure are resolved. The image was acquired as the tip scanned from left to right and from the bottom to the top of the image in this case. (b) Examples of tip changes both induced by voltage pulsing and occurring spontaneously on Si(100)-(2x1). (c) Spontaneous tip changes during qPlus imaging of Si(100)-(2x1).⁷⁵



⁷³ Philip Moriarty, personal communication to Robert A. Freitas Jr., 11 June 2009 and 26 June 2009. Franz J. Giessibl, S. Hembacher, H. Bielefeldt, J. Mannhart, “Subatomic Features on the Silicon (111)-(7x7) Surface Observed by Atomic Force Microscopy,” *Science* 289(21 July 2000):422-425; <http://www.sciencemag.org/cgi/content/full/289/5478/422>.

⁷⁴ Philip Moriarty, Natalio Krasnogor, Richard Woolley, “Automated Optimisation of Scanning Probes: Accelerating Nanoscience,” University of Nottingham, U.K., funding proposal, 2009.

⁷⁵ Philip Moriarty, Natalio Krasnogor, Richard Woolley, “Automated Optimisation of Scanning Probes: Accelerating Nanoscience,” University of Nottingham, U.K., funding proposal, 2009.

3.2 Asperity and Nanotube Tips

A least favored but possibly viable choice for DMS work would be to employ the sub-nanometer asperity (and related) tips shown in Table 2-1. This approach would restrict us to diamond, diamond-like carbon (DLC), carbon nanotube, and silicon tips that are already commercially available “off the shelf”. Especially noteworthy is the NT-MDT⁷⁶ DLC-based spike-probe tip with an asperity that is only a few carbon atoms wide at the tip (Figure 3-2A). This atomically-imprecise tip has been used by Klinov et al.⁷⁷ to scan short poly(dG)-poly(dC) DNA fragments deposited on modified HOPG (highly oriented pyrolytic graphite), enabling the researchers to detect single-stranded regions in double-stranded poly(dG)-poly(dC) and double-stranded and single-stranded regions in poly(dG)-poly(dG)-poly(dC) triplexes, as well as to resolve the helical pitch of the triplex molecules (Figure 3-2B). Single-walled carbon nanotubes (SWCNTs) having near-atomic precision also have been attached to SPM tips (Figure 3-2C).⁷⁸

It may be possible to grow asperity-like metal tips that might be directly suitable for DMS. For example, in 2009 Sun et al.⁷⁹ synthesized ultrathin single crystal platinum nanowires (Figure 3-3) with diameters of 2.5 nm and lengths up to 100 nm on nitrogen-doped CNTs (N-CNTs) using a straightforward wet-chemical method in environmentally friendly water solution at room temperature, without using any stabilizing agent. Wong et al.⁸⁰ have described carbon nanotubes functionalized with -COOH and other chemically active groups at their apex, for use as atomically sharp AFM probes.

⁷⁶ NT-MDT (Molecular Devices and Tools for Nanotechnology, Moscow, Russia, <http://www.ntmdt.com>), “Super sharp Diamond-Like Carbon (DLC) tips,” from their “SPM Probe and Accessories” catalog, 2008; http://www.ntmdt.com/download/accessories_catalog.pdf.

⁷⁷ Dmitry Klinov, Benjamin Dwir, Eli Kapon, Natalia Borovok, Tatiana Molotsky, Alexander Kotlyar, “High-resolution atomic force microscopy of duplex and triplex DNA molecules,” *Nanotechnology* 18(6 June 2007):225102..

⁷⁸ J. Martinez, T.D. Yuzvinsky, A.M. Fennimore, A. Zettl, R. Garcia, C. Bustamante, “Length control and sharpening of atomic force microscope carbon nanotube tips assisted by an electron beam,” *Nanotechnology* 16(2005):2493-2496; <http://socrates.berkeley.edu/~tyuz/pub/nanotechnology16.pdf>. Cattien V. Nguyen, Kuo-Jen Chao, Ramsey M.D. Stevens, Lance Delzeit, Alan Cassell, Jie Han, M. Meyyappan, “Carbon nanotube tip probes: stability and lateral resolution in scanning probe microscopy and application to surface science in semiconductors,” *Nanotechnology* 12(September 2001):363-367; <http://www.iop.org/EJ/abstract/0957-4484/12/3/326/>. J.H. Hafner, C.L. Cheung, T.H. Oosterkamp, C.M. Lieber, “High-Yield Assembly of Individual Single-Walled Carbon Nanotube Tips for Scanning Probe Microscopies,” *J. Phys. Chem. B.* 105(2001):743-746; http://cmliris.harvard.edu/publications/2000s/2001/jPCB105_743.pdf.

⁷⁹ Shuhui Sun, Gaixia Zhang, Yu Zhong, Hao Liu, Ruying Li, Xiaorong Zhou, Xueliang Sun, “Ultrathin single crystal Pt nanowires grown on N-doped carbon nanotubes,” *Chem. Commun.* (2009):7048-7050.

⁸⁰ Stanislaus S. Wong, Ernesto Joselevich, Adam T. Woolley, Chin Li Cheung & Charles M. Lieber, “Covalently functionalized nanotubes as nanometresized probes in chemistry and biology,” *Nature* 394(2 July 1998):52-55; <http://leitl.org/docs/nano/394052.pdf>.

Figure 3-2. Probe sharpness determines resolution. (A) Super-sharp (<1 nm) diamond-like carbon (DLC) “asperity tip” from NT-MDT.⁸¹ **(B)** DNA strand diameter (~ 2 nm) can be resolved⁸² using DLC spike-probe tip;⁸³ small unwound single-strand DNA fragments can be seen (bold arrow on scan) and even the helical pitch of the DNA molecule can be resolved (thin arrows). **(C)** SWCNT tip (0.5 – 1.4 nm).⁸⁴

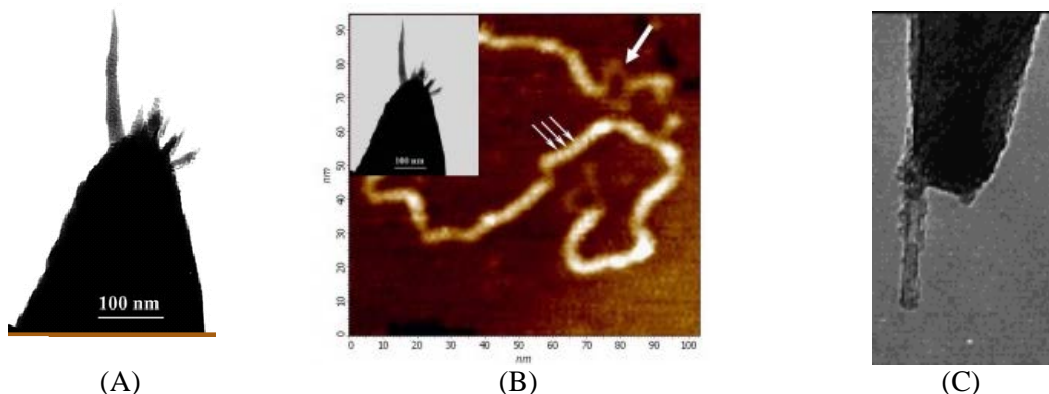
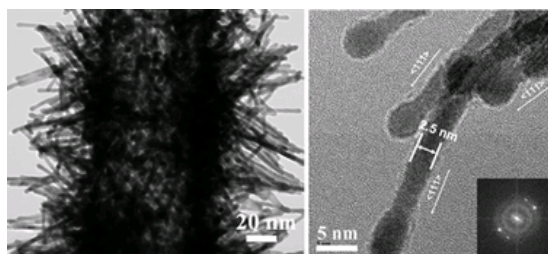


Figure 3-3. Single-crystal platinum asperities grown on CNT.⁸⁵



⁸¹ NT-MDT (Molecular Devices and Tools for Nanotechnology, Moscow, Russia, <http://www.ntmdt.com>), “Super sharp Diamond_Like Carbon (DLC) tips,” from their “SPM Probe and Accessories” catalog, 2008; http://www.ntmdt.com/download/accessories_catalog.pdf.

⁸² Dmitry Klinov, Benjamin Dwir, Eli Kapon, Natalia Borovok, Tatiana Molotsky, Alexander Kotlyar, “High-resolution atomic force microscopy of duplex and triplex DNA molecules,” *Nanotechnology* 18(6 June 2007):225102.. “DNA in nanotechnology,” 2007; <http://www.nanovip.com/node/4971>.

⁸³ NT-MDT (Molecular Devices and Tools for Nanotechnology, Moscow, Russia, <http://www.ntmdt.com>), “Super sharp Diamond_Like Carbon (DLC) tips,” from their “SPM Probe and Accessories” catalog, 2008; http://www.ntmdt.com/download/accessories_catalog.pdf.

⁸⁴ Dieter Winkler, Udo Weigel, Stefan Grimm, “Method Of Preparing An Ultra Sharp Tip, Apparatus For Preparing An Ultra Sharp Tip, And Use Of An Apparatus,” IPC8 Class: AC25D534FI, USPC Class: 205205, Patent application number: 20100006447; <http://www.faqs.org/patents/app/20100006447>.

⁸⁵ Shuhui Sun, Gaixia Zhang, Yu Zhong, Hao Liu, Ruying Li, Xiaorong Zhou, Xueliang Sun, “Ultrathin single crystal Pt nanowires grown on N-doped carbon nanotubes,” *Chem. Commun.* (2009):7048-7050.

Such asperity-type tips probably won't be highly reliable and will not be atomically precise, but they might work well enough for DMS if enough trials can be attempted and if the error rate proves low enough. Unfortunately, extensive physical experimentation with fabricating and using these tips will be required to determine their suitability because there is no easy way to simulate them to high accuracy, due to their nonuniform and atomically-imprecise structure and given the large atom count that would be involved. There will also be a lot of variation in tip structure and quality from one tip to the next, even when successive tips are all obtained from the same source or process. In this scenario, the obvious strategy would be to build atomically precise replacement tips as quickly as possible using the initial DMS bootstrap system.

3.3 Nanowire Tips

Another approach is to use nanowires as AFM tips.⁸⁶ Many different types of nanowires exist, including metallic (e.g., Ni, Pt, Au), semiconducting (e.g., Si, InP, GaN, etc.), and insulating (e.g., SiO₂, TiO₂, ZnO).

Tungsten nanowires with nanoscale widths can be grown⁸⁷ using the technique of electron-beam-induced deposition (EBID), which is often used for direct-writing of three-dimensional dielectric, semiconductor, and metallic materials with nanoscale precision and resolution. In this work,⁸⁸ slow one-dimensional lateral scanning produced >20 nm diameter textured β -tungsten nanowire cores surrounded by an oxide secondary layer, while stationary vertical growth produced single-crystal (100)-oriented W₃O nanowires. See more on EBID in [Section 3.8](#). Tungsten nanowires of ~5 nm diameter have also been tested for their field emission properties.⁸⁹

⁸⁶ Munekazu Motoyama, Neil P. Dasgupta, Fritz B. Prinz, "Electrochemical Deposition of Metallic Nanowires as a Scanning Probe Tip," J. Electrochem. Soc., Volume 156(20 August 2009):D431-D438. See also: Munekazu Motoyama, Friedrich B. Prinz, "Nanoscale Topography Measurements with a Metal Nanowire AFM Tip," ECS Trans. 19(2009):85-96. (Researchers are at Stanford University) A.B.H. Tay, J.T.L. Thong, "Fabrication of super-sharp nanowire atomic force microscope using a field emission induced growth technique," Rev. Sci. Instrum. 75(10 October 2004):3248-3255; <http://www.nanoworkstation.com/fileadmin/public/publications/2004-rsi-75.pdf> or <http://www.kleindiek.com/fileadmin/public/publications/2004-rsi-75.pdf>. See also: A.B.H. Tay, J.T.L. Thong, "High-resolution nanowire atomic force microscope probe grown by a field-emission induced process," Appl. Phys. Lett. 84(21 June 2004):5207-5209; <http://nanoworkstation.com/fileadmin/public/publications/2004-apl-84.pdf>.

⁸⁷ K.L. Klein, S.J. Randolph, J.D. Fowlkes, L.F. Allard, H.M. Meyer III, M.L. Simpson, P.D. Rack, "Single-crystal nanowires grown via electron-beam-induced deposition," Nanotechnology 19(27 August 2008):345705.

⁸⁸ K.L. Klein, S.J. Randolph, J.D. Fowlkes, L.F. Allard, H.M. Meyer III, M.L. Simpson, P.D. Rack, "Single-crystal nanowires grown via electron-beam-induced deposition," Nanotechnology 19(27 August 2008):345705.

⁸⁹ K.S. Yeong, J.T.L. Thong, "Field-emission properties of ultrathin 5 nm tungsten nanowire," J. Appl. Phys. 100(14 December 2006):114325.

Another technique is field emission induced growth,⁹⁰ which has been used to grow a single metallic nanowire on an atomic force microscope (AFM) tip. In this experiment, tungsten nanowire AFM probes were produced with great consistency and high reproducibility. The tungsten nanowires were grown onto a silicon substrate to lengths between 100-1500 nm with a radius of curvature at the tip end typically between 1-2 nm⁹¹ (Figure 3-4). Experiments using the fabricated tungsten nanowire AFM probe demonstrated its ability to produce high-resolution AFM images and improved profiling of structures with steep sidewalls due to its very sharp tip and high aspect ratio.

Another technique for making nanowires is electrodeposition. For example, pure metallic molybdenum nanowires 15 nm in diameter and up to 500 nm in length (Figure 3-5) have been prepared by electrodeposition.⁹² Another method is vapor-liquid-solid (VLS), which has been used to grow ZnO nanowires 10-15 nm in diameter and 2-10 microns in length on sapphire, silica and silicon substrates atop 50-100 nm gold dots.⁹³ VLS-grown crystalline boron nanowires have been EBID-welded to AFM probe tips and then imaged via SEM.⁹⁴ Crystalline boron nanowires

⁹⁰ A.B.H. Tay, J.T.L. Thong, "Fabrication of super-sharp nanowire atomic force microscope using a field emission induced growth technique," Rev. Sci. Instrum. 75(10 October 2004):3248-3255; <http://www.nanoworkstation.com/fileadmin/public/publications/2004-rsi-75.pdf> or <http://www.kleindiek.com/fileadmin/public/publications/2004-rsi-75.pdf>. See also: A.B.H. Tay, J.T.L. Thong, "High-resolution nanowire atomic force microscope probe grown by a field-emission induced process," Appl. Phys. Lett. 84(21 June 2004):5207-5209; <http://nanoworkstation.com/fileadmin/public/publications/2004-apl-84.pdf>. K.S. Yeong, J.B.K. Law, J.T.L. Thong, "Field-emission-induced growth of nanowire between electrodes," Appl. Phys. Lett. 88(1 December 2006):193116.

⁹¹ A.B.H. Tay, J.T.L. Thong, "Fabrication of super-sharp nanowire atomic force microscope using a field emission induced growth technique," Rev. Sci. Instrum. 75(10 October 2004):3248-3255; <http://www.nanoworkstation.com/fileadmin/public/publications/2004-rsi-75.pdf> or <http://www.kleindiek.com/fileadmin/public/publications/2004-rsi-75.pdf>. See also: A.B.H. Tay, J.T.L. Thong, "High-resolution nanowire atomic force microscope probe grown by a field-emission induced process," Appl. Phys. Lett. 84(21 June 2004):5207-5209; <http://nanoworkstation.com/fileadmin/public/publications/2004-apl-84.pdf>.

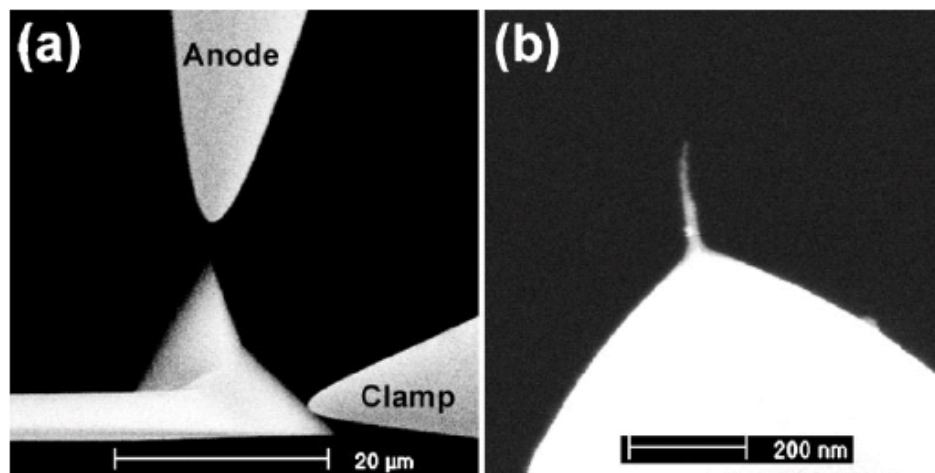
⁹² Michael P. Zach, Kwok H. Ng, Reginald M. Penner, "Molybdenum Nanowires by Electrodeposition," Science 290(15 December 2000):2120-2123; [http://chem.ps.uci.edu/~rmpenner/PDFs/59_Science_290\(2000\)2120.pdf](http://chem.ps.uci.edu/~rmpenner/PDFs/59_Science_290(2000)2120.pdf).

⁹³ E.C. Greyson, Y. Babayan, T.W. Odom, "Directed Growth of Ordered Arrays of Small Diameter ZnO Nanowires," Adv. Mat. 16(2004):1348-1352; <http://chemgroups.northwestern.edu/odom/Publications/TWO-23.pdf>.

⁹⁴ C.H. Lin, M. Chang, X. Li, J.R. Deka, "Measurement of Mechanical Properties of Boron Nanowire Using Nano-manipulation System," in: Srichand Hinduja, Kuang-Chao Fan, eds., Proceedings of the 35th International MATADOR Conference, Springer, London, 2007, pp. 275-278.

have also been synthesized by the chemical vapor deposition (CVD) method onto preformed metal catalyst particles.⁹⁵

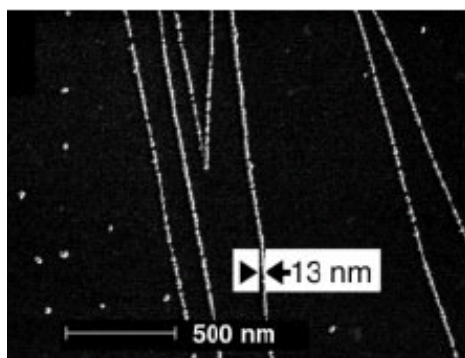
Figure 3-4. (a) SEM image showing the orientation of the AFM tip and the two etched tungsten sharp tips that are attached to the micromanipulators positioned for field-emission induced growth; **(b)** SEM image of a 200 nm long tungsten nanowire AFM tip with a 1-2 nm tip radius curvature; the tungsten nanowire appears much thicker than as-grown in the SEM image due to contamination during viewing.⁹⁶



⁹⁵ Carolyn Jones Otten, Oleg R. Lourie, Min-Feng Yu, John M. Cowley, Mark J. Dyer, Rodney S. Ruoff, William E. Buhro, "Crystalline boron nanowires," J. Am. Chem. Soc. 124(2002):4564-4565; <https://netfiles.uiuc.edu/mfyu/www/Documents/Publications/JACS-2002.pdf>.

⁹⁶ A.B.H. Tay, J.T.L. Thong, "Fabrication of super-sharp nanowire atomic force microscope using a field emission induced growth technique," Rev. Sci. Instrum. 75(10 October 2004):3248-3255; <http://www.nanoworkstation.com/fileadmin/public/publications/2004-rsi-75.pdf> or <http://www.kleindiek.com/fileadmin/public/publications/2004-rsi-75.pdf> . See also: A.B.H. Tay, J.T.L. Thong, "High-resolution nanowire atomic force microscope probe grown by a field-emission induced process," Appl. Phys. Lett. 84(21 June 2004):5207-5209; <http://nanoworkstation.com/fileadmin/public/publications/2004-apl-84.pdf>.

Figure 3-5. Low-magnification SEM image of graphite surface following the electrodeposition of MoOx nanowires the linearity, number density, and uniformity of electrodeposited nanowires.⁹⁷



It has long been known that tips for AFM/STM work can be made with radii of ~ 5 nm using EBID⁹⁸ and other techniques,⁹⁹ and EBID-fabricated carbon supertips have “customizable shapes with features down to below 10 nm”.¹⁰⁰ If reasonably pure single-crystal (111)-oriented W nanowires could be produced, they might be used as low-radius curvature tips suitable for faceting work (Section 5.3). This would be especially useful if such tungsten nanowires can be EBID-grown directly onto the ends of qPlus AFM tips in a specific orientation and shape, then Ir-coated to produce high-aspect-ratio pyramidal single-atom tips at the working apex of the qPlus tip (Section 6.1). Alternatively, the tip could be grown on a small jig structure that could be processed separately, then later mechanically attached to the qPlus terminus (Section 6.3) – in the event that the MEMS-based qPlus sensor cannot tolerate the moderately high annealing temperatures required to produce the Ir-pyramidal single atom tip.

⁹⁷ Michael P. Zach, Kwok H. Ng, Reginald M. Penner, “Molybdenum Nanowires by Electrodeposition,” Science 290(15 December 2000):2120-2123; [http://chem.ps.uci.edu/~rmpenner/PDFs/59_Science_290\(2000\)2120.pdf](http://chem.ps.uci.edu/~rmpenner/PDFs/59_Science_290(2000)2120.pdf).

⁹⁸ Hans W.P. Koops, Johannes Kretz, Michael Rudolph, Markus Weber, Gerold Dahm, Kam L. Lee, “Characterization and application of materials grown by electron-beam-induced deposition,” Jpn. J. Appl. Phys. 33(30 December 1994):7099-7107.

⁹⁹ K. Wiesauer, G. Springholz, “Fabrication of semiconductor nanostructures by nanoindentation of photoresist layers using atomic force microscopy,” J. Appl. Phys. 88(15 December 2000):7289-7297; http://www.hlphys.uni-linz.ac.at/hl/perskarin/publikat/jap88_7289_00_nano.pdf.

¹⁰⁰ P. Boggild, T.M. Hansen, K. Molhave (Mikroelektronik Centret, Technical University of Denmark), “Nanotweezers for manipulation of free-hanging nanowires,” abstract FF14, <http://www.nbi.dk/dfs/abs2001final/ff14.html> ; presentation at Physics and Industrial Innovation Session, Chairman F. Grey (Mikroelektronik Centret, Technical University of Denmark), sponsored by Danish Physical Society, 2001; <http://www.nbi.dk/dfs/abs2001final/ff00.html>.

Noble metals will also self-organize into isolated nanowires on semiconductor surfaces, though it appears that full contact with the surface is required (i.e., no self-supporting or free-standing wires are formed) and mechanical removal of the wires from the surface has not yet been attempted. For example, Schafer et al.¹⁰¹ have fabricated self-organizing noble metal atomic nanowires on the Ge(100) surface: “Atomic structures of quasi-one-dimensional (1D) character can be grown on semiconductor substrates by metal adsorption. Significant progress concerning study of their 1D character has been achieved recently by condensing noble metal atoms on the Ge(001) surface. In particular, Pt and Au yield high quality reconstructions with low defect densities. For Pt/Ge(001), we find hot substrate growth is the preferred method for self-organization. Despite various dimerized bonds, these atomic wires exhibit metallic conduction at room temperature, as documented by low-bias STM. For the recently discovered Au/Ge(001) nanowires, we have developed a deposition technique that allows complete substrate coverage. The Au nanowires are extremely well separated spatially, exhibit a continuous 1D charge density, and are of solid metallic conductance.”

Nano-needles have been fabricated. In one chemical process,¹⁰² tungsten oxide tapered needles with nanotips were synthesized on a large scale by reacting tungsten nanopowders with hydrous nickel nitrate in hydrogen atmosphere. The resulting tungsten oxide needles have lengths more than 100 μm , root diameters of several hundred nanometers and tip diameters of several nanometers, showing a perfectly axisymmetric configuration. HRTEM and SAED analyses showed that the synthesized tungsten oxide tapered needles have a single-crystal structure with a growth direction of (010). Tungsten oxide nanowires, submicro-/micro-whiskers and microtubules could be facilely obtained under different experimental conditions (the ratio between tungsten and hydrous nickel nitrate, the size of tungsten powders, and the reaction atmosphere).

Nanoscale whiskers have also been fabricated and could be used for tips. For example, Al nanowhiskers 23-30 nm in thickness (Figure 3-6A) have been grown on a surface-oxidized Si substrate using an electron beam evaporation apparatus, wherein aluminum is deposited at a glancing angle on a high-temperature substrate (HT-GLAD).¹⁰³ Diamond nanowhiskers 50-100

¹⁰¹ J. Schafer, S. Meyer, C. Blumenstein, K. Roensch, R. Claessen, S. Mietke, M. Klinke, T. Podlich, R. Matzdorf, A. Stekolnikov, S. Sauer, F. Bechstedt, “Self-organized atomic nanowires of noble metals on Ge(001): atomic structure and electronic properties,” *New J. Phys.* 11(2009):125011.

¹⁰² Shiliang Wang, Yuehui He, Jin Zou, Peng Cao, Yao Jiang, Baiyun Huang, C.T. Liu, P.K. Liaw, “Synthesis of tungsten oxide tapered needles with nanotips,” *Journal of Crystal Growth* 303(15 May 2007):574-579.

¹⁰³ Motofumi Suzuki, Koji Nagai, Sadamu Kinoshita, Kaoru Nakajima, Kenji Kimura, Tomoki Okano, Kaoru Sasakawa, “Vapor phase growth of Al whiskers induced by glancing angle deposition at high temperature,” *Appl. Phys. Lett.* 89(2006):133103; http://repository.kulib.kyoto-u.ac.jp/dspace/bitstream/2433/24186/1/AplPhysLett_89_133103.pdf. Motofumi Suzuki, Koji Nagai, Sadamu Kinoshita, Kaoru Nakajima, Kenji Kimura, Tomoki Okano, Kaoru Sasakawa, “Morphological evolution of Al whiskers grown by high temperature glancing angle deposition,” *J. Vac. Sci. Technol. A* 25(July 2007):1098-1102. Motofumi Suzuki, Hideki Hara, Ryo Kita, Kenji Hamachi, Koji Nagai, Kaoru Nakajima, Kenji Kimura, “Growth of Metal Nanowhiskers on Patterned Substrate by High Temperature Glancing Angle Deposition,” *Journal of the Electrochemical Society* 157(December 2009):K34-K38.

nm¹⁰⁴ in width have been fabricated; single-crystal Ag,¹⁰⁵ AgBiS₂,¹⁰⁶ single-crystal Al,¹⁰⁷ single-crystal Au,¹⁰⁸ 20-nm Bi₂S₃,¹⁰⁹ CdS,¹¹⁰ single-crystal Cu,¹¹¹ 15-30 nm Cu₂O,¹¹² Fe,¹¹³ GaAs,¹¹⁴

¹⁰⁴ Eun-Song Baik, Young-Joon Baik, Dongryul Jeon, "Aligned diamond nanowhiskers," *J. Mater. Res.* 15(April 2000):923-926. Chaoyang Li, Akimitsu Hatta, "Comparison of Properties of Diamond Nanowhiskers Obtained by Etching Diamond Films with Different Metal Coatings in Radio Frequency Plasma," *Jpn. J. Appl. Phys.* 45(2006):8378-8380.

¹⁰⁵ Gunther Richter, Karla Hillerich, Daniel S. Gianola, Reiner Monig, Oliver Kraft, Cynthia A. Volkert, "Ultrahigh Strength Single Crystalline Nanowhiskers Grown by Physical Vapor Deposition," *Nano Lett.* 9(August 2009):3048-3052;
http://gianola.seas.upenn.edu/pubs/PDFs/Richter_nanowhisk_published_nanolett_2009.pdf.

¹⁰⁶ Bo Xie, Shengwen Yuan, Yang Jiang, Jun Lu, Qing Li, Yue Wu, Weichao Yu, Houbo Zhang, Yitai Qian, "Molecular Template Preparation of AgBiS₂ Nanowhiskers," *Chemistry Letters* 31(2002):612-613.

¹⁰⁷ Gunther Richter, Karla Hillerich, Daniel S. Gianola, Reiner Monig, Oliver Kraft, Cynthia A. Volkert, "Ultrahigh Strength Single Crystalline Nanowhiskers Grown by Physical Vapor Deposition," *Nano Lett.* 9(August 2009):3048-3052;
http://gianola.seas.upenn.edu/pubs/PDFs/Richter_nanowhisk_published_nanolett_2009.pdf.

¹⁰⁸ Gunther Richter, Karla Hillerich, Daniel S. Gianola, Reiner Monig, Oliver Kraft, Cynthia A. Volkert, "Ultrahigh Strength Single Crystalline Nanowhiskers Grown by Physical Vapor Deposition," *Nano Lett.* 9(August 2009):3048-3052;
http://gianola.seas.upenn.edu/pubs/PDFs/Richter_nanowhisk_published_nanolett_2009.pdf.

¹⁰⁹ Rong He, Xuefeng Qian, Jie Yin, Zikang Zhu, "Preparation of Bi₂S₃ nanowhiskers and their morphologies," *Journal of Crystal Growth* 252(2003):505-510; <http://202.127.1.11/jcg/252/25275.pdf>.

¹¹⁰ Pavle V. Radovanovic, Carl J. Barrelet, Silvija Gradeak, Fang Qian, Charles M. Lieber, "General Synthesis of Manganese-Doped II–VI and III–V Semiconductor Nanowires," *Nano Lett.* 5(2005):1407-1411.

¹¹¹ Gunther Richter, Karla Hillerich, Daniel S. Gianola, Reiner Monig, Oliver Kraft, Cynthia A. Volkert, "Ultrahigh Strength Single Crystalline Nanowhiskers Grown by Physical Vapor Deposition," *Nano Lett.* 9(August 2009):3048-3052;
http://gianola.seas.upenn.edu/pubs/PDFs/Richter_nanowhisk_published_nanolett_2009.pdf.

¹¹² Ying Yu, Fei-Peng Du, Jimmy C. Yu, Yuan-Yi Zhuang, Po-Keung Wong, "One-dimensional shape-controlled preparation of porous Cu₂O nano-whiskers by using CTAB as a template," *Journal of Solid State Chemistry* 177(2004):4640-4647.

¹¹³ Motofumi Suzuki, Hideki Hara, Ryo Kita, Kenji Hamachi, Koji Nagai, Kaoru Nakajima, Kenji Kimura, "Growth of Metal Nanowhiskers on Patterned Substrate by High Temperature Glancing Angle Deposition," *Journal of the Electrochemical Society* 157(December 2009):K34-K38.

¹¹⁴ V. Khorenko, I. Regolin, S. Neumann, Q.T. Do, W. Prost, F.-J. Tegude, "Characterisation of GaAs nanowhiskers grown on GaAs and Si substrates," *International Conference on Indium Phosphide and Related Materials*, 8-12 May 2005, pp. 363-366.

GaN,¹¹⁵ InAs (Figure 3-6B),¹¹⁶ InGaAs,¹¹⁷ Mn,¹¹⁸ MnP and Mn₂P,¹¹⁹ 70-300 nm Na_xWO₃,¹²⁰ Pb,¹²¹ 3-nm Si,¹²² 100-nm Si,¹²³ single-crystal Si,¹²⁴ SiC,¹²⁵ SiGe,¹²⁶ SnO₂,¹²⁷ WO₃,¹²⁸ ZnO,¹²⁹ and ZnS¹³⁰ nanowhiskers have also been grown.

¹¹⁵ Anna Cavallini, Laura Polenta, Marco Rossi, Thomas Richter, Michel Marso, Ralph Meijers, Raffaella Calarco, Hans Lüth, "Defect Distribution along Single GaN Nanowhiskers," Nano Letters 6(July 2006):1548-1551.

¹¹⁶ Masamitsu Yazawa, Masanari Koguchi, Akiko Muto, Kenji Hiruma, "Semiconductor nanowhiskers," Advanced Materials 5(2004):577-580.

¹¹⁷ D. Sudfeld, I. Regolin, J. Kaumlstner, G. Dumpich, V. Khorenko, W. Prost, F.-J. Tegude, "Single InGaAs nanowhiskers characterized by analytical transmission electron microscopy," Phase Transitions 79(September 2006):727-737.

¹¹⁸ Wu Er-Dong, Guo Xiu-Mei, "Mn Nanowhiskers of a Novel Hexagonal Phase Grown from Hydrogen Activated Laves Phase Alloys," Chinese Phys. Lett. 25(2008):2607-2609.

¹¹⁹ A.D. Bouravleuv, H. Sosiati, T. Ishibashi, N. Kuwano, K. Sato, "MBE fabrication of Mn_xP nanowhiskers," J. Phys.: Conf. Ser. 100(2008):052052; http://home.sato-gallery.com/research/jpconf8_100_052052.pdf.

¹²⁰ R. Azimirad, M. Goudarzi, O. Akhavan, A.Z. Moshfegh, "The effect of heating time on growth of Na_xWO₃ nanowhiskers," Vacuum 82(August 2008):821-826.

¹²¹ Z.M. Sun, M.W. Barsoum, "Spontaneous room temperature extrusion of Pb nano-whiskers from leaded brass surfaces," J. Mater. Res. 20(May 2005):1087-1089; <http://staff.aist.go.jp/z.m.sun/Pub/PDF/Spontaneous%20room%20temperature%20extrusion%20of%20Pb%20nano-whiskers%20from%20leaded%20brass%20surfaces.pdf>.

¹²² N. Ozaki, Y. Ohno, S. Takeda, "Silicon nanowhiskers grown on a hydrogen-terminated silicon {111} surface," Appl. Phys. Lett. 73(1998):3700-3702.

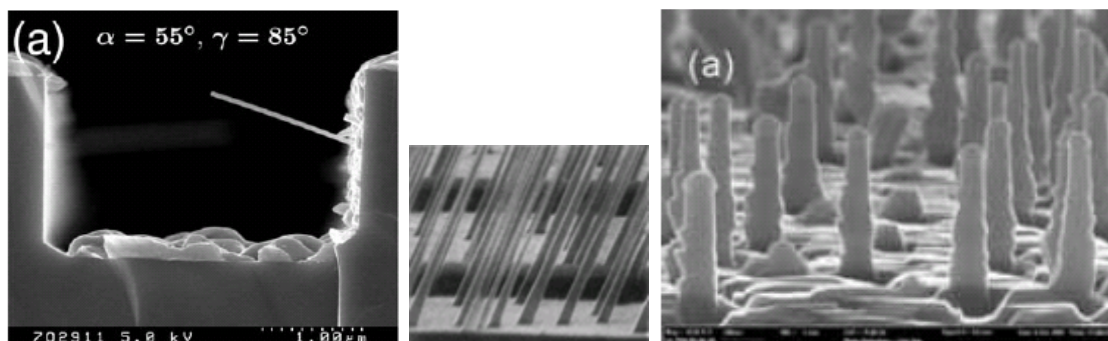
¹²³ F.M. Ross, J. Tersoff, M.C. Reuter, "Sawtooth Faceting in Silicon Nanowires," Phys. Rev. Lett. 95(29 September 2005):146104. See also: R. Dujardin, V. Poydenot, T. Devillers, P. Gentile, V. Fabre Nicolin, A. Barski, "Growth of Si and SiGe Nanowhiskers by Molecular Beam Epitaxy: X-Ray Scattering and Electron Microscopy Investigations," poster at TNT2006, Grenoble, France, 4-8 September 2006; http://www.tntconf.org/2006/Abstracts/Posters/TNT2006_Dujardin.pdf.

¹²⁴ Gunther Richter, Karla Hillerich, Daniel S. Gianola, Reiner Monig, Oliver Kraft, Cynthia A. Volkert, "Ultrahigh Strength Single Crystalline Nanowhiskers Grown by Physical Vapor Deposition," Nano Lett. 9(August 2009):3048-3052; http://gianola.seas.upenn.edu/pubs/PDFs/Richter_nanowhisk_published_nanolett_2009.pdf.

¹²⁵ Y.J. Wu, W. Qin, Z.X. Yang, J.S. Wu, Y.F. Zhang, "Preparation of high-quality β-SiC nanowhiskers by using carbon fibres as carbon source," J. Mater. Sci. 39(August 2004):5563-5565.

¹²⁶ Lincoln J. Lauhon, Mark S. Gudiksen, Deli Wang, Charles M. Lieber, "Epitaxial core-shell and core-multishell nanowire heterostructures," Nature 420(2002):57-61; http://hamers.chem.wisc.edu/chem630_fall2004/problem_sets/nature01141.pdf.

Figure 3-6. (A) Left: SEM image of the cross section of an Al nanowhisker.¹³¹ (B) Middle: InAs nanowhiskers.¹³² (C) Right: Si nanowhiskers.¹³³



¹²⁷ S.H. Luo, Q. Wan, W.L. Liu, M. Zhang, Z.F. Di, S.Y. Wang, Z.T. Song, C.L. Lin, J.Y. Dai, "Vacuum electron field emission from SnO₂ nanowhiskers synthesized by thermal evaporation," *Nanotechnology* 15(2004):1424-1427.

¹²⁸ Y. Baek, Y. Song, K. Yong, "A Novel Heteronanostructure System: Hierarchical W Nanothorn Arrays on WO₃ Nanowhiskers," *Advanced Materials* 18(10 November 2006):3105-3110.

¹²⁹ Hai-Bo Lin, Mao-Sheng Cao, Quan-Liang Zhao, Xiao-Ling Shi, Da-Wei Wang, Fu-Chi Wang, "Mechanical reinforcement and piezoelectric properties of nanocomposites embedded with ZnO nanowhiskers," *Scripta Materialia* 59(October 2008):780-783.

¹³⁰ Pavle V. Radovanovic, Carl J. Barrelet, Silvija Gradeak, Fang Qian, Charles M. Lieber, "General Synthesis of Manganese-Doped II–VI and III–V Semiconductor Nanowires," *Nano Lett.* 5(2005):1407-1411.

¹³¹ M. Suzuki, H. Hara, R. Kita, K. Hamachi, K. Nagai, K. Nakajima, K. Kimura, "Growth of Metal Nanowhiskers on the Patterned Substrate by Glancing Angle Deposition at High Temperature," *Electrochemical Society meeting*; <http://www.electrochem.org/meetings/scheduler/abstracts/216/2198.pdf>.

¹³² Masamitsu Yazawa, Masanari Koguchi, Akiko Muto, Kenji Hiruma, "Semiconductor nanowhiskers," *Advanced Materials* 5(2004):577-580.

¹³³ F.M. Ross, J. Tersoff, M.C. Reuter, "Sawtooth Faceting in Silicon Nanowires," *Phys. Rev. Lett.* 95(29 September 2005):146104. See also: R. Dujardin, V. Poydenot, T. Devillers, P. Gentile, V. Fabre Nicolin, A. Barski, "Growth of Si and SiGe Nanowhiskers by Molecular Beam Epitaxy: X-Ray Scattering and Electron Microscopy Investigations," poster at TNT2006, Grenoble, France, 4-8 September 2006; http://www.tntconf.org/2006/Abstracts/Posters/TNT2006_Dujardin.pdf.

NIST has also proposed¹³⁴ mounting a GaN nanowire on a silicon cantilever AFM tip to enable more precise NSOM-like nanoscale optical scanning capabilities.

3.4 Hut Structures

Self-assembled “hut” structures are another possibility, if they can be induced to grow at the tip of a suitably high-aspect flat-apex tip handle. For example, the formation and growth of self-assembled metastable Ge hut clusters (Figure 3-7),¹³⁵ and the distribution of strain around their base, are fascinating problems, as is their peculiar propensity to form (501)-facets as their sides,¹³⁶ e.g., when Ge atoms are added to Si(100) surface in 4-6 monolayer thickness.¹³⁷ Ge nanocrystals grown on Si(100)-(2x1) surfaces by molecular beam epitaxy (MBE) also are observed to form a relatively high density of Ge islands with small “pyramids,” “domes,” and “faceted domes” of various sizes co-existing in the film.¹³⁸ Scanning tunneling microscopy (STM) and high resolution cross-sectional transmission electron microscopy (XTEM) studies¹³⁹ reveal that a large fraction of these islands, especially the dome-shaped Ge islands, have an aspect ratio of ~1(diameter):1 (height), though this is likely too blunt to be useful for DMS bootstrapping tips.

¹³⁴ Kris A. Bertness, Norman A. Sanford, “Tip-mounted Nanowire Light Source Instrumentation,” Docket 08-010 Review, 20 May 2008, NIST/Optoelectronics Division/EEEL;
<http://www.google.com/url?sa=t&source=web&ct=res&cd=1&ved=0CAkQFjAA&url=http%3A%2F%2Fsapps.nist.gov%2Ftechtransfer%2Fdocs%2FTip-Mounted%2520Nanowire%2520Light%2520Source%2520Instrumentation.ppt&rct=j&q=nanowire+%22as+an+AFM+tip%22&ei=mcF1S5XpDMOpnQel2pCrCQ&usg=AFQjCNGbcs0lhacesumK24na8LM1qXDJZw>.

¹³⁵ Y.-W. Mo, D.E. Savage, B.S. Swartzentruber, M.G. Lagally, “Kinetic Pathway in Stranski-Krastanov Growth of Ge on Si(001),” Phys. Rev. Lett. 65(20 August 1990):1020-1023.

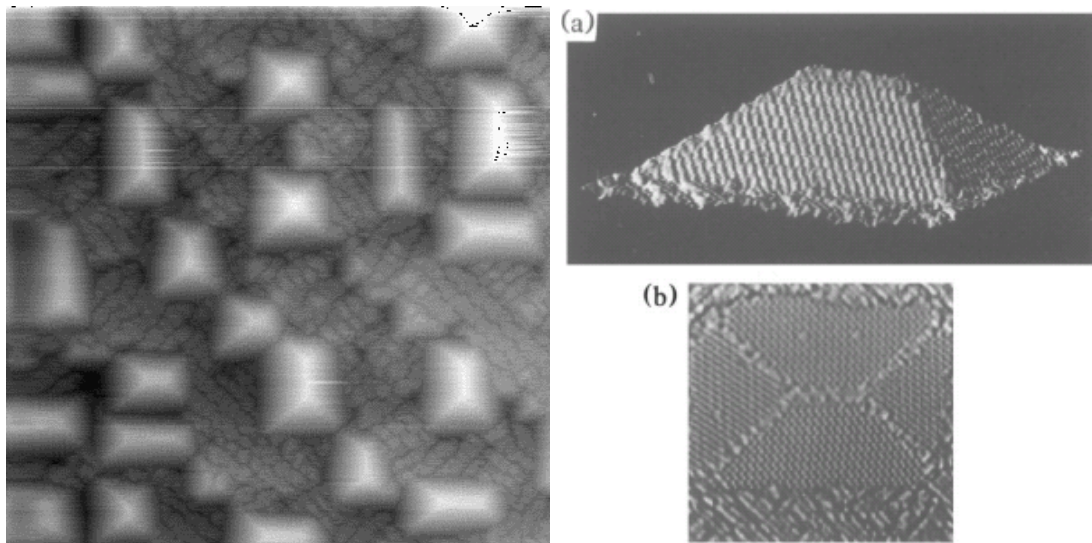
¹³⁶ <http://www.cmmmp.ucl.ac.uk/~drb/Thesis/Masterch8.html>.

¹³⁷ Y.-W. Mo, D.E. Savage, B.S. Swartzentruber, M.G. Lagally, “Kinetic Pathway in Stranski-Krastanov Growth of Ge on Si(001),” Phys. Rev. Lett. 65(20 August 1990):1020-1023.

¹³⁸ K. Bhattacharjeea, Anupam Roy, Jay Ghataka, P.V. Satyama, B.N. Deva, “Ultrasmall Ge islands with low diameter-to-height aspect ratio on Si(100)-(2x1) surfaces,” Applied Surface Science 256(30 October 2009):356-360; http://www.sciencedirect.com/science?_ob=ArticleURL&_udi=B6THY-4W7YXMH-F&_user=10&_rdoc=1&_fmt=&_orig=search&_sort=d&_docanchor=&view=c&_searchStrId=1102988067&_rerunOrigin=scholar.google&_acct=C000050221&_version=1&_urlVersion=0&_userid=10&md5=93d7077e3462b4f62a914d920d9fc656.

¹³⁹ K. Bhattacharjeea, Anupam Roy, Jay Ghataka, P.V. Satyama, B.N. Deva, “Ultrasmall Ge islands with low diameter-to-height aspect ratio on Si(100)-(2x1) surfaces,” Applied Surface Science 256(30 October 2009):356-360; http://www.sciencedirect.com/science?_ob=ArticleURL&_udi=B6THY-4W7YXMH-F&_user=10&_rdoc=1&_fmt=&_orig=search&_sort=d&_docanchor=&view=c&_searchStrId=1102988067&_rerunOrigin=scholar.google&_acct=C000050221&_version=1&_urlVersion=0&_userid=10&md5=93d7077e3462b4f62a914d920d9fc656.

Figure 3-7. Left: An STM image of “hut” clusters formed (number density typically $\sim 7 \times 10^{10}/\text{cm}^2$)¹⁴⁰ when 4-6 layers of germanium are grown on silicon, with the hut sides running along (100)-like directions (which are elastically soft) and the faces all (501)-like; image courtesy of Ilan Goldfarb.¹⁴¹ **Right:** STM images of a single Ge “hut” cluster – (a) perspective image with a scan area of 40 nm x 40 nm, showing a hut height of 2.8 nm; (b) curvature-mode grey-scale image, showing the crystal structure on all four facets as well as the dimer rows in the 2D Ge layer around the cluster; the 2D layer dimer rows are 45° to the axis of the cluster.¹⁴²



The huts were the first Ge/Si island type to be discovered,¹⁴³ but now they are considered to be only metastable, because in annealing experiments huts transform into pyramids.¹⁴⁴ Germanium

¹⁴⁰ Y.-W. Mo, D.E. Savage, B.S. Swartzentruber, M.G. Lagally, “Kinetic Pathway in Stranski-Krastanov Growth of Ge on Si(001),” Phys. Rev. Lett. 65(20 August 1990):1020-1023.

¹⁴¹ <http://www.cmmp.ucl.ac.uk/~drb/Thesis/Masterch8.html>.

¹⁴² Y.-W. Mo, D.E. Savage, B.S. Swartzentruber, M.G. Lagally, “Kinetic Pathway in Stranski-Krastanov Growth of Ge on Si(001),” Phys. Rev. Lett. 65(20 August 1990):1020-1023.

¹⁴³ Y.-W. Mo, D.E. Savage, B.S. Swartzentruber, M.G. Lagally, “Kinetic Pathway in Stranski-Krastanov Growth of Ge on Si(001),” Phys. Rev. Lett. 65(20 August 1990):1020-1023.

¹⁴⁴ G. Medeiros-Ribeiro, T.I. Kamins, D.A.A. Ohlberg, R. Stanley Williams, “Annealing of Ge nanocrystals on Si(001) at 550 °C: Metastability of huts and the stability of pyramids and domes,” Phys. Rev. B 58(1998):3533-3536; http://dns.ntu-ccms.ntu.edu.tw/references/1Sorted-References/PHYS_REV_B/Volume_58/PHYS_REV_B-58-3533-1998.pdf.

can form defect-free pyramidal islands on Si(100)-(2x1) with a height of 15 nm and a width of 60 nm using chemical vapor deposition.¹⁴⁵

Pyramids and domes can coexist over a wide range of coverage, temperature, growth and annealing conditions, and the growth and shape transition mechanisms of these two island types have been extensively studied and debated for over a decade.¹⁴⁶ The experimental size distribution¹⁴⁷ shows indications of size-limited behavior for both pyramids and domes, and a dependence on the substrate crystallographic orientation. For instance, deposition of a single 2.5 nm thick layer of Si_{0.55}Ge_{0.45} on Si(001) substrate with $\theta = 4^\circ$ polar miscut results in a surface covered with oriented triangular structures.¹⁴⁸ The structures are actually composed of three facets reminiscent of self-assembled Ge pyramids on Si(001): a (001) square bound by $\langle 100 \rangle$ steps, and two {105} parallelograms – a pattern of SiGe surface faceting with three facet types reported to be unique for a semiconductor surface.¹⁴⁹

The growth of germanium (which has a 4% larger lattice constant than silicon) on a Si(001) substrate has been described by layer-plus-island mode. The wetting layer, a uniformly strained germanium film, grows pseudomorphically to a thickness of 2-3 monolayers, followed by the formation of three-dimensional islands on top of the uniform film.¹⁵⁰ These islands have a

¹⁴⁵ Marco Riedel, Bert Muller, Erich Wintermantel, “Protein adsorption and monocyte activation on germanium nanopylramids,” *Biomaterials* 22(2001):2307-2316; http://eva.unibas.ch/download/19426-Riedel_Biom_2001.pdf.

¹⁴⁶ R. Stanley Williams, Gilberto Medeiros-Ribeiro, Theodore I. Kamins, Douglas A.A. Ohlberg, “Thermodynamics of the Size and Shape of Nanocrystals: Epitaxial Ge on Si(001),” *Annu. Rev. Phys. Chem.* 51(October 2000):527-551; http://dns.ntu-ccms.ntu.edu.tw/references/ANNU_REV_PHYS_CHEM-51-527-2000.pdf. C. Teichert, “Self-organization of nanostructures in semiconductor heteroepitaxy,” *Phys. Rep.* 365(2002):335-432; <http://nanotech.iu4.bmstu.ru/archive/ran/Self-organization%20of%20nanostructures%20in%20semiconductor%20heteroepitaxy.pdf>. Karl Brunner, “Si/Ge nanostructures,” *Rep. Prog. Phys.* 65(2002):27-72; <http://lib.semi.ac.cn:8080/tsh/dzzy/wsqr/IOP/rep-prog-phys/rep65-27.pdf>.

¹⁴⁷ F.M. Ross, J. Tersoff, R.M. Tromp, “Coarsening of Self-Assembled Ge Quantum Dots on Si(001),” *Phys. Rev. Lett.* 80(2 February 1998):984-987; http://dns.ntu-ccms.ntu.edu.tw/references/PHYS_REV_LETT-80-5-984.pdf.

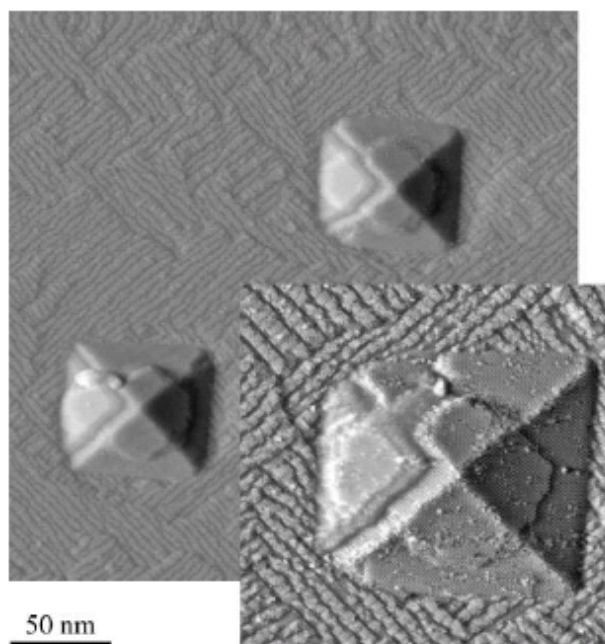
¹⁴⁸ C. Teichert, “Self-organization of nanostructures in semiconductor heteroepitaxy,” *Phys. Rep.* 365(2002):335-432; <http://nanotech.iu4.bmstu.ru/archive/ran/Self-organization%20of%20nanostructures%20in%20semiconductor%20heteroepitaxy.pdf>.

¹⁴⁹ C. Teichert, “Self-organization of nanostructures in semiconductor heteroepitaxy,” *Phys. Rep.* 365(2002):335-432; <http://nanotech.iu4.bmstu.ru/archive/ran/Self-organization%20of%20nanostructures%20in%20semiconductor%20heteroepitaxy.pdf>.

¹⁵⁰ Y.-W. Mo, D.E. Savage, B.S. Swartzentruber, M.G. Lagally, “Kinetic Pathway in Stranski-Krastanov Growth of Ge on Si(001),” *Phys. Rev. Lett.* 65(20 August 1990):1020-1023. D.J. Eaglesham, M. Cerullo, “Dislocation-free Stranski-Krastanow growth of Ge on Si(100),” *Phys. Rev. Lett.* 64(1990):1943-1946.

pyramidal or prism-like shape and are free of dislocations.¹⁵¹ At lower coverage the nanopyrramids are square or elongated huts with (105) facets implying angles of 11.3° with the flat substrate.¹⁵² Scanning tunneling microscopy images in Figure 3-8 represent such pyramids.

Figure 3-8. Scanning tunneling microscopy images of germanium nanopyrramids (hut clusters) grown on Si(001)-(2x1) at a substrate temperature of 550 °C with a deposition rate of 0.16 monolayers/s by molecular beam epitaxy (germanium coverage 5.8 monolayers). The pyramids have a height of about 6 nm and a base 60 nm x 60 nm, and exhibit well-defined (105) facets. The atomic structure is visible in the inset, where the magnification is further increased by a factor of two. The facet on the left is not well resolved due to the imperfect STM tip.¹⁵³



¹⁵¹ D.J. Eaglesham, M. Cerullo, "Dislocation-free Stranski-Krastanow growth of Ge on Si(100)," Phys. Rev. Lett. 64(1990):1943-1946.

¹⁵² Y.-W. Mo, D.E. Savage, B.S. Swartzentruber, M.G. Lagally, "Kinetic Pathway in Stranski-Krastanov Growth of Ge on Si(001)," Phys. Rev. Lett. 65(20 August 1990):1020-1023.

¹⁵³ Marco Riedel, Bert Muller, Erich Wintermantel, "Protein adsorption and monocyte activation on germanium nanopyrramids," Biomaterials 22(2001):2307-2316; http://eva.unibas.ch/download/19426-Riedel_Biom_2001.pdf.

These hut clusters are about 6 nm high and 60 nm wide. Their formation on atomic scale is made visible using high-temperature scanning tunneling microscopy.¹⁵⁴ At higher coverages, the shape changes, and nanopramids, termed dome clusters, are formed.¹⁵⁵ Here, the side planes are (113) and (102) facets, which gives rise to angles of 25.2° and 26.6°, respectively. Their base is comparable with that of hut clusters but their height exceeds the cluster height by more than a factor of two. More important, the Wenzel ratio, that is for pyramids basically $1/\cos(\alpha)$, where α denotes the angle between facet and substrate, is larger by a factor of six for the dome clusters than for the hut clusters with respect to the flat surface.¹⁵⁶

Si nanopyramid arrays on silicon have also been fabricated by a dry etching method via nanosphere lithography.¹⁵⁷

3.5 Metal Surface Faceting

It is well known in surface science that metal adsorbates can induce faceting and other morphological changes on a metal crystal surface (Figure 3-9).¹⁵⁸ (Reversible surface-step coalescence into facets can be described in terms of equilibrium thermodynamics – Herring¹⁵⁹ first quantified the requirements on the variation of the surface free energy with orientation for such a phase separation to occur. The stability of any given surface orientation on such a crystal is governed by a convexity requirement on the surface free energy as a function of orientation.)

¹⁵⁴ M. Kastner, B. Voigtlander, “Kinetically self-limiting growth of Ge islands on Si(001),” *Phys. Rev. Lett.* 82(1999):2745-2748.

¹⁵⁵ D.J. Eaglesham, M. Cerullo, “Dislocation-free Stranski-Krastanow growth of Ge on Si(100),” *Phys. Rev. Lett.* 64(1990):1943-1946. F.M. Ross, J. Tersoff, R.M. Tromp, “Coarsening of self-assembled Ge quantum dots on Si(001),” *Phys. Rev. Lett.* 80(1998):984-987. G. Medeiros-Ribeiro, A.M. Bratkovski, T.I. Kamins, D.A.A. Ohlberg, R.S. Williams, “Shape transition of germanium nanocrystals on a silicon (0 0 1) surface from pyramids to domes,” *Science* 279(1998):353-355. F.M. Ross, R.M. Tromp, M.C. Reuter, “Transition states between pyramids and domes during Ge/Si island growth,” *Science* 286(1999):1931-1934.

¹⁵⁶ Marco Riedel, Bert Muller, Erich Wintermantel, “Protein adsorption and monocyte activation on germanium nanopramids,” *Biomaterials* 22(2001):2307-2316; http://eva.unibas.ch/download/19426-Riedel_Biom_2001.pdf.

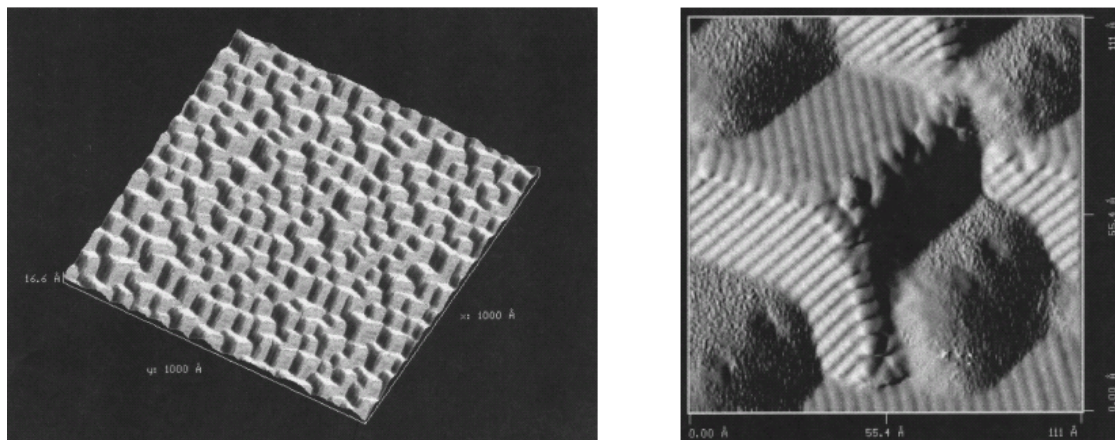
¹⁵⁷ Ho-Yen Hsieh, Sheng-Huang Huang, Kuo-Feng Liao, Chih-Huang Lai, Lih-Juann Chen, “Fabrication of Well-ordered Si Pyramids by Nanosphere Lithography and Dry Etching,” presentation KK4.29, Symposium KK: Nanoscale Pattern Formation, MRS 2007 Fall Meeting, 26-29 November 2007, Materials Research Society Symposium Proceedings Series, Volume 1059E (Proceedings Library, www.mrs.org/publications_library); http://www.mrs.org/s_mrs/doc.asp?CID=11403&DID=202761.

¹⁵⁸ A. Cetrionio, J.P. Jones, “Reconstruction at a metallic interface studied by field ion and field emission microscopy,” *Surf. Sci.* 40(November 1973):227-248. E.D. Williams, N.C. Bartelt, “Thermodynamics of Surface Morphology,” *Science* 251(25 January 1991):393-400.

¹⁵⁹ C. Herring, “Some Theorems on the Free Energies of Crystal Surfaces,” *Phys. Rev.* 82(1951):87-93.

Faceting is a physical-chemistry surface phenomenon that can be exploited to create atomically-sharp tips (e.g., see [Section 5.3](#)).

Figure 3-9. Left: STM image of a completely faceted W(111) surface induced by an ultrathin Pd film (~ 1.2 ML) upon annealing to 1075 K for 3 min, forming three-sided pyramids with $\{211\}$ facets; the dimensions are $1000 \times 1000 \text{ \AA}^2$ and the vertical scale is 16.6 \AA . **Right:** STM image of a faceted Pd/W(111) surface with a coverage of ~ 1.5 ML; the dimensions are $110 \times 110 \text{ \AA}^2$ and the vertical scale is 14.0 \AA ; the atomic row-and-trough structure demonstrates the $\text{bcc}\{211\}$ facets.¹⁶⁰



Among the best-known is the faceting of Pd/W(111) to form nanoscale three-sided pyramids with $\{011\}$ facets, which has been observed by STM, and $\{112\}$ faceting that can transform the entire Pd/W(111) surface to a morphology composed entirely of three-sided pyramidal $\{112\}$ facets.¹⁶¹ (The driving force for the transition is a surface energy difference between film-covered W(111) and W(211) surfaces.)¹⁶² The $\{011\}$ faceting of Pd/W(111) occurs in coexistence with $\{112\}$ faceting upon prolonged annealing (**Figure 3-10**) – $\{112\}$ facets grow in size from 3-15 nm (length of base edge) with increasing annealing temperatures, while the dimensions of $\{011\}$

¹⁶⁰ T.E. Madey, C.H. Nien, K. Pelhos, J.J. Kolodziej, I.M. Abdelrehim, H.S. Tao, "Faceting induced by ultrathin metal films: structure, electronic properties and reactivity," Surface Science 438(1999):191-206; http://www.isr.umd.edu/gwrubloff/teaching/enma490fall03/resources/current/final_report/120203_Anne/ref_11.pdf.

¹⁶¹ C.-H. Nien, T.E. Madey, Y.W. Tai, T.C. Leung, J.G. Che, C.T. Chan, "Coexistence of $\{011\}$ facets with $\{112\}$ facets on W(111) induced by ultrathin films of Pd," Phys. Rev. B 59(1999):10335-10340.

¹⁶² J.G. Che, C.T. Chan, C.H. Kuo, T.C. Leung, "Faceting Induced by Ultrathin Metal Films: A First Principles Study," Phys. Rev. Lett. 79(24 November 1997):4230-4233; <http://www.physics.fudan.edu.cn/tps/people/jgche/paper/prl79-4230.pdf>.

facets appear to be limited to ~ 2.5 nm.¹⁶³ Some late-transition-metals like Au, Ir, Pd, Pt and Rh cause faceting when monolayered on clean but atomically rough Mo(111) or W(111) bcc(111) surfaces,¹⁶⁴ making pyramids up to 100 nm in size,¹⁶⁵ while other metals like Cu and Ag on Mo(111) do not.¹⁶⁶

Madey's experimental team studied ultrathin films of transition and noble metals on Mo(111) and W(111)¹⁶⁷ and found that pyramidal faceting occurs upon dosing with Pt, Au, Ir, Rh, O,¹⁶⁸ Cl,¹⁶⁹ or S.¹⁷⁰ In contrast, monolayer films of Ti, Cr, Fe, Ni, Cu, Ag and Gd do not induce massive reconstruction or faceting on W(111) and Mo(111) surfaces.¹⁷¹ The authors speculated: "The

¹⁶³ C.-H. Nien, T.E. Madey, Y.W. Tai, T.C. Leung, J.G. Che, C.T. Chan, "Coexistence of {011} facets with {112} facets on W(111) induced by ultrathin films of Pd," Phys. Rev. B 59(1999):10335-10340.

¹⁶⁴ T.E. Madey, J. Guan, C.H. Nien, C.Z. Dong, H.S. Tao, R.A. Campbell, "Faceting Induced by Ultrathin Metal Films on W(111) and Mo(111):. Structure, Reactivity, and Electronic Properties," Surf. Rev. and Lett. 3(1996):1315-1328. T.E. Madey, C.H. Nien, K. Pelhos, J.J. Kolodziej, I.M. Abdelrehim, H.S. Tao, "Faceting induced by ultrathin metal films: structure, electronic properties and reactivity," Surface Science 438(1999):191-206;
http://www.isr.umd.edu/gwrubloff/teaching/enma490fall03/resources/current/final_report/120203_Anne/ref_11.pdf. J.J. Kolodziej, T.E. Madey, J.W. Keister, J.E. Rowe, "Photoelectron spectroscopy studies of growth, thermal stability, and alloying for transition metal-tungsten (111) bimetallic systems," Phys. Rev. B 65(2002):075413;
http://www.physics.rutgers.edu/~madey/Publications/Full_Publications/PDF/madey_PRB_2002_JJK.pdf.

¹⁶⁵ Kalman Pelhos, Ihab M. Abdelrehim, Cheng-Hsun Nien, Theodore E. Madey, "Structural Changes of the W(211) Surface Induced by Ultrathin Films of Rh, Pt, and Pd," J. Phys. Chem. B 105(2001):3708-3717;
http://www.physics.rutgers.edu/~madey/Publications/Full_Publications/PDF/madey_JPCb_2001_P.pdf.

¹⁶⁶ J.G. Che, C.T. Chan, C.H. Kuo, T.C. Leung, "Faceting Induced by Ultrathin Metal Films: A First Principles Study," Phys. Rev. Lett. 79(24 November 1997):4230-4233;
<http://www.physics.fudan.edu.cn/tps/people/jgche/paper/prl79-4230.pdf>. C.T. Chan, J.G. Che, T.C. Leung, "First principles studies of overlayer-induced faceting," Prog. Surf. Sci. 59(1998):1-11;
<http://www.physics.fudan.edu.cn/tps/people/jgche/paper/pss59-1.pdf>.

¹⁶⁷ T.E. Madey, J. Guan, C.H. Nien, C.Z. Dong, H.S. Tao, R.A. Campbell, "Faceting Induced by Ultrathin Metal Films on W(111) and Mo(111):. Structure, Reactivity, and Electronic Properties," Surf. Rev. and Lett. 3(1996):1315-1328.

¹⁶⁸ J.C. Tracy, J.M. Blakely, "A study of faceting of tungsten single crystal surfaces," Surf. Sci. 13(1968):313-336.

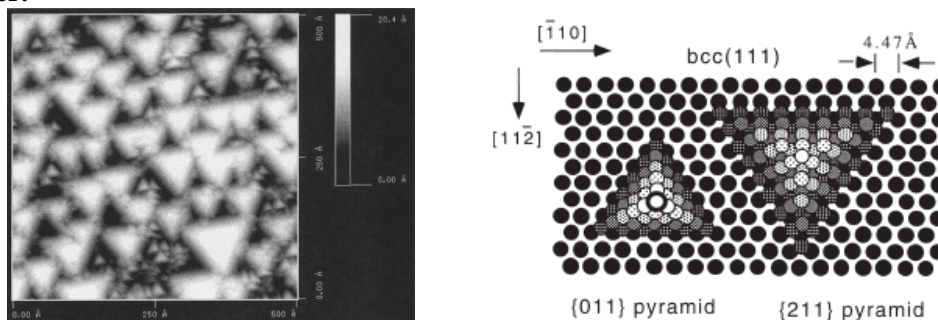
¹⁶⁹ F. Bonszek, T. Engel, and E. Bauer, "Cl adsorption layers on W(110) and (111) surfaces," Surf. Sci. 97(1980):595-608.

¹⁷⁰ P.J.F. Harris, "Sulphur-induced faceting of platinum catalyst particles," Nature 323(30 October 1986):792-794.

¹⁷¹ T.E. Madey, J. Guan, C.H. Nien, C.Z. Dong, H.S. Tao, R.A. Campbell, "Faceting Induced by Ultrathin Metal Films on W(111) and Mo(111):. Structure, Reactivity, and Electronic Properties," Surf. Rev. and Lett. 3(1996):1315-1328. M.J. Gladys, G. Jackson, J.E. Rowe, T.E. Madey, "High resolution

faceting appears to be thermodynamically driven but kinetically limited: faceting is caused by an increased anisotropy in surface free energy that occurs for the film-covered surfaces. An interesting correlation has been observed for both substrates: faceting occurs for overlayer elements having Pauling electronegativities greater than 2.0, suggesting that surface electronic effects are controlling the structural instability of both Mo(111) and W(111).” Low index clean metal surfaces seldom facet since the surface energy anisotropy is usually small, but stable metal surfaces can facet upon adsorption of O and Cl,¹⁷² and even carbon (from CO) is known to induce W¹⁷³ and Pt(210)¹⁷⁴ faceting (though producing an entirely different topography).¹⁷⁵

Figure 3-10. Pd facets on W. Left: Top view of an STM image (500 Å x 500 Å) showing the coexistence of {011} facets with {211} facets on a Pd-W(111) surface; the as-deposited coverage of Pd is 1.0 ML; two types of three-sided pyramid form upon annealing for 6 min; atomic-resolution images (not shown here) identify the large facets as {211}, and the atomic structures on tiny facets are quantitatively consistent with {011}. Right: Top view of a hard-sphere model showing the atomic structures of a pyramid with {011} facets and a pyramid with {211} facets on a bcc(111) surface; the indicated value of the atomic spacing corresponds to a bulk truncation structure of W(111), containing a pseudomorphic Pd overlayer.¹⁷⁶



photoemission study of growth, alloying, and intermixing of ultrathin ruthenium films on W(111) and W(211),” *Surf. Sci.* 544(2003):193-208; <http://202.127.1.11/surface%20science/544/544206.pdf>.

¹⁷² F. Bonszek, T. Engel, and E. Bauer, “Cl adsorption layers on W(110) and (111) surfaces,” *Surf. Sci.* 97(1980):595-608.

¹⁷³ M. Drechsler, “On the equilibrium shape of metal crystals,” in: Vu Thien Binh, ed., *Surface Mobilities on Solid Materials*, Plenum Press, New York, 1983, p. 405.

¹⁷⁴ M. Sander, R. Imbihl, R. Schuster, J.V. Barth, G. Ertl, “Microfacetted of Pt(210) induced by oxygen adsorption and by catalytic CO oxidation,” *Surf. Sci.* 271(1992):159-169.

¹⁷⁵ M. Drechsler, “On the equilibrium shape of metal crystals,” in: Vu Thien Binh, ed., *Surface Mobilities on Solid Materials*, Plenum Press, New York, 1983, p. 405.

¹⁷⁶ T.E. Madey, C.H. Nien, K. Pelhos, J.J. Kolodziej, I.M. Abdelrehim, H.S. Tao, “Faceting induced by ultrathin metal films: structure, electronic properties and reactivity,” *Surface Science* 438(1999):191-206; http://www.isr.umd.edu/gwrubloff/teaching/enma490fall03/resources/current/final_report/120203_Anne/ref_11.pdf.

Szczepkowicz et al.¹⁷⁷ explain further: “Planar surfaces of many metals undergo facet formation when they are covered with oxygen or other adsorbates, and are annealed to elevated temperature. These include bcc W(111) and Mo(111), fcc Ir(210), Pt(210), Ni(210), and various Cu surfaces. All of these are atomically rough, non-close-packed surfaces with relatively high surface free energies. The presence of adsorbate increases the anisotropy in surface free energy, as well as lowering the average surface free energy. The increased anisotropy means that the faceted surface with its higher exposed surface area has a lower energy than the initially planar surface. Thus, faceting is driven by thermodynamics – the minimization of total surface free energy – but is controlled by the kinetics of diffusion, nucleation and growth.”

A simple solid-on-solid model of faceting on curved surfaces¹⁷⁸ predicts a reversible phase transition at which a faceted surface transforms to an almost spherical one, and that the temperature of this phase transition is an increasing function of the surface curvature. Experiments by Madey’s group¹⁷⁹ confirmed the validity of this model, which also predicts that the shape of the facets is different for flat and curved surfaces. According to this work,¹⁸⁰ adsorbate-induced pyramid-like {211} facets are formed on an initially flat W(111) surface, whereas steplike {211} facets are formed on an initially curved W surface (tip apex with curvature radius ~200 nm)¹⁸¹ (Figure 3-11).

¹⁷⁷ Andrzej Szczepkowicz, Antoni Ciszewski, Robert Bryl, Czesław Oleksy, Cheng-Hsun Nien, Qifei Wu, Theodore E. Madey, “A comparison of adsorbate-induced faceting on flat and curved crystal surfaces,” Surf. Sci. 599(2005):55-68; <http://www.zmp.ifd.uni.wroc.pl/asz/joint-paper-published.pdf>.

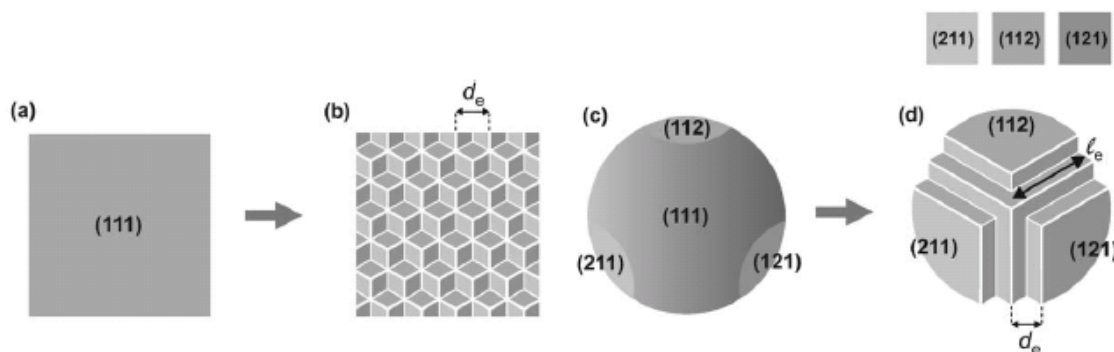
¹⁷⁸ D. Niewieczerzał, C. Oleksy, “Simulation of adsorbate-induced faceting on curved surfaces,” Surf. Sci. 600(1 January 2006):56-65. See also: C. Oleksy, “Solid-on-solid model of overlayer-induced faceting,” Surf. Sci. 549(1 February 2004):246-254.

¹⁷⁹ Andrzej Szczepkowicz, Antoni Ciszewski, Robert Bryl, Czesław Oleksy, Cheng-Hsun Nien, Qifei Wu, Theodore E. Madey, “A comparison of adsorbate-induced faceting on flat and curved crystal surfaces,” Surf. Sci. 599(2005):55-68; <http://www.zmp.ifd.uni.wroc.pl/asz/joint-paper-published.pdf>.

¹⁸⁰ Andrzej Szczepkowicz, Antoni Ciszewski, Robert Bryl, Czesław Oleksy, Cheng-Hsun Nien, Qifei Wu, Theodore E. Madey, “A comparison of adsorbate-induced faceting on flat and curved crystal surfaces,” Surf. Sci. 599(2005):55-68; <http://www.zmp.ifd.uni.wroc.pl/asz/joint-paper-published.pdf>.

¹⁸¹ Andrzej Szczepkowicz, Antoni Ciszewski, “Faceting of curved tungsten surface induced by palladium,” Surf. Sci. 515(2002):441-452; http://www.zmp.ifd.uni.wroc.pl/asz/Pd_W_faceting_preprint.pdf.

Figure 3-11. The formation of {211} facets on a flat crystal: (a), (b), and on a spherical crystal: (c), (d).¹⁸²

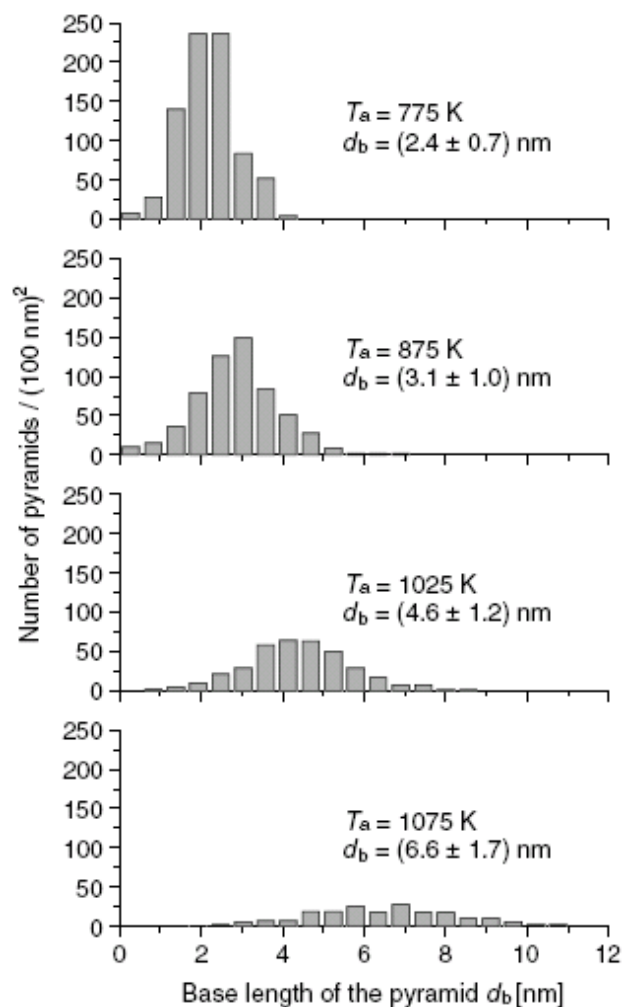


The size distribution of the Pd/W facet pyramids can be characterized by two parameters: (1) the expected size of the pyramids, (2) the spread of pyramid sizes. These are heavily influenced by the annealing temperature (Figure 3-12). For both flat and curved surfaces, the number of facets was smaller for experiments with higher annealing temperatures. For Pd deposited on a surface with curvature radius ~ 200 nm, facet measurements (see Figure 3-11d) yielded $d_e = 9.3$ nm, $l_e = 19$ nm after annealing at 1000 K, $d_e = 9.6$ nm, $l_e = 32$ nm after annealing at 1100 K, and $d_e = 10.2$ nm, $l_e = 26$ nm after annealing at 1200 K.¹⁸³ Note that these pyramids are not very tall – for Pd/W, the $d_b(\text{flat})/\text{rms}(z)$ ratio is 17-31 (typ. ~ 24); in other words, the pyramid is about 24 times wider at the base than it is tall, a very poor aspect ratio (Figure 3-13).

¹⁸² Andrzej Szczepkiewicz, Antoni Ciszewski, Robert Bryl, Czesław Oleksy, Cheng-Hsun Nien, Qifei Wu, Theodore E. Madey, "A comparison of adsorbate-induced faceting on flat and curved crystal surfaces," Surf. Sci. 599(2005):55-68; <http://www.zmp.ifd.uni.wroc.pl/asz/joint-paper-published.pdf>.

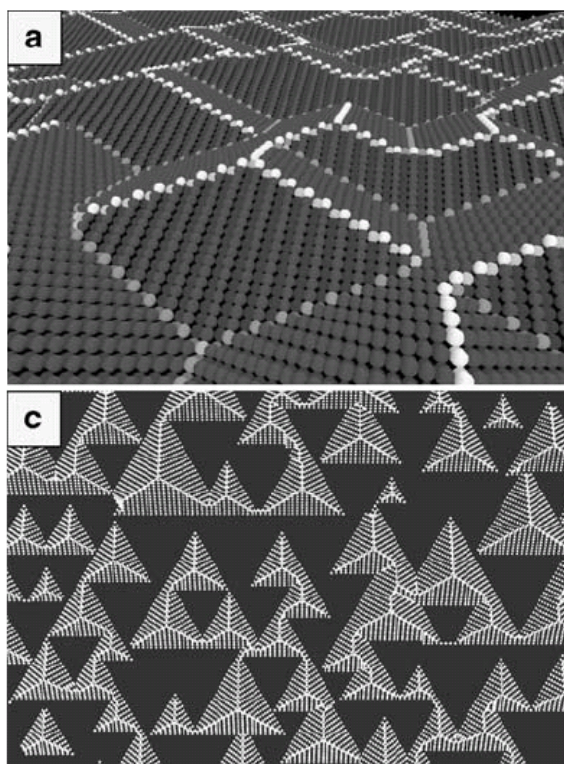
¹⁸³ Andrzej Szczepkiewicz, Antoni Ciszewski, Robert Bryl, Czesław Oleksy, Cheng-Hsun Nien, Qifei Wu, Theodore E. Madey, "A comparison of adsorbate-induced faceting on flat and curved crystal surfaces," Surf. Sci. 599(2005):55-68; <http://www.zmp.ifd.uni.wroc.pl/asz/joint-paper-published.pdf>.

Figure 3-12. Temperature dependence of the pyramid size distribution on flat Pd/W(111) surface.¹⁸⁴



¹⁸⁴ Andrzej Szczepkiewicz, Antoni Ciszewski, Robert Bryl, Czesław Oleksy, Cheng-Hsun Nien, Qifei Wu, Theodore E. Madey, "A comparison of adsorbate-induced faceting on flat and curved crystal surfaces," Surf. Sci. 599(2005):55-68; <http://www.zmp.ifd.uni.wroc.pl/asz/joint-paper-published.pdf>.

Figure 3-13. Initially flat bcc (111) surface undergoes {211} faceting:¹⁸⁵ (a) Angle view shows atomic details; all surface atoms are shown. (c) Restricted top view; only the atoms above the average surface height are shown.

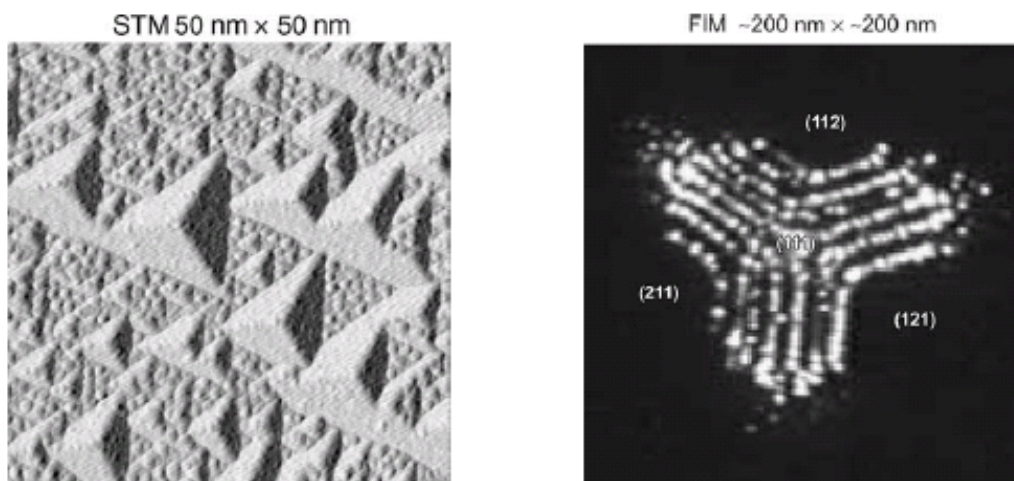


In studying palladium-induced faceting of tungsten, it is very important to make sure that there is no residual oxygen on the surface of the sample, otherwise oxygen-induced faceting will dominate over the palladium-induced surface effects.¹⁸⁶ In fact, oxygen has been long known to induce faceting of both curved and planar tungsten surfaces (Figure 3-14).

¹⁸⁵ Andrzej Szczepkiewicz, Antoni Ciszewski, Robert Bryl, Czesław Oleksy, Cheng-Hsun Nien, Qifei Wu, Theodore E. Madey, "A comparison of adsorbate-induced faceting on flat and curved crystal surfaces," Surf. Sci. 599(2005):55-68; <http://www.zmp.ifd.uni.wroc.pl/asz/joint-paper-published.pdf>.

¹⁸⁶ Andrzej Szczepkiewicz, Antoni Ciszewski, Robert Bryl, Czesław Oleksy, Cheng-Hsun Nien, Qifei Wu, Theodore E. Madey, "A comparison of adsorbate-induced faceting on flat and curved crystal surfaces," Surf. Sci. 599(2005):55-68; <http://www.zmp.ifd.uni.wroc.pl/asz/joint-paper-published.pdf>.

Figure 3-14. Left: Flat W(111) surface after oxygen exposure (0.5 L) and annealing (1075 K, 180 s); scanning tunneling microscopy at room temperature; x-slope-filtered view. Right: Curved tungsten surface after oxygen exposure (0.7 ± 0.3 L) and annealing (1120 K, 80 s); field ion microscopy at liquid nitrogen temperature (He + Ne, 32 kV); edges of the facets are imaged as bright lines; the image covers the crystallographic orientations around the W(111) direction within the angular radius of $20\text{--}30^\circ$.¹⁸⁷



Although the faceted topography changes with the crystallographic orientation on a curved surface, at the (111) crystal pole the topography should be pyramid-like as on a flat (111) crystal.¹⁸⁸ Since on both flat and curved surfaces the facet size, width of the facet size distribution, and surface rms roughness increase with annealing temperature,¹⁸⁹ it seems possible that a highly curved tungsten tip (e.g., 5-10 nm radius of curvature) oriented axially along the (111) pole might suffice to grow a single pyramid that could provide a single-atom AFM tip. This possibility should be investigated further.

¹⁸⁷ Andrzej Szczepkiewicz, Antoni Ciszewski, Robert Bryl, Czesław Oleksy, Cheng-Hsun Nien, Qifei Wu, Theodore E. Madey, "A comparison of adsorbate-induced faceting on flat and curved crystal surfaces," Surf. Sci. 599(2005):55-68; <http://www.zmp.ifd.uni.wroc.pl/asz/joint-paper-published.pdf>.

¹⁸⁸ Andrzej Szczepkiewicz, Antoni Ciszewski, Robert Bryl, Czesław Oleksy, Cheng-Hsun Nien, Qifei Wu, Theodore E. Madey, "A comparison of adsorbate-induced faceting on flat and curved crystal surfaces," Surf. Sci. 599(2005):55-68; <http://www.zmp.ifd.uni.wroc.pl/asz/joint-paper-published.pdf>.

¹⁸⁹ Andrzej Szczepkiewicz, Antoni Ciszewski, Robert Bryl, Czesław Oleksy, Cheng-Hsun Nien, Qifei Wu, Theodore E. Madey, "A comparison of adsorbate-induced faceting on flat and curved crystal surfaces," Surf. Sci. 599(2005):55-68; <http://www.zmp.ifd.uni.wroc.pl/asz/joint-paper-published.pdf>.

As noted, oxygenated metals can also be induced to form pyramidal “faceted” structures. One example is iridium, which forms a clean-faceted surface¹⁹⁰ that could, in principle, be used to fabricate an ultrasharp metal tip. Here’s how: Oxygen chemisorbs dissociatively on Ir(210) at room temperature, forming three-sided pyramid-shaped facets with (311) and (110) orientations on the oxygen-covered Ir(210) surface when annealed to $T \geq 600$ K (Figure 3-15).¹⁹¹ The average size of the pyramids is ~30 nm.¹⁹² The surface remains faceted for substrate temperatures $T < 850$ K. For $T > 850$ K, the substrate structure reverts to the oxygen-covered (210) planar state and does so reversibly, provided that oxygen is not lost due to desorption or via chemical reactions (whereupon the planar (210) structure returns if the temperature rises above 600 K). A clean oxygen-free faceted metal surface can then be prepared through by employing low temperature surface cleaning methods: using either CO oxidation or the reaction of H_2 to form H_2O , oxygen can be removed from the oxidized Ir metal surface while preserving (“freezing”) the clean faceted Ir metal pyramidal structure, which remains stable for $T < 600$ K.¹⁹³ DFT simulations of Ir facet stability have been reported.¹⁹⁴ On faceted Ir(210) surfaces, recent studies have also revealed structure sensitivity in chemical reactions such as in the decomposition of acetylene¹⁹⁵ and ammonia,¹⁹⁶ and in the oxidation of CO.¹⁹⁷

¹⁹⁰ Ivan Ermanoski, Kalman Pelhos, Wenhua Chen, Jamie S. Quinton, Theodore E. Madey, “Oxygen-induced nano-faceting of Ir(210),” *Surf. Sci.* 549(10 January 2004):1-23. Payam Kaghazchi, Felice C. Simeone, Khaled A. Soliman, Ludwig A. Kibler, Timo Jacob, “Bridging the gap between nanoparticles and single crystal surfaces,” *Faraday Discuss.* 140(2008):69-80;
<http://www.rsc.org/delivery/ArticleLinking/DisplayHTMLArticleForFree.cfm?JournalCode=FD&Year=2009&ManuscriptID=b802919a&Iss=0> and
<http://www.rsc.org/delivery/ArticleLinking/DisplayArticleForFree.cfm?doi=b802919a&JournalCode=FD>.

¹⁹¹ Ivan Ermanoski, “Nanoscale properties of planar and faceted iridium(210),” PhD dissertation, Rutgers - The State University Of New Jersey - New Brunswick, 2005;
<http://gradworks.umi.com/31/95/3195677.html>.

¹⁹² Khaled A. Soliman, Felice C. Simeone, Ludwig A. Kibler, “Electrochemical behaviour of nano-faceted Ir(210),” *Electrochemistry Communications* 11(January 2009):31-33.

¹⁹³ Ivan Ermanoski, Kalman Pelhos, Wenhua Chen, Jamie S. Quinton, Theodore E. Madey, “Oxygen-induced nano-faceting of Ir(210),” *Surf. Sci.* 549(10 January 2004):1-23.

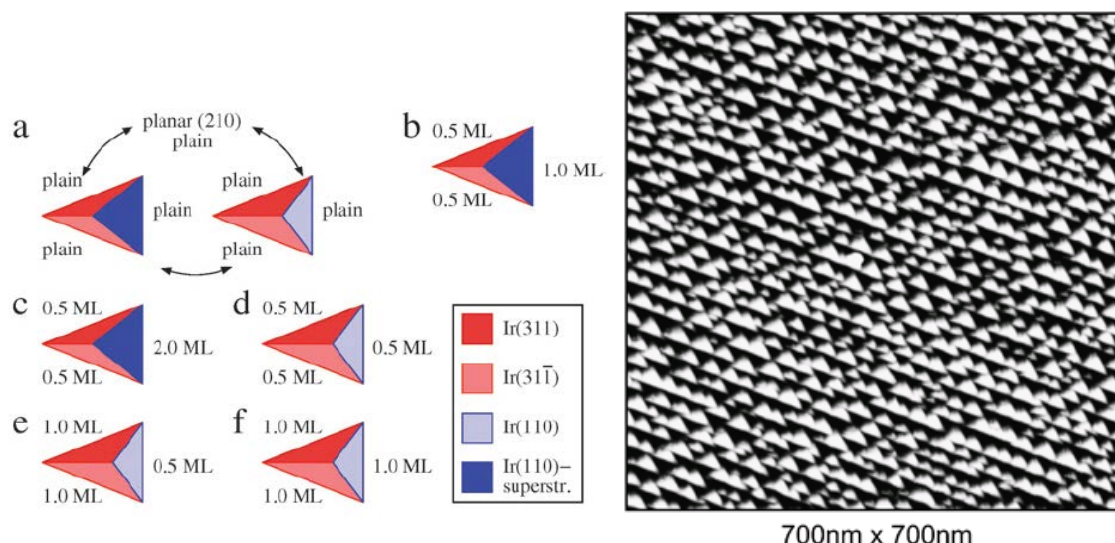
¹⁹⁴ P. Kaghazchi, T. Jacob, I. Ermanoski, W. Chen, T.E. Madey, “First-principles studies on oxygen-induced faceting of Ir(210),” *ACS Nano.* 2(June 2008):1280-1288.

¹⁹⁵ Wenhua Chen, Ivan Ermanoski, Qifei Wu, T.E. Madey, Henry H. Hwu, Jingguang G. Chen, “Adsorption and Decomposition of Acetylene on Planar and Faceted Ir(210),” *J. Phys. Chem. B* 107(2003):5231-5242;
http://www.physics.rutgers.edu/~madey/Publications/Full_Publications/PDF/madey_JPCb_2003_C.pdf.

¹⁹⁶ Wenhua Chen, Ivan Ermanoski, Theodore E. Madey, “Decomposition of Ammonia and Hydrogen on Ir Surfaces: Structure Sensitivity and Nanometer-Scale Size Effects,” *J. Am. Chem. Soc.* 127(2005):5014-5015;
http://www.physics.rutgers.edu/~madey/Publications/Full_Publications/PDF/madey_JACS_2005.pdf.

¹⁹⁷ Wenhua Chen, Ivan Ermanoski, Timo Jacob, Theodore E. Madey, “Structure Sensitivity in the Oxidation of CO on Ir Surfaces,” *Langmuir* 22(2006):3166-3173;

Figure 3-15. Left: Models of the different surface structures that are present on Ir(210) at specific electrode potentials; for all surfaces, 1 ML is defined as one oxygen atom per surface unit cell. **Right:** STM-image for nano-faceted Ir(210).¹⁹⁸



Studies on adsorbate-induced faceting of atomically rough surfaces have mostly focused on bcc metals such as W(111)¹⁹⁹ and Mo(111),²⁰⁰ or fcc metals such as Cu(210),²⁰¹ Ir(210),²⁰²

http://www.physics.rutgers.edu/~madey/Publications/Full_Publications/PDF/madey_Langmuir_2006_C.pdf.

¹⁹⁸ Payam Kaghzazchi, Felice C. Simeone, Khaled A. Soliman, Ludwig A. Kibler, Timo Jacob, "Bridging the gap between nanoparticles and single crystal surfaces," Faraday Discuss. 140(2008):69-80; <http://www.rsc.org/delivery/ArticleLinking/DisplayHTMLArticleForFree.cfm?JournalCode=FD&Year=2009&ManuscriptID=b802919a&Iss=0> and <http://www.rsc.org/delivery/ArticleLinking/DisplayArticleForFree.cfm?doi=b802919a&JournalCode=FD>.

¹⁹⁹ K. Pelhos, J.B. Hannon, G.L. Kellogg, T.E. Madey, "LEEM investigation of the faceting of the Pt covered W(111) surface," Surf. Sci. 432(1999):115-124.

²⁰⁰ 157. C. Zhang, M.A. van Hove, G.A. Somorjai, "The interaction of oxygen with the Mo(100) and Mo(111) single-crystal surfaces: Chemisorption and oxidation at high temperatures," Surf. Sci. 149(2 January 1985):326-340. K.J. Song, J.C. Lin, M.Y. Lai, Y.L. Wang, "Faceting Phase Transitions of Mo(111) Induced by Pd, Au, and Oxygen Overlayers," Surf. Sci. 327(1995):17-32. D.B. Danko, M. Kuchowicz, J. Kolaczewicz, "Adsorbate-induced surface rearrangement of the system Pd/Mo(111)," Surf. Sci. 552(2004):111-122.

²⁰¹ R.E. Kirby, C.S. McKee, L.V. Renny, "Faceting of Cu(210) and Ni(210) by activated nitrogen," Surf. Sci. 97(1980):457-477. A.T.S. Wee, J.S. Foord, R.G. Egdell, J.B. Pethica, "Superstructure formation and faceting in the Cu(210)-O system studied by scanning tunneling microscopy," Phys. Rev. B 58(1998):R7548-R7551.

Ni(210),²⁰³ and Pt(210).²⁰⁴ At least one *hcp* metal surface, Re(123⁻1), has also been examined for faceting.²⁰⁵ Oxygenated atomically-rough rhenium Re(123⁻1) makes wedge-terminated ridges that are almost pyramidal in shape (Figure 3-16) and are stable indefinitely at room temperature.²⁰⁶ Off-center four-sided pyramids are also induced by oxygen on atomically-rough Re(112⁻1) surface²⁰⁷ (Figure 3-17). Monolayer coatings of Re on W(112) remain atomically sharp even after annealing to 1000 K.²⁰⁸

²⁰² Ivan Ermanoski, Kalman Pelhos, Wenhua Chen, Jamie S. Quinton, Theodore E. Madey, "Oxygen-induced nano-faceting of Ir(210)," *Surf. Sci.* 549(10 January 2004):1-23.

²⁰³ R.E. Kirby, C.S. McKee, L.V. Renny, "Faceting of Cu(210) and Ni(210) by activated nitrogen," *Surf. Sci.* 97(1980):457-477. R.E. Kirby, C.S. McKee, M.W. Roberts, "Low temperature oxygen and activated nitrogen faceting of Ni(210) surfaces," *Surf. Sci.* 55(May 1976):725-728.

²⁰⁴ M. Sander, R. Imbihl, R. Schuster, J.V. Barth, G. Ertl, "Microfacetting of Pt(210) induced by oxygen adsorption and by catalytic CO oxidation," *Surf. Sci.* 271(1992):159-169.

²⁰⁵ Hao Wang, Wenhua Chen, Theodore E. Madey, "Morphological evolution in oxygen-induced faceting of Re(123⁻1)," *Phys. Rev. B* 74(2006):205426;
http://www.physics.rutgers.edu/~madey/Publications/Full_Publications/PDF/madey_PRB_2006_W.pdf.
 Hao Wang, "Adsorbate-induced nanoscale faceting of rhenium surfaces," PhD dissertation, Rutgers - The State University Of New Jersey - New Brunswick, 2008, 153 pages;
<http://gradworks.umi.com/33/44/3344853.html>.

²⁰⁶ Hao Wang, Wenhua Chen, Theodore E. Madey, "Morphological evolution in oxygen-induced faceting of Re(123⁻1)," *Phys. Rev. B* 74(2006):205426;
http://www.physics.rutgers.edu/~madey/Publications/Full_Publications/PDF/madey_PRB_2006_W.pdf.
 Hao Wang, Ally S.Y. Chan, Wenhua Chen, Payam Kaghazchi, Timo Jacob, Theodore E. Madey, "Facet Stability in Oxygen-Induced Nanofaceting of Re(123⁻1)," *ACS Nano* 1(2007):449-455; http://www.fhi-berlin.mpg.de/th/publications/ACS_NANO-1-449-2007.pdf.

²⁰⁷ Hao Wang, "Adsorbate-induced nanoscale faceting of rhenium surfaces," PhD dissertation, Rutgers - The State University Of New Jersey - New Brunswick, 2008, 153 pages;
<http://gradworks.umi.com/33/44/3344853.html>. Payam Kaghazchi, Timo Jacob, Hao Wang, Wenhua Chen, Theodore E. Madey, "First-principles studies on adsorbate-induced faceting of Re(112⁻1)," *Phys. Rev. B* 79(April 2009):132107; <http://www.fhi-berlin.mpg.de/th/publications/PRB-79-132107-2009.pdf>.
 See also: Timo Jacob, "Electrochemical surface faceting of Re(112⁻1)," *Electrochimica Acta* 54(1 September 2009):5023-5029.

²⁰⁸ Chonglin Chen, Tien T. Tsong, "Atomic structure of a rhenium monolayer on the W(112) surface," *Philosophical Magazine Letters* 72(November 1995):285-290.

Figure 3-16. STM images of faceted O/Re(123̄1) surfaces prepared by dosing 3 L O₂ (0.9 ML) at 300 K followed by annealing at 800 K for 2 min. (a) 500 Å x 500 Å, raw data; (b) after the X slope taken. (c) and (d) show measured and ideal azimuthal angles of edge lines formed by facets, respectively.²⁰⁹

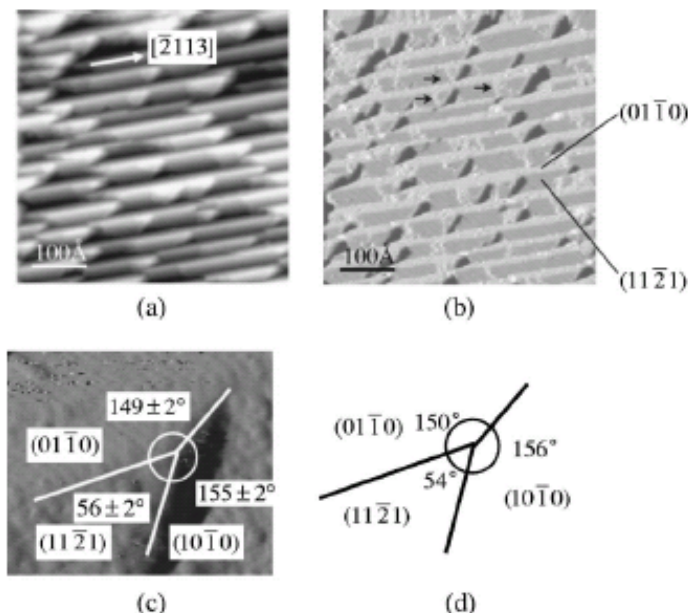
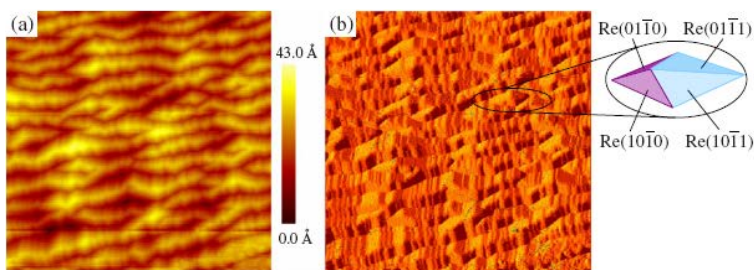


Figure 3-17. (a) STM and (b) x-slope images of the faceted Re(112̄1) surface prepared by oxygen adsorption (exposure of 300 L) at 1000 K; both figures show a surface area of 1000 x 1000 Å².²¹⁰



²⁰⁹ Hao Wang, Wenhua Chen, Theodore E. Madey, "Morphological evolution in oxygen-induced faceting of Re(123̄1)," Phys. Rev. B 74(2006):205426; http://www.physics.rutgers.edu/~madey/Publications/Full_Publications/PDF/madey_PRB_2006_W.pdf.

²¹⁰ Payam Kaghazchi, Timo Jacob, Hao Wang, Wenhua Chen, Theodore E. Madey, "First-principles studies on adsorbate-induced faceting of Re(112̄1)," Phys. Rev. B 79(April 2009):132107; <http://www.fhi-berlin.mpg.de/th/publications/PRB-79-132107-2009.pdf>. See also: Timo Jacob, "Electrochemical surface faceting of Re(112̄1)," Electrochimica Acta 54(1 September 2009):5023-5029.

Pyramidal faceting has also been observed by Ru on W(111) after annealing to >800 K (optimally at 970 K), although atom exchange and intermixing at the Ru/W interface is seen for a fractional monolayer of Ru on W(211) or W(111) – in sharp contrast to other metal monolayers studied on W, which “float” on the outer surface upon annealing.²¹¹ It is possible that a >1.0 ML coating of Ru on W(111) would induce a purer layer of pyramidal Ru atop the mixed Ru/W interface layer – potentially of great utility for a DMS tooltip – but this supposition remains to be confirmed by experiment. Even a mixed-phase pyramid could be useful for DMS if the geometry is repeatable and atomically precise.

Faceting has also been observed for O on Cu(100),²¹² O on Cu(110),²¹³ O on Cu(115),²¹⁴ NaCl on Cu(532),²¹⁵ Sb on Ge(103),²¹⁶ oxygen-induced shape transformation of Rh on MgO substrate,²¹⁷ O on Nb(111),²¹⁸ Te on Pd(100),²¹⁹ Pd on Ta(111),²²⁰ and O on AlPdMn quasicrystal.²²¹ The

²¹¹ M.J. Gladys, G. Jackson, J.E. Rowe, T.E. Madey, “High resolution photoemission study of growth, alloying, and intermixing of ultrathin ruthenium films on W(111) and W(211),” *Surf. Sci.* 544(2003):193-208; <http://202.127.1.11/surface%20science/544/544206.pdf>.

²¹² Guangwen Zhou, Judith C. Yang, Jeffery A. Eastman, John E. Pearson, “Control of the Nanoscale Morphology of Oxide Islands by Interfacial Elastic Strain via Temperature or Alloying,” presentation KK4.1, Symposium KK: Nanoscale Pattern Formation, MRS 2007 Fall Meeting, 26-29 November 2007, Materials Research Society Symposium Proceedings Series, Volume 1059E (Proceedings Library, www.mrs.org/publications_library); http://www.mrs.org/s_mrs/doc.asp?CID=11403&DID=202761.

²¹³ J.C Boulliard, M.P Sotto, “Structural study of the oxygen adsorption on the (hk0) stepped faces of the (110) copper face,” *Surf. Sci.* 177(2 November 1986):139-156.

²¹⁴ D.A. Walko, I.K. Robinson, “Energetics of oxygen-induced faceting on Cu(115),” *Phys. Rev. B* 64(2001):045412; http://groups.mrl.uiuc.edu/robinson/~ikrpub02/.%5CDOn_prb2.pdf.

²¹⁵ S. Folsch, A. Riemann, J. Repp, G. Meyer, K.H. Rieder, “From atomic kinks to mesoscopic surface patterns: Ionic layers on vicinal metal surfaces,” *Phys. Rev. B* 66(2002):161409; http://www.physics.wvu.edu/riemana/paper/2002_PRB_Cu532.pdf.

²¹⁶ G. Falkenberg, R.L. Johnson, “Adsorbate-induced faceting of high-index semiconductor surfaces: antimony adsorbed on Ge(103),” *Appl. Surf. Sci.* 142(April 1999):81-87.

²¹⁷ P. Nolte, A. Stierle, N.Y. Jin-Phillipp, N. Kasper, T.U. Schulli, H. Dosch, “Shape Changes of Supported Rh Nanoparticles During Oxidation and Reduction Cycles,” *Science* 321(19 September 2008):1654-1658.

²¹⁸ Chung-Hsiang Huang, “Reversible segregation of oxygen onto Nb(111) and associated faceting,” PhD thesis, 18 July 2006; <http://www.cetd.com.tw/ec/thesisDetail.aspx?etdun=U0001-1307200620121600>.

²¹⁹ D. Kolthoff, T. Dullweber, H. Pfnür, “Adsorbate-induced faceting of a nearly close-packed surface: Te-Pd(100),” *Surf. Sci.* 447(2000):259-271.

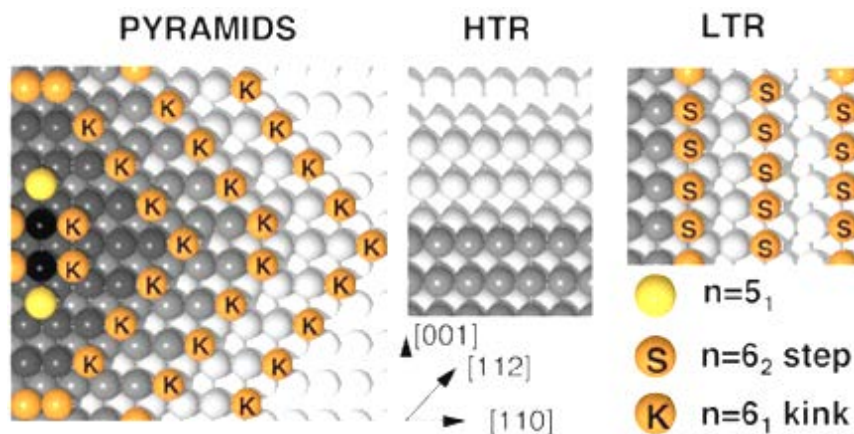
²²⁰ R. Szukiewicz, J. Kolaczkiwicz, “Thermal stability of the Ta (111) surface covered with Pd,” *Vacuum* 74(3 May 2004):55-68.

²²¹ S. Burkardt, M. Erbudak, “Oxygen-induced surface faceting of the threefold-symmetry surface of icosahedral AlPdMn quasicrystal,” *Surf. Sci.* 603(15 July 2009):2248-2253.

ECR plasma-etched (211)B surface consists of asymmetric pyramids formed by (110), (101), (100), and (111) surfaces with the apex of the asymmetric pyramid 1.3 Å in height.²²²

Pyramidal faceting has also been observed on pure single-metal surfaces. For example, Molle et al.²²³ report a novel interfacial state characterized by rhomboidal pyramid islanding after Xe ion irradiation of flat Rh(110) and Cu(110) metal surfaces, with majority steps oriented along nonequilibrium low-symmetry directions – a far-from-equilibrium self-organized morphology. The formation of the novel rhomboidal pyramid state and its transition to the well-known rippled phases results from a delicate interplay of kinetic processes which are controlled by temperature, ion flux, and impact energy. The morphology of the Rh rhomboidal pyramid nanostructure (Figure 3-18) is metastable because the pyramids tend to relax towards the flat fcc(110) morphology upon annealing above 560 K.²²⁴

Figure 3-18. Model of the rhomboidal pyramid nanocrystals (determined in accordance with the LEED data and for the high temperature ripples and low temperature ripples phases) showing the geometry and the undercoordinated step sites, with the number of exposed layers (and the lateral dimensions) scaled down by a factor of 2.5.²²⁵



²²² J.D. Benson, A.J. Stoltz, J.B. Varesi, L.A. Almeida, E.P.G. Smith, S.M. Johnson, M. Martinka, A.W. Kaleczyc, J.K. Markunas, P.R. Boyd, J.H. Dinan, "Surface Structure of Plasma-Etched (211)B HgCdTe," J. Electronic Mater. 34(June 2005):726-732.

²²³ A. Molle, F. Buatier de Mongeot, A. Molinari, F. Xiaerding, C. Boragno, U. Valbusa, "Self-Organized Formation of Rhomboidal Nanopyramids on fcc(110) Metal Surfaces," Phys. Rev. Lett. 93(2004):256103.

²²⁴ F. Buatier de Mongeot, A. Toma, A. Molle, S. Lizzit, L. Petaccia, A. Baraldi, "Carbon Monoxide Dissociation on Rh Nanopyramids," Phys. Rev. Lett. 97(August 2006):056103; <http://www.elettra.trieste.it/science/update/docs/200610.pdf>.

²²⁵ F. Buatier de Mongeot, A. Toma, A. Molle, S. Lizzit, L. Petaccia, A. Baraldi, "Carbon Monoxide Dissociation on Rh Nanopyramids," Phys. Rev. Lett. 97(August 2006):056103; <http://www.elettra.trieste.it/science/update/docs/200610.pdf>.

3.6 Graphene-on-Metal Dome Structures

Another long-shot alternative is to make use of the semi-deterministic growth of graphene domes on flat Ir(111) surface recently reported by Lacovig et al.²²⁶ A combination of high-resolution photoelectron spectroscopy and *ab initio* calculations showed that carbon nanoislands formed during the growth of a long-range ordered graphene layer on Ir(111) assume a peculiar domelike shape (Figure 3-19). The researchers studied, both experimentally and via confirmatory DFT-based computational simulations using VASP, the aggregation of carbon atoms into graphene clusters (1) upon annealing to different temperatures an Ir(111) surface saturated with C₂H₄ at 300 K and (2) during C₂H₄ exposure at 820 K, 970 K, and 1270 K. These two procedures resulted in different morphologies of the C clusters as seen with STM.²²⁷ In the second (high-temperature) case the clusters grow exclusively at step edges because of rapid C diffusion and occupation of preferred configurations, but in the first (low temperature) case flat C island formation takes place also on the terraces and an overall coverage of 0.29 ML is obtained. The transition from carbidic C to a low interacting graphene layer proceeds via formation of dome-shaped C nanoislands whose interaction with the Ir substrate takes place only at the cluster edge.

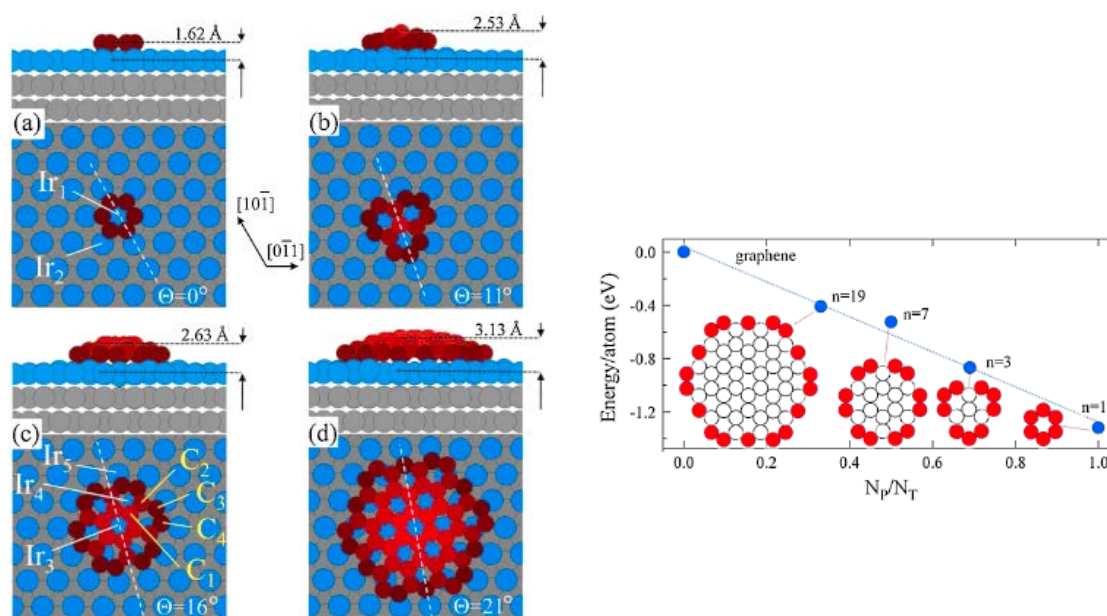
The geometry of a single ($n = 1$) honeycomb ring (Figure 3-19A) is quite simple: The C atoms, placed in bridge sites, sit in a planar configuration with a C-Ir distance of 1.62 Å and the symmetry axes oriented along the (101) direction. However, an increase in n has drastic effects on cluster morphology. The cluster with $n = 3$ abandons the flat configuration and bends upwards assuming a domelike shape: the central C atom is now at a distance of 2.53 Å from the Ir surface, and only the C atoms at the periphery remain close to the Ir substrate. This process is paralleled by a rotation of the symmetry axes by 11°. For still larger cluster sizes the unsticking process goes on further: the top C atoms for $n = 7$ and $n = 19$ move apart by 2.63 Å and 3.13 Å, respectively, while the cluster undergoes further rotation, not too far from the value of 30° of a graphene layer with a C-C distance of 1.42 Å. Even for a very small C island, the interaction of Ir atoms placed just below the center of the dome is very small (Figure 3-19B). Only the Ir atoms directly bonded with the C atoms at the cluster edge strongly.²²⁸

²²⁶ Paolo Lacovig, Monica Pozzo, Dario Alfe, Paolo Vilmercati, Alessandro Baraldi, Silvano Lizzit, "Growth of Dome-Shaped Carbon Nanoislands on Ir(111): The Intermediate between Carbidity Clusters and Quasi-Free-Standing Graphene," *Phys. Rev. Lett.* 103(16 October 2009):166101.

²²⁷ Johann Coraux, Alpha T. N'Diaye, Martin Engler, Carsten Busse, Dirk Wall, Niemma Buckanie, Frank-J Meyer zu Heringdorf, Raoul van Gastel, Bene Poelsema, Thomas Michely, "Growth of graphene on Ir(111)," *New J. Phys.* 11(4 February 2009):023006.

²²⁸ Paolo Lacovig, Monica Pozzo, Dario Alfe, Paolo Vilmercati, Alessandro Baraldi, Silvano Lizzit, "Growth of Dome-Shaped Carbon Nanoislands on Ir(111): The Intermediate between Carbidity Clusters and Quasi-Free-Standing Graphene," *Phys. Rev. Lett.* 103(16 October 2009):166101.

Figure 3-19. (A) Left: Calculated structural models of the C clusters formed by n honeycomb rings with (a) $n = 1$, (b) $n = 3$, (c) $n = 7$, and (d) $n = 19$; Ir_i ($i = 1; \dots; 6$) and C_j ($j = 1; \dots; 4$) represent different Ir and C local configurations, respectively; the distance of the central C atoms from the Ir substrate as well as the orientation of the cluster with respect to the (101) direction of Ir(111) are also shown. (B) Right: Evolution of the binding energy/atom as a function of the ratio of C atoms at the periphery N_P and the total number N_T in each C cluster.²²⁹



If this process could be closely controlled, a graphene dome of specific n might be self-assembled on a flat Ir surface (e.g., at the apex of a truncated flat-apex conical probe), with the intent to use the most apical C atom at the center of the dome structure as the DMS bonding atom of a low-aspect-ratio but atomically deterministic DMS tip.

3.7 Pyramidal Cavity Templating

Another group of possible methods for making atomically-imprecise tips might generally be described as pyramidal cavity templating. One such approach, pursued by the Odom group at Northwestern University during the mid-2000s,²³⁰ involved using lithography to make pyramidal nanoparticles (Figure 3-20) which could then, in principle, be attached to a larger AFM handle

²²⁹ Paolo Lacovig, Monica Pozzo, Dario Alfe, Paolo Vilmercati, Alessandro Baraldi, Silvano Lizzit, "Growth of Dome-Shaped Carbon Nanoislands on Ir(111): The Intermediate between Carbide Clusters and Quasi-Free-Standing Graphene," Phys. Rev. Lett. 103(16 October 2009):166101.

²³⁰ J. Henzie, J.E. Barton, C.L. Stender, T.W. Odom, "Large-area Nanoscale Patterning: Chemistry meets Fabrication," Accts. Chem. Res. 39(2006):249-257;
<http://chemgroups.northwestern.edu/odom/Publications/TWO-33.pdf>.

structure. The process involves making a layer with holes in it, etching away some material underneath (which will be a pyramidal, not round, inverted cavity when crystalline material is used), evaporating another material into the pyramidal cavity to fill it (optionally in multiple layers), then etching away more material to free the nanopyramid shapes from the cavities in which they have been formed.

In 2004,²³¹ laser-assisted embossing was used to create arrays of nanowells in which crystals of various materials could grow (Figure 3-20A). Later work in 2005²³² produced mesoscale metal (Au/Ni) pyramids having corners with a curvature radius of ~2 nm (Figure 3-20B), by using mesoscale holes (100-300 nm) in a chromium film as an etch mask to fabricate pyramidal pits and then as a deposition mask to form the metallic pyramids. By 2006,²³³ the group produced arrays of gold pyramids mounted on much larger pyramidal silicon pedestals and blocks of material embedded with the gold pyramids (Figure 3-20C). Given the group's demonstration of two-material nanopyramids (Figure 3-20D),²³⁴ it seems plausible that some variant of this fabrication process might yield metal pyramids affixed at their base (rather than their apex) to a larger handle structure, which then might be useful as a DMS tooltip. For example, EBID could be used to grow the handle after which the silicon wells are etched away, leaving the nanopyramid attached to the handle.

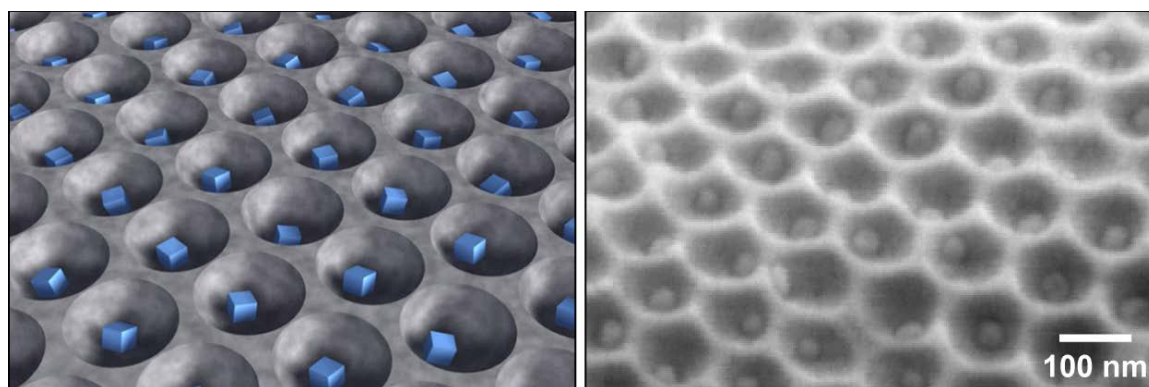
²³¹ J.E. Barton, T.W. Odom, "Mass-limited Growth in Zeptoliter-Beakers: A General Approach to Nanoparticle Synthesis," *Nano Letters* 4(2004):1525-1528; <http://chemgroups.northwestern.edu/odom/Publications/TWO-21.pdf>.

²³² J. Henzie, E.-S. Kwak, T.W. Odom, "Mesoscale Metallic Pyramids with Nanoscale Tips," *Nano Letters* 5(2005):1199-1202; <http://chemgroups.northwestern.edu/odom/Publications/TWO-27.pdf>.

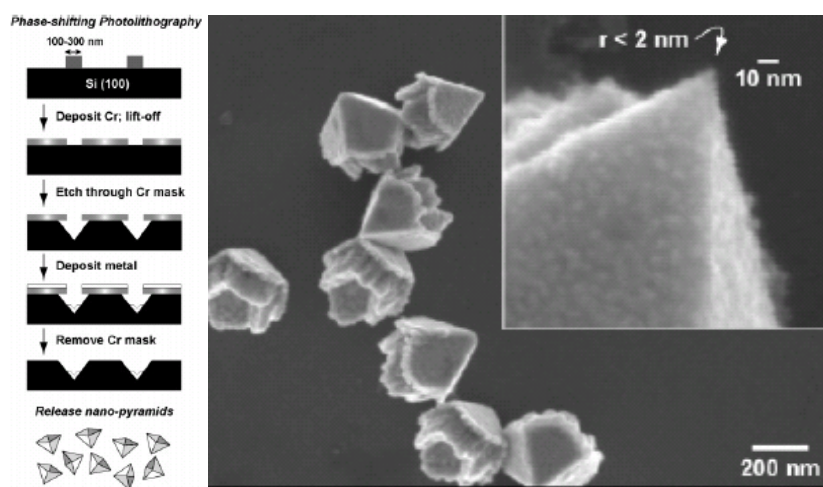
²³³ J. Henzie, K.L. Shuford, E.-S. Kwak, G.C. Schatz, T.W. Odom, "Manipulating the Optical Properties of Pyramidal Nanoparticle Arrays," *J. Phys. Chem. B* 110(2006):14028-14031; <http://chemgroups.northwestern.edu/odom/Publications/TWO-34.pdf>.

²³⁴ J. Lee, W. Hasan, M.H. Lee, T.W. Odom, "Optical Properties and Magnetic Manipulation of Bi-Material Nanopyramids," *Adv. Mater.* 19(2007):4387; <http://dx.doi.org/10.1002/adma.200701505>. 188.

Figure 3-20. (A) Crystals grown in nanowells using laser-assisted embossing.²³⁵ (B) Metal nanopyramids with <2 nm curvature radius apex.²³⁶ (C) Lithographically prepared array of inverted gold nanopyramids.²³⁷ (D) Two-material (Ni/Au) nanopyramid.²³⁸



(A)



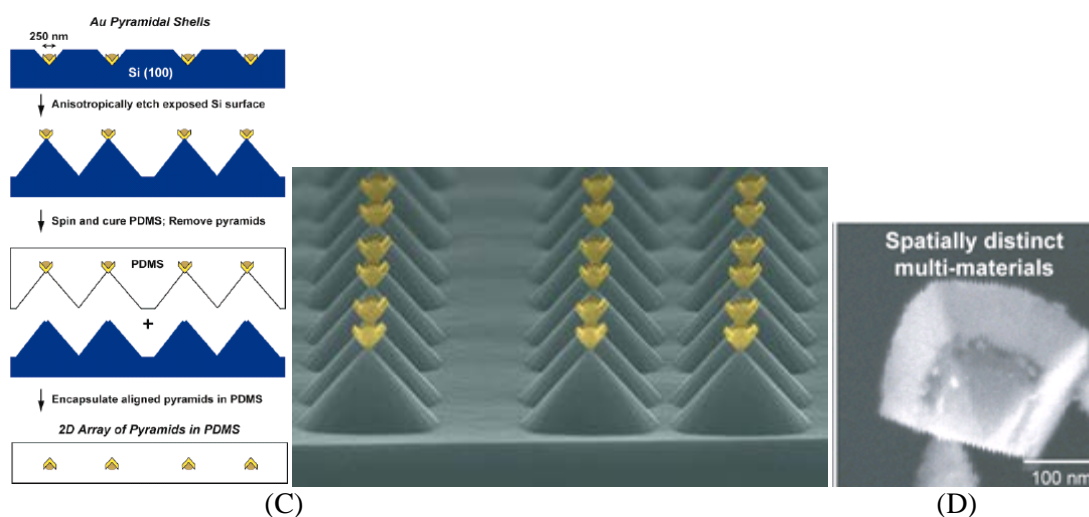
(B)

²³⁵ J.E. Barton, T.W. Odom, "Mass-limited Growth in Zeptoliter-Beakers: A General Approach to Nanoparticle Synthesis," *Nano Letters* 4(2004):1525-1528; <http://chemgroups.northwestern.edu/odom/Publications/TWO-21.pdf>.

²³⁶ J. Henzie, E.-S. Kwak, T.W. Odom, "Mesoscale Metallic Pyramids with Nanoscale Tips," *Nano Letters* 5(2005):1199-1202; <http://chemgroups.northwestern.edu/odom/Publications/TWO-27.pdf>.

²³⁷ J. Henzie, K.L. Shuford, E.-S. Kwak, G.C. Schatz, T.W. Odom, "Manipulating the Optical Properties of Pyramidal Nanoparticle Arrays," *J. Phys. Chem. B* 110(2006):14028-14031; <http://chemgroups.northwestern.edu/odom/Publications/TWO-34.pdf>.

²³⁸ J. Lee, W. Hasan, C.L. Stender, T.W. Odom, "Pyramids: A Platform for Designing Multifunctional Plasmonic Particles," *Acc. Chem. Res.* 41(2008):1762; <http://dx.doi.org/10.1021/ar800126p>.

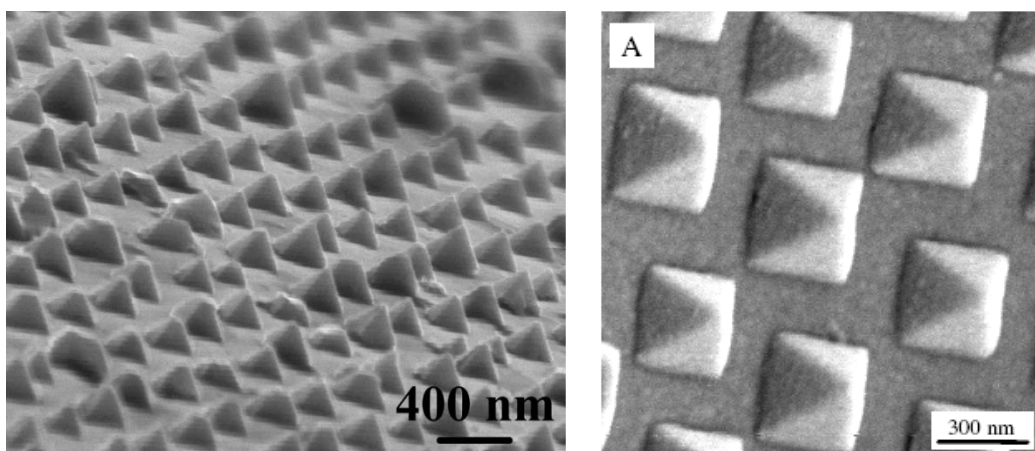
Figure 3-20. (cont'd).

Other groups have used simple self-assembly-based templating approaches for fabricating wafer-scale, periodic metallic nanopyramid arrays with nanoscale tips (Figure 3-21A). For example, spin-coated, non-close-packed monolayer colloidal crystals can be used as templates to create chromium nanohole arrays, which are utilized as etching masks to fabricate inverted silicon pyramidal pits by anisotropic KOH etching; wafer-scale metallic pyramid arrays with sharp nanotips can then be replicated from silicon templates by a simple adhesive peeling process²³⁹ (although often the resulting nanopyramids are polycrystalline). As revealed in the figure, there are a lot of broken pyramids that occur during the peeling process. In 2009 the same group reported²⁴⁰ an improved process in which nanopyramids composed of organic ETPTA (ethoxylated trimethylolpropane triacrylate monomer) are sputter-coated with gold. The uncoated ETPTA nanopyramids have tip curvature of under 5 nm, and for thin gold coatings this good sharpness is largely retained (Figure 3-21B).

²³⁹ Chih-Hung Sun, Nicholas C. Linn, Peng Jiang, “Templated Fabrication of Periodic Metallic Nanopyramid Arrays,” *Chem. Mater.* 19(2007):4551-4556.

²⁴⁰ Nicholas C. Linn, Chih-Hung Sun, Ajay Arya, Peng Jiang, Bin Jiang, “Surface-enhanced Raman scattering on periodic metal nanotips with tunable sharpness,” *Nanotechnology* 20(2009):225303; http://www.mth.pdx.edu/~bjiang/papers/2009_nanotech.pdf

Figure 3-21. (A) Left: Pure gold metal nanopyramid array created by templated fabrication.²⁴¹ (B) Right: SEM image of an ETPTA organic polymer nanopyramid array overcoated with 30 nm thick gold layer.²⁴²



Au and Ag nanopyramids have also been fabricated using nanoimprint lithography in polymethylmethacrylate (PMMA),²⁴³ and colloidal nanocrystal templating of Au nanopyramidal arrays has been demonstrated.²⁴⁴

3.8 EBID Fabrication of SPM Tips

According to a brief survey by Utke et al.,²⁴⁵ commercial cantilevers with ultrasharp high-aspect-ratio tips are used in AFM configuration to sense a variety of properties with nanometer resolution, such as topography, magnetic polarization, ferroelectric domains, and temperature. High resolution, high-aspect-ratio tips can be made by focused electron beam (FEB) induced

²⁴¹ Chih-Hung Sun, Nicholas C. Linn, Peng Jiang, “Templated Fabrication of Periodic Metallic Nanopyramid Arrays,” *Chem. Mater.* 19(2007):4551-4556.

²⁴² Nicholas C. Linn, Chih-Hung Sun, Ajay Arya, Peng Jiang, Bin Jiang, “Surface-enhanced Raman scattering on periodic metal nanotips with tunable sharpness,” *Nanotechnology* 20(2009):225303; http://www.mth.pdx.edu/~bjiang/papers/2009_nanotech.pdf.

²⁴³ B. Cui, L. Clime, K. Li, T. Veres, “Fabrication of large area nanoprism arrays and their application for surface enhanced Raman spectroscopy,” *Nanotechnology* 19(2008):145302; <http://ece.uwaterloo.ca/~bcui/Publication/2008%20Nanoprism%20Nanotech.pdf>.

²⁴⁴ Tzung-Hua Lin, Nicholas C. Linn, Lemis Tarajano, Bin Jiang, Peng Jiang, “Electrochemical SERS at Periodic Metallic Nanopyramid Arrays,” *J. Phys. Chem. C* 113(2009):1367-1372; http://www.mth.pdx.edu/~bjiang/papers/2009_jpcc.pdf.

²⁴⁵ Ivo Utke, Patrik Hoffmann, John Melngailis, “Gas-assisted focused electron beam and ion beam processing and fabrication,” *J. Vac. Sci. Technol. B* 26(July 2008):1197-1276.

deposition in a simple single step process²⁴⁶ by focusing the primary beam on the cantilever and depositing a pillar of the desired material (Figure 3-22).

EBID-made tips have been fabricated for use in scanning probe (STM) work out of tungsten²⁴⁷ and carbon.²⁴⁸ Mechanically resistant, high-aspect-ratio, high resolution AFM tips of diamondlike carbon are a commercial product from Nanotools.²⁴⁹ The mechanical properties are close to diamond (elastic modulus ~ 0.5 TPa)²⁵⁰ and their use as a mechanical high resolution patterning tool has been demonstrated.²⁵¹

Scientific studies on FEB tip deposition investigated the role of electron beam energy,²⁵² precursor pressure,²⁵³ secondary electron emission,²⁵⁴ different precursors,²⁵⁵ and electron beam size.²⁵⁶ As extensively discussed in the previous sections on modeling, it should be kept in mind

²⁴⁶ B. Hubner, H.W.P. Koops, H. Pagnia, N. Sotnik, J. Urban, M. Weber, "Tips for scanning tunneling microscopy produced by electron-beam-induced deposition," *Ultramicroscopy* 42(1992):1519-1525. 195.

²⁴⁷ Shinji Matsui, Toshinori Ichihashi, Masakazu Baba, Akinobu Satoh, "Electron beam induced selective etching and deposition technology," *Superlattices and Microstructures* 7(1990):295-301.

²⁴⁸ Y. Akama, E. Nishimura, A. Sakai, "New scanning tunneling microscopy tip for measuring surface topography," *J. Vac. Sci. Technol. A* 8(January 1990):429-433. K.I. Schiffmann, "Investigation of fabrication parameters for the electron-beam-induced deposition of contamination tips used in atomic force microscopy," *Nanotechnology* 4(1993):163-169.

²⁴⁹ Nanotools; <http://www.nano-tools.com/>

²⁵⁰ G. Jänschen, P. Hoffmann, A. Kriele, H. Lorenz, A.J. Kulik, G. Dietler, "Mechanical properties of high-aspect-ratio atomic-force microscope tips," *Appl. Phys. Lett.* 80(2002):4623-4625.

²⁵¹ M. Wendel, H. Lorenz, J.P. Kotthaus, "Sharpened electron beam deposited tips for high resolution atomic force microscope lithography and imaging," *Appl. Phys. Lett.* 67(1995):3732-3734.

²⁵² K.I. Schiffmann, "Investigation of fabrication parameters for the electron-beam-induced deposition of contamination tips used in atomic force microscopy," *Nanotechnology* 4(1993):163-169. M. Weber, "Scattering of non-relativistic electrons in tip structures," *J. Phys. D: Appl. Phys.* 27(1994):1363-1369. Philip D. Rack, Jason D. Fowlkes, Steven J. Randolph, "In situ probing of the growth and morphology in electron-beam-induced deposited nanostructures," *Nanotechnology* 18(2007):465602.

²⁵³ Young R. Choi Philip D. Rack, Steven J. Randolph, Daryl A. Smith, David C. Joy, "Pressure effect of growing with electron beam-induced deposition with tungsten hexafluoride and tetraethylorthosilicate precursor," *Scanning* 28(2006):311-318.

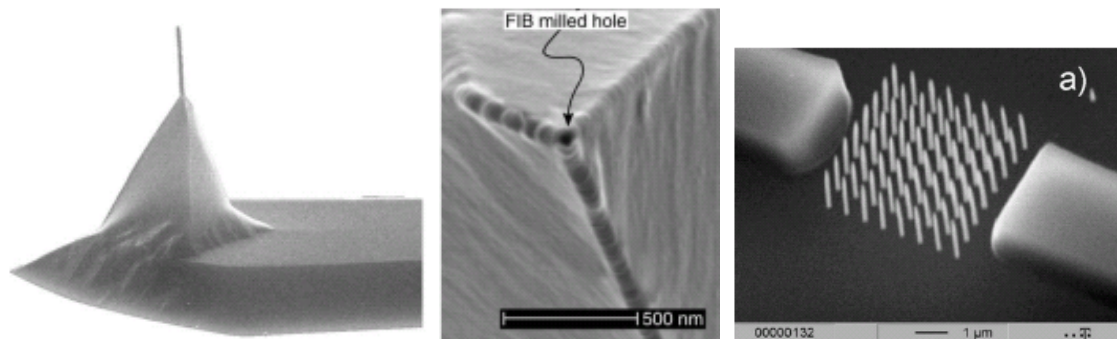
²⁵⁴ N. Silvis-Cividjian, C.W. Hagen, L.H.A. Leunissen, P. Kruit, "The role of secondary electrons in electron-beam-induced-deposition spatial resolution," *Microelectron. Eng.* 61-62(July 2002):693-699.

²⁵⁵ T. Bret, I. Utke, A. Bachmann, P. Hoffmann, "In situ control of the focused-electron-beam-induced deposition process," *Appl. Phys. Lett.* 83(2003):4005-4007.

²⁵⁶ I. Utke, R. Berger, L. Scandella, P. Hoffmann, "High-resolution magnetic Co supertips grown by a focused electron beam," *Appl. Phys. Lett.* 80(2002):4792-4794.

that the tip apex resolution depends on the balance of precursor replenishment and depletion for a given beam size. This balance is very difficult to quantify experimentally. There has been some experimental work²⁵⁷ concerning the ultimate resolution of freestanding rod deposits by FEB.

Figure 3-22. High resolution FEB and FIB functionalized sensors.²⁵⁸ Left: FEB deposited MFM tip on commercial silicon AFM sensor. Center: 40 nm diameter FIB milled hole into a magnetic coating of commercial silicon sensor. Right: FEB deposited band gap filter.



The potential of automated FEB processing of cantilever wafers (image recognition, positioning, and autofocus) has been investigated.²⁵⁹ Apart from commercialized hard, high-aspect ratio,

²⁵⁷ Shinji Matsui, Toshinari Ichihashi, "In situ observation on electron-beam-induced chemical vapor deposition by transmission electron microscopy," *Appl. Phys. Lett.* 53(1988):842-844. S. Matsui, T. Ichihashi, M. Mito, "Electron beam induced selective etching and deposition technology," *Journal of Vacuum Science & Technology B* 7(September/October 1989):1182 -1190. V.V. Aristov, A.Y. Kasumov, N.A. Kislov, O.V. Kononenko, V.N. Matveev, V.A. Tulin, I.I. Khodos, Y.A. Gorbatov, V.I. Nikolaichik, "A new approach to fabrication of nanostructures," *Nanotechnology* 6(April 1995):35-39. J. Fujita, M. Ishida, T. Ichihashi, Y. Ochiai, T. Kaito, S. Matsui, "Carbon nanopillar laterally grown with electron beam-induced chemical vapor deposition," *Journal of Vacuum Science & Technology B* 21(November 2003):2990-2993; <http://dx.doi.org/10.1116/1.1624259>. Z.Q. Liu, K. Mitsuishi, K. Furuya, "The growth behavior of self-standing tungsten tips fabricated by electron-beam-induced deposition using 200 keV electrons," *J. Appl. Phys.* 96(2004):3983-3986.

²⁵⁸ L. Folks, M.E. Best, P.M. Rice, B.D. Terris, D. Weller, J.N. Chapman, "Perforated tips for high-resolution in-plane magnetic force microscopy," *Appl. Phys. Lett.* 76(2000):909-911. H.W.P. Koops, O.E. Hoinkis, M.E.W. Honsberg, R. Schmidt, R. Blum, G. Böttger, A. Kuligk, C. Liguda, M. Eich, "Two-dimensional photonic crystals produced by additive nanolithography with electron beam-induced deposition act as filters in the infrared," *Microelectron. Eng.* 57-58(2001):995.

²⁵⁹ Johannes H Kindt, Georg E Fantner, James B Thompson, Paul K Hansma, "Automated wafer-scale fabrication of electron beam deposited tips for atomic force microscopes using pattern recognition," *Nanotechnology* 15(September 2004):1131-1134.

sharp AFM tips, several functional scanning probe sensors have been fabricated and analyzed at laboratory scale – including the characterization of magnetic FEB tips²⁶⁰ and the measurement of magnetic properties of FEB structures.²⁶¹ Optical fibers for scanning near field microscopy were functionalized with FEB deposited plasmonic gold structures²⁶² and carbon waveguides,²⁶³ and scanning thermal sensors have been demonstrated.²⁶⁴ FEB and FIB (focused ion beam) deposited silicon oxide nanostructures were used to reduce fluorescence quenching in apertureless scanning near field optical microscopy and create surface plasmon resonant tips, which avoids far field illumination and related background noise signals.²⁶⁵ Sidewall roughness has been measured with a specially FEB designed AFM tip.²⁶⁶ Convex nanopyramids can be formed by Si(111) facets because the anisotropic etch rate in hydrazine is lower for (111) than for (001) planes (in this case the effect was due to a decrease in the etch rate with increasing ion-beam exposure).²⁶⁷ FIB deposition of tips suffers from comparatively “bad” resolution. The physical sputtering inherent to FIB is predominantly used in trimming of sensors, such as recording heads in magnetic hard disk storage,²⁶⁸ AFM sensors,²⁶⁹ or nanodispensers.²⁷⁰

²⁶⁰ I. Utke, F. Cicoira, G. Jaenchen, P. Hoffmann, L. Scandella, B. Dwir, E. Kapon, D. Laub, P. Buffat, N. Xanthopoulos, H.J. Mathieu, “Focused electron beam induced deposition of high resolution magnetic scanning probe tips,” Materials Research Society Symposium Proceedings No. 706, 2002, pp. 307-312. Y.M. Lau, P.C. Chee, J.T.L. Thong, V. Ng, “Properties and applications of cobalt-based material produced by electron-beam-induced deposition,” Journal of Vacuum Science & Technology A 20(July 2002):1295-1302. <http://dx.doi.org/10.1116/1.1481040>.

²⁶¹ M. Takeguchi, M. Shimojo, R. Che, K. Furuya, “Fabrication of a nano-magnet on a piezo-driven tip in a TEM sample holder,” J. Mater. Sci. 41(May 2006):2627-2630. Masaki Takeguchi, Masayuki Shimojo, Kazuo Furuya, “Fabrication of magnetic nanostructures using electron beam induced chemical vapour deposition,” Nanotechnology 16(August 2005):1321-1325.

²⁶² O. Sqalli, I. Utke, P. Hoffmann, F. Marquis-Weible, “Gold elliptical nanoantennas as probes for near field optical microscopy,” J. Appl. Phys. 92(2002):1078-1083.

²⁶³ M. Castagne, M. Benfedda, S. Lahimer, P. Falgayrettes, J.P. Fillard, “Near field optical behaviour of C supertips,” Ultramicroscopy 76(April 1999):187-194.

²⁶⁴ I.W. Rangelow, T. Gotszalka, N. Abedinov, P. Grabieca, K. Edinger, “Thermal nano-probe,” Microelectron. Eng. 57-58(September 2001):737-748. K. Edinger, T. Gotszalk, I.W. Rangelow, “Novel high resolution scanning thermal probe,” J. Vac. Sci. Technol. B 19(November 2001):2856-2860.

²⁶⁵ E.J. Sanchez, J.T. Krug, X.S. Xie, “Ion and electron beam assisted growth of nanometric Si_mO_n structures for near-field microscopy,” Rev. Sci. Instrum. 73(2002):3901-3907.

²⁶⁶ S. Matsui, T. Ichihashi, Y. Ochiai, K. Baba, H. Watanabe, A. Sato, “Nanostructure technology developed through electron-beam-induced surface reaction,” in: S. Namba, C. Hamaguchi, T. Ando, eds., Science and Technology of Mesoscopic Structures, Springer, Tokyo, 1992, pp. 334-352.

²⁶⁷ M. Koh, S. Sawara, T. Shinada, T. Goto, Y. Ando, I. Ohdomari, “Simple nanostructuring on silicon surface by means of focused beam patterning and wet etching,” Appl. Surf. Sci. 162-163(1 August 2000):599-603.

²⁶⁸ T. Koshikawa, A. Nagai, Y. Yokoyama, T. Hoshino, “A New Write Head Trimmed at Wafer Level by Focus Ion Beam,” IEEE Trans. Magn. 34(July 1998):1471-1473. S.K. Khizroev, M.H. Kryder, Y. Ikeda,

3.9 Molecular Beam Epitaxy (MBE) and CVD-Based Nanopyramids

Molecular beam epitaxy (MBE) is one of several methods of depositing single crystals. MBE takes place in high vacuum or ultra high vacuum (10^{-8} Pa, practically free space). In MBE, a source material is heated to produce an evaporated beam of particles. These particles travel through the vacuum to the substrate, where they condense. MBE has lower throughput than other forms of epitaxy.²⁷¹

The most important aspect of MBE is the slow deposition rate (typically less than 1000 nm per hour) which allows the films to grow epitaxially. The slow deposition rates require proportionally better vacuum to achieve the same impurity levels as other deposition techniques. Molecular beam epitaxy enables accurate control of vertical composition since it is inherent to this growth process. The deposition of complex layers such as dopant profiles with nanometer thickness²⁷² and arbitrary doping concentration with high crystalline quality is feasible. For lateral patterning without etching, differential epitaxy²⁷³ or selective epitaxy on SiO₂ patterned Si

K. Rubin, P. Arnett, M. Best, D.A. Thompson, "Recording heads with track widths suitable for 100 Gbit/in² density," IEEE Trans. Magn. 35(September 1999):2544-2546. Dmitri Litvinov, Sakhrat Khizroev, "Focused ion beams in future nanoscale probe recording," Nanotechnology 13(April 2002):179-184.

²⁶⁹ L. Folks, M.E. Best, P.M. Rice, B.D. Terris, D. Weller, J.N. Chapman, "Perforated tips for high-resolution in-plane magnetic force microscopy," Appl. Phys. Lett. 76(2000):909-911. M.R. Koblishka, U. Hartmann, T. Sulzbach, "Resolving magnetic nanostructures in the 10-nm range using MFM at ambient conditions," Mater. Sci. Eng. C 23(15 December 2003):747-751.

²⁷⁰ A. Meister, M. Liley, J. Brugger, R. Pugin, H. Heinzelmann, "Nanodispenser for attoliter volume deposition using atomic force microscopy probes modified by focused-ion-beam milling," Appl. Phys. Lett. 85(2004):6260-6262; http://kism2.epfl.ch/record/58432/files/Meister_2004_APL.pdf.

²⁷¹ **Epitaxy** refers to the method of depositing a monocrystalline film on a monocrystalline substrate. The deposited film is denoted as epitaxial film or epitaxial layer. Epitaxial films may be grown from gaseous or liquid precursors. Because the substrate acts as a seed crystal, the deposited film takes on a lattice structure and orientation identical to those of the substrate. This is different from other thin-film deposition methods which deposit polycrystalline or amorphous films, even on single-crystal substrates. **Homoepitaxy** is a kind of epitaxy performed with only one material. In homoepitaxy, a crystalline film is grown on a substrate or film of the same material. This technology is used to grow a film which is more pure than the substrate and to fabricate layers having different doping levels. **Heteroepitaxy** is a kind of epitaxy performed with materials that are different from each other. In heteroepitaxy, a crystalline film grows on a crystalline substrate or film of a different material. This technology is often used to grow crystalline films of materials for which single crystals cannot otherwise be obtained and to fabricate integrated crystalline layers of different materials.

²⁷² I. Eisele, "Delta-type doping profiles in silicon," Appl. Surf. Sci. 36(1989):39-51. H.P. Zeindl, E. Hammerl, W. Kiunke, I. Eisele, "Delta doping superlattices in silicon," J. Electron. Mater. 19(October 1990):1119-1122.

²⁷³ Yusuke Ota, "Silicon molecular beam epitaxy," Thin Solid Films 106(12 August 1983):1-136, 3. H.J. Herzog, E. Kasper, "Silicon Layers Grown by Differential Molecular Beam Epitaxy," J. Electrochem. Soc. 132(September 1985):2227-2231.

substrates²⁷⁴ are available. However, the mesa side walls may show structural imperfections depending on the interface between the oxide and the single-crystalline layer.²⁷⁵ We've already discussed MBE-fabricated hut structures in [Section 3.4](#), but there are several other nanopyramidal structures that are also of potential interest – most notably, pure silicon.

Silicon exhibits a very strong preference to form (111) limited planes as boundaries of mesoscopic structures, as is nicely evident in the work of Baumgärtner et al.²⁷⁶ where silicon has been deposited by MBE onto a Si(100) wafer through a square-shaped 250 nm x 250 nm aperture. The resulting structure is a pyramid with (111) plane boundaries, rather than a pile with a square cross section. To do this, a method of using micro-shadow masks to achieve lateral pattern sizes in the nanometer regime by a self-assembling growth mechanism has been successfully applied to silicon technology.²⁷⁷ The process starts with a mask pattern size in the order of half a micron which can be fabricated by modern optical lithography, thus guaranteeing a high throughput. Self-assembling MBE growth then leads to nanometer-scale features. Depending on the growth parameters, pyramid-like tips or long wedges are formed. The sidewalls are free-standing (111) or (311) facets and hence they are crystallographic damage-free surfaces.²⁷⁸

Before MBE growth a micro-shadow mask is first formed on the substrate ([Figure 3-23a](#)).²⁷⁹ Si(100) substrates are cleaned and thermally oxidized at $T = 1050\text{ }^{\circ}\text{C}$ to 1 micron oxide thickness. A silicon nitride layer of about 100 nm thickness is deposited onto the oxide using a low pressure chemical vapor deposition (LPCVD) process at $T = 700\text{ }^{\circ}\text{C}$. Optical or electron beam lithography in combination with CF_4 plasma etching is used to pattern the nitride layer. The width of the

²⁷⁴ H. Hirayama, M. Hiroi, T. Ide, “{311} facets of selectively grown epitaxial Si layers on SiO_2 -patterned Si(100) surfaces,” *Phys. Rev. B* 48(15 December 1993):17331-17337.

²⁷⁵ H. Hirayama, M. Hiroi, T. Ide, “{311} facets of selectively grown epitaxial Si layers on SiO_2 -patterned Si(100) surfaces,” *Phys. Rev. B* 48(15 December 1993):17331-17337.

²⁷⁶ H. Baumgärtner, F. Kaesen, H. Gossner, I. Eisele, “Formation of single-crystalline silicon nanostructures by self-assembling growth with molecular beam epitaxy,” *Applied Surface Science* 130-132(June 1998):747-754; <http://forschung.unibw.de/berichte/2002/gsgu46gfgkvsuemqvub9v8ixmfruxa.pdf>. See also: H. Baumgärtner, W. Hansch, F. Wittmann, I. Eisele, *Curr. Top. Cryst. Growth Res.* 2(1995):283.

²⁷⁷ E. Hammerl, F. Wittmann, J. Messarosch, I. Eisele, V. Huber, H. Oppolzer, “High Definition Mesa Growth by Silicon MBE,” *Mater. Res. Soc. Symp. Proc.* 220(1991):27. E. Hammerl, I. Eisele, “Local silicon molecular beam epitaxy with microshadow masks,” *Appl. Phys. Lett.* 62(3 May 1993):2221-2223. Harald Gossner, Hermann Baumgärtner, Erwin Hammerl, Franz Wittmann, Ignaz Eisele, Thomas Heinzl, Heribert Lorenz, “Self-Organizing Growth of Nanometer Mesa Structures on Silicon (100) Substrates,” *Jpn. J. Appl. Phys.* 33(1994):2268-2271. I. Eisele, H. Baumgärtner, W. Hansch, in: K. Eberl, P.M. Petroff, P. Demeester, eds., *Low dimensional Structures Prepared by Epitaxial Growth or Regrowth on Patterned Substrates*, Kluwer Academic Publisher, 1995, p. 161.

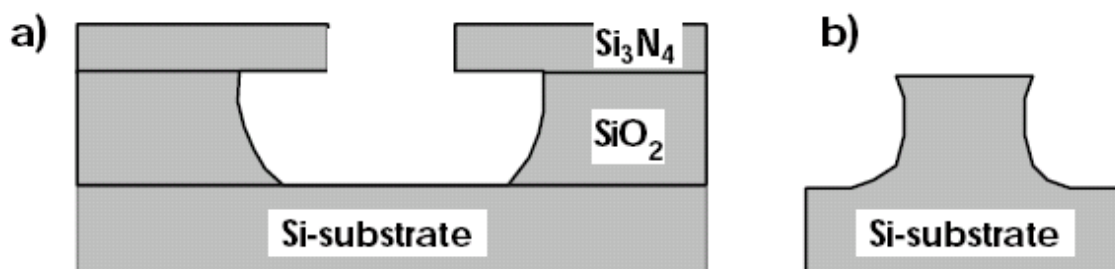
²⁷⁸ E. Hammerl, F. Wittmann, J. Messarosch, I. Eisele, V. Huber, H. Oppolzer, “High Definition Mesa Growth by Silicon MBE,” *Mater. Res. Soc. Symp. Proc.* 220(1991):27.

²⁷⁹ E. Hammerl, I. Eisele, “Local silicon molecular beam epitaxy with microshadow masks,” *Appl. Phys. Lett.* 62(3 May 1993):2221-2223.

square- or line-shaped mask aperture is of the order of half a micron. The oxide is then selectively etched down to the substrate in buffered hydrofluoric acid, and the shadow mask is formed for the subsequent MBE deposition by under-etching the nitride layer.

After the cleaning, the (100) substrates are anisotropically etched in a SF_6 plasma. The size of the square-shaped mesas varies between 300 nm and 3 micron with a height of about half a micron. The etch process is performed such that a small undercut of the mesa sidewalls is obtained (Figure 3-23b). The anisotropy of the etch process was not yet optimized so the base of the sidewalls is rounded to some extent, but the actual shape of the mesa template does not substantially affect the growth mechanism. After a final clean the substrates are transferred to the MBE system. The base pressure in the ultrahigh vacuum chamber is 0.3×10^{-9} mbar rising to 2×10^{-9} mbar during evaporation. The MBE process starts with a thermal desorption of the native oxide on the substrate surface for 5 min at $T = 900^\circ\text{C}$. The growth rate for the deposition of pure undoped silicon is 0.1 nm/s and is controlled by a quadrupole mass spectrometer. During the growth the substrates are heated to temperatures between 500°C and 730°C as measured by pyrometry.

Figure 3-23. a) Schematic cross-section of a micro-shadow mask and b) of a nonplanar prepatterned substrate for the self-assembling MBE growth of silicon tips and wedges.²⁸⁰

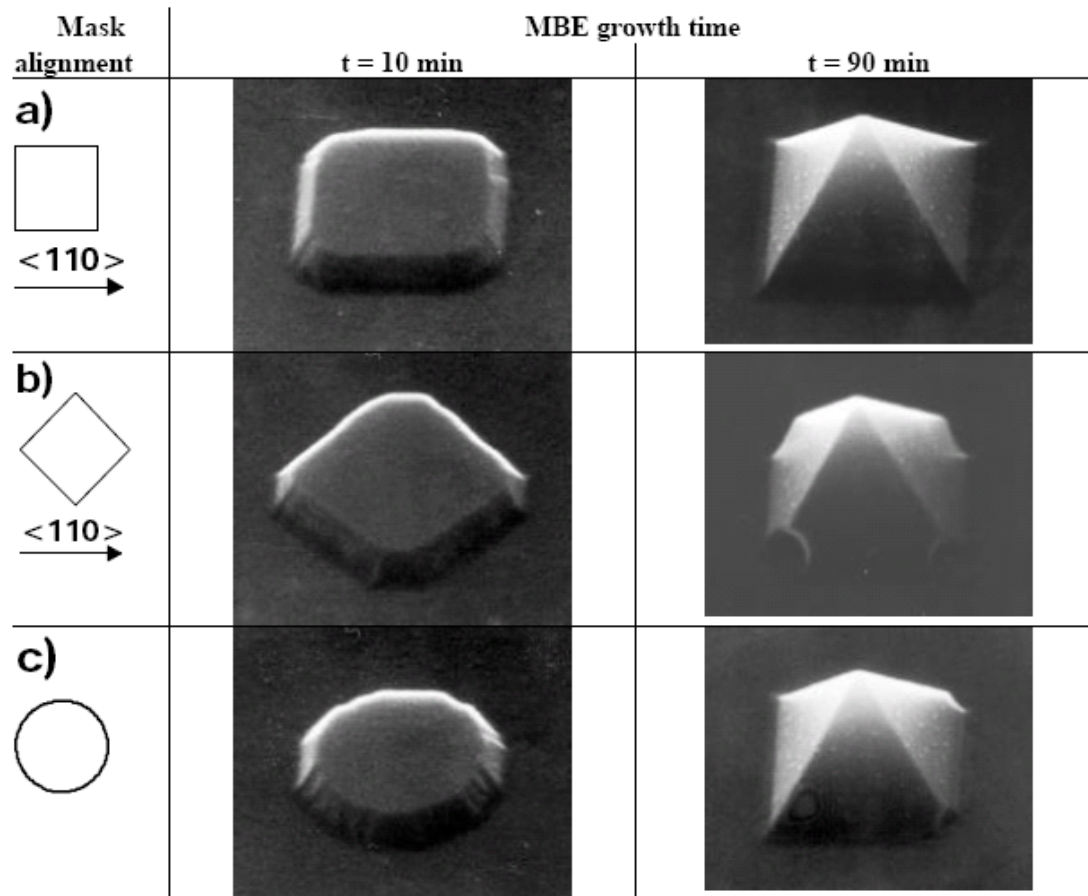


In Figure 3-24 the self-assembling growth of pyramids at two different chronological states is depicted. For square-shaped micro-shadow masks and a sufficient growth time the deposition results in ultrasharp pyramids limited by (111) sidewalls. In the right column of Figure 3-24a the result is shown for a 250 nm mask aperture and a growth time of $t = 90$ min. The radius of the tip

²⁸⁰ H. Baumgärtner, F. Kaesen, H. Gossner, I. Eisele, "Formation of single-crystalline silicon nanostructures by self-assembling growth with molecular beam epitaxy," Applied Surface Science 130-132(June 1998):747-754; <http://forschung.unibw.de/berichte/2002/gsgu46gfgkvsuemqvub9v8ixmfruxa.pdf>. See also: H. Baumgärtner, W. Hansch, F. Wittmann, I. Eisele, Curr. Top. Cryst. Growth Res. 2(1995):283.

is estimated to be less than 5 nm which is the resolution limit of the SEM.²⁸¹ For a shorter growth time ($t = 10$ min) only a truncated pyramid is deposited (Figure 3-24a, left column).

Figure 3-24. SEM micrographs of six silicon nanopyramid samples grown by MBE with micro-shadow masks at two different growth states after 10 and 90 min; the alignment with respect to the crystallographic orientation and the shape of the mask aperture have been changed; in all cases the size of the mask opening amounts to 250 nm and the growth temperature is kept constant at 500 °C.²⁸²



²⁸¹ I. Eisele, H. Baumgärtner, W. Hansch, in: K. Eberl, P.M. Petroff, P. Demeester, eds., Low dimensional Structures Prepared by Epitaxial Growth or Regrowth on Patterned Substrates, Kluwer Academic Publisher, 1995, p. 161.

²⁸² H. Baumgärtner, F. Kaesen, H. Gossner, I. Eisele, "Formation of single-crystalline silicon nanostructures by self-assembling growth with molecular beam epitaxy," Applied Surface Science 130-132(June 1998):747-754; <http://forschung.unibw.de/berichte/2002/gsgu46fgkvsuemqvub9v8ixmfruxa.pdf>. See also: H. Baumgärtner, W. Hansch, F. Wittmann, I. Eisele, Curr. Top. Cryst. Growth Res. 2(1995):283.

The baseline of the (111) facets on the Si(100) substrate surface is oriented in the (110) direction. The self-assembling process leads to the formation of (111) facets if the mask edge is aligned parallel to the (110) (Figure 3-24a). Turning the mask by 45° also results in a turning of the truncated structure at the early state of the deposition (Figure 3-24b). The sidewalls are still mainly determined by the mask shape, but small (111) facets already appear at the edges. Continuing the deposition process, the facets grow further at the expense of the other nonfaceted sidewalls. At the end the same pyramid is formed as the one that is formed for an alignment of the mask in the (110) direction. This experiment clearly demonstrates the self-assembling growth mechanism of the deposition process which is confirmed by the last example in Figure 3-24c. In this case a round mask hole is used. At the beginning of the growth this hole is imaged, but again the (111) facets are already visible. Continuing the growth, a perfect pyramid is formed after $t = 90$ min. Thus the shape of the grown features depends on the mask shape only on the coarse scale, while small fluctuations in the mask geometry don't much affect the shape of the grown structures. This is a very important result with respect to a straightforward and reproducible process run for an industrial production. To summarize: Depending on the growth parameters, ultrasharp single-crystalline tips or wedges with crystallographic (111) and/or (311) sidewalls and high thermal stability can be grown using a simple process technology (MBE).²⁸³ As shown by scanning electron micrographs the tip radius amounts to less than 5 nm. Low-power plasma-enhanced CVD can also be used to deposit arrays of (100)-oriented silicon nanopyramids²⁸⁴ and silicon nanocones.²⁸⁵

Mendez-Garcia et al.²⁸⁶ have studied the surface atomic structure of GaAs(631) and the GaAs growth by molecular beam epitaxy (MBE) on this plane. After the oxide desorption process at 585 °C reflection high-energy electron diffraction (RHEED) showed along the (-120) direction a 2x surface reconstruction for GaAs(631)A and a 1x pattern for GaAs(631)B. After annealing the substrates for 60 min, small hilly-like features appeared on the A surface after which 500 nm-thick GaAs layers were grown on GaAs(631)A at 585 °C. AFM images at the end of growth showed the self-formation of nanoscale structures with a pyramidal shape enlarged along the $(5-9-3)$ direction, and transversal views of the bulk-truncated GaAs(631) surface model showed arrays of atomic grooves along this direction (which could influence the formation of the

²⁸³ H. Baumgärtner, F. Kaesen, H. Gossner, I. Eisele, "Formation of single-crystalline silicon nanostructures by self-assembling growth with molecular beam epitaxy," *Applied Surface Science* 130-132(June 1998):747-754; <http://forschung.unibw.de/berichte/2002/gsgu46fgkvsuemqvub9v8ixmfruxa.pdf>. See also: H. Baumgärtner, W. Hansch, F. Wittmann, I. Eisele, *Curr. Top. Cryst. Growth Res.* 2(1995):283.

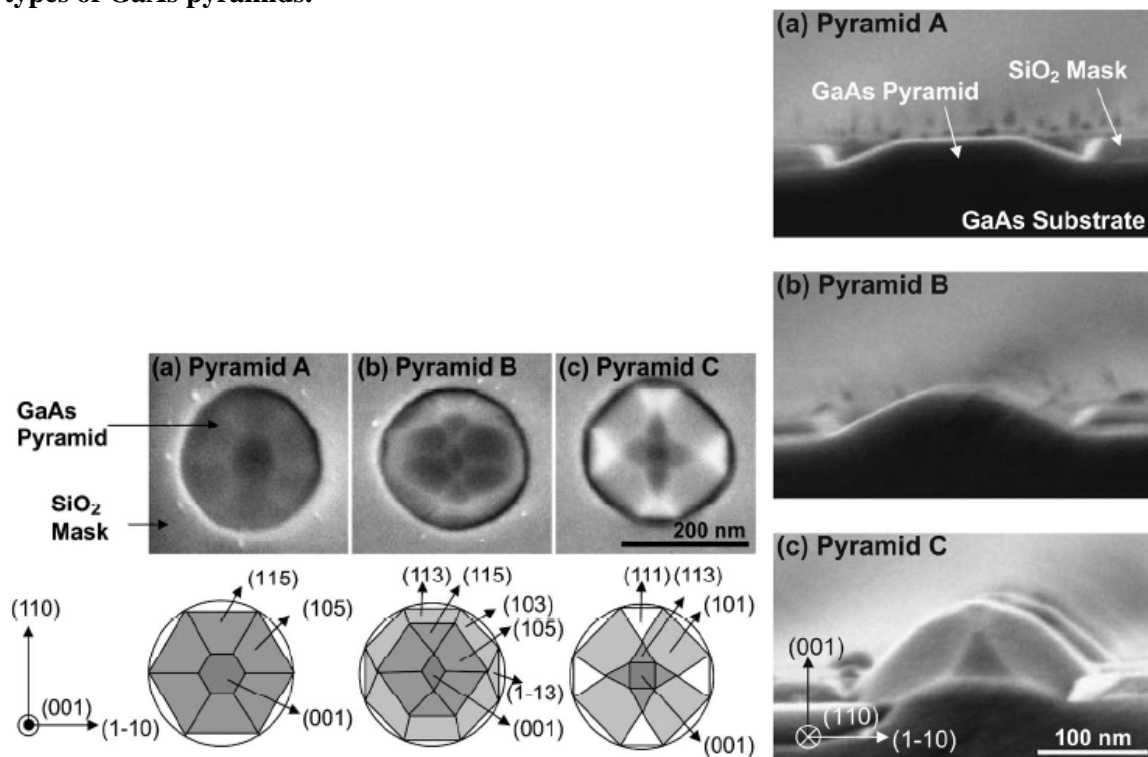
²⁸⁴ Gong-Ru Lin, Chi-Kuan Lin, Li-Jen Chou, Yu-Lun Chueh, "Synthesis of Si nanopyramids at SiO_x/Si interface for enhancing electroluminescence of Si-rich SiO_x," *Appl. Phys. Lett.* 89(1 September 2006):093126.

²⁸⁵ S. Xu, I. Levchenko, S.Y. Huang, K. Ostrikov, "Self-organized vertically aligned single-crystal silicon nanostructures with controlled shape and aspect ratio by reactive plasma etching," *Appl. Phys. Lett.* 95(18 September 2009):111505.

²⁸⁶ V.H. Méndez-García, F.J. Ramirez-Arenas, A. Lastras-Martínez, E. Cruz-Hernandez, A. Pulzara-Mora, J.S. Rojas-Ramirez, M. Lopez-Lopez, "Structure and homoepitaxial growth of GaAs(631)," *Applied Surface Science* 252(30 May 2006):5530-5533.

pyramidal structures). Faceted nanopatterned GaAs pyramids²⁸⁷ can be grown via CVD; **Figure 3-25** shows the three unique GaAs pyramid shapes A, B, and C in top and side view, indicating a pyramidal height ranging from 30-90 nm in pyramids A, B, and C, respectively. Simulated growth MBE morphologies for GaAs show the same formations.²⁸⁸

Figure 3-25. Left: Top-view SEM images and the corresponding structural schematics of three unique types of GaAs pyramids. **Right:** Cross-sectional SEM images of the three types of GaAs pyramids.²⁸⁹



²⁸⁷ P.S. Wong, G. Balakrishnan, N. Nuntawong, J. Tatebayashi, D.L. Huffaker, "Controlled InAs quantum dot nucleation on faceted nanopatterned pyramids," Appl. Phys. Lett. 90(2007):183103; http://www.ee.ucla.edu/~huffaker/Documents/117_APL_90_183103_PQDs.pdf.

²⁸⁸ M. Ohtsuka, A. Suzuki, "Simulation of epitaxial growth over patterned substrates," J. Crystal Growth 95(February 1989):55-59.

²⁸⁹ P.S. Wong, G. Balakrishnan, N. Nuntawong, J. Tatebayashi, D.L. Huffaker, "Controlled InAs quantum dot nucleation on faceted nanopatterned pyramids," Appl. Phys. Lett. 90(2007):183103; http://www.ee.ucla.edu/~huffaker/Documents/117_APL_90_183103_PQDs.pdf.

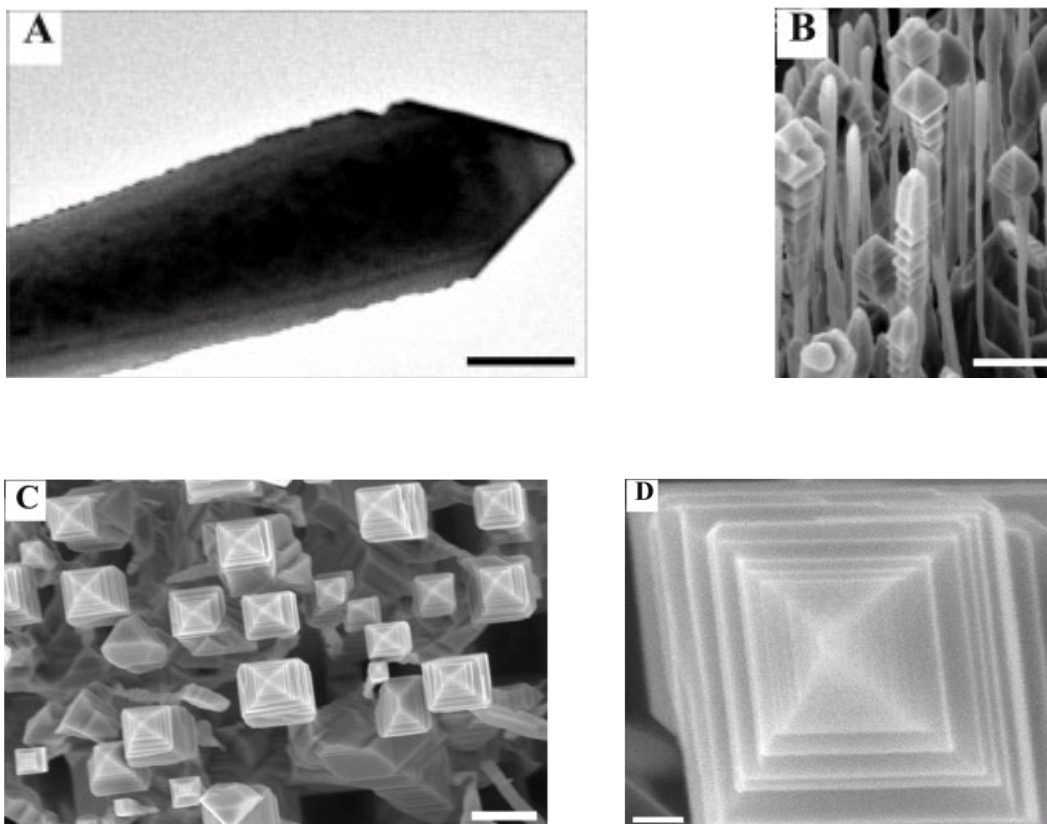
Denisov et al.²⁹⁰ has investigated the formation of heteroepitaxial structures with InAs nanoclusters in an Si matrix during molecular-beam epitaxy with variations in the parameters of these structures due to thermal annealing. The deposition of InAs onto the Si(100) surface at certain temperatures brings about the formation of tetrahedral nanopyramids with {111} orientation of the lateral faces. InAs nanoislands can be epitaxially overgrown with silicon, which leads to gradual smoothing of the three-dimensional relief. After annealing under vacuum, the Si/InAs/Si(100) structures are stable at temperatures up to 700 °C.

Large-scale single-crystal magnetite (Fe₃O₄) nanopyramids have been fabricated in arrays by CH₄ and N₂ plasma sputtering of hematite (0001) wafers without using any template or catalyst.²⁹¹ After a 2-hour sputtering time, the magnetite nanopyramids stand about 3 microns tall and is capped with a fairly uniform “Egyptian pyramid” structure at the very top having many layers, four triangular faces, a rectangular base typically 400-500 nm on an edge and a flat plateau at the tip measuring ~20 nm square (**Figure 3-26**).

²⁹⁰ D.V. Denisov, I.T. Serenkov, V.I. Sakharov, G.É. Tsyrlin, V.M. Ustinov, “Molecular-beam epitaxy and properties of heterostructures with InAs nanoclusters in an Si matrix,” *Physics of the Solid State* 45(November 2003):2194-2202; translated from *Fizika Tverdogo Tela*, Vol. 45, No. 11, 2003, pp. 2090-2098.

²⁹¹ Fei Liu, Peijiang Cao, Huairuo Zhang, Jifa Tian, Congwen Xiao, Chengmin Shen, Jianqi Li, Hongjun Gao, “Novel Nanopyramid Arrays of Magnetite,” *Adv. Mater.* 17(2005):1893-1897;
<http://nano.iphy.ac.cn/N04/subgroup/cvd-chem%20lab%20publication/Adv%20Mater-Nanopyramid.pdf>.

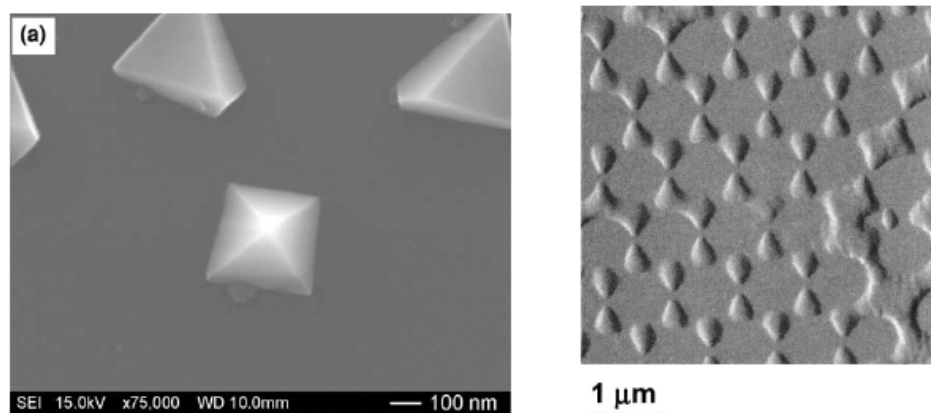
Figure 3-26. Single-crystal magnetite nanopyramids. (A) Typical TEM image of the nanopyramid; scale bar = 100 nm. (B) Side view and (C) top view of the nanopyramids; scale bars = 1 micron. (D) High-resolution image of the nanopyramid cap; scale bar = 100 nm.²⁹²



²⁹² Fei Liu, Peijiang Cao, Huairuo Zhang, Jifa Tian, Congwen Xiao, Chengmin Shen, Jianqi Li, Hongjun Gao, "Novel Nanopyramid Arrays of Magnetite," *Adv. Mater.* 17(2005):1893-1897;
<http://nano.iphy.ac.cn/N04/subgroup/cvd-chem%20lab%20publication/Adv%20Mater-Nanopyramid.pdf>.

Nanopyramids of In_2O_3 have been formed²⁹³ on Si(111) substrate via atmospheric-pressure CVD (Figure 3-27A).²⁹⁴ BaTiO_3 forms 3-sided nanopyramids (Figure 3-27B) having a height of ~45 nm and a width of ~200 nm at half-height, using nanosphere lithography.²⁹⁵

Figure 3-27. (A) Left: In_2O_3 pyramidal nanocrystals were grown on a Si(111) substrate surface at 600 °C via the reaction of In and NH_4Cl .²⁹⁶ (B) Right: Contact mode AFM image (deflection image) of the annealed well-ordered BaTiO_3 pyramidal nanostructures.²⁹⁷



²⁹³ Ye Zhang, Hongbo Jia, Dapeng Yu, Xuhui Luo, Zhensheng Zhang, Xihong Chen, Cheoljin Lee, "Shape-controllable synthesis of indium oxide structures: Nanopyramids and nanorods," J. Mater. Res. 18(December 2003):2793-2798. See also: H.B. Jia, Y. Zhang, X.H. Chen, J. Shu, X.H. Luo, Z.S. Zhang, D.P. Yu, Appl. Phys. Lett. 82(2003):4146. P. Guha, S. Kar, S. Chaudhuri, "Direct synthesis of single crystalline In_2O_3 nanopyramids and nanocolumns and their photoluminescence properties," Appl. Phys. Lett. 85(25 October 2004):3851-3853. Soumitra Kar, Supriya Chakrabarti, Subhadra Chaudhuri, "Morphology dependent field emission from In_2O_3 nanostructures," Nanotechnology 17(28 June 2006):3058-3062. Matthew Zervos, Demetra Tsokkou, Maria Pervolaraki, Andreas Othonos, "Low Temperature Growth of In_2O_3 and InN Nanocrystals on Si(111) via Chemical Vapour Deposition Based on the Sublimation of NH_4Cl in In," Nanoscale Res. Lett. 4(2009):491-497; <http://www.nanoarchive.org/5532/1/fulltext.pdf>.

²⁹⁴ Matthew Zervos, Demetra Tsokkou, Maria Pervolaraki, Andreas Othonos, "Low Temperature Growth of In_2O_3 and InN Nanocrystals on Si(111) via Chemical Vapour Deposition Based on the Sublimation of NH_4Cl in In," Nanoscale Res. Lett. 4(2009):491-497; <http://www.nanoarchive.org/5532/1/fulltext.pdf>.

²⁹⁵ Wenhui Ma, Catalin Harnagea, Dietrich Hesse, Ulrich Gosele, "Well-ordered arrays of pyramid-shaped ferroelectric BaTiO_3 nanostructures," Appl. Phys. Lett. 83(3 November 2003):3770-3773; http://www.mpi-halle.mpg.de/mpi/publi/pdf/4679_03.pdf.

²⁹⁶ Matthew Zervos, Demetra Tsokkou, Maria Pervolaraki, Andreas Othonos, "Low Temperature Growth of In_2O_3 and InN Nanocrystals on Si(111) via Chemical Vapour Deposition Based on the Sublimation of NH_4Cl in In," Nanoscale Res. Lett. 4(2009):491-497; <http://www.nanoarchive.org/5532/1/fulltext.pdf>.

²⁹⁷ Wenhui Ma, Catalin Harnagea, Dietrich Hesse, Ulrich Gosele, "Well-ordered arrays of pyramid-shaped ferroelectric BaTiO_3 nanostructures," Appl. Phys. Lett. 83(3 November 2003):3770-3773; http://www.mpi-halle.mpg.de/mpi/publi/pdf/4679_03.pdf.

Nanopyramids (with varying geometries and surface roughness) have also been reported for AlN,²⁹⁸ BiVO₄,²⁹⁹ CdO,³⁰⁰ CdS,³⁰¹ CdSe,³⁰² GaN,³⁰³ InP,³⁰⁴ LaTiO₃(001) on SrTiO₃(100) substrate,³⁰⁵ NaTaO₃,³⁰⁶ PbS,³⁰⁷ Pb(Zr_{0.52}Ti_{0.48})O₃ (PZT),³⁰⁸ In-doped SnO₂,³⁰⁹ and ZnO.³¹⁰

²⁹⁸ Jie Zheng, Xubo Song, Bo Yu, "Asymmetrical AlN nanopyramids induced by polar surfaces," Appl. Phys. Lett. 90(2007):193121.

²⁹⁹ Jinzhan Su, Liejin Guo, Sorachon Yoriya, Craig A. Grimes, "Aqueous Growth of Pyramidal-Shaped BiVO₄ Nanowire Arrays and Structural Characterization: Application to Photoelectrochemical Water Splitting," Cryst. Growth Des. 10(2010):856-861.

³⁰⁰ Uros Cvelbar, Kostya (Ken) Ostrikov, Miran Mozetic, "Reactive oxygen plasma-enabled synthesis of nanostructured CdO: tailoring nanostructures through plasma-surface interactions," Nanotechnology 19(2008):405605.

³⁰¹ Guoan Tai, Wanlin Guo, "Sonochemistry-assisted microwave synthesis and optical study of single-crystalline CdS nanoflowers," Ultrasonics Sonochemistry 15(April 2008):350-356; <http://nsi.nuaa.edu.cn/html/edit/uploadfile/system/20090921/20090921172855229.pdf>.

³⁰² J.H. Cheng, H.Y. Chao, Y.H. Chang, C.H. Hsu, C.L. Cheng, T.T. Chen, Y.F. Chen, M.W. Chu, "Growth and characterization of CdSe nanoneedles and other one-dimensional CdSe nanostructures," Physica E 40(2008):2000-2003; <http://ntur.lib.ntu.edu.tw/bitstream/246246/163727/1/131.pdf>.

³⁰³ Hock M. Ng, Nils G. Weimann, Aref Chowdhury, "GaN nanotip pyramids formed by anisotropic etching," J. Appl. Phys. 94(1 July 2003):650. Chaowang Liu, Alexander Satka, Lethy Krishnan Jagadamma, Paul R. Edwards, Duncan Allsopp, Robert W. Martin, Philip Shields, Jaroslav Kovac, Frantisek Uherek, Wang Wang, "Light Emission from InGaN Quantum Wells Grown on the Facets of Closely Spaced GaN Nano-Pyramids Formed by Nano-Imprinting," Appl. Phys. Express 2(2009):121002.

³⁰⁴ T. Ujihara, Y. Yoshida, W.S. Lee, Y. Takeda, "Size uniformity of InAs dots on mesa-structure templates on (001) InP substrates grown by droplet metal-organic vapor phase epitaxy method," Appl. Phys. Lett. 89(2006):083110.

³⁰⁵ Lei Bi, Hyun-Suk Kim, Gerald F. Dionne, C.A. Ross, Hanjong Paik, Yun Chang Park, "Orientation control and self-assembled nanopyramid structure of LaFeO₃ films epitaxially grown on SrTiO₃(001) substrates," Appl. Phys. Lett. 95(December 2009):121908.

³⁰⁶ Xingfu Zhou, Ying Chen, Hua Mei, Zhaolin Hu, Yiqun Fan, "A facile route for the preparation of morphology-controlled NaTaO₃ films," Applied Surface Science 255(30 December 2008):2803-2807.

³⁰⁷ R.R. Hawaldar, G.G. Umarji, S.A. Ketkar, S.D. Sathaye, U.P. Mulik, D.P. Amalnerkar, "Nanoscale multilayer PbS thin films fabricated by liquid-liquid interface reaction technique for solar photovoltaic applications," Materials Science and Engineering: B 132(25 July 2006):170-173.

³⁰⁸ J.X. Zhang, J.Y. Dai, W. Lu, H.L.W. Chan, B. Wu, D.X. Li, "A novel nanostructure and multiferroic properties in Pb(Zr_{0.52}Ti_{0.48})O₃/CoFe₂O₄ nanocomposite films grown by pulsed-laser deposition," J. Phys. D: Appl. Phys. 41(7 December 2008):235405.

³⁰⁹ D. Maestre, A. Cremades, J. Piqueras, L. Gregoratti, "Thermal growth and structural and optical characterization of indium tin oxide nanopyramids, nanoislands, and tubes," J. Appl. Phys. 103(12 May 2008):093531.

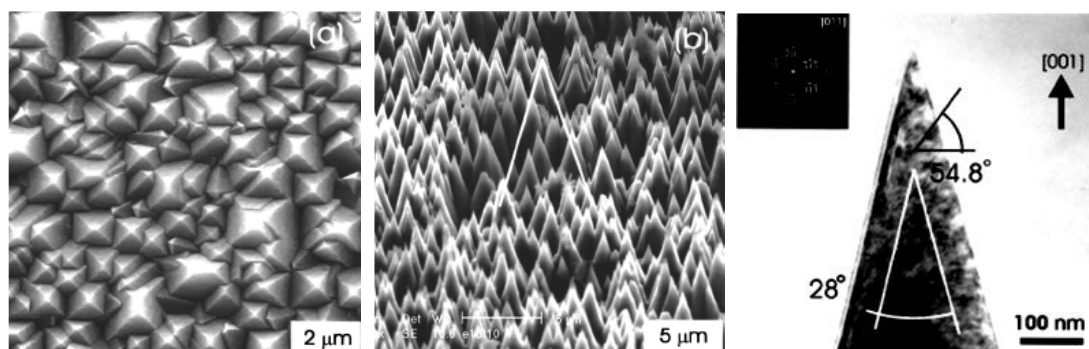
In 2003, Zhang et al.³¹¹ fabricated arrays of single-crystal diamond nanocones (uniformly distributed over large areas on silicon substrates) (Figure 3-28) by performing bias-assisted reactive ion etching in hydrogen plasma of a diamond film deposited on a silicon substrate using a commercial microwave plasma CVD reactor equipped with a 1.5 kW microwave generator. Each diamond cone is a single crystal with an apical angle as small as 28° and a very sharp tip radius of ~2 nm (~10 carbon atoms wide), with its (001) axis perpendicular to the substrate surface and parallel to the other cones in the array. Other methods are known for preparing diamond cones with tip radius of 10-50 nm³¹² but many yield nanocrystalline diamond, diamond-like carbon (DLC), or amorphous carbon structures.

³¹⁰ Jason B. Baxter, Feng Wu, Eray S. Aydil, "Growth mechanism and characterization of zinc oxide hexagonal columns," Appl. Phys. Lett. 83(2003):3797-3799. G.A. Emelchenko, "Deliverable No. 29.5: Report on Design parameters of ZnO-based resonator," PHOREMOST Project, Project Number: 511616, EU IST-511616, Institute of Solid State Physics RAS, June 2006; http://www.phoremot.org/UserFiles/File/Documents/Deliverables_Month24/Phoremot_D29.5.pdf. Hongsheng Chen, Junjie Qi, Yue Zhang, Xiaomei Zhang, Qingliang Lia, Yunhua Huang, "Controlled growth and field emission properties of zinc oxide nanopyramid arrays," Applied Surface Science 253(15 September 2007):8901-8904.

³¹¹ W.J. Zhang, X.M. Meng, C.Y. Chan, Y. Wu, I. Bello, S.T. Leeb, "Oriented single-crystal diamond cones and their arrays," Appl. Phys. Lett. 82(21 April 2003):2622-2624; http://137.99.79.133/halld/diamonds/BNLdev-1-2009/ApplPhysLett_82_2622.pdf. See also: W. J. Zhang, Y. Wu, W.K. Wong, X.M. Meng, C.Y. Chan, I. Bello, Y. Lifshitz, S.T. Lee, "Structuring nanodiamond cone arrays for improved field emission," Appl. Phys. Lett. 83(October 2003):3365-3367.

³¹² Chii-Ruey Lin, Tzyy-Jiann Wang, Kwang-Chang Chen, Chih-Hong Chang, "Nano-tip diamond-like carbon fabrication utilizing plasma sheath potential drop technique," Materials Chemistry and Physics 72(1 November 2001):126-129. Zongli Wang, Changzhi Gu, Junjie Li, Zheng Cui, "A novel method for making high aspect ratio solid diamond tips," Microelectronic Engineering 78-79(March 2005):353-358. Z.L. Wang, Q. Wang, H.J. Li, J.J. Li, P. Xu, Q. Luo, A.Z. Jin, H.F. Yang, C.Z. Gu, "The field emission properties of high aspect ratio diamond nanocone arrays fabricated by focused ion beam milling," Science and Technology of Advanced Materials 6(October 2005):799-803. Q. Yang, T. Hamilton, C. Xiao, A. Hirose, A. Moewes, "Plasma-enhanced synthesis of diamond nanocone films," Thin Solid Films 494(3 January 2006):110-115. Q. Wang, J.J. Li, A.Z. Jin, Z.L. Wang, P. Xu, C.Z. Gu, "The growth and characterization of diamond cone arrays formed by plasma etching," Diamond and Related Materials 15(April-August 2006):866-869. Q. Wang, Z.L. Wang, J.J. Li, Y. Huang, Y.L. Li, C.Z. Gu, Z. Cui, "Field electron emission from individual diamond cone formed by plasma etching," Appl. Phys. Lett. 89(8 August 2006):063105.

Figure 3-28. Left: SEM image of a (001)-oriented pyramidal-shaped diamond film prepared for cone-array fabrication. **Middle:** A single-crystal diamond cone array collected from a sample tilted in an angle of 45° towards the SEM detector; note that nearly all diamond cones are uniform in both size and aspect ratio. **Right:** Low-magnification TEM image of a single diamond cone with a ~ 2 nm tip elucidating its sharpness and orientation; the corresponding transmission electron diffraction inserted indicates its single-crystal nature.³¹³



3.10 Field-Assisted Tip Sharpening

Under the influence of a high electrostatic field, electrons can be emitted from a metallic surface into vacuum; this purely quantum mechanical phenomenon is called field emission. Much of the material in the following four sections is drawn from the excellent review by Lucier.³¹⁴

The field ion microscope (FIM) is operated in a UHV chamber which is back-filled with an imaging gas, usually an inert gas such as helium, neon or argon, to partial pressures typically in the 10^{-5} mbar range. The specimen is a sharp tip, which is positively biased to high voltages of several kV and often cooled down to liquid nitrogen temperatures. A magnified, high resolution image of the tip apex surface is produced on a phosphorous screen placed some centimeters away from the specimen through the physical process called field ionization. There is a value of the electric field for which the contrast in a FIM image is best and maximum surface detail can be

³¹³ W.J. Zhang, X.M. Meng, C.Y. Chan, Y. Wu, I. Bello, S.T. Leeb, "Oriented single-crystal diamond cones and their arrays," Appl. Phys. Lett. 82(21 April 2003):2622-2624; http://137.99.79.133/halld/diamonds/BNLdev-1-2009/ApplPhysLett_82_2622.pdf. See also: W. J. Zhang, Y. Wu, W.K. Wong, X.M. Meng, C.Y. Chan, I. Bello, Y. Lifshitz, S.T. Lee, "Structuring nanodiamond cone arrays for improved field emission," Appl. Phys. Lett. 83(October 2003):3365-3367.

³¹⁴ Anne-Sophie Lucier, "Preparation and Characterization of Tungsten Tips Suitable for Molecular Electronics Studies," M.S. Thesis, Center for the Physics of Materials, Department of Physics, McGill University, Montreal, Quebec, Canada, February 2004; <http://www.physics.mcgill.ca/~peter/theses/lucier.pdf>. See also: Anne-Sophie Lucier, Henrik Mortensen, Yan Sun, and Peter Grütter, "Determination of the atomic structure of scanning probe microscopy tungsten tips by field ion microscopy," Phys. Rev. B 72, 235420 (2005).

obtained. This value is called the best image field (BIF) and depends notably on the imaging gas used.³¹⁵ Although the definition of a “best image” could be somewhat subjective, many investigators seem to have agreed over the years that fields of 44 V/nm for helium, 37.5 V/nm for neon and 22 V/nm for argon and hydrogen yield the clearest FIM images.³¹⁶ The existence of a BIF also implies that there must be a corresponding best image voltage (BIV) that has to be applied to the tip in order to get the sharpest FIM image.³¹⁷

A useful application of the FIM regarding the preparation of tungsten tips is the possibility of engineering the atomic structure of the apex through the physical process called field evaporation. If properly mastered, field evaporation can lead to a controlled removal of individual tungsten atoms from the tip; a stable apex terminating in very few atoms can then be achieved. Under the influence of a strong electric field, atoms bound to the tip surface may escape into vacuum in the form of ions. If the emitted ions were lattice atoms, the phenomenon is called field evaporation. If these ions were adsorbates on the tip, then the process is referred to as field desorption. There is no theoretical distinction between these two cases – field evaporation is often thought of as a particular type of field desorption.³¹⁸

One consequence of the field evaporation process is the development of an atomically smooth tip surface as the voltage is gradually raised towards the BIV. Since the local electric field is enhanced above protrusions and sharp edges, the most prominent surface atoms will field evaporate at a lower voltage than the atoms belonging to smooth regions of the apex;³¹⁹ a uniform apex surface composed of various well resolved crystallographic poles is thus exposed at BIV. Since the resulting apex shape has a nearly hemispherical end-form, the image distortion is minimal³²⁰ and the surface can look as ordered as the bulk lattice.³²¹ One can then conclude that

³¹⁵ T.T. Tsong, *Atom-Probe Field Ion Microscopy*, Cambridge University Press, 1990. J.A. Panitz, “Field-ion microscopy-a review of basic principles and selected applications,” *J. Phys. E: Sci. Instrum.* 15(December 1982):1281-1294; http://japanitz.com/japanitz/publications_files/Field-ion%20microscopy-a%20review%20of%20basic%20principles%20and%20selected%20applications.pdf.

³¹⁶ T.T. Tsong, *Atom-Probe Field Ion Microscopy*, Cambridge University Press, 1990.

³¹⁷ K.M. Bowkett, D.A. Smith, “Field-Ion Microscopy,” in: *Defects in Crystalline Solids*, Volume 2, North Holland Publishing Company, 1970. T.T. Tsong, *Atom-Probe Field Ion Microscopy*, Cambridge University Press, 1990.

³¹⁸ T.T. Tsong, *Atom-Probe Field Ion Microscopy*, Cambridge University Press, 1990. M.K. Miller, A. Cerezo, M.G. Hetherington, G.D.W. Smith, *Atom Probe Field Ion Microscopy*, Oxford University Press, 1996. J.A. Panitz, “Field-ion microscopy-a review of basic principles and selected applications,” *J. Phys. E: Sci. Instrum.* 15(December 1982):1281-1294; http://japanitz.com/japanitz/publications_files/Field-ion%20microscopy-a%20review%20of%20basic%20principles%20and%20selected%20applications.pdf.

³¹⁹ M.K. Miller, A. Cerezo, M.G. Hetherington, G.D.W. Smith, *Atom Probe Field Ion Microscopy*, Oxford University Press, 1996.

³²⁰ T.T. Tsong, *Atom-Probe Field Ion Microscopy*, Cambridge University Press, 1990.

³²¹ J.A. Panitz, “Field-ion microscopy-a review of basic principles and selected applications,” *J. Phys. E: Sci. Instrum.* 15(December 1982):1281-1294; http://japanitz.com/japanitz/publications_files/Field-ion%20microscopy-a%20review%20of%20basic%20principles%20and%20selected%20applications.pdf.

while FIM is a unique tip characterization tool, it induces substantial blunting of the tip apex which compromises the ultimate resolution achieved by the STM. To obtain an atomically sharp tip, a smooth and stable field evaporated end-form should first be obtained at BIV, followed by careful successive field evaporation of single atoms until a sharp apex configuration is achieved.

Since the evaporation field of the tip material is higher than the BIF of the imaging gas, field evaporation of a single atom from a stable and atomically smooth apex surface is experimentally achieved as follows: while carefully observing the “live” FIM image, one increases the tip voltage very slowly above the BIV until the onset of field evaporation. Once an apex atom “disappears” from the FIM image, the voltage must then be quickly lowered back to its BIV value to prevent further field evaporation of lattice atoms. These field evaporation steps are repeated until the desired apex configuration is obtained.

Lucier³²² successfully applied this technique to a (111) oriented tungsten tip. The field evaporation steps reduced the number of atoms on the topmost layer of the apex from 5 to 3. The resulting (111) trimer was the sharpest apex Lucier could obtain. Lucier did not manage to engineer an apex terminating in a single atom since the trimer field evaporated as a single unit. If the trimer is accidentally field evaporated, it is possible to resume the controlled field evaporation process on the freshly exposed (111) layer in order to recover a sharp apex. However, since the process of field evaporation is statistical in nature, it is very difficult to predict the exact order of the evaporation sequence for more than a couple of steps. Note also that because field evaporation is thermally activated, the field evaporation rate will depend notably on the vibrational amplitude of the surface atoms. Controlled removal of single atoms will thus be much easier at low temperatures, due to the higher stability of the atomic structure above BIV.

Some thought must also be given to the choice of the crystallographic orientation of the top electrode, since the ease with which it can be atomically engineered and the stability of the resulting apex configuration depends on the work function of the apex plane and on its activation energy for surface diffusion. Since planes with a higher work function have a slightly lower evaporation field due to the details of their electronic structure and to the larger amount of energy returned to the lattice upon reentering of the electrons in the tip surface,³²³ and since these planes are closely packed and thus have a larger interplanar spacing which enhances the field at their edges, atoms belonging to these planes will be preferentially evaporated at lower voltages. This explains why the (110) planes, which have the highest work function ($\Phi_{110} = 5.25$ eV) for tungsten and a large step heights of 2.23 Å, always develop into larger, more open facets on all

³²² Anne-Sophie Lucier, “Preparation and Characterization of Tungsten Tips Suitable for Molecular Electronics Studies,” M.S. Thesis, Center for the Physics of Materials, Department of Physics, McGill University, Montreal, Quebec, Canada, February 2004; <http://www.physics.mcgill.ca/~peter/theses/lucier.pdf>. See also: Anne-Sophie Lucier, Henrik Mortensen, Yan Sun, and Peter Grütter, “Determination of the atomic structure of scanning probe microscopy tungsten tips by field ion microscopy,” *Phys. Rev. B* 72, 235420 (2005).

³²³ K.M. Bowkett, D.A. Smith, “Field-Ion Microscopy,” in: *Defects in Crystalline Solids*, Volume 2, North Holland Publishing Company, 1970. T.T. Tsong, *Atom-Probe Field Ion Microscopy*, Cambridge University Press, 1990. M.K. Miller, A. Cerezo, M.G. Hetherington, G.D.W. Smith, *Atom Probe Field Ion Microscopy*, Oxford University Press, 1996.

our FIM images taken at BIV. These planes are quite difficult to engineer in a controlled fashion, due to the lower energy required to field evaporate the atoms. The onset of field evaporation tends to happen at a voltage too close to BIV to allow field evaporation of single atoms. If the voltage is slightly raised above BIV, an entire layer of (110) atoms quickly field evaporates. Lucier found that any apex configuration obtained on a (110) plane is not stable for more than a couple of minutes at BIV.

The (111) orientation, with a lower work function $\Phi_{111} = 4.47$ eV, a more loosely packed structure and a smaller interplanar spacing ($s = 0.91$ Å), is much easier to engineer. Since the gap between the BIV value and the field evaporation voltage is greater for the (111) plane than it is for the (110) plane, the (111) trimer remains very stable at BIV. Another advantage of the (111) trimer is its high stability against surface diffusion. The diffusion rate of single atoms on the (111) plane is basically negligible even at room temperature,³²⁴ since the activation energy for single atom self-diffusion is ~ 1.8 eV for the tungsten (111) plane.³²⁵ Atoms on the (110) plane are much more mobile and surface diffusion on this plane is quite rapid – the activation energy for surface diffusion on the (110) plane is about ~ 0.9 eV.³²⁶ A similar method called field-enhanced diffusion-growth (FDG)³²⁷ can form a nano-protrusion terminated with a few atoms or less at room temperature (unlike the conventional method by Binh et al.).

We can conclude that a (111) oriented tungsten tip can more easily be engineered into a sharp and stable apex terminating in 3 atoms. Additionally, a single atom tip can be obtained from the 3-atom tip by vapor deposition of an atom onto the (111) trimer, a technique already successfully developed by Fink.³²⁸ Due to the loosely packed structure of the trimer and the high activation energy for surface diffusion on the (111) plane, the vapor deposited atom creates a very stable protrusion.³²⁹ Furthermore, this single-atom protrusion could be made of a different metal than the underlying tungsten tip, and could even have a lower evaporation field (bulk property) than

³²⁴ M.K. Miller, A. Cerezo, M.G. Hetherington, G.D.W. Smith, *Atom Probe Field Ion Microscopy*, Oxford University Press, 1996. O. Nishikawa, M. Tomitori, F. Katsuki, "Arrangement and stability of atoms at the apex of a scanning tip," *J. Microscopy* 152(1988):637-641.

³²⁵ H.W. Fink, "Mono-atomic tips for scanning tunneling microscopy," *IBM J. Res. Develop.* 30(1986):460-465.

³²⁶ T.T. Tsong, *Atom-Probe Field Ion Microscopy*, Cambridge University Press, 1990.

³²⁷ K. Nagaoka, H. Fujii, K. Matsuda, M. Komaki, Y. Murata, C. Oshima, T. Sakurai, "Field emission spectroscopy from field-enhanced diffusion-growth nano-tips," *Appl. Surf. Sci.* 182(5 October 2001):12-19.

³²⁸ H.W. Fink, "Mono-atomic tips for scanning tunneling microscopy," *IBM J. Res. Develop.* 30(1986):460-465.

³²⁹ M.K. Miller, A. Cerezo, M.G. Hetherington, G.D.W. Smith, *Atom Probe Field Ion Microscopy*, Oxford University Press, 1996.

the BIF of helium, as has been experimentally demonstrated by the imaging of gold atoms deposited on a (111) tungsten tip.³³⁰

In common use, ultrasharp tips can become blunted (Figure 3-29A). A popular method to sharpen a blunt tungsten tip, called field-assisted annealing, consists in annealing the tip in the presence of an electric field with a high gradient in order to create a sharp asperity at the apex.³³¹ While the oxygen treatment described in Section 3.11 leads to a sharpening of the tip by increasing the tungsten evaporation rate with respect to the surface diffusion rate, the field assisted annealing technique lowers the overall blunting rate by generating a surface diffusion flux opposite to the heat induced matter transport.

The mechanics of the field assisted annealing technique can be explained as follows.³³² When a voltage is applied to a tip, a surface field gradient develops along the tip and this field gradient induces a surface diffusion flux from regions of low field strength to those of higher field strength. Since the field increases with curvature, atoms are thus forced to move from the shank back to the apex. This counterbalances the self-diffusion of atoms caused by capillary forces. For temperatures between 1600 and 1800 K and for an applied voltage of 2 to 3 kV, the directional effect of the applied electric field dominates over the matter transport due to capillary forces and from this, a sharp protrusion can “build up” at the apex (Figure 3-29B). More specifically, the local rearrangement of atoms leads to an enlargement of some low index planes. This enlargement self-terminates when two neighboring planes meet each other and a sharp protrusion results from the intersection at the apex of the so-called “build-up” planes.

It has been reported that this “build-up” process works beautifully for (111) oriented tungsten tips. A three-atom protrusion can be routinely obtained from the meeting of the three (112) “build-up” planes.³³³ However, the ease with which asperities can be created on the (111) family of planes might prevent this technique from being successfully applied to some other tip orientations: undesired side protrusions from the (111) planes have been observed when

³³⁰ A. Schirmeisen, *Metallic Adhesion and Tunneling at the Atomic Scale*, PhD thesis, McGill University, Canada, 1999.

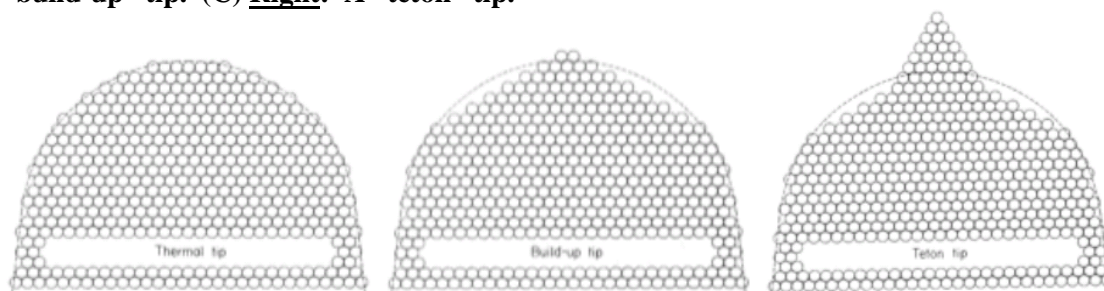
³³¹ U. Staufer, L.P. Muray, D.P. Kern, T.H.P. Chang, “Investigation of emitter tips for scanning tunneling microscope-based microprobe systems,” *J. Vac. Sci. Technol. B* 9(November 1991):2962-2966. J.A. Meyer, S.J. Stranick, J.B. Wang, P.S. Weiss, “Field emission current-voltage curves as a diagnostic for scanning tunneling microscope tips,” *Ultramicroscopy*, 42-44(July 1992):1538-1541. V.T. Binh, J. Marien, “Characterization of microtips for scanning tunneling microscopy,” *Surf. Sci.* 202(1 August 1988):L539-L549. V.T. Binh, “In Situ Fabrication and Regeneration of Microtips for Scanning Tunnelling Microscopy,” *J. Microsc.* 152(November 1988):355-361.

³³² V.T. Binh, J. Marien, “Characterization of microtips for scanning tunneling microscopy,” *Surf. Sci.* 202(1 August 1988):L539-L549. V.T. Binh, “In Situ Fabrication and Regeneration of Microtips for Scanning Tunnelling Microscopy,” *J. Microsc.* 152(November 1988):355-361.

³³³ V.T. Binh, J. Marien, “Characterization of microtips for scanning tunneling microscopy,” *Surf. Sci.* 202(1 August 1988):L539-L549. V.T. Binh, “In Situ Fabrication and Regeneration of Microtips for Scanning Tunnelling Microscopy,” *J. Microsc.* 152(November 1988):355-361.

annealing a (310) oriented tungsten tip in an electric field.³³⁴ The “build-up” technique also proved to be effective in the creation of sharp (100) oriented tungsten tips – in this case, the protrusion resulted from the intersection of four (110) planes.³³⁵

Figure 3-29. (A) Left: Schematic representation of a tungsten thermal tip. (B) Middle: A “build-up” tip. (C) Right: A “teton” tip.³³⁶



The sharpening effect can be enhanced if the “build-up” process is combined to the oxygen treatment described in [Section 3.11](#). The resulting technique is called the corrosion-field process and leads to the formation of a pyramidal microtip erected on top of a support tip of larger radius; for a (111) oriented tungsten tip, this “teton” tip geometry ([Figure 3-29C](#)) usually ends with a single atom.³³⁷

3.11 Tip Sharpening by Oxygen Annealing

Tungsten tip sharpening can result from the interaction of tungsten with oxygen at high temperatures; the sharpening of W tips by oxidation and annealing was first reported by Müller in 1938.³³⁸ When the tip is annealed in an oxygen atmosphere, the oxygen reacts with the tungsten atoms at the surface of the tip, forming various tungsten oxides which are volatile at

³³⁴ U. Stauffer, L.P. Muray, D.P. Kern, T.H.P. Chang, “Investigation of emitter tips for scanning tunneling microscope-based microprobe systems,” *J. Vac. Sci. Technol. B* 9(November 1991):2962-2966.

³³⁵ Y. Kuk, P.J. Silverman, “Role of tip structure in scanning tunneling microscopy,” *Appl. Phys. Lett.* 48(9 June 1986):1597-1599.

³³⁶ V.T. Binh, J. Marien, “Characterization of microtips for scanning tunneling microscopy,” *Surf. Sci.* 202(1 August 1988):L539-L549. V.T. Binh, “In Situ Fabrication and Regeneration of Microtips for Scanning Tunnelling Microscopy,” *J. Microsc.* 152(November 1988):355-361.

³³⁷ 38. V.T. Binh, J. Marien, “Characterization of microtips for scanning tunneling microscopy,” *Surf. Sci.* 202(1 August 1988):L539-L549. V.T. Binh, “In Situ Fabrication and Regeneration of Microtips for Scanning Tunnelling Microscopy,” *J. Microsc.* 152(November 1988):355-361.

³³⁸ E.W. Müller, “Further observations with the field electron microscope,” *Z. für Physik* 108(1938):668-680.

these temperatures. This surface corrosion process leads to an overall removal of material from the tip, provided that the tungsten evaporation rate due to this oxygen treatment is higher than the blunting rate induced by the surface diffusion of atoms on the tip.³³⁹ Therefore, sharpening of the tip will only happen for very specific oxygen pressures and annealing temperatures.

It has been demonstrated that optimal results can be obtained by introducing an oxygen pressure of 5×10^{-4} mbar in a UHV chamber through a gas inlet system and annealing the tip at 1300 K for a few minutes up to many hours; the length of the treatment depends on the initial tip shape and the desired final tip radius.³⁴⁰ The tip temperature is a very critical parameter. Too low a temperature will result in a slow reaction time with no significant sharpening and too high a temperature will cause an increase of the apex radius. It has been reported that the corrosion reaction happens at a preferential rate for certain crystallographic planes, which gives rise to a strong faceting of the tip surface³⁴¹ and seems to lead to a particularly efficient sharpening of (111) oriented tungsten tips.³⁴² However, this method has been successfully used to sharpen polycrystalline tungsten tips as well.³⁴³ Another consequence of the oxygen treatment is the occasional formation of several microtips at the apex,³⁴⁴ although this finger-like structure is not a desirable feature for DMS tips.

Interaction with oxygen also produces facetization of Mo(111) and Mo(100) surfaces.³⁴⁵

³³⁹ Vu Thien Binh, A. Piquet, H. Roux, R. Uzan, M. Drechsler, "Sharpening of metal tips by heat treatment in vacuum," J. Phys. E: Sci. Instrum. 9(May 1976):377-381.

³⁴⁰ H. Wengelnik, H. Neddermeyer, "Oxygen-induced sharpening process of W(111) tips for scanning tunneling microscope use," J. Vac. Sci. Technol. A 8(January 1990):438-440.

³⁴¹ H. Wengelnik, H. Neddermeyer, "Oxygen-induced sharpening process of W(111) tips for scanning tunneling microscope use," J. Vac. Sci. Technol. A 8(January 1990):438-440. H.S. Kim, M.L. Yu, U. Staufer, L.P. Murray, D.P. Kern, T.H.P. Chang, "Oxygen processed field emission tips for microcolumn applications," J. Vac. Sci. Technol. B 11(November 1993):2327-2331.

³⁴² H. Wengelnik, H. Neddermeyer, "Oxygen-induced sharpening process of W(111) tips for scanning tunneling microscope use," J. Vac. Sci. Technol. A 8(January 1990):438-440.

³⁴³ J. Mendez, M. Luna, A.M. Baro, "Preparation of STM W tips and characterization by FEM, TEM and SEM," Surf. Sci. 266(15 April 1992):294-298.

³⁴⁴ H. Wengelnik, H. Neddermeyer, "Oxygen-induced sharpening process of W(111) tips for scanning tunneling microscope use," J. Vac. Sci. Technol. A 8(January 1990):438-440. J. Mendez, M. Luna, A.M. Baro, "Preparation of STM W tips and characterization by FEM, TEM and SEM," Surf. Sci. 266(15 April 1992):294-298.

³⁴⁵ C. Zhang, M.A. van Hove, G.A. Somorjai, "The interaction of oxygen with the Mo(100) and Mo(111) single-crystal surfaces: Chemisorption and oxidation at high temperatures," Surf. Sci. 149(2 January 1985):326-340.

3.12 Electrochemical Etching and Annealing

Electrochemical etching of a metal wire is routinely used to generate sharp STM tips. The basic idea is to dip a small diameter metal wire into an electrolyte solution in which a counterelectrode is sitting and to apply an AC or DC voltage between these two electrodes until enough dissolution of the wire has happened so that it displays a sharp tip shape. The choice of the electrolyte and of the voltage applied depends on the material used to make the tip.³⁴⁶ Among the reasons why tungsten (W) is such a popular material for the production of STM tips is that an extremely sharp tip can be obtained in a single electrochemical step using fairly mild chemicals. One drawback is that the tungsten tip will most likely undergo surface contamination due to its poor resistance to oxidation. However, a proper annealing treatment in UHV can provide a quick and efficient solution to this problem.

Lucier³⁴⁷ made W tips from either a 0.1 mm diameter polycrystalline wire or a 0.13 mm diameter (very high cost) single crystal W(111) oriented wire. The most common electrolytes used for W etching are NaOH and KOH – the community seems divided as to which one is best³⁴⁸ – but Lucier³⁴⁹ used a freshly prepared 7.5 mol/L KOH solution which yielded satisfying results. A

³⁴⁶ L.E. Murr, *Electron and Ion Microscopy and Microanalysis: Principles and Applications*, Second Edition, Marcel Dekker, 1991. K.M. Bowkett, D.A. Smith, "Field-Ion Microscopy," in: *Defects in Crystalline Solids*, Volume 2, North Holland Publishing Company, 1970. T.T. Tsong, *Atom-Probe Field Ion Microscopy*, Cambridge University Press, 1990. M.K. Miller, A. Cerezo, M.G. Hetherington, G.D.W. Smith, *Atom Probe Field Ion Microscopy*, Oxford University Press, 1996.

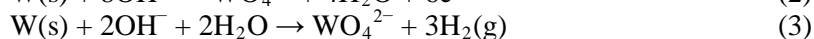
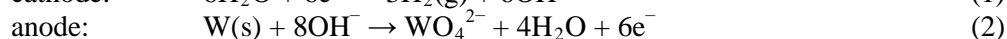
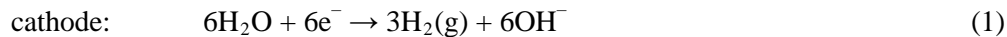
³⁴⁷ Anne-Sophie Lucier, "Preparation and Characterization of Tungsten Tips Suitable for Molecular Electronics Studies," M.S. Thesis, Center for the Physics of Materials, Department of Physics, McGill University, Montreal, Quebec, Canada, February 2004; <http://www.physics.mcgill.ca/~peter/theses/lucier.pdf>. See also: Anne-Sophie Lucier, Henrik Mortensen, Yan Sun, and Peter Grütter, "Determination of the atomic structure of scanning probe microscopy tungsten tips by field ion microscopy," *Phys. Rev. B* 72, 235420 (2005).

³⁴⁸ H. Lemke, T. Goddenhenrich, H.P. Bochem, U. Hartmann, C. Heiden, "Improved microtips for scanning probe microscopy," *Rev. Sci. Instrum.* 61(October 1990):2538-2541. A.I. Oliva, A. Romero G.J.L. Pena, E. Anguiano, M. Aguilar, "Electrochemical preparation of tungsten tips for a scanning tunneling microscope," *Rev. Sci. Instrum.* 67(May 1996):1917-1921. L. Ottaviano, L. Lozzi, S. Santucci, "Scanning Auger microscopy study of W tips for scanning tunneling microscopy," *Rev. Sci. Instrum.* 74(2003):3368-3378. L.E. Murr, *Electron and Ion Microscopy and Microanalysis: Principles and Applications*, Second Edition, Marcel Dekker, 1991. K.M. Bowkett, D.A. Smith, "Field-Ion Microscopy," in: *Defects in Crystalline Solids*, Volume 2, North Holland Publishing Company, 1970. T.T. Tsong, *Atom-Probe Field Ion Microscopy*, Cambridge University Press, 1990. M.K. Miller, A. Cerezo, M.G. Hetherington, G.D.W. Smith, *Atom Probe Field Ion Microscopy*, Oxford University Press, 1996.

³⁴⁹ Anne-Sophie Lucier, "Preparation and Characterization of Tungsten Tips Suitable for Molecular Electronics Studies," M.S. Thesis, Center for the Physics of Materials, Department of Physics, McGill University, Montreal, Quebec, Canada, February 2004; <http://www.physics.mcgill.ca/~peter/theses/lucier.pdf>. See also: Anne-Sophie Lucier, Henrik Mortensen, Yan Sun, and Peter Grütter, "Determination of the atomic structure of scanning probe microscopy tungsten tips by field ion microscopy," *Phys. Rev. B* 72, 235420 (2005).

large-working-distance optical microscope sits in front of the setup so that the tip etching can be carefully observed.

The overall chemical reaction governing this particular electrochemical etching technique is the following:³⁵⁰



The etching takes place at the air/electrolyte interface, and Equation 2 indicates that the tungsten undergoes an oxidative dissolution to tungstate anions (WO_4^{2-}) which are soluble in water. However, the actual reaction is more complex than it appears:³⁵¹ the tungsten is first oxidized to intermediate tungsten oxides; these are in turn non-electrochemically dissolved to yield the soluble tungstate anions which show greatest stability in a basic medium. The reaction also involves the reduction of water, with bubbles of gaseous hydrogen and OH^- ions produced at the cathode (Equation 1).

One can wonder how this reaction actually generates a tip shape out of a cylindrical wire. The explanation³⁵² roots in the fact that capillary forces yield the formation of a meniscus of solution around the tip wire when it is immersed into the electrolyte. The shape of the meniscus plays a very important role in determining the final shape of the tip as the etching rate at the top of the meniscus is a lot slower than at the bottom. This can be explained by the presence of a concentration gradient due to the diffusion of OH^- ions to the tip. Furthermore, the soluble tungstate produced during the reaction flows towards the lower end of the tip wire, generating a dense viscous layer which prevents this region from being etched away. Thus, a necking phenomenon is observed in the meniscus where the etching rate is enhanced. At some point, this part of the wire becomes so thin that its tensile strength cannot sustain the weight of the lower end of the wire – the latter then breaks off, leaving behind a sharp tip. This is commonly referred to as the “drop-off” method (Figure 3-30). (It is claimed by some³⁵³ that adding a mass to the end of the wire may increase the yield of sharp tips.)

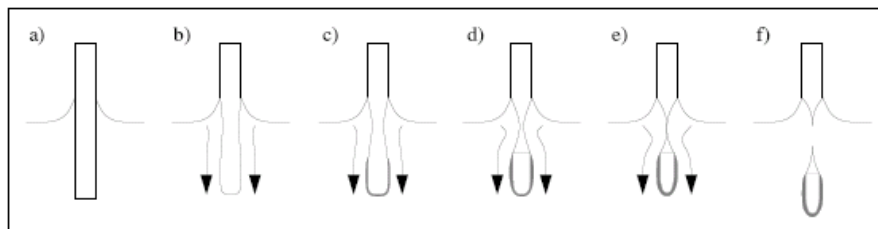
³⁵⁰ J.P. Ibe, P.P. Bey Jr., S.L. Brandow, R.A. Brizzolara, N.A. Burnham, D.P. DiLella, K.P. Lee, C.R.K. Marrian, R.J. Colton, “On the electrochemical etching of tips for scanning tunneling microscopy,” J. Vac. Sci. Technol. A 8(July 1990):3570-3575.

³⁵¹ J.P. Ibe, P.P. Bey Jr., S.L. Brandow, R.A. Brizzolara, N.A. Burnham, D.P. DiLella, K.P. Lee, C.R.K. Marrian, R.J. Colton, “On the electrochemical etching of tips for scanning tunneling microscopy,” J. Vac. Sci. Technol. A 8(July 1990):3570-3575.

³⁵² J.P. Ibe, P.P. Bey Jr., S.L. Brandow, R.A. Brizzolara, N.A. Burnham, D.P. DiLella, K.P. Lee, C.R.K. Marrian, R.J. Colton, “On the electrochemical etching of tips for scanning tunneling microscopy,” J. Vac. Sci. Technol. A 8(July 1990):3570-3575.

³⁵³ Pilkyu Kim, Sungho Jeong, Mun Seok Jeong, Do-Kyeong Ko, Jongmin Lee, “Effects of process parameters on the electrochemical etching of sharp metallic tips with an attached mass,” Rev. Sci. Instrum. 78(26 September 2007):096105.

Figure 3-30. Illustration of the drop-off method: a) shows the formation of the meniscus. b) to e) illustrate the flow of WO_4^{2-} towards the lower end of the wire, the formation of a dense layer of WO_4^{2-} around the bottom of the wire, and the necking phenomenon in the meniscus. In f), the lower part breaks off: the drop-off has occurred.³⁵⁴



Once the etching is completed, it is imperative that the tip should be cleaned immediately by carefully dipping it for a few seconds in distilled water, then rinsing it with acetone and ethanol. The purpose of this step is to remove residues left by the etching process. The tip should then be gently dried with clean compressed nitrogen.

If the electrochemical etching is successful and has been followed by the cleaning procedure described above, then the freshly-made W tip when observed under an optical microscope should crudely resemble the tip presented in [Figure 3-31](#). It should reveal a smooth surface and have a very sharp end that cannot be resolved. Note that on the left image of [Figure 3-31](#) the part of the wire closest to the tip appears more reflective than the rest of it. This is due to a pre-etching operation³⁵⁵ during which 1 mm of the wire is immersed in the electrolyte and etched for 5 seconds, followed by the cleaning steps explained before. This pre-etching, while not removing a significant amount of material, leaves a much smoother and cleaner wire to etch, and seems to improve the quality and reproducibility of the subsequent “real” etching step.³⁵⁶

Of course, not all etched tips will look as nice as the one shown in [Figure 3-31](#). Often the electrochemical etching does not go as smoothly as described above. In fact, Lucier³⁵⁷ reports

³⁵⁴ Anne-Sophie Lucier, “Preparation and Characterization of Tungsten Tips Suitable for Molecular Electronics Studies,” M.S. Thesis, Center for the Physics of Materials, Department of Physics, McGill University, Montreal, Quebec, Canada, February 2004; <http://www.physics.mcgill.ca/~peter/theses/lucier.pdf>. See also: Anne-Sophie Lucier, Henrik Mortensen, Yan Sun, and Peter Grütter, “Determination of the atomic structure of scanning probe microscopy tungsten tips by field ion microscopy,” *Phys. Rev. B* 72, 235420 (2005).

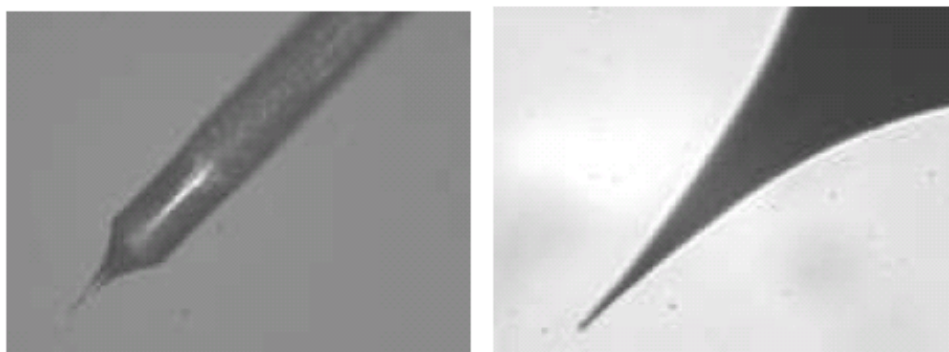
³⁵⁵ I. Ekvall, E. Wahlstrom, D. Claesson, H. Olin, E. Olsson, “Preparation and characterization of electrochemically etched W tips for STM,” *Meas. Sci. Technol.* 10(January 1999):11-18.

³⁵⁶ A. Schirmeisen, *Metallic Adhesion and Tunneling at the Atomic Scale*, PhD thesis, McGill University, Canada, 1999.

³⁵⁷ Anne-Sophie Lucier, “Preparation and Characterization of Tungsten Tips Suitable for Molecular Electronics Studies,” M.S. Thesis, Center for the Physics of Materials, Department of Physics, McGill University, Montreal, Quebec, Canada, February 2004; <http://www.physics.mcgill.ca/~peter/theses/lucier.pdf>. See also: Anne-Sophie Lucier, Henrik Mortensen,

that ~40% of all freshly etched tips have to be discarded due to obvious gross flaws. Many factors must be well controlled to obtain a reasonable success rate.³⁵⁸

Figure 3-31. Freshly electrochemically etched tungsten tip observed under an optical microscope with a 10X magnification on the left and a 50X magnification on the right.³⁵⁹



One can also imagine that a symmetric meniscus will yield a symmetric tip. This is achieved when the angle between the immersed wire and the air/electrolyte interface is close to 90° . However, this is not an easy task and lots of practice is required to be able to mount the tip wire truly perpendicularly onto the tip holder. Figure 3-32 shows scanning electron microscope (SEM) images of two tips etched at different angles with respect to the air/electrolyte interface. The left image shows a tip etched perpendicularly to the liquid surface and its shape exhibits remarkable symmetry, while the tip in the right image illustrates the effect of an asymmetric meniscus.

The length of the immersed part of the wire is another determining parameter in the final tip shape. It is quite intuitive to understand that too small a dipping length will not yield a necking

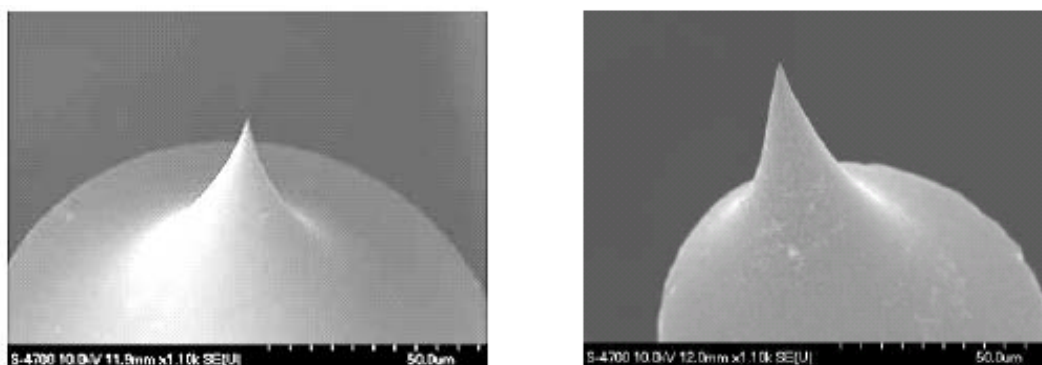
Yan Sun, and Peter Grütter, "Determination of the atomic structure of scanning probe microscopy tungsten tips by field ion microscopy," Phys. Rev. B 72, 235420 (2005).

³⁵⁸ J.P. Ibe, P.P. Bey Jr., S.L. Brandow, R.A. Brizzolara, N.A. Burnham, D.P. DiLella, K.P. Lee, C.R.K. Marrian, R.J. Colton, "On the electrochemical etching of tips for scanning tunneling microscopy," J. Vac. Sci. Technol. A 8(July 1990):3570-3575. Pilkyu Kim, Sungho Jeong, Mun Seok Jeong, Do-Kyeong Ko, Jongmin Lee, "Effects of process parameters on the electrochemical etching of sharp metallic tips with an attached mass," Rev. Sci. Instrum. 78(26 September 2007):096105.

³⁵⁹ Anne-Sophie Lucier, "Preparation and Characterization of Tungsten Tips Suitable for Molecular Electronics Studies," M.S. Thesis, Center for the Physics of Materials, Department of Physics, McGill University, Montreal, Quebec, Canada, February 2004; <http://www.physics.mcgill.ca/~peter/theses/lucier.pdf>. See also: Anne-Sophie Lucier, Henrik Mortensen, Yan Sun, and Peter Grütter, "Determination of the atomic structure of scanning probe microscopy tungsten tips by field ion microscopy," Phys. Rev. B 72, 235420 (2005).

phenomenon.³⁶⁰ However, contradiction exists among authors as to whether or not the quality of the tip increases with the dipping length. It was reported³⁶¹ that the longer the submerged wire, the larger the radius of curvature of the tip. The explanation is that as the length increases, the weight of the part hanging below the neck increases as well; this can cause a premature drop-off and thus possibly produce blunt tips. On the other hand, it was also claimed³⁶² that a longer immersed wire yields a sharper tip. Lucier³⁶³ found that a dipping length of 0.5 mm generally gave good results.

Figure 3-32. SEM images showing the effect that the symmetry of the meniscus has on the tip shape. Left: tip obtained from a symmetric meniscus. Right: tip obtained from an asymmetric meniscus.³⁶⁴



³⁶⁰ A. Schirmeisen, *Metallic Adhesion and Tunneling at the Atomic Scale*, PhD thesis, McGill University, Canada, 1999.

³⁶¹ J.P. Ibe, P.P. Bey Jr., S.L. Brandow, R.A. Brizzolara, N.A. Burnham, D.P. DiLella, K.P. Lee, C.R.K. Marrian, R.J. Colton, "On the electrochemical etching of tips for scanning tunneling microscopy," *J. Vac. Sci. Technol. A* 8(July 1990):3570-3575.

³⁶² A.I. Oliva, A. Romero G.J.L. Pena, E. Anguiano, M. Aguilar, "Electrochemical preparation of tungsten tips for a scanning tunneling microscope," *Rev. Sci. Instrum.* 67(May 1996):1917-1921.

³⁶³ Anne-Sophie Lucier, "Preparation and Characterization of Tungsten Tips Suitable for Molecular Electronics Studies," M.S. Thesis, Center for the Physics of Materials, Department of Physics, McGill University, Montreal, Quebec, Canada, February 2004; <http://www.physics.mcgill.ca/~peter/theses/lucier.pdf>. See also: Anne-Sophie Lucier, Henrik Mortensen, Yan Sun, and Peter Grütter, "Determination of the atomic structure of scanning probe microscopy tungsten tips by field ion microscopy," *Phys. Rev. B* 72, 235420 (2005).

³⁶⁴ Anne-Sophie Lucier, "Preparation and Characterization of Tungsten Tips Suitable for Molecular Electronics Studies," M.S. Thesis, Center for the Physics of Materials, Department of Physics, McGill University, Montreal, Quebec, Canada, February 2004; <http://www.physics.mcgill.ca/~peter/theses/lucier.pdf>. See also: Anne-Sophie Lucier, Henrik Mortensen, Yan Sun, and Peter Grütter, "Determination of the atomic structure of scanning probe microscopy tungsten tips by field ion microscopy," *Phys. Rev. B* 72, 235420 (2005).

Although tungsten is probably the most widely used material to prepare tips for STM applications in UHV, other metals could offer certain advantages. Iridium is an interesting candidate since it is a very stiff material that is much more inert to oxidation than tungsten. On the other hand, its lower chemical reactivity makes it harder to etch and often requires the use of dangerous chemicals.³⁶⁵ A method using relatively benign electrolytes has nonetheless been suggested,³⁶⁶ and Lucier³⁶⁷ has applied it to a 0.25 mm diameter polycrystalline iridium wire.

This published technique advises the use of a CaCl_2 solution of 30% to 50% saturated concentration, an AC voltage between 20 and 30 V, a graphite counter electrode and a dipping length of 3 mm. Since the drop-off phenomenon does not occur in this reaction, the voltage has to be turned off manually when the electrochemical activity stops. The parameters that gave the best results were a 40% saturated concentration and an AC voltage of 20 V. In contrast to the etching of tungsten tips, the starting current is very low (here, around 0.4 A) and the time that must elapse until there is no more noticeable activity in the solution is very long, up to 45 minutes. A typical iridium tip made using this procedure is shown in **Figure 3-33**. An interesting feature is the overall shape of iridium tips. The absence of a pronounced curvature along the tip shank is quite common with AC etching and from the lack of a strong necking effect. This is made obvious in **Figure 3-34** where SEM images show the differences in shape between a tungsten tip (left) and an iridium tip (right). One can notice how much more concave the shape is in the case of tungsten.

³⁶⁵ L.E. Murr, *Electron and Ion Microscopy and Microanalysis: Principles and Applications*, Second Edition, Marcel Dekker, 1991. K.M. Bowkett, D.A. Smith, "Field-Ion Microscopy," in: *Defects in Crystalline Solids*, Volume 2, North Holland Publishing Company, 1970. T.T. Tsong, *Atom-Probe Field Ion Microscopy*, Cambridge University Press, 1990.

³⁶⁶ A.J. Nam, A. Teren, T.A. Lusby, A.J. Melmed, "Benign making of sharp tips for STM and FIM: Pt, Ir, Au, Pd, and Rh," *J. Vac. Sci. Technol. B* 13(July 1995):1556-1559.

³⁶⁷ Anne-Sophie Lucier, "Preparation and Characterization of Tungsten Tips Suitable for Molecular Electronics Studies," M.S. Thesis, Center for the Physics of Materials, Department of Physics, McGill University, Montreal, Quebec, Canada, February 2004; <http://www.physics.mcgill.ca/~peter/theses/lucier.pdf>. See also: Anne-Sophie Lucier, Henrik Mortensen, Yan Sun, and Peter Grütter, "Determination of the atomic structure of scanning probe microscopy tungsten tips by field ion microscopy," *Phys. Rev. B* 72, 235420 (2005).

Figure 3-33. Freshly electrochemically etched iridium tip observed under an optical microscope with a 10X magnification on the left and a 50X magnification on the right.³⁶⁸

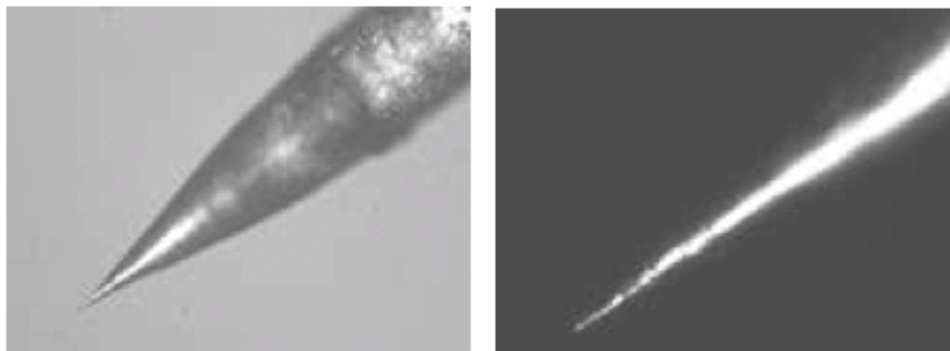
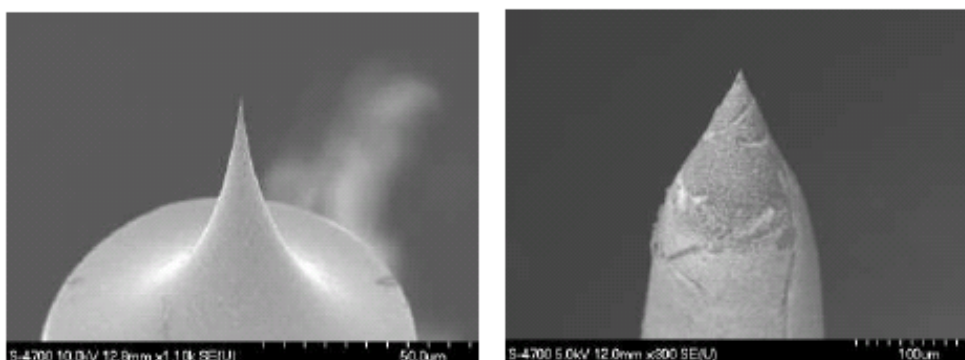


Figure 3-34. SEM images comparing the overall shape of two electrochemically etched tips. The left image shows a tungsten tip and the right image, an iridium tip. (Please note the difference in magnification and scale between these two images.)³⁶⁹



³⁶⁸ Anne-Sophie Lucier, "Preparation and Characterization of Tungsten Tips Suitable for Molecular Electronics Studies," M.S. Thesis, Center for the Physics of Materials, Department of Physics, McGill University, Montreal, Quebec, Canada, February 2004; <http://www.physics.mcgill.ca/~peter/theses/lucier.pdf>. See also: Anne-Sophie Lucier, Henrik Mortensen, Yan Sun, and Peter Grütter, "Determination of the atomic structure of scanning probe microscopy tungsten tips by field ion microscopy," Phys. Rev. B 72, 235420 (2005).

³⁶⁹ Anne-Sophie Lucier, "Preparation and Characterization of Tungsten Tips Suitable for Molecular Electronics Studies," M.S. Thesis, Center for the Physics of Materials, Department of Physics, McGill University, Montreal, Quebec, Canada, February 2004; <http://www.physics.mcgill.ca/~peter/theses/lucier.pdf>. See also: Anne-Sophie Lucier, Henrik Mortensen, Yan Sun, and Peter Grütter, "Determination of the atomic structure of scanning probe microscopy tungsten tips by field ion microscopy," Phys. Rev. B 72, 235420 (2005).

Tungsten tips resulting from a successful electrochemical etching process are quickly transferred to the preparation chamber of a UHV system for a further cleaning step, as their surface is inevitably covered with contaminants which cannot be removed by mere rinsing in water, acetone and ethanol. It is well known that an oxide layer (mainly WO_3 , aka. tungsten trioxide) develops on the tip shank during electrochemical etching,³⁷⁰ though it is not quite understood how the growth of this amorphous layer relates to the tip etching parameters.³⁷¹ It has been suggested that a higher DC etching voltage could yield a particularly thick oxide layer,³⁷² but authors who actually looked at this layer with a transmission electron microscope (TEM) agree that it is usually a few nanometers thick³⁷³ regardless of the etching conditions. Auger microscopy and energy dispersive x-ray analysis have also revealed the presence of other surface contaminants such as carbon, nitrogen, alkali metal hydroxides (e.g. KOH), and microcrystals (e.g., WO_3K) which are left on the tip from the electrochemical bath and after exposure to the atmosphere.³⁷⁴

For tips used in STM work, the various contaminants listed above will undoubtedly cause instabilities in the tunnel junction, affecting image quality and increasing the noise level.³⁷⁵ The

³⁷⁰ E. Paparazzo, L. Moretto, S. Selci, M. Righini, I. Farne, "Effects of HF attack on the surface and interface microchemistry of W tips for use in the STM microscope: a scanning Auger microscopy (SAM) study," *Vacuum* 52(April 1999):421-426. J. Garnaes, F. Kragh, K.A. Mørch, A.R. Tholen, "Transmission electron microscopy of scanning tunneling tips," *J. Vac. Sci. Technol. A* 8(January 1990):441-444.

³⁷¹ I. Ekvall, E. Wahlstrom, D. Claesson, H. Olin, E. Olsson, "Preparation and characterization of electrochemically etched W tips for STM," *Meas. Sci. Technol.* 10(January 1999):11-18. D.K. Biegelsen, F.A. Ponce, J.C. Tramontana, S.M. Koch, "Ion milled tips for scanning tunneling microscopy," *Appl. Phys. Lett.* 50(16 March 1987):696-698.

³⁷² J.P. Ibe, P.P. Bey Jr., S.L. Brandow, R.A. Brizzolara, N.A. Burnham, D.P. DiLella, K.P. Lee, C.R.K. Marrian, R.J. Colton, "On the electrochemical etching of tips for scanning tunneling microscopy," *J. Vac. Sci. Technol. A* 8(July 1990):3570-3575.

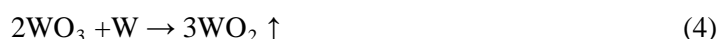
³⁷³ I. Ekvall, E. Wahlstrom, D. Claesson, H. Olin, E. Olsson, "Preparation and characterization of electrochemically etched W tips for STM," *Meas. Sci. Technol.* 10(January 1999):11-18. J. Mendez, M. Luna, A.M. Baro, "Preparation of STM W tips and characterization by FEM, TEM and SEM," *Surf. Sci.* 266(15 April 1992):294-298. J. Garnaes, F. Kragh, K.A. Mørch, A.R. Tholen, "Transmission electron microscopy of scanning tunneling tips," *J. Vac. Sci. Technol. A* 8(January 1990):441-444. D.K. Biegelsen, F.A. Ponce, J.C. Tramontana, S.M. Koch, "Ion milled tips for scanning tunneling microscopy," *Appl. Phys. Lett.* 50(16 March 1987):696-698. A. Schirmeisen, *Metallic Adhesion and Tunneling at the Atomic Scale*, PhD thesis, McGill University, Canada, 1999.

³⁷⁴ A.I. Oliva, A. Romero G.J.L. Pena, E. Anguiano, M. Aguilar, "Electrochemical preparation of tungsten tips for a scanning tunneling microscope," *Rev. Sci. Instrum.* 67(May 1996):1917-1921. L. Ottaviano, L. Lozzi, S. Santucci, "Scanning Auger microscopy study of W tips for scanning tunneling microscopy," *Rev. Sci. Instrum.* 74(2003):3368-3378. A. Cricenti, E. Paparazzo, M.A. Scarselli, L. Moretto, S. Selci, "Preparation and characterization of tungsten tips for scanning tunneling microscopy," *Rev. Sci. Instrum.* 65(May 1994):1558-1560. I. Ekvall, E. Wahlstrom, D. Claesson, H. Olin, E. Olsson, "Preparation and characterization of electrochemically etched W tips for STM," *Meas. Sci. Technol.* 10(January 1999):11-18.

³⁷⁵ A. Cricenti, E. Paparazzo, M.A. Scarselli, L. Moretto, S. Selci, "Preparation and characterization of tungsten tips for scanning tunneling microscopy," *Rev. Sci. Instrum.* 65(May 1994):1558-1560. L.A. Hockett, S.E. Creager, "A convenient method for removing surface oxides from tungsten STM tips," *Rev.*

presence of an insulating oxide layer can even lead to a tip crash, since the resistance of this layer is most likely greater than the tunnel gap resistance corresponding to the set current – the tip can touch the sample's surface before the desired current can be reached.³⁷⁶ Sometimes a controlled tip crash may allow a more stable tunnel junction to be recovered, either by breaking the oxide layer covering the tip or by transferring some atoms from the sample to the tip,³⁷⁷ but in DMS we require a sharp atomically defined tip so intentional crashing is not an option! There are more appropriate, controllable and reproducible ways to remove the contaminants (especially the undesired oxide layer) in order to clean the tungsten tips – most commonly, thermal annealing.

Heating the tip to high temperature in UHV is a very efficient way to desorb the contamination layer. At temperatures above 1000 K, the following reaction takes place:³⁷⁸



From Equation 4, it can be seen that the tungsten trioxide (WO_3) covering the tip will react with tungsten to form tungsten dioxide (WO_2) which is volatile and sublimates around 1075 K.³⁷⁹ A clean metallic tungsten surface is therefore left behind.³⁸⁰ Another advantage of this annealing

Sci. Instrum. 64(January 1993):263-264. R. Zhang, D.G. Ivey, "Preparation of sharp polycrystalline tungsten tips for scanning tunneling microscopy imaging," J. Vac. Sci. Technol. B 14(January 1996):1-10. I. Ekvall, E. Wahlstrom, D. Claesson, H. Olin, E. Olsson, "Preparation and characterization of electrochemically etched W tips for STM," Meas. Sci. Technol. 10(January 1999):11-18.

³⁷⁶ A.I. Oliva, A. Romero G.J.L. Pena, E. Anguiano, M. Aguilar, "Electrochemical preparation of tungsten tips for a scanning tunneling microscope," Rev. Sci. Instrum. 67(May 1996):1917-1921. R. Wiesendanger, Scanning Probe Microscopy and Spectroscopy: Methods and Applications, Cambridge University Press, 1994. D.K. Biegelsen, F.A. Ponce, J.C. Tramontana, S.M. Koch, "Ion milled tips for scanning tunneling microscopy," Appl. Phys. Lett. 50(16 March 1987):696-698.

³⁷⁷ L.A. Hockett, S.E. Creager, "A convenient method for removing surface oxides from tungsten STM tips," Rev. Sci. Instrum. 64(January 1993):263-264. J. Garnaes, F. Kragh, K.A. Mørch, A.R. Tholen, "Transmission electron microscopy of scanning tunneling tips," J. Vac. Sci. Technol. A 8(January 1990):441-444. R.J. Colton, S.M. Baker, J.D. Baldeschwieler, W.J. Kaiser, "'Oxide-free' tip for scanning tunneling microscopy," Appl. Phys. Lett., 51(3 August 1987):305-307.

³⁷⁸ C.J. Chen, Introduction to Scanning Tunneling Microscopy, Oxford University Press, 1993. S.W.H. Yih, C.T. Wang, Tungsten: Sources, Metallurgy, Properties, and Applications, Plenum Press, 1979.

³⁷⁹ C.J. Chen, Introduction to Scanning Tunneling Microscopy, Oxford University Press, 1993. K.C. Li, C.Y. Wang, Tungsten: Its History, Geology, Ore-Dressing, Metallurgy, Chemistry, Analysis, Applications, and Economics, Reinhold Publishing Corporation, 3rd Edition, 1955.

³⁸⁰ C.J. Chen, Introduction to Scanning Tunneling Microscopy, Oxford University Press, 1993. L. Ottaviano, L. Lozzi, S. Santucci, "Scanning Auger microscopy study of W tips for scanning tunneling microscopy," Rev. Sci. Instrum. 74(2003):3368-3378. I. Ekvall, E. Wahlstrom, D. Claesson, H. Olin, E. Olsson, "Preparation and characterization of electrochemically etched W tips for STM," Meas. Sci. Technol. 10(January 1999):11-18.

process is that it heals the crystallographic defects generated by the electrochemical etching and the drop-off, and it also smoothes out the tip surface.³⁸¹

While being successful at removing the contamination layer from the electrochemically etched tungsten tips,³⁸² the annealing process also has been reported to routinely lead to the blunting of these heated tips.³⁸³ After trying various annealing temperatures and times, Lucier³⁸⁴ got the best results by flash-annealing the tip for 2 seconds at a bright orange glow (usually corresponding to a current of 3.0-4.5 A), then lowering the current to ~2.0 A for at least 5 minutes. It seemed better to use a short annealing time and to perfect the tip cleaning with FIM, rather than to take the risk of dulling our tips by annealing them for too long. Because of potential tip blunting during the annealing process, some refinements have been proposed. For example, annealing the tip in the presence of a high gradient electric field or annealing the tip in an oxygen atmosphere can efficiently clean the tip while lowering the overall blunting rate – and if properly mastered, these refinements can also allow the resharpener of a blunt tip inside the UHV preparation chamber.

Annealing of freshly electrochemically etched tungsten tips is among the most widely used techniques to remove surface contaminants, but several other popular methods exist:

³⁸¹ A. Schirmeisen, *Metallic Adhesion and Tunneling at the Atomic Scale*, PhD thesis, McGill University, Canada, 1999. Vu Thien Binh, A. Piquet, H. Roux, R. Uzan, M. Drechsler, “Sharpening of metal tips by heat treatment in vacuum,” *J. Phys. E: Sci. Instrum.* 9(May 1976):377-381. H.S. Kim, M.L. Yu, U. Staufer, L.P. Murray, D.P. Kern, T.H.P. Chang, “Oxygen processed field emission tips for microcolumn applications,” *J. Vac. Sci. Technol. B* 11(November 1993):2327-2331.

³⁸² A. Cricenti, E. Paparazzo, M.A. Scarselli, L. Moretto, S. Selci, “Preparation and characterization of tungsten tips for scanning tunneling microscopy,” *Rev. Sci. Instrum.* 65(May 1994):1558-1560. U. Staufer, L.P. Muray, D.P. Kern, T.H.P. Chang, “Investigation of emitter tips for scanning tunneling microscope-based microprobe systems,” *J. Vac. Sci. Technol. B* 9(November 1991):2962-2966.

³⁸³ Vu Thien Binh, A. Piquet, H. Roux, R. Uzan, M. Drechsler, “Sharpening of metal tips by heat treatment in vacuum,” *J. Phys. E: Sci. Instrum.* 9(May 1976):377-381. H.S. Kim, M.L. Yu, U. Staufer, L.P. Murray, D.P. Kern, T.H.P. Chang, “Oxygen processed field emission tips for microcolumn applications,” *J. Vac. Sci. Technol. B* 11(November 1993):2327-2331. J.L. Boling, W.W. Dolan, “Blunting of Tungsten Needles by Surface Diffusion,” *J. Appl. Phys.* 29(March 1958):556-559. V.T. Binh, R. Uzan, “Tip shape evolution: Capillarity-induced matter transport by surface diffusion. I,” *Surf. Sci.* 179(2 January 1987):540-560. V.T. Binh, A. Piquet, H. Roux, R. Uzan, M. Drechsler, “Simultaneous Free Evaporation and Surface Diffusion,” *Surf. Sci.* 44(August 1974):598-616. U. Staufer, L.P. Muray, D.P. Kern, T.H.P. Chang, “Investigation of emitter tips for scanning tunneling microscope-based microprobe systems,” *J. Vac. Sci. Technol. B* 9(November 1991):2962-2966.

³⁸⁴ Anne-Sophie Lucier, “Preparation and Characterization of Tungsten Tips Suitable for Molecular Electronics Studies,” M.S. Thesis, Center for the Physics of Materials, Department of Physics, McGill University, Montreal, Quebec, Canada, February 2004; <http://www.physics.mcgill.ca/~peter/theses/lucier.pdf>. See also: Anne-Sophie Lucier, Henrik Mortensen, Yan Sun, and Peter Grütter, “Determination of the atomic structure of scanning probe microscopy tungsten tips by field ion microscopy,” *Phys. Rev. B* 72, 235420 (2005).

(1) **HF Chemical Cleaning.** The idea behind this technique³⁸⁵ is to dip the tip in hydrofluoric (HF) acid right after completion of the electrochemical etching to solubilize the tungsten oxides. Tungsten itself does not react with HF but all of its oxides are soluble in a concentrated HF solution, so a clean tungsten tip should result from this treatment. The suggested dipping time is 10-30 seconds, and the recommended concentration is 51% HF in water. Lucier³⁸⁶ examined the efficiency of this technique by comparing the performance of treated and untreated tips in STM imaging and spectroscopy. Treated tips turned out to have highly superior imaging capabilities and displayed a truly metallic behavior in spectroscopy. Auger microscopy studies have also confirmed the ability of HF attack to remove oxides from the tip.³⁸⁷ However, it has been reported by others that a similar HF chemical cleaning treatment, with a slightly lower solution concentration, gave quite irreproducible and unpredictable results.³⁸⁸ It was also observed that HF cleaning can lead to a significant blunting of the tip.³⁸⁹

(2) **Ion Milling.** Ion milling involves directing argon ions to the tip surface in order to remove the contamination layer by sputtering. In a typical setup, the tip is either rotated in a flux of argon ions with the ion beam at a certain incident angle, or placed right under the ion beam so that its axis coincides with the beam. The bombardment time and flux energy vary with the particular geometry of the setup, but exposures of tens of minutes at a few keV are often encountered in the literature.³⁹⁰ Ion milling is an effective way to clean the tips and it has the advantage of further decreasing the radius of the tip apex since sputtering also removes tungsten atoms.³⁹¹ However, a short annealing step is usually necessary afterwards to heal the damage

³⁸⁵ L.A. Hockett, S.E. Creager, "A convenient method for removing surface oxides from tungsten STM tips," *Rev. Sci. Instrum.* 64(January 1993):263-264.

³⁸⁶ Anne-Sophie Lucier, "Preparation and Characterization of Tungsten Tips Suitable for Molecular Electronics Studies," M.S. Thesis, Center for the Physics of Materials, Department of Physics, McGill University, Montreal, Quebec, Canada, February 2004; <http://www.physics.mcgill.ca/~peter/theses/lucier.pdf>. See also: Anne-Sophie Lucier, Henrik Mortensen, Yan Sun, and Peter Grütter, "Determination of the atomic structure of scanning probe microscopy tungsten tips by field ion microscopy," *Phys. Rev. B* 72, 235420 (2005).

³⁸⁷ E. Paparazzo, L. Moretto, S. Selci, M. Righini, I. Farne, "Effects of HF attack on the surface and interface microchemistry of W tips for use in the STM microscope: a scanning Auger microscopy (SAM) study," *Vacuum* 52(April 1999):421-426.

³⁸⁸ I. Ekvall, E. Wahlstrom, D. Claesson, H. Olin, E. Olsson, "Preparation and characterization of electrochemically etched W tips for STM," *Meas. Sci. Technol.* 10(January 1999):11-18.

³⁸⁹ L. Ottaviano, L. Lozzi, S. Santucci, "Scanning Auger microscopy study of W tips for scanning tunneling microscopy," *Rev. Sci. Instrum.* 74(2003):3368-3378.

³⁹⁰ L. Ottaviano, L. Lozzi, S. Santucci, "Scanning Auger microscopy study of W tips for scanning tunneling microscopy," *Rev. Sci. Instrum.* 74(2003):3368-3378. R. Zhang, D.G. Ivey, "Preparation of sharp polycrystalline tungsten tips for scanning tunneling microscopy imaging," *J. Vac. Sci. Technol. B* 14(January 1996):1-10. D.K. Biegelsen, F.A. Ponce, J.C. Tramontana, S.M. Koch, "Ion milled tips for scanning tunneling microscopy," *Appl. Phys. Lett.* 50(16 March 1987):696-698.

³⁹¹ R. Wiesendanger, *Scanning Probe Microscopy and Spectroscopy: Methods and Applications*, Cambridge University Press, 1994. R. Zhang, D.G. Ivey, "Preparation of sharp polycrystalline tungsten

caused by ion sputtering.³⁹² It has been reported that multiple tips might result from the ion milling process on polycrystalline tips, due to the lamellar texture of polycrystalline tungsten wire.³⁹³ The formation of a neck just below the tip apex has also been observed and has been attributed to the trajectory of the ions and the local roughness of the tip surface.³⁹⁴

(3) **Self-Sputtering.** Cleaning the tip by self-sputtering has effects very similar to ion milling. Self-sputtering occurs when the UHV chamber is filled with neon at a pressure around 10^{-4} mbar, and then a high negative voltage is applied to the tip. Under these conditions, the electric field at the tip apex will ionize the noble gas atoms and cause these positive ions to be accelerated back towards the tip, thus inducing sputtering. As with ion milling, self-sputtering leads to the removal of contaminants and to further sharpening of the tip. The difference is that this process can be conveniently monitored through the field emission current ([Section 3.10](#)) generated by the tip apex.³⁹⁵ One can then follow the evolution of the tip apex shape, as a higher field emission current corresponds to a sharper tip.

(4) **OPD.** A one-step, nontemplated, low-cost electrochemical method for the growth of gold nanopyramidal, nanorod-like, and spherical nanostructures have been fabricated on polycrystalline gold substrates through electrochemical overpotential deposition (OPD) by manipulating the deposition potentials and concentrations of HAuCl_4 .³⁹⁶ X-ray diffraction and electrochemical analyses revealed that the nanopyramids (which have anisotropic structures) are more extensively dominated by (111) facets than the other nanostructures. Oxygen reduction activity of a gold electrode with the pyramidal structures was lower than those of the electrodes with the other nanostructures since the activity at the gold (111) surface is lower than that at the (100) and (110) surfaces.

tips for scanning tunneling microscopy imaging,” J. Vac. Sci. Technol. B 14(January 1996):1-10. D.K. Biegelsen, F.A. Ponce, J.C. Tramontana, S.M. Koch, “Ion milled tips for scanning tunneling microscopy,” Appl. Phys. Lett. 50(16 March 1987):696-698.

³⁹² H.S. Kim, M.L. Yu, U. Staufer, L.P. Murray, D.P. Kern, T.H.P. Chang, “Oxygen processed field emission tips for microcolumn applications,” J. Vac. Sci. Technol. B 11(November 1993):2327-2331. U. Staufer, L.P. Muray, D.P. Kern, T.H.P. Chang, “Investigation of emitter tips for scanning tunneling microscope-based microprobe systems,” J. Vac. Sci. Technol. B 9(November 1991):2962-2966.

³⁹³ R. Zhang, D.G. Ivey, “Preparation of sharp polycrystalline tungsten tips for scanning tunneling microscopy imaging,” J. Vac. Sci. Technol. B 14(January 1996):1-10. D.K. Biegelsen, F.A. Ponce, J.C. Tramontana, S.M. Koch, “Ion milled tips for scanning tunneling microscopy,” Appl. Phys. Lett. 50(16 March 1987):696-698.

³⁹⁴ I. Ekvall, E. Wahlstrom, D. Claesson, H. Olin, E. Olsson, “Preparation and characterization of electrochemically etched W tips for STM,” Meas. Sci. Technol. 10(January 1999):11-18.

³⁹⁵ I. Ekvall, E. Wahlstrom, D. Claesson, H. Olin, E. Olsson, “Preparation and characterization of electrochemically etched W tips for STM,” Meas. Sci. Technol. 10(January 1999):11-18. O. Albrektsen, H.W.M. Salemink, K.A. Mørch, A.R. Tholen, “Reliable tip preparation for high-resolution scanning tunneling microscopy,” J. Vac. Sci. Technol. B 12(November 1994):3187-3190.

³⁹⁶ Yang Tian, Haiqing Liu, Guohua Zhao, Tetsu Tatsuma, “Shape-Controlled Electrodeposition of Gold Nanostructures,” J. Phys. Chem. B 110(2 November 2006):23478-23481.

Randall et al.³⁹⁷ report that Zyvex is using electrochemically etched W and HfB₂ tips produced by a self-limiting field-directed sputter sharpening³⁹⁸ process that yields very sharp apex structures having ~2 nm radius of curvature.

3.13 Other Ways of Making Sharp Tips

“Possibly there are as many tip-preparation procedures as there are people making tips.”³⁹⁹ This statement reflects the amazing variety of existing approaches to producing sharp tips and makes it clear that an exhaustive review of these techniques would be a rather tedious task. Researchers continue to innovate by creating their own procedures or by trying new combinations of known techniques. Useful descriptions of many popular methods are available in the literature;⁴⁰⁰ only a quick overview is provided here.

As a general rule, tip-forming techniques tend to fall within one of the two following categories: (1) mechanical procedures and (2) physicochemical procedures. Mechanical procedures were popular in the early age of STM⁴⁰¹ due to their simplicity and their ability to yield atomically resolved images. This category includes techniques such as cutting a metal wire at an angle with a wire cutter, a scissor, or a razor blade,⁴⁰² or fragmenting bulk pieces of material into small pointy pieces,⁴⁰³ or grinding a metal rod in order to get a sharp tip shape.⁴⁰⁴ Mechanical

³⁹⁷ J.N. Randall, J.W. Lyding, S. Schmucker, J.R. Von Ehr, J. Ballard, R. Saini, H. Xu, Y. Ding, “Atomic precision lithography on Si,” *J. Vac. Sci. Technol. B* 27(November/December 2009):2764-2768.

³⁹⁸ Joseph W. Lyding, Scott Schmucker, U.S. Patent Application No. 20080105539 (pending).

³⁹⁹ I. Ekvall, E. Wahlstrom, D. Claesson, H. Olin, E. Olsson, “Preparation and characterization of electrochemically etched W tips for STM,” *Meas. Sci. Technol.* 10(January 1999):11-18.

⁴⁰⁰ Allan J. Melmed, “Art and Science and other Aspects of Making Sharp Tips,” *J. Vac. Sci. Technol. B* 9(March/April 1991):601-608. R. Wiesendanger, *Scanning Probe Microscopy and Spectroscopy: Methods and Applications*, Cambridge University Press, 1994. Mircea Fotino, “Tip sharpening by normal and reverse electrochemical etching,” *Rev. Sci. Instrum.* 64(January 1993):159-167. D. Bonnell, ed., *Scanning Probe Microscopy and Spectroscopy: Theory, Techniques, and Applications*, Wiley-VCH, 2nd Edition, 2001.

⁴⁰¹ 38. Mircea Fotino, “Tip sharpening by normal and reverse electrochemical etching,” *Rev. Sci. Instrum.* 64(January 1993):159-167.

⁴⁰² D. Bonnell, ed., *Scanning Probe Microscopy and Spectroscopy: Theory, Techniques, and Applications*, Wiley-VCH, 2nd Edition, 2001. Gary W. Stupian, Martin S. Leung, “A scanning tunneling microscope based on a motorized micrometer,” *Rev. Sci. Instrum.* 60(February 1989):181-185. A. Cricenti, E. Paparazzo, M.A. Scarselli, L. Moretto, S. Selci, “Preparation and characterization of tungsten tips for scanning tunneling microscopy,” *Rev. Sci. Instrum.* 65(May 1994):1558-1560.

⁴⁰³ A.J. Melmed, R.D. Shull, C.K. Chiang, H.A. Fowler, “Possible Evidence for Superconducting Layers in Single Crystal YBa₂Cu₃O_{7-x} by Field Ion Microscopy,” *Science*, 239(8 January 1988):176-178.

procedures commonly leave a ragged surface at the end of the tip and the numerous tiny asperities that often protrude from the apex almost always guarantee atomic resolution on flat surfaces. Even a broken pencil lead managed to successfully image the structure of highly ordered pyrolytic graphite.⁴⁰⁵ However, mechanically prepared tips display an irregular shape and a large macroscopic radius of curvature.⁴⁰⁶ During STM imaging they perform quite irreproducibly and often show poor stability, particularly on rough surfaces. The presence of several minitips at their apex can also lead to multiple image signals and other artifacts.⁴⁰⁷

Physicochemical procedures can yield extremely sharp and symmetric tips in a more reproducible fashion than mechanical procedures and seem to be the methods of choice nowadays.⁴⁰⁸

Electrochemical etching, either as described in [Section 3.12](#) or along with additional refinements,⁴⁰⁹ is probably the most popular tip preparation method. It is sometimes performed as a two-step procedure, where the second step consists of “zone electropolishing” the tip to further sharpen it in a very controlled manner. During zone electropolishing, the tip is moved by a micromanipulator through a thin film of electrolyte contained in a loop of metal (which acts as the counter electrode) so that very small amounts of material can be removed locally.⁴¹⁰ (Note that this extra step was not required for the etching procedure described in [Section 3.12](#) because very sharp tungsten tips could already be obtained.) Various other physicochemical procedures exist. For instance, sharp tips can be made by chemical vapor deposition⁴¹¹ or electron beam

⁴⁰⁴ G. Binnig, H. Rohrer, Ch. Gerber, E. Weibel, “Surface Studies by Scanning Tunneling Microscopy,” *Phys. Rev. Lett.* 49(5 July 1982):57-61; http://www.tu-chemnitz.de/physik/FPRAK/F-Praktikum/Versuche/Literatur_RTM.pdf.

⁴⁰⁵ R.J. Colton, S.M. Baker, J.D. Baldeschwieler, W.J. Kaiser, “ ‘Oxide-free’ tip for scanning tunneling microscopy,” *Appl. Phys. Lett.*, 51(3 August 1987):305-307.

⁴⁰⁶ R. Wiesendanger, *Scanning Probe Microscopy and Spectroscopy: Methods and Applications*, Cambridge University Press, 1994.

⁴⁰⁷ R. Wiesendanger, *Scanning Probe Microscopy and Spectroscopy: Methods and Applications*, Cambridge University Press, 1994. D. Bonnell, ed., *Scanning Probe Microscopy and Spectroscopy: Theory, Techniques, and Applications*, Wiley-VCH, 2nd Edition, 2001.

⁴⁰⁸ Allan J. Melmed, “Art and Science and other Aspects of Making Sharp Tips,” *J. Vac. Sci. Technol. B* 9(March/April 1991):601-608.

⁴⁰⁹ H. Lemke, T. Goddenhenrich, H.P. Bochem, U. Hartmann, C. Heiden, “Improved microtips for scanning probe microscopy,” *Rev. Sci. Instrum.* 61(October 1990):2538-2541. Allan J. Melmed, “Art and Science and other Aspects of Making Sharp Tips,” *J. Vac. Sci. Technol. B* 9(March/April 1991):601-608. Mircea Fotino, “Nanotips by reverse electrochemical etching,” *Appl. Phys. Lett.* 60(8 June 1992):2935-2937.

⁴¹⁰ Allan J. Melmed, “Art and Science and other Aspects of Making Sharp Tips,” *J. Vac. Sci. Technol. B* 9(March/April 1991):601-608. D. Bonnell, ed., *Scanning Probe Microscopy and Spectroscopy: Theory, Techniques, and Applications*, Wiley-VCH, 2nd Edition, 2001.

⁴¹¹ T.S. Ravi, R.B. Marcus, T. Gmitter, H.H. Busta, J.T. Niccum, “Fabrication of atomically sharp tungsten tips,” *Appl. Phys. Lett.* 57(1 October 1990):1413-1415.

deposition⁴¹² onto pre-existing tips, as well as by ion milling.⁴¹³ Ultimate control on the tip apex shape can be achieved with field ion microscopy techniques ([Section 3.10](#)), where consecutive field evaporation of single atoms can yield a particular atomic configuration of the apex.

⁴¹² Y. Akama, E. Nishimura, A. Sakai, “New scanning tunneling microscopy tip for measuring surface topography,” *J. Vac. Sci. Technol. A* 8(January 1990):429-433.

⁴¹³ D.K. Biegelsen, F.A. Ponce, J.C. Tramontana, S.M. Koch, “Ion milled tips for scanning tunneling microscopy,” *Appl. Phys. Lett.* 50(16 March 1987):696-698.

4. Patterned Atomic Layer Epitaxy (ALE)

Atomic Layer Epitaxy (ALE) of Si is an experimentally-demonstrated cyclic Chemical Vapor Deposition (CVD) process that deposits a monolayer (or a well defined fraction of a monolayer) per ALE cycle.⁴¹⁴ The deposition self-limits due to the Si atoms that bind epitaxially to the surface, carrying with them an atom or molecule that “protects” the newly deposited surface from further deposition. In another part of the ALE cycle, the protecting or passivating species are globally removed from the surface, effectively deprotecting the surface and allowing a subsequent monolayer of atoms to be deposited in the next ALE cycle. In several cases, notably using disilane Si_2H_6 as a precursor gas, the passivating species is H. A patterned Si ALE process (Section 4.2) then is accomplished by replacing the global removal of H with a patterned removal of H. ALE cycles then will only deposit Si in the areas that have been deprotected via atomically precise H depassivation lithography, providing atomic resolution in all three dimensions.

One ALE technique involves using two different passivating species where one may be selectively removed without disturbing the other. For instance, both Cl and H will successfully passivate Si(100) surfaces. H will desorb from the Si surface at lower temperatures than Cl. By using the patterned Cl layer to first passivate a Si surface, ALE may be used to grow Si in that patterned area. If the ALE process is one that uses hydrogen as the passivating chemistry, then the ALE process may be continued without additional patterning by using temperature as the depassivating process for the H passivated Si. Because the Cl will remain in place, then the ALE process will only grow Si in the area that was originally patterned in the Cl passivation layer. The process may be continued for as many deposition cycles as desired for that pattern.

ALE is often considered to be a special case of the more general process called Atomic Layer Deposition or ALD: the focus of ALE is depositing epitaxial layers, meaning perfect crystal structure, whereas ALD seeks to deposit one layer at a time with the focus on film uniformity, not single crystal structure. Notes Aaltonen:⁴¹⁵ “ALD is a gas phase thin film deposition method which can be regarded as a special modification of the more widely used chemical vapor deposition (CVD) technique. In ALD, the precursors are led into the reaction chamber in alternate pulses while in CVD, the precursors are led into the reaction chamber simultaneously. The alternate precursor pulses in ALD are separated by inert gas purging (in flow type reactors) or by evacuation of the reactor (in high-vacuum type reactors). The precursors react with the surface groups on the substrate, or chemisorb on the substrate surface. In properly chosen process conditions, the surface reactions are self-limiting, which leads to highly controlled film growth. If the surface reactions become saturated, a constant film growth rate is obtained over the whole substrate surface, and films with excellent conformality and good large-area uniformity

⁴¹⁴ John Randall, “Atomically Precise Manufacturing Processes,” Paper 01, Part 3, Proceedings of the Roadmap Working Group, Foresight/Battelle Nanotechnology Roadmap, 2007.

⁴¹⁵ Titta Aaltonen, “Atomic Layer Deposition of Noble Metal Thin Films”, Academic Dissertation, Helsinki 2005;
<http://www.cambridgenanotech.com/theses/Atomic%20Layer%20Deposition%20of%20Noble%20Metal%20Thin%20Films.pdf>.

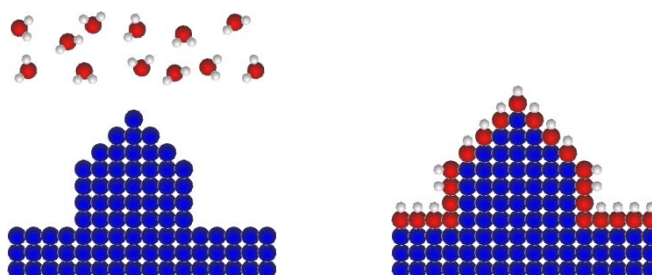
are obtained. The set of successive pulses of two or more precursors, separated by purge periods, is called an ALD cycle. The film growth rate is usually measured as the film thickness obtained during one ALD cycle. The film thickness can be easily and accurately controlled by the number of the applied growth cycles.”

ALE has not yet been used to fabricate atomically precise single-atom tips (SATs), but we believe that this process or its derivatives could be used for this purpose, as described below.

4.1 ALE-Coated Single-Atom SPM Tips

One alternative to obtain atomically sharp silicon tip might be to start with a single-atom metal tip such as those that are often prepared by applying a metal thin film over a tungsten tip ([Table 2-1](#)), and coat them instead with a single monolayer of silicon atoms, yielding (in principle) a single Si atom, or perhaps just a few Si atoms, at the tip ([Figure 4-1](#)). These tips would hopefully be better in quality than the silicon field emission tips⁴¹⁶ previously mentioned in [Section 2](#) and [Table 2-1](#), and should provide more reliable tips than the current practice among experimentalists of banging single-atom Ir-W tips into silicon surface until one Si atom at random comes to reside on the tip, among the jumble of other Si atoms collecting there, thus providing single-atom resolution with a silicon tip ([Section 3](#)). Silicon tip chemistry for DMS is the basis of our original bootstrap proposal, hence single-atom Si tips should work as or more reliably than single-atom metal tips, all else equal.

Figure 4-1. Illustration of tip building sequence using ALE to deposit silicon (red atoms) on a tungsten tip (blue atoms) using hydrogen (white atoms) as the passivating agent.



Numerous ALE processes have been developed for Si and Ge with a wide variety of precursors (e.g., SiH_4 , Si_2H_6 , SiCl_2H_2 , GeH_4 , Ge_2H_6 , $\text{GeH}_2(\text{CH}_3)_2$, GeCl_4). ALE technologies for Si on Si

⁴¹⁶ Ding Meng, Sha Guobin, A.I. Akinwande, “Silicon field emission arrays with atomically sharp tips: turn-on voltage and the effect of tip radius distribution,” *IEEE Transactions on Electron Devices* 49(December 2002):2333-2342.

substrate,⁴¹⁷ insulating SiO₂ on Si substrate,⁴¹⁸ P/B doping on SiGe,⁴¹⁹ Si on Ge,⁴²⁰ and semiconductor on silver substrate⁴²¹ are well known, but the ALD of metals on Si and SiO₂ substrates has traditionally been quite challenging. Even so, by 2005 a large number of metallic elements (Al, Co, Cu, Fe, Ir, Mo, Ni, Pd, Pt, Rh, Ru, Ta, Ti, W) had been deposited either by using a thermally activated process or with additional activation.⁴²² Further investigation would be required to determine if silicon ALE is available (or can be developed) for reliably depositing a Si monolayer onto single-atom tip metal surfaces such as Ir, Pt, or W.

4.2. Atomically-Precise Single-Atom Tips from PALE

Patterned Atomic Layer Epitaxy, or PALE, might be used to produce almost atomically-precise atomically-sharp tooltips to greatly improve the efficiency of the initial bootstrapping process for DMS – after which DMS could be used to fabricate fully atomically-precise atomically-sharp

⁴¹⁷ Titta Aaltonen, “Atomic Layer Deposition of Noble Metal Thin Films”, Academic Dissertation, Helsinki 2005;

<http://www.cambridgenanotech.com/theses/Atomic%20Layer%20Deposition%20of%20Noble%20Metal%20Thin%20Films.pdf>.

⁴¹⁸ Ofer Sneh, Steven M. George, “Thermal Stability of Hydroxyl Groups on a Well-Defined Silica Surface,” *J. Phys. Chem.* 99(1995):4639-4647; http://pubs.acs.org/cgi-bin/abstract.cgi/jpchax/1995/99/i13/f-pdf/f_j100013a039.pdf?sessid=600613. S. Morishita, Y. Uchida, M. Matsumura, “Atomic-Layer Chemical-Vapor-Deposition of SiO₂ by Cyclic Exposures of CH₃OSi(NCO)₃ and H₂O₂,” *Jpn. J. Appl. Phys.* 34(1995):5738-5742; <http://jap.ipap.jp/link?JJAP/34/5738>. O. Sneh, M.L. Wisem A.W. Ott, L.A. Okada, S.M. George, “Atomic layer growth of SiO₂ on Si(100) using SiCl₄ and H₂O in a binary reaction sequence,” *Surf. Sci.* 334(1995):135-152. J.W. Klaus, A.W. Ott, J.M. Johnson, S.M. George, “Atomic layer controlled growth of SiO₂ films using binary reaction sequence chemistry,” *Appl. Phys. Lett.* 70(3 March 1997):1092; <http://link.aip.org/link/?APPLAB/70/1092/1>. Kei-ichi Yamaguchi, Shigeru Imai, Naoto Ishitobi, Masashi Takemoto, Hidejiro Miki, Masakiyo Matsumura, “Atomic-layer chemical-vapor-deposition of silicon dioxide films with an extremely low hydrogen content,” *Applied Surface Science* 130-132(June 1998):202-207. Eva Aro, Suvi Haukka, Marko Tuominen, “Atomic-Layer-Chemical-Vapor-Deposition of Films That Contain Silicon Dioxide,” European Patent EP1248865, Filing Date 12/04/2000; www.freepatentsonline.com/EP1248865.html.

⁴¹⁹ B. Tillack, “Atomic layer doping of SiGe,” Proceedings of the Twelfth European Conference on Chemical Vapour Deposition, 1999, *Journal de Physique IV: Proceedings* 1(1999):295-305.

⁴²⁰ Keiji Ikeda, Satoshi Sugahara, Yasutaka Uchida, Tomonori Nagai, Masakiyo Matsumura, “Formation of an atomically abrupt Si/Ge hetero-interface,” *Japanese Journal of Applied Physics* 37(1998):1311-1315.

⁴²¹ M. Luisa Foresti, Francesca Forni, Massimo Innocenti, Francesca Loglio, Giovanni Pezzatini, “Deposition and characterization of ultrathin layers of compound semiconductors on Ag(111),” *Abstr. Papers, Am. Chem. Soc.* (2001), 221st COLL-345.

⁴²² Antti Niskanen, *Radical Enhanced Atomic Layer Deposition of Metals and Oxides*, Academic Dissertation, Helsinki, 2006; <https://oa.doria.fi/dspace/bitstream/10024/2729/1/radicale.pdf>. See also: A. Niskanen, T. Hatanpää, K. Arstila, M. Leskelä, M. Ritala, “Radical Enhanced Atomic Layer Deposition of Metallic Silver Films,” submitted to *Mater. Chem.* 2006.

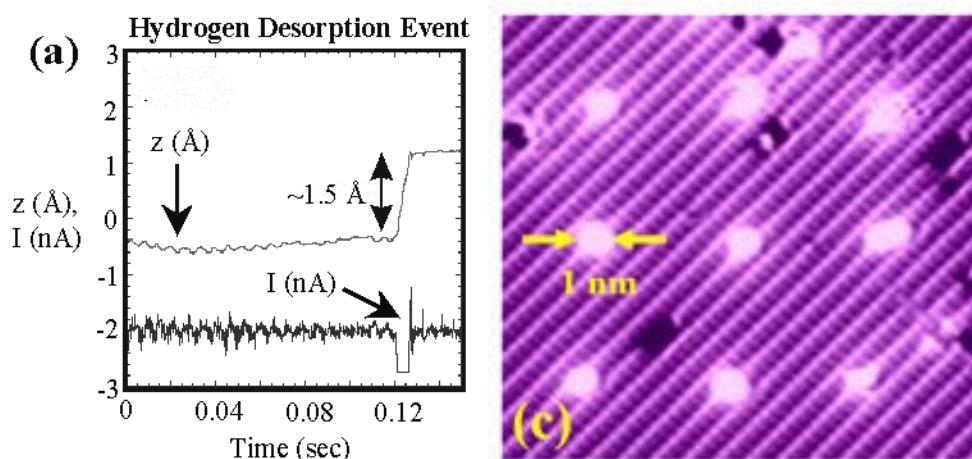
nanoscale tooltips for later generations of the molecular workstation. At least one company (Zyvex) has received a patent on the process and was actively pursuing experimental development work using grants from private and government sources totaling ~\$25M as of 2009.

PALE is a positionally-controlled variant of atomic layer deposition (ALD) or atomic layer epitaxy (ALE) ([Section 4.1](#)). PALE, which has been proposed by researchers at Zyvex,⁴²³ is an extension of ALD or ALE in which scanning probe technology is employed for positional control to selectively deprotect specific atomic sites on a surface ([Figure 4-2](#)), after which atomic layer epitaxy is used to add a single atomic layer of a second material from the vapor phase at the positionally selected depassivated sites in a CVD-type reaction with an ambient gas ([Figure 4-3](#)). Repeating this process can allow atomically precise three-dimensional structures to be built up one atomic layer at a time. For example, Lyding's group at the Beckman Institute has successfully grown silicon nanostructures by selectively depassivating a hydrogen-terminated silicon surface at atomically precise locations using Feedback Controlled Lithography,⁴²⁴ then depositing silicon onto the sites from the gas phase, demonstrating that atomically precise deprotection is possible with an STM tip that is not itself atomically precise.

⁴²³ J.N. Randall et al., "Patterned atomic layer epitaxy," United States Patent 20050223968, 13 October 2005. See also: Mikko Ritala, Markku Leskelä, "Atomic layer epitaxy – a valuable tool for nanotechnology?" *Nanotechnology* 10(March 1999):19-24.

⁴²⁴ M.C. Hersam, G.C. Abeln, J.W. Lyding, "An approach for efficiently locating and electrically contacting nanostructures fabricated via UHV-STM lithography on Si(100)," *Microelectronic Engineering* 47(June 1999):235-237. See also: Mark C. Hersam, Nathan P. Guisinger, and Joseph W. Lyding, "Silicon-Based Molecular Nanotechnology," Seventh Foresight Conference on Molecular Nanotechnology, 15-17 Oct. 1999, Santa Clara, CA. <http://www.foresight.org/conferences/mnt7/Papers/Hersam/index.html>.

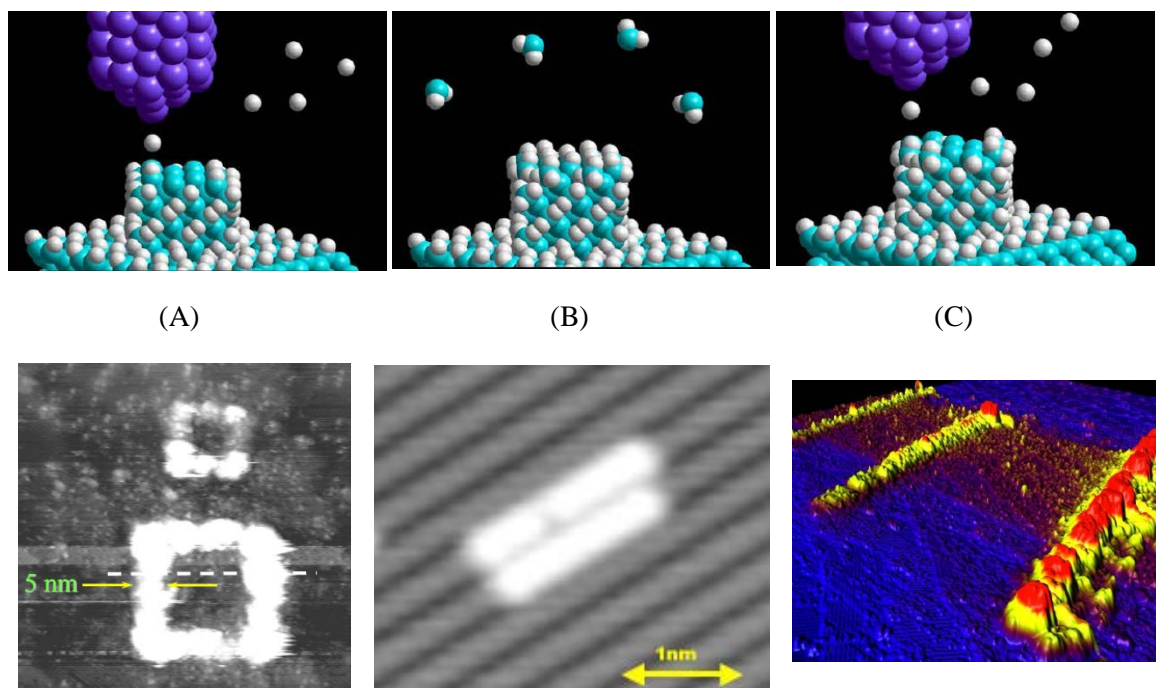
Figure 4-2. Site specific hydrogen desorption. (a) The feedback { z } and tunneling current { I } signals are monitored as a function of time while patterning at 3V, 2 nA; hydrogen atom desorption is clearly observed as a ~ 1.5 Å step in z and occurs in ~ 0.005 sec.⁴²⁵ (c) 3×3 array of individual dangling bonds nanopatterned with feedback controlled lithography on Si(100)- 2×1 :H in ultra-high vacuum.⁴²⁶



⁴²⁵ M.C. Hersam, G.C. Abeln, J.W. Lyding, "An approach for efficiently locating and electrically contacting nanostructures fabricated via UHV-STM lithography on Si(100)," *Microelectronic Engineering* 47(June 1999):235-237. See also: Mark C. Hersam, Nathan P. Guisinger, and Joseph W. Lyding, "Silicon-Based Molecular Nanotechnology," Seventh Foresight Conference on Molecular Nanotechnology, 15-17 Oct. 1999, Santa Clara, CA. <http://www.foresight.org/conferences/mnt7/Papers/Hersam/index.html>.

⁴²⁶ Mark Hersam, "Conductive Scanning Probe Microscopy Nanopatterning," The Hersam Research Group: Single Molecule Sensing, Characterization, and Actuation, 2007; <http://www.hersam-group.northwestern.edu/nanopatterning.html>.

Figure 4-3. Silicon patterned ALE at Zyvex: (A) STM tip removes H atoms from the Si surface; (B) a precursor gas is used to dose the surface, whereupon protected Si atoms are deposited only where H has been removed; (C) Completed deposition is verified, then the deprotection and patterning is repeated. **Below:** Experimental demonstration of PALE by Joe Lyding – room temperature, 10^{-8} torr disilane, 10 minutes/row, 5V-1nA / 7V-1nA / 6V-1nA, 6 nm high features.⁴²⁷



This process has been developed by Lyding's group at the Beckman Institute. Silicon nanostructures⁴²⁸ and copper phthalocyanine (Cu(Pc)) and norbornadiene⁴²⁹ were successfully grown by selectively depassivating a hydrogen-terminated silicon surface at atomically precise locations using Feedback Controlled Lithography, then depositing the atoms or molecules by

⁴²⁷ Zyvex research activities, accessed March 2008; <http://www.zyvex.com/Research/activities.html>.

⁴²⁸ Joseph Lyding, "Silicon-Based (Carbon) Nanotechnology," seminar presented at the University of Sheffield, 27 January 2004. <http://www.shef.ac.uk/sheffield/jsp/polopoly.jsp?a=15946>.

⁴²⁹ Hersam, Mark C.; Guisinger, Nathan P.; and Lyding, Joseph W. 1999a. "Silicon-Based Molecular Nanotechnology," Seventh Foresight Conference on Molecular Nanotechnology, 15-17 Oct. 1999, Santa Clara, CA. <http://www.foresight.org/conferences/mnt7/Papers/Hersam/index.html>.

adsorption onto the sites from the gas phase. The work by Lyding and Hersam⁴³⁰ demonstrates that atomic precision deprotection is possible with an STM tip that is not atomically precise, but is simply capable of atomic resolution imaging. However, reliable manufacturing will require a reproducible tooltip.

In March 2008, Zyvex announced that it had assembled \$15 million in funding for its Atomically Precise Manufacturing Consortium. The project includes a mixture of funding from the Defense Advanced Research Projects Agency, the Texas Emerging Technology Fund and cost sharing from the team members. “Increasing the precision of manufacturing has driven both technology and science for the past couple of centuries and what we are doing is just an extension of that drive,” said John Randall, vice president of Zyvex Labs, the prime contractor for the research project. “What is revolutionary is having digital control over where we add atoms to a robust solid material.” In addition to UT Dallas and Zyvex, the research team includes the University of Illinois at Urbana-Champaign, the University of North Texas, the University of Central Florida, the University of Texas at Austin, the National Institute of Standards and Technology, General Dynamics, Molecular Imprints Inc. and Integrated Circuit Scanning Probe Instruments.

The Atomically Precise Manufacturing Project currently consists of three coordinated efforts: MicroAutomation, Molecularly Precise Tools, and Patterned Atomic Layer Epitaxy. The latter initiative is perhaps the most important to Nanofactory Corporation’s diamondoid nanofactory program. Notes Randall: “Atomic layer deposition builds amorphous materials; atomic layer epitaxy (ALE) builds crystalline materials. Start with a protected (passivated) surface: every available bond has a hydrogen atom. If you deprotect the surface, removing the hydrogen, then you can deposit a layer of atoms. If you choose the right precursor gas, you add only one monolayer which is protected as it’s added. Then you can deprotect and add exactly one more layer of atoms. There are a number of precursor gases available. There are literally hundreds of systems to grow things with atomic precision in one dimension. Now, if you combine this with the ability to deprotect the surface in selected locations....With a scanning tunneling microscope, you can remove single hydrogen atoms with atomic precision. If you do this layer by layer, you can build 3D structures. Professor Joe Lyding at University of Illinois has done repeated desorption/deposition.”

According to a Zyvex website:⁴³¹ “The Patterned Atomic Layer Epitaxy Project will combine two known experimental techniques to produce atomically precise nanostructures. In our view, this is the best approach to a molecular assembler that can make reasonable progress before molecularly precise tools are available. We have identified a target process and material system that will be capable of producing complex, atomically precise (in all three dimensions) nanostructures in a robust material. The prototype reactors will not be massively parallel and will be capable of only limited output. We have identified several approaches to massive parallelism that will be evaluated as we develop the prototype tools. The prototype system, even with its limited capabilities, will be able to produce valuable products that require only very small

⁴³⁰ M.C. Hersam, G.C. Abeln, J.W. Lyding, “An approach for efficiently locating and electrically contacting nanostructures fabricated via UHV-STM lithography on Si(100),” *Microelectronic Engineering* 47(June 1999):235-237.

⁴³¹ Zyvex research activities, accessed March 2008; <http://www.zyvex.com/Research/activities.html>.

atomically precise structures. When the APM Project produces a superior tip for patterning, this will greatly improve patterned atomic layer epitaxy and enable its scale-up to large parallelism. However, such tools will also enable significant progress in molecular pick and place technology. Zyvex will constantly be evaluating the best path to a massively parallel molecular assembler.”

Notes Randall:⁴³² For a Si process two different passivation layers would be required, one (passivation A) that is a robust mask that can be patterned with Atomic Precision and would be stable while an ALE process that used a different passivation chemistry (passivation B) was used to deposit Si in that patterned area. Part of that requirement would be for passivation B to be cleanly removed from the Si surface repeatably (every ALE cycle) with some global depassivation process while not removing passivation A. One technique involves using two different passivating species, where one may be selectively removed without disturbing the other, as already described above. The process may be continued for as many deposition cycles as desired for that pattern. Control of the growth on the sidewalls of the ALE grown structure may be an issue.

A dual-material ALE process could also have a reduced patterning requirement as well as a number of other advantages. Consider an atomically flat section of Ge(100) that was passivated with some species that can be patterned. An ALE process is used to deposit a monolayer of Si in the patterned layer. (Note that heteroepitaxy of Si on Ge and Ge on Si has been established with ALE processes.) At this point a dual material ALE process could be used to selectively deposit Si on Si and Ge on Ge where the cyclic process would alternatively deposit a monolayer of Si and a monolayer of Ge. In this way the growth surface would stay atomically flat and there would be no sidewalls to contend with. After a designed number of deposited monolayers, the pattern could be changed and complex 3D heterostructures could be created. Since there are very selective etches to remove Ge, the Ge material could be used as a sacrificial layer, allowing for releasable 3D structures. Thus a dual material ALE process such as Si/Ge would be able to create releasable complex 3D structures. Simple atomically precise Si artifacts such as a wall of silicon that was a known number of atoms wide and tall would be an excellent CD standard for SEMs or AFMs, and several other atomically precise standards could be produced. The cost of producing a single metrology standard even with a single STM tip doing the patterning could be easily under \$1000.

According to an online article⁴³³ by Tihamer Toth-Fejel dated 6 October 2009, giving an update on the Zyvex TPN effort: “The Zyvex-led Atomically Precise Manufacturing Consortium has recently met their DARPA-funded Tip-Based Nanofabrication project’s Phase I metrics by writing 100 dangling bond wires, half of them 36.6 nm x 3.5 nm and half 24.5 nm x 3.5 nm in 5.66 minutes. [These “wires” are just lines of depassivation positionally etched on hydrogenated silicon surface, each line ~10 atoms wide.] That is 1.5 million atoms per hour, but the error rate was $\pm 6.4\%$, which is unacceptable for [molecular manufacturing] (unless they implement error

⁴³² John Randall, “Atomically Precise Manufacturing Processes,” Paper 01, Part 3, Proceedings of the Roadmap Working Group, Foresight/Battelle Nanotechnology Roadmap, 2007.

⁴³³ Tihamer Toth-Fejel, “Productive Nanosystems and the 2009 Financial Meltdown,” Nanotechnology-Now, 6 October 2009; <http://www.nanotech-now.com/columns/?article=357>.

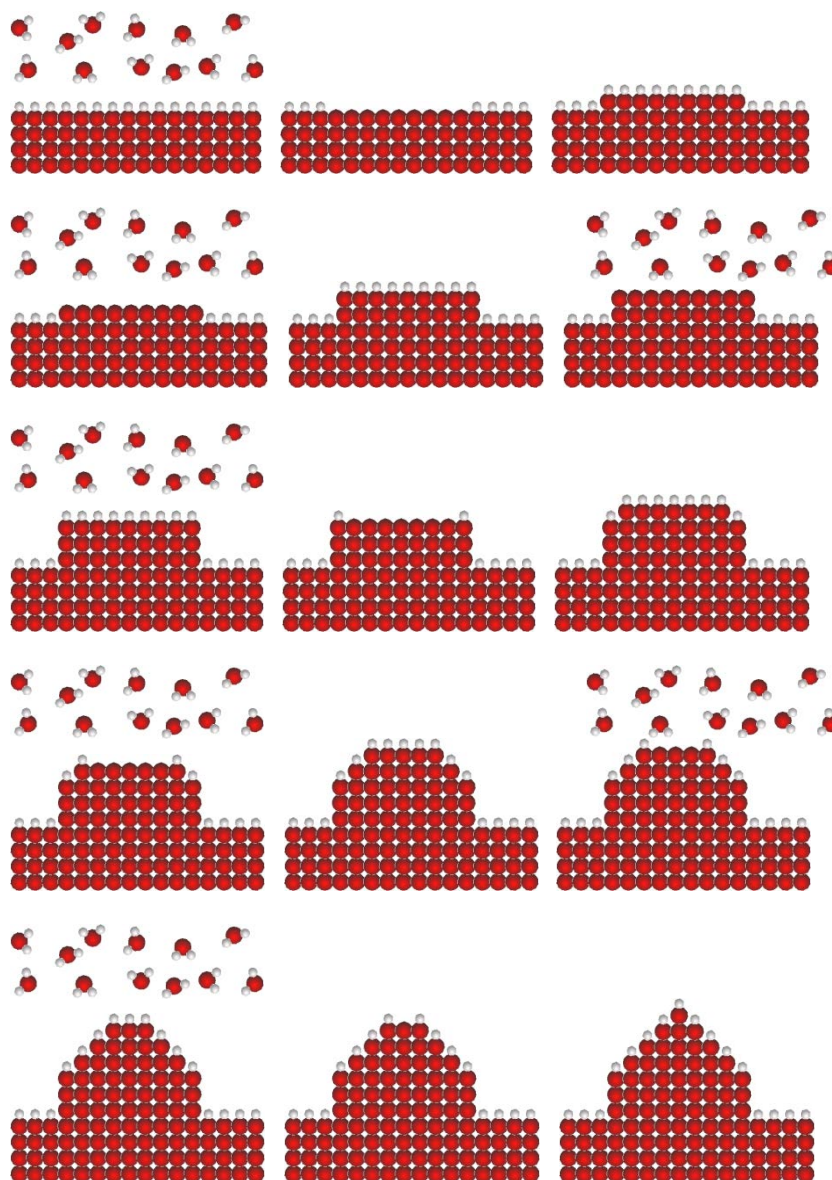
correction, which for Patterned Atomic Layer Epitaxy may or may not be easy because the high mobility of hydrogen at the operating temperature of the process)."

According to further comments by Tihamer Toth-Fejel on 20 October 2009 at the Lifeboat Foundation blog, in response to an assertion that "Zyvex is working on atomically perfect quantum dots (with size control to 0.2 nanometers)": "It's not just the precise size, but also the shape. Second, there is the precise placement and orientation of those QDs....Zyvex was thinking about building quantum dots at the beginning of the project, but we are no longer concentrating on them (unless someone here can think of a killer application that only requires a few thousand perfect quantum dots, at \$1 each)....The big problem with using our method – Patterned Atomic Layer Epitaxy – to make quantum dots is that all the applications for QDs (e.g., solar cells, biological labeling, etc.) are analogous to putting pebbles in concrete. With the possible exception of quantum dot cellular automata, there is no reason that quantum dots need to be atomically precise. In other words, it's not economically worthwhile to use Patterned ALE for QDs; not even close. As I stated at the Unither Nanomedicine Conference (assuming we succeed in phase III), the estimated costs for building bulk amounts of anything using Patterned ALE are astronomical – a one-person dose of Freitas' respirocites⁴³⁴ would optimistically cost \$360 quadrillion. That's the bad news. But nanoimprint might lower that cost by about one magnitude. A primitive bootstrap, in which the STM array would be used to build another array with smaller, and more numerous probe tips, would require about 16 weeks of build time, plus an indeterminate amount of research time, possibly reducing the cost of one dose of respirocites by two magnitudes. Only 15 generations to go!...I'm just making assumptions and cranking numbers here. We still need to achieve atomic precision at a rate of 10 million atoms/hour for \$300 by 2012, and there are some serious technical barriers that must be overcome. Plus there is the additional problem that Patterned ALE can't do error correction after the ALE step (though it can do it during/after the patterning step)."

Once PALE is a proven technology, perhaps by 2012 (according to optimistic Zyvex estimates as of 2009, and comments by Toth-Fejel), one plan would be to build a PALE tip from scratch on an atomically flat silicon SPM tip using the Zyvex process, once they can do it. We assume that we can build or obtain, say, a rectangular silicon rod of dimensions $1\ \mu\text{m} \times 1\ \mu\text{m} \times 1\ \text{mm}$ long, where the tip end of the rod tapers down to a $10\ \text{nm} \times 10\ \text{nm}$ square surface that is atomically flat. Very crudely, an isosceles triangle (in cross-section) with a $\theta = 60^\circ$ apex tip angle has a height H equal to halfwidth $W/2$ divided by the tangent of the half-angle $\theta/2$, therefore the PALE tip height is $H = (W/2) / \tan(\theta/2) = (10\ \text{nm} / 2) / \tan(60^\circ / 2) = 8.66\ \text{nm}$ for a tip with a flat $10\ \text{nm} \times 10\ \text{nm}$ flat end on which the tip is built up layer by layer using PALE (Figure 4-4). If the silicon layers are Si(110) crystal planes and are, say, $1.92\ \text{\AA}$ apart, then to build up a $8.66\ \text{nm}$ stack made of these layers will require $8.66\ \text{nm} / (0.192\ \text{nm/layer}) \approx 45$ layers to be laid down by PALE. At ~ 1 hour/layer, this does not seem excessive.

⁴³⁴ Freitas RA Jr. Exploratory design in medical nanotechnology: a mechanical artificial red cell. *Artif Cells Blood Substit Immobil Biotechnol.* 1998 Jul;26(4):411-30; <https://www.tandfonline.com/doi/pdf/10.3109/10731199809117682>. A longer version of this paper appears at: <https://web.archive.org/web/20100420085137/http://www.foresight.org/Nanomedicine/Respirocites.html>.

Figure 4-4. Schematic illustration of hypothetical atomically-sharp silicon tip-building sequence using PALE to deposit silicon on silicon (red atoms) using hydrogen (white atoms) as the passivating agent. The dehydrogenated sections in every other frame is created via positionally-controlled SPM tip-based electrical desorption of individual H atoms, one by one.



Unfortunately, the most recent results⁴³⁵ indicate that progress at Zyvex toward making atomically precise tips is moving considerably slowly than early optimists had hoped, and that the tips we need probably won't be available until well after 2012, possibly by a great many years.

A related epitaxial self-assembly process for single-atom silicon tips is the subject of a patent by another group.⁴³⁶

⁴³⁵ K.E.J. Goh, S. Chen, H. Xu, J. Ballard, J.N. Randall, J.R. Von Ehr, "Using patterned H-resist for controlled three-dimensional growth of nanostructures," *Appl. Phys. Lett.* 98(2011):163102.

⁴³⁶ Karl D. Hobart, Francis J. Kub, Henry F. Gray, Mark E. Twigg, Phillip E. Thompson, Jonathan Shaw, "Atomically sharp field emission cathodes," U.S. Patent 6113451, 5 September 2000; <http://www.patentstorm.us/patents/6113451/fulltext.html>.

5. Single-Atom Tips (SATs)

Atomically sharp and stable tips are of great importance in scanning probe microscopy. Many ways to produce sharp tips of various materials for SPM have been developed, including electrolytic (electrochemical) polishing/etching, chemical polishing/etching, ion milling, cathode sputtering, whisker growth, electron-beam deposition, flame polishing, mechanical sharpening, cutting, machining, fragmenting, and so on.⁴³⁷ As previously noted, the sharpest possible tip terminates in a single atom. A single atom tip (a tip with an atom protruding at its apex) is necessary for obtaining true atomic resolution.⁴³⁸ Leaving aside the question of aspect ratio, the survey presented in [Section 2](#) mentioned that a number of single-atom tips (SATs) have been fabricated and widely used by experimentalists, some of them for decades. We review these tips in this Section.

A variety of almost single-atom tips are also known. For example, a silicon field emission tip with 3-4 atoms at the tip has a tip radius with a log-normal distribution having a peak at 0.75 nm, an expected value of 1.8 nm, and a shape parameter of 0.74 nm, which was achieved by isotropic etching of silicon and low-temperature oxidation sharpening.⁴³⁹ In theory a planar-triangular tri-atom tip could bond a C or Ge atom at the missing apex, which could possibly be useful for DMS. Alternatively, a tri-atom SAT could be directly used for DMS provided that the tip was characterized to atomic precision and the presence of the other tip atoms would not enable pathologies to occur when DMS was performed using one of the tip atoms.

One fundamental goal of the Atom-Based Standards and Fabrication project at NIST⁴⁴⁰ is to “develop methods for repeatably producing atomically-sharp tungsten and alternative-material tips, and evaluate their atomic resolution imaging capabilities. This includes a systematic evaluation of different crystalline materials capable of producing single atom tips or atomic structures defined for high resolution sub-nanometer imaging.” This effort, while potentially useful to us, appears aimed primarily at imaging rather than positional chemistry applications.

⁴³⁷ Allan J. Melmed, “Art and Science and other Aspects of Making Sharp Tips,” *J. Vac. Sci. Technol. B* 9(March/April 1991):601-608.

⁴³⁸ Masaharu Komiyama, Katsuyuki Tazawa, Kazuya Tsujimichi, Akiyasu Hirotsu, Momiji Kubo, Akira Miyamoto, “Simulations of the Effects of Tip Apex Geometries on Atomic Force Microscopy Images,” *Jpn. J. Appl. Phys.* 35(1996):4101-4104. See also: V. Koutsos, E. Manias, G. Ten Brinke, G. Hadzioann, “Atomic Force Microscopy and Real Atomic Resolution. Simple Computer Simulations,” *Europhys. Lett.* 26(10 April 1994):103-107;
http://zeus.plmsc.psu.edu/~manias/PDFs/afm-atom-resol_epl94o.pdf.

⁴³⁹ Ding Meng, Sha Guobin, A.I. Akinwande, “Silicon field emission arrays with atomically sharp tips: turn-on voltage and the effect of tip radius distribution,” *IEEE Transactions on Electron Devices* 49(December 2002):2333-2342.

⁴⁴⁰ “Atom-Based Standards and Fabrication,” Manufacturing Engineering Laboratory, NIST, 28 May 2009;
<http://www.nist.gov/mel/ped/nm/absf.cfm>.

5.1 Field-Assisted Tungsten SATs

The first (tungsten) single-atom tip was made in 1986 by Fink.⁴⁴¹ Fink reported a “deposition” method of creating a single atom W tip by first using a field- and thermal-induced tip-forming process to produce a three-atom island on the (111) facet of a clean W tip, followed by thermal deposition of a single W atom on top of this island. Fink used field-ion microscopy techniques to create stable tips whose very ends are made up of just one individual atom, deposited from the gas phase onto an upper terrace of a pyramidal (111)-oriented tungsten tip – with the first three layers of the tip consisting of one, three, and seven atoms, respectively.

Other similar methods have since been reported.⁴⁴² Since the 1980s, various experimental techniques have been proposed for the production of tungsten nanotips with a well controlled geometry,⁴⁴³ including neon ion sputtering⁴⁴⁴ and thermo-field treatment.⁴⁴⁵ For example, Vu Thien Binh⁴⁴⁶ and others have developed the “build-up” and “pseudo-stationary profile (PSP)” techniques based on ultrahigh-vacuum heat treatments in the presence of an electrical field. Ness and Gautier⁴⁴⁷ were among the first to perform theory studies on possible transition metal SATs.

⁴⁴¹ H.W. Fink, “Mono-atomic tips for scanning tunneling microscopy,” IBM J. Res. Develop. 30(1986):460-465. H.W. Fink, “Point Source for Ions and Electrons,” Physica Scripta 38(1988):260-263.

⁴⁴² V.T. Binh, N. Garcia, “On the electron and metallic ion emission from nanotips fabricated by field-surface-melting technique – experiments on W and Au tips,” Ultramicroscopy 42-44(1992):80-90. R. Morin, H.W. Fink, “Highly monochromatic electron point-source beams,” Appl. Phys. Lett. 65(1994):2362.

⁴⁴³ V.T. Binh, “In Situ Fabrication and Regeneration of Microtips for Scanning Tunnelling Microscopy,” J. Microsc. 152(November 1988):355-361. H.W. Fink, “Point Source for Ions and Electrons,” Physica Scripta 38(1988):260-263. H.W. Fink, “Point Source for Ions and Electrons,” Physica Scripta 38(1988):260-263. V.T. Binh, N. Garcia, “Atomic metallic ion emission, field surface melting and scanning tunneling microscopy tips,” J. Physique I 1(May 1991):605-612. S. Horch, R. Morin, “Field emission from atomic size sources,” J. Appl. Phys. 74(15 September 1993):3652-3657.

⁴⁴⁴ J. Unger, Y.A. Vlasov, N. Ernst, “Probe hole field electron/field ion microscopy and energy spectroscopy of ultrasharp [111]-oriented tungsten tips,” Appl. Surf. Sci. 87-88(2 March 1995):45-52. W. Qian, M.R. Scheinfein, J.C.H. Spence, “Brightness measurements of nanometer-sized field-emission-electron sources,” J. Appl. Phys. 73(1 June 1993):7041-7045.

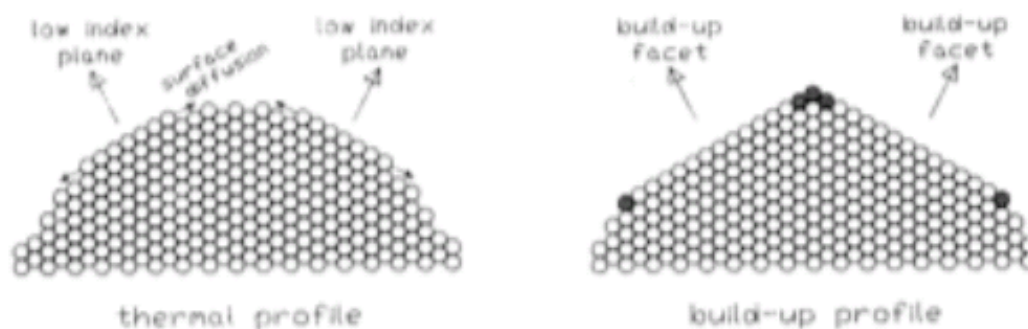
⁴⁴⁵ J. Unger, Y.A. Vlasov, N. Ernst, “Probe hole field electron/field ion microscopy and energy spectroscopy of ultrasharp [111]-oriented tungsten tips,” Appl. Surf. Sci. 87-88(2 March 1995):45-52.

⁴⁴⁶ V.T. Binh, J. Marien, “Characterization of microtips for scanning tunneling microscopy,” Surf. Sci. 202(1 August 1988):L539-L549. V.T. Binh, “In Situ Fabrication and Regeneration of Microtips for Scanning Tunnelling Microscopy,” J. Microsc. 152(November 1988):355-361.

⁴⁴⁷ H. Ness, F. Gautier, “The electronic structure and stability of transition metal nanotips – part I,” J. Phys. Condens. Matter 7(1995):6625-6640. H. Ness, F. Gautier, “The electronic structure of transition metal interacting tip and sample and atomic force microscopy – part II,” J. Phys. Condens. Matter 7(1995):6641-6661.

In the “build-up” method,⁴⁴⁸ an initially nearly hemispherical field emitter tip surface (Figure 5-1A) deforms into a polyhedral shape when the emitter is heated in the presence of a high electric field.⁴⁴⁹ The build-up process consists essentially of a local rearrangement by surface diffusion of the atoms of some low index facets, leading to an enlargement of these planes (Figure 5-1B). This local migration occurs because of the presence of a gradient in the electric field between the center of the facet and the vicinal regions. The facet enlargement will stop by itself when two neighboring facets meet each other – that is, when they are separated by a one-atom boundary line. For a tungsten tip, it is well-known that the build-up phenomenon leads to the enlargement of the (011) and (112) planes.⁴⁵⁰ Thus if the tip axis is in the (111) direction then the build-up “equilibrium” geometry shows at the apex a microfacet resulting from the meeting of the three (112) build-up planes.

Figure 5-1. Schematic representation of the build-up process, the enlargement of the facets are due to surface diffusion under the gradient of the electric field over the facets. (A) Left: thermal profile. (B) Right: build-up profile.⁴⁵¹



⁴⁴⁸ V.T. Binh, J. Marien, “Characterization of microtips for scanning tunneling microscopy,” *Surf. Sci.* 202(1 August 1988):L539-L549. Vu Thien Binh, J. Marien, 3rd French-German Symposium on Field Emission and their Applications, Rouen, France, September 1987; Vu Thien Binh, Workshop on Mathematical Treatments and Image Processings of STM, Luminy, France, October 1987. H.W. Fink, “Mono-atomic tips for scanning tunneling microscopy,” *IBM J. Res. Develop.* 30(1986):460-465.

⁴⁴⁹ P.C. Bettler, F.M. Charbonnier, “Activation Energy for the Surface Migration of Tungsten in the Presence of a High-Electric Field,” *Phys. Rev.* 119(1960):85-93. L.W. Swanson, L.C. Crouser, “Angular Confinement of Field Electron and Ion Emission,” *J. Appl. Phys.* 40(November 1969):4741-4749.

⁴⁵⁰ P.C. Bettler, F.M. Charbonnier, “Activation Energy for the Surface Migration of Tungsten in the Presence of a High-Electric Field,” *Phys. Rev.* 119(1960):85-93.

⁴⁵¹ V.T. Binh, J. Marien, “Characterization of microtips for scanning tunneling microscopy,” *Surf. Sci.* 202(1 August 1988):L539-L549.

In the “PSP” method,⁴⁵² under the simultaneous action of surface diffusion and evaporation (or corrosion) the tip geometry evolves from the initial hemispherical geometry to reach a constant geometry called pseudo-stationary profile.⁴⁵³ This means that the profile, and in particular the tip radius value, results from an equilibrium between surface diffusion and evaporation or corrosion rate. This method is routinely used to obtain FEM tips in situ and under ultra-high vacuum.⁴⁵⁴ In order to obtain tungsten “microtips”⁴⁵⁵ or “teton”⁴⁵⁶ tips (Figure 5-2), processes using heat treatments in UHV and in the presence of oxygen atmosphere and electric field are used. It appears⁴⁵⁷ that obtaining the “teton” tips is independent of the initial geometry of the tip (pseudo-stationary profile principle).⁴⁵⁸ Owing to this “blind” method, a reproducible tip can be obtained by only setting the parameters of temperature, electric field, and oxygen pressure. The PSP technique allows in situ sharpening and regeneration of the tips. A geometrical estimation using FIM gives values of ~5 nm for the dimensions of the “teton” tip base width and height.

Nanotips can be sharpened in situ in a reproducible manner – using such techniques it is possible to obtain W protrusions ending in one atom.⁴⁵⁹ Analysis of the structure of these W tips at the atomic scale has been performed by field ion microscopy.⁴⁶⁰ The successive field ion diagrams of these W tips, obtained after a progressive field evaporation, show a monatomic apex, a 3-atom

⁴⁵² V.T. Binh, J. Marien, “Characterization of microtips for scanning tunneling microscopy,” *Surf. Sci.* 202(1 August 1988):L539-L549.

⁴⁵³ V.T. Binh, R. Uzan, “Tip shape evolution: Capillarity-induced matter transport by surface diffusion. I,” *Surf. Sci.* 179(2 January 1987):540-560.

⁴⁵⁴ Vu Thien Binh, A. Piquet, H. Roux, R. Uzan, M. Drechsler, “Sharpening of metal tips by heat treatment in vacuum,” *J. Phys. E: Sci. Instrum.* 9(May 1976):377-381. Vu Thien Binh, in: *Semiconductor Interfaces, Formation and Properties*, Springer Proc. Phys. 22(1987):126.

⁴⁵⁵ V.T. Binh, J. Marien, “Characterization of microtips for scanning tunneling microscopy,” *Surf. Sci.* 202(1 August 1988):L539-L549.

⁴⁵⁶ V.T. Binh, N. Garcia, “Atomic metallic ion emission, field surface melting and scanning tunneling microscopy tips,” *J. Physique I* 1(May 1991):605-612.

⁴⁵⁷ V.T. Binh, J. Marien, “Characterization of microtips for scanning tunneling microscopy,” *Surf. Sci.* 202(1 August 1988):L539-L549.

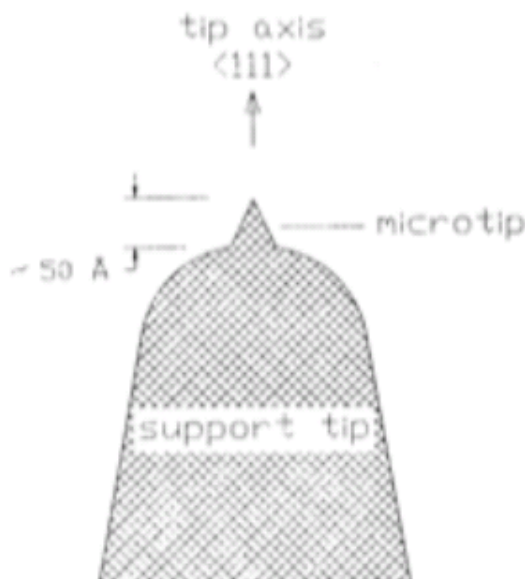
⁴⁵⁸ V.T. Binh, R. Uzan, “Tip shape evolution: Capillarity-induced matter transport by surface diffusion. I,” *Surf. Sci.* 179(2 January 1987):540-560.

⁴⁵⁹ V.T. Binh, J. Marien, “Characterization of microtips for scanning tunneling microscopy,” *Surf. Sci.* 202(1 August 1988):L539-L549. V.T. Binh, “In Situ Fabrication and Regeneration of Microtips for Scanning Tunnelling Microscopy,” *J. Microsc.* 152(November 1988):355-361. V.T. Binh, N. Garcia, “Atomic metallic ion emission, field surface melting and scanning tunneling microscopy tips,” *J. Physique I* 1(May 1991):605-612.

⁴⁶⁰ V.T. Binh, J. Marien, “Characterization of microtips for scanning tunneling microscopy,” *Surf. Sci.* 202(1 August 1988):L539-L549. V.T. Binh, “In Situ Fabrication and Regeneration of Microtips for Scanning Tunnelling Microscopy,” *J. Microsc.* 152(November 1988):355-361.

second layer, a 7-atom third layer and so on, with these tips always found to be localized around the (111) axis of the W tip's support.

Figure 5-2. Schematic drawing of a “teton” tip obtained by the PSP technique.⁴⁶¹



Three-atom tungsten W(111) tips have also been reported (Figure 5-4A).⁴⁶² For instance, Gross et al.⁴⁶³ use nanowires in the preparation of trimer tungsten tips. Their experiments were conducted at 150 K and under good UHV ($\sim 2 \times 10^{-11}$ Torr). From their paper:

“The tip was fabricated from a 0.1-mm-thick (111)-oriented W single-crystal wire by means of electrochemical etching in a concentrated potassium hydroxide solution. Tip shaping involved a series of steps performed in situ. First, the tip was flash heated to approximately $1000 \pm \text{C}$ in order to remove oxides and surface contaminants. Then the tip was operated in the field emission mode

⁴⁶¹ V.T. Binh, J. Marien, “Characterization of microtips for scanning tunneling microscopy,” *Surf. Sci.* 202(1 August 1988):L539-L549.

⁴⁶² Anne-Sophie Lucier, “Preparation and Characterization of Tungsten Tips Suitable for Molecular Electronics Studies,” M.S. Thesis, Center for the Physics of Materials, Department of Physics, McGill University, Montreal, Quebec, Canada, February 2004; <http://www.physics.mcgill.ca/~peter/theses/lucier.pdf>. See also: Anne-Sophie Lucier, Henrik Mortensen, Yan Sun, and Peter Grütter, “Determination of the atomic structure of scanning probe microscopy tungsten tips by field ion microscopy,” *Phys. Rev. B* 72, 235420 (2005).

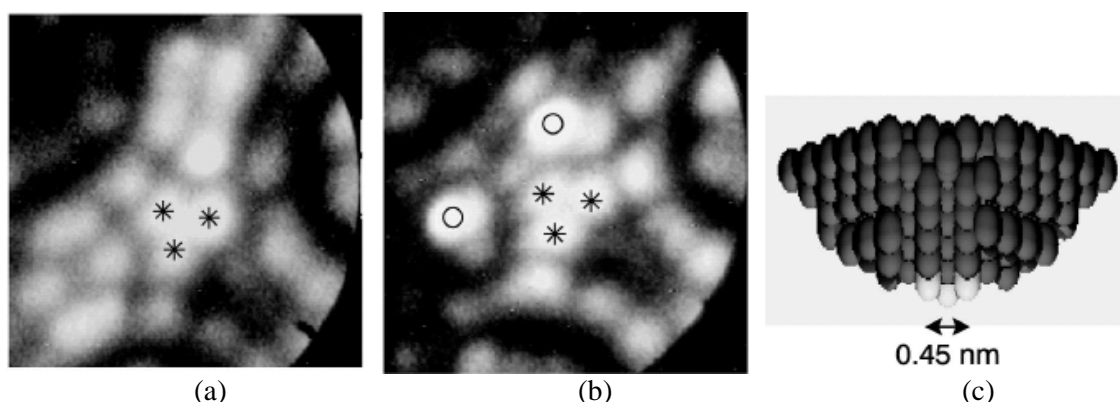
⁴⁶³ G. Cross, A. Schirmeisen, A. Stalder, P. Grütter, M. Tschudy, U. Dürig, “Adhesion Interaction between Atomically Defined Tip and Sample,” *Phys. Rev. Lett.* 80(25 May 1998):4685-4688; <http://www.physics.mcgill.ca/~peter/publications/prl1.pdf>.

for some 2 min at currents up to 5 mA. The apex was tailored to its final trimer shape by means of field evaporation under visual control using field ion microscopy (FIM).⁴⁶⁴ Typical imaging and evaporation potentials were 4.2 and 4.5 kV, respectively, and ultrapure He was used as imaging gas. A typical experimental run took about 2.5 h. An FIM image of the initial trimer tip used in the experiment reported here and the corresponding sphere model are shown in **Figure 5-3(a)** and **Figure 5-3(c)**, respectively. We found that this tip structure is stable for hours; specifically no evidence of surface migration was observed. However, one rest gas atom per hour is typically adsorbed and imaged on the tip.”

Interestingly, the tungsten trimer tip was used to test short-range attractive forces by bringing it into contact with a flat Au(111) surface. A force vs. tip-sample separation distance curve shows that: (1) the range of tip-sample distances over which substantial attractive forces are observed extends over more than 1 nm, (2) hysteresis corresponding to an energy dissipation of ~ 7 eV (calculated from the area enclosed by the approach and retraction force curves) is observed in the range of maximum adhesion interaction, (3) there is no evidence of a spontaneous jump to contact, which normally occurs in metal contacts, and (4) the repulsive branch of the force curve is essentially linear and reversible. The slope of the force curve in the repulsive regime (indicated by the dashed line) yields a contact stiffness of the order of 40 N/m, a number can be reproduced using standard elastic contact theory. Regarding Van der Waals interactions, FIM images indicate a tip radius of the order of 2.5 nm. Assuming a typical value of 3×10^{-19} J for the Hamaker constant gives adhesion forces that are at least 1 order of magnitude smaller than the measured values. This experiment exhibits adhesion forces of the order of several nanonewtons over a rather large range of tip-sample distances; the tip-sample system can support a rather large contact pressure of up to 25 GPa with no observable changes in the atomic structure of the tip.

⁴⁶⁴ H.W. Fink, “Mono-atomic tips for scanning tunneling microscopy,” IBM J. Res. Develop. 30(1986):460-465.

Figure 5-3. Field ion projection image of the (111)-oriented W tip (a) before and (b) after the adhesion experiment. Trimer atoms are marked with an asterisk (*). Note that with the exception of two additional adatoms [bright spots marked with a circle (O)] no irreversible tip changes occurred even though the apex atoms had been exposed to tensile and compressive forces of the order of 2 nN per atom, corresponding to uniaxial contact stresses of the order of 25 GPa. The two atoms marked with “O” are compatible with rest gas adsorbed during the 2.5-h lapse between acquiring image (a) and (b). The variations in intensities between (a) and (b) are due to the strong dependence of FIM image intensities on the local atomic structure such as that introduced by the two adsorbates. (c) Hard-sphere model of the tip apex reconstructed from FIM images (apex trimer highlighted in bright tones, vertical scale is expanded by a factor of 1.8).⁴⁶⁵



Other well-known examples include the single-atom W tip (FIM image),⁴⁶⁶ produced in 2006 using field-assisted chemical etching in vacuum to trim the tip shank to form a nanometer-sharp tip, and the “Teton tip” (Figure 5-4B).⁴⁶⁷ This technique for fabricating nanotips is based on spatially controlling the reaction of nitrogen gas with the surface atoms of a tungsten tip in a field

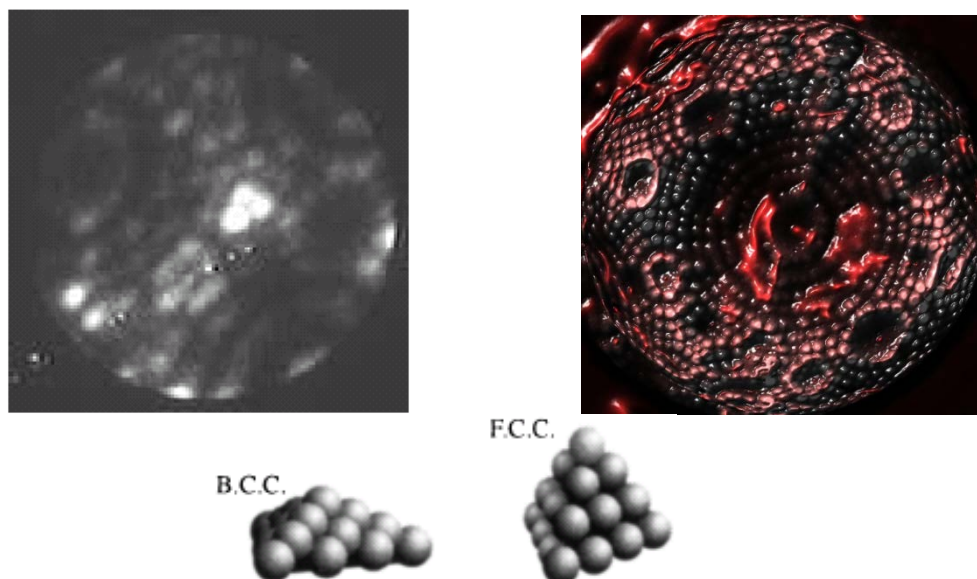
⁴⁶⁵ G. Cross, A. Schirmeisen, A. Stalder, P. Grütter, M. Tschudy, U. Dürig, “Adhesion Interaction between Atomically Defined Tip and Sample,” *Phys. Rev. Lett.* 80(25 May 1998):4685-4688; <http://www.physics.mcgill.ca/~peter/publications/prl1.pdf>.

⁴⁶⁶ Moh’d Rezeq, Jason Pitters, Robert Wolkow, “Tungsten nanotip fabrication by spatially controlled field-assisted reaction with nitrogen,” *J. Chem. Phys.* 124(28 May 2006):204716, <http://www.aip.org/png/2006/264.htm> (image), <http://www.phys.ualberta.ca/~wolkow> (movie); see also: “University of Alberta Nanotechnology Researchers Create Sharpest Tip Ever Known,” 11 July 2006, University of Alberta press release, <http://www.azonano.com/news.asp?newsID=2606>. Moh’d Rezeq, Christian Joachim, N. Chandrasekhar, “Nanotip apex modification with atomic precision and single atom tips restoration,” *Microelectronic Engineering* 86(April-June 2009):996-998.

⁴⁶⁷ 38. V.T. Binh, J. Marien, “Characterization of microtips for scanning tunneling microscopy,” *Surf. Sci.* 202(1 August 1988):L539-L549. V.T. Binh, “In Situ Fabrication and Regeneration of Microtips for Scanning Tunnelling Microscopy,” *J. Microsc.* 152(November 1988):355-361.

ion microscope (FIM); confining this field-assisted etching reaction to the shank enables the production of single-atom tips.⁴⁶⁸

Figure 5-4. (A) Top left: Three-atom apex W(111) tip (<0.6 nm).⁴⁶⁹ (B) Top right: FIM image of single-atom tip (~ 0.3 nm, inside centermost ring).⁴⁷⁰ (C) Bottom: bcc (left) and fcc (right) (111)-oriented W pyramids.⁴⁷¹



⁴⁶⁸ Moh'd Rezeq, Jason Pitters, Robert Wolkow, "Tungsten nanotip fabrication by spatially controlled field-assisted reaction with nitrogen," J. Chem. Phys. 124(28 May 2006):204716, <http://www.aip.org/png/2006/264.htm> (image), <http://www.phys.ualberta.ca/~wolkow> (movie); see also: "University of Alberta Nanotechnology Researchers Create Sharpest Tip Ever Known," 11 July 2006, University of Alberta press release, <http://www.azonano.com/news.asp?newsID=2606>.

⁴⁶⁹ Anne-Sophie Lucier, "Preparation and Characterization of Tungsten Tips Suitable for Molecular Electronics Studies," M.S. Thesis, Center for the Physics of Materials, Department of Physics, McGill University, Montreal, Quebec, Canada, February 2004; <http://www.physics.mcgill.ca/~peter/theses/lucier.pdf>. See also: Anne-Sophie Lucier, Henrik Mortensen, Yan Sun, and Peter Grütter, "Determination of the atomic structure of scanning probe microscopy tungsten tips by field ion microscopy," Phys. Rev. B 72, 235420 (2005).

⁴⁷⁰ Moh'd Rezeq, Jason Pitters, Robert Wolkow, "Tungsten nanotip fabrication by spatially controlled field-assisted reaction with nitrogen," J. Chem. Phys. 124(28 May 2006):204716, <http://www.aip.org/png/2006/264.htm> (image), <http://www.phys.ualberta.ca/~wolkow> (movie); see also: "University of Alberta Nanotechnology Researchers Create Sharpest Tip Ever Known," 11 July 2006, University of Alberta press release, <http://www.azonano.com/news.asp?newsID=2606>.

⁴⁷¹ A.L. Vázquez de Parga, O.S. Hernán, R. Miranda, A. Levy Yeyati, N. Mingo, A. Martin-Rodero, F. Flores, "Electron Resonances in Sharp Tips and Their Role in Tunneling Spectroscopy," Phys. Rev. Lett. 80(12 January 1998):357-360; <http://people.nas.nasa.gov/~mingo/WWW/natalio/publications/pr198.pdf>

The initial tip was prepared from a polycrystalline tungsten wire of 0.4 mm in diameter by electrochemical etching. The tip was loaded into an ultra high vacuum (UHV) homemade FIM setup,⁴⁷² then resistively heated at 1000 °C to desorb various contaminants from the tip surface. Subsequently, the tip was transferred into the FIM chamber with a background pressure of 1×10^{-10} Torr, and placed in front of the FIM screen (a combination of a phosphor screen and microchannel plates). The tip was maintained at LN2 temperature while helium gas was introduced at 8×10^{-6} Torr for imaging. Later the tip voltage was increased gradually to further clean the tip and to field-evaporate all metallic mini-protrusions from the apex surface. An atomically clean tip surface of a radius ~ 11 nm was obtained at a voltage = 5.9 kV. The tip axial orientation and azimuthal angular rotation was determined by comparing the FIM image with a standard stereographic map of a (bcc) lattice,⁴⁷³ as shown in **Figure 5-5a**. These tip conditions was maintained throughout the experiment for reliable modeling of the subsequently fabricated nanotips. Then N₂ gas was introduced in the chamber in a way to perform the field assisted etching.⁴⁷⁴ The FIM image in **Figure 5-5b** was taken during the sharpening process and shows a reduced apex area. Finally a single atom apex was formed in **Figure 5-5c** at 2 kV. The removal of the last atom by slightly increasing the applied voltage revealed an apex with a few atoms on the topmost layer (**Figure 5-5d**). The structure of the tip is further illustrated in **Figure 5-6**.

In one study,⁴⁷⁵ atomically sharp STM tips were made of polycrystalline W wire that was electrochemically etched. The tips were cleaned in situ by applying 1 kV to the tip and approaching a clean tantalum foil until a field emission current of 10 mA was established. This current was kept constant for several minutes by readjusting the tip-foil distance until the current is stable. Tips cleaned with this method produced reproducible I-V spectra. This high-current, field-emission cleaning process⁴⁷⁶ is believed to lead to local melting and recrystallization of the tip end, whereby the facets with the highest density of atoms, e.g., W(110) and W(111), are most likely to be present. They considered semi-infinite pyramidal tips built from perfect (100) and

⁴⁷² Moh'd Rezeq, Jason Pitters, Robert Wolkow, "Tungsten nanotip fabrication by spatially controlled field-assisted reaction with nitrogen," J. Chem. Phys. 124(28 May 2006):204716, <http://www.aip.org/png/2006/264.htm> (image), <http://www.phys.ualberta.ca/~wolkow> (movie); see also: "University of Alberta Nanotechnology Researchers Create Sharpest Tip Ever Known," 11 July 2006, University of Alberta press release, <http://www.azonano.com/news.asp?newsID=2606>.

⁴⁷³ E. Muller, T.T. Tsong, Field Ion Microscopy: Principles and Applications, American Elsevier Publishing Company, Inc. (1969).

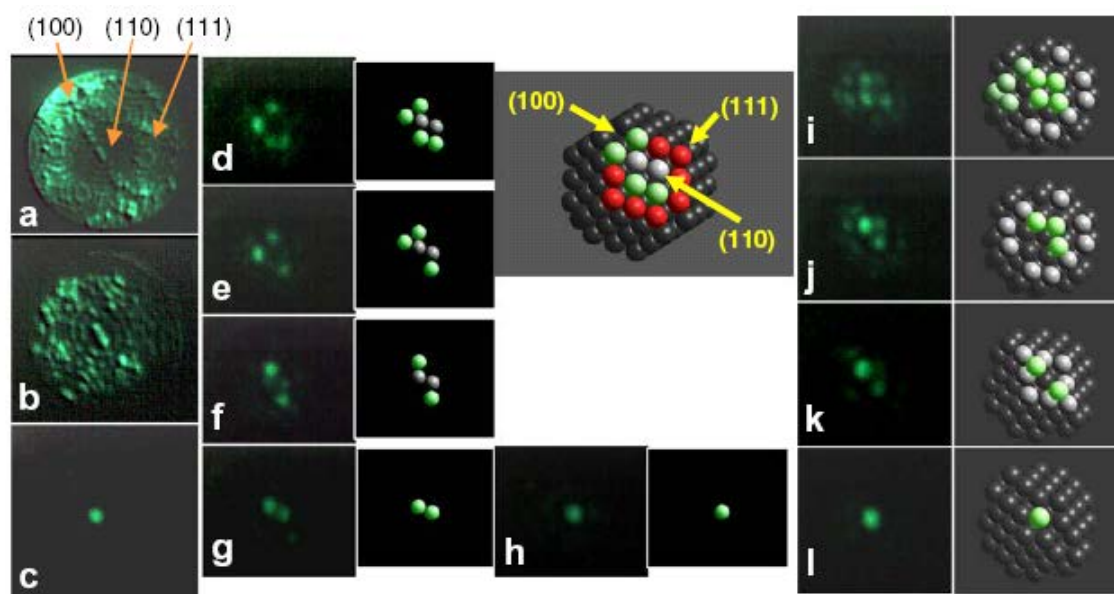
⁴⁷⁴ Moh'd Rezeq, Jason Pitters, Robert Wolkow, "Tungsten nanotip fabrication by spatially controlled field-assisted reaction with nitrogen," J. Chem. Phys. 124(28 May 2006):204716, <http://www.aip.org/png/2006/264.htm> (image), <http://www.phys.ualberta.ca/~wolkow> (movie); see also: "University of Alberta Nanotechnology Researchers Create Sharpest Tip Ever Known," 11 July 2006, University of Alberta press release, <http://www.azonano.com/news.asp?newsID=2606>.

⁴⁷⁵ A.L. Vázquez de Parga, O.S. Hernán, R. Miranda, A. Levy Yeyati, N. Mingo, A. Martin-Rodero, F. Flores, "Electron Resonances in Sharp Tips and Their Role in Tunneling Spectroscopy," Phys. Rev. Lett. 80(12 January 1998):357-360; <http://people.nas.nasa.gov/~mingo/WWW/natalio/publications/prl98.pdf>

⁴⁷⁶ R.M. Feenstra, J.A. Stroscio, A.P. Fein, "Tunneling spectroscopy of the Si(111) 2x1 surface," Surf. Sci. 181(1 March 1987):295-306.

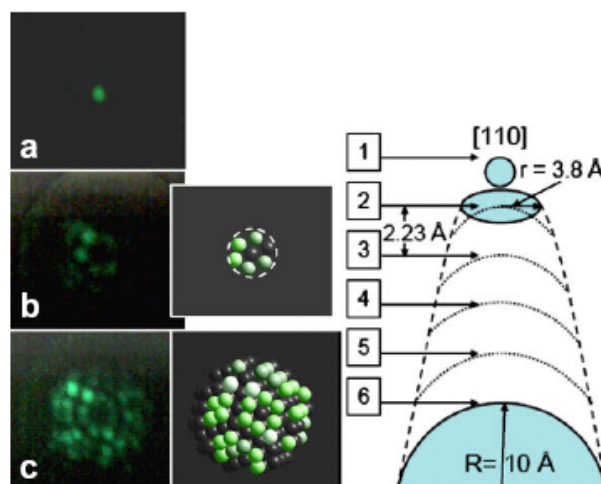
(111) planes stacked both in the bcc and the fcc structures (Figure 5-4C) and concluded that the fcc tips were most likely to have been present experimentally.

Figure 5-5. (a) An atomically clean W(110) tip apex at 5.9 kV. (b) A reduced apex during the etching process. (c) A single atom tip at 2 kV. (d) An atomic layer after the removal of a previously topmost atom. Atoms arrangement can be extracted from the far right spherical crystal model (radius = 8.5 Å). (d)-(h) FIM images and next ball models illustrate the restoration of the single atom tip. (i)-(l) FIM images (left) and ball models from a spherical crystal of a radius = 7.7 Å (right) illustrate the restoration of a subsequent single atom tip.⁴⁷⁷



⁴⁷⁷ Moh'd Rezeq, Christian Joachim, N. Chandrasekhar, "Nanotip apex modification with atomic precision and single atom tips restoration," *Microelectronic Engineering* 86(April-June 2009):996-998.

Figure 5-6. (a) A single atom tip. (b) The underneath atomic layer. (c) A nanotip after the removal of five top layers. The schematic, far right, estimates the nanotip shape based on the ball models in (b) and (c). The tip voltage was increased from 2 kV in (a) to 2.3 kV in (c).⁴⁷⁸



Oriented single crystalline tips⁴⁷⁹ can be more sharp and stable because of the lower concentration of defects – e.g., sharp tip apices can be obtained on W(001) and Mo(001) tips using coaxial ion etching (oriented in Mo(110) direction)⁴⁸⁰ and thermal-field treatments⁴⁸¹ but the high price of such single crystalline probes has until fairly recently⁴⁸² restricted their usage in high resolution STM studies. Studies of individual W adatoms on W(111) surface⁴⁸³ shows that it is fairly difficult to cause a single W atom to diffuse (activation energy ~ 1.9 eV), and even smaller

⁴⁷⁸ Moh'd Rezeq, Christian Joachim, N. Chandrasekhar, "Nanotip apex modification with atomic precision and single atom tips restoration," *Microelectronic Engineering* 86(April-June 2009):996-998.

⁴⁷⁹ See, for example: Applied Physics Technologies, "STM Tips," 2008; <http://www.a-p-tech.com/stmtips.htm>.

⁴⁸⁰ S. Morishita, F. Okuyama, "Sharpening of monocrystalline molybdenum tips by means of inert-gas ion sputtering," *J. Vac. Sci. Technol. A* 9(January 1991):167-169.

⁴⁸¹ Juying Dou, Ergang Chen, Changchun Zhu, Deqing Yang, "New method for imaging atoms," *J. Vac. Sci. Technol. B* 18(2000):2681-2683; Shin Fujita, Hiroshi Shimoyama, "Thermal-field treatment for creating single-crystal tungsten tips with ultimate sharpness," *J. Vac. Sci. Technol. B* 26(2008):738-744.

⁴⁸² A.N. Chaika, V.N. Semenov, V.G. Glebovskiy, S.I. Bozhko, "Scanning tunneling microscopy with single crystalline W(001) tips: High resolution studies of Si(557)5x5 surface," *Appl. Phys. Lett.* 95(2009):173107.

⁴⁸³ T.Y. Fu, W.J. Weng, T.T. Tsong, "Dynamic study of W atoms and clusters on W(111) surfaces," *Applied Surface Science* 254(30 September 2008):7831-7834.

clusters are unlikely to migrate at room temperature or below, e.g., diffusion barrier is ~ 1.6 eV for 2-atom clusters, rising to ~ 2.0 eV for 10-atom clusters.

According to Hwang et al.,⁴⁸⁴ who define “single-atom tip” as a “metal tip ending with one atom at its apex,” it is difficult to repeatably prepare a reliable single atom tip for commercial applications. They note that there are several conventional methods for preparing single atom tips, most involving the use of electric fields. One method uses a high electric field gradient to produce directional surface mobility to generate a protrusion terminated with one atom.⁴⁸⁵ Other methods use high-energy electrons to heat metal tips, combined with field forming effect, to generate single atom tips, or field surface melting⁴⁸⁶ or ion bombardment in combination with field evaporation and vacuum sputtering to place a single tungsten atom on top of a small tungsten (111) facet.⁴⁸⁷ However, Hwang et al. complain that these conventional preparations of an SAT are “complicated and with poor yield rates. The single atom tip so prepared does not have a thermodynamically stable structure either, thus the operation lifetime is short and regeneration of single atom tips is very difficult or impossible. The metal tips so prepared don’t have a well-defined structure of atoms at their apex and applications of such metal tips outside the ultra-high vacuum system are not possible. These drawbacks hinder the single atom tip from commercial applications [which is why] such single atom tips have so far been used only in the laboratories.” (It should be noted that many of these complaints arise in context of the usual application of these tips as electron or ion beam sources, in which the sharp tip may be rapidly corroded by contact with ambient O₂, N₂, or H₂O, or the energy barriers to tip atom migration may be more easily overcome by the high fields involved.)

One example of the aforementioned techniques is the fabrication of highly angular nanostructures on a tip surface via the thermal-field (TF) treatment of metal tips in which a polyhedral shape builds up on a tip if it is heated under a strong electrostatic field.⁴⁸⁸ In 1968, Crew et al.⁴⁸⁹ first

⁴⁸⁴ Ing-shouh Hwang, Hong-shi Kuo, Tien T. Tsong, Tsu-yi Fu, “Single-atom tip and preparation method thereof,” United States Patent 7507320, filing date 10/09/2004, publication date 03/24/2009; <http://www.freepatentsonline.com/7507320.pdf>.

⁴⁸⁵ H.W. Fink, “Mono-atomic tips for scanning tunneling microscopy,” IBM J. Res. Develop. 30(1986):460-465. A.P. Janssen, J. P. Jones, “The sharpening of field emitter tips by ion sputtering,” J. Phys. D 4(January 1971):118-123.

⁴⁸⁶ V.T. Binh, N. Garcia, “Atomic metallic ion emission, field surface melting and scanning tunneling microscopy tips,” J. Physique I 1(May 1991):605-612. V.T. Binh, N. Garcia, “On the electron and metallic ion emission from nanotips fabricated by field-surface-melting technique – experiments on W and Au tips,” Ultramicroscopy 42-44(1992):80-90.

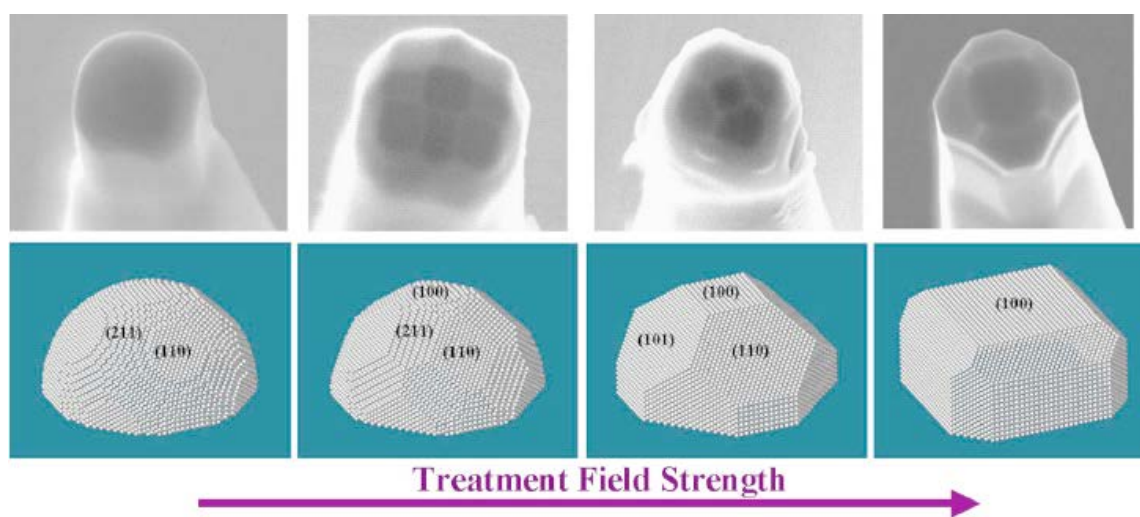
⁴⁸⁷ H.W. Fink, “Mono-atomic tips for scanning tunneling microscopy,” IBM J. Res. Develop. 30(1986):460-465. P.C. Bettler, F.M. Charbonnier, “Activation Energy for the Surface Migration of Tungsten in the Presence of a High-Electric Field,” Phys. Rev. 119(1960):85-93.

⁴⁸⁸ P.C. Bettler, F.M. Charbonnier, “Activation Energy for the Surface Migration of Tungsten in the Presence of a High-Electric Field,” Phys. Rev. 119(1960):85-93.

⁴⁸⁹ A.V. Crewe, D.N. Eggenberger, J. Wall, L.M. Welter, “Electron Gun Using a Field Emission Source,” Rev. Sci. Instrum. 39(April 1968):576.

proposed to utilize this buildup phenomenon in order to restore the low extraction voltage of blunted field emitters, a method called the “remolding” technique. In 2008, Fujita and Shimoyama⁴⁹⁰ at Meijo University (Tokyo) used thermal-field treatment to create (111)-oriented tungsten SATs (just one or a few atoms at the tip). They show an example of the tip shape evolution of (100)-oriented tungsten as a function of the TF treatment field strength (Figure 5-7). Note that the tip initially takes a hemispherical shape due to surface tension effects, but once the field exceeds a certain strength the tip evolves into polyhedrons covered by a set of low index crystal planes. Tip shape appears closely related to the equilibrium crystal shape as determined by the surface free energy anisotropy. As a result, the TF treatment allows control of the surface tension anisotropy via the application of a strong electrostatic field to the tip,⁴⁹¹ giving the possibility of creating a very sharp apex on the polyhedrons.

Figure 5-7. Summary of the shape evolution of the (100)-oriented tungsten tip emitter with increasing electric field under the TF treatment; the SEM images and the emitter tip shapes constructed by the bcc hard sphere model are presented.⁴⁹²



To create a nanotip with single-atom sharpness, the tip was first processed as above at high temperature (2300 K) until the (111) apex became bounded by (110) planes (i.e., (A) to (E) in

⁴⁹⁰ Shin Fujita, Hiroshi Shimoyama, “Thermal-field treatment for creating single-crystal tungsten tips with ultimate sharpness,” J. Vac. Sci. Technol. B 26(March 2008):738-744.

⁴⁹¹ Shin Fujita, Hiroshi Shimoyama, “Mechanism of surface-tension reduction by electric-field application: Shape changes in single-crystal field emitters under thermal-field treatment,” Phys. Rev. B 75(15 June 2007):235431.

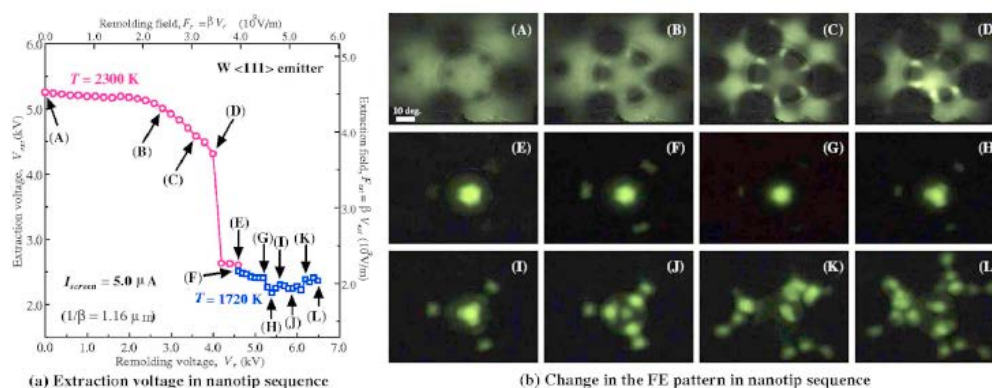
⁴⁹² Shin Fujita, Hiroshi Shimoyama, “Thermal-field treatment for creating single-crystal tungsten tips with ultimate sharpness,” J. Vac. Sci. Technol. B 26(March 2008):738-744.

Figure 5-8(b)). Then the treatment temperature was lowered to 1720 K while maintaining the constant remolding voltage at 4600 V (i.e., (E) to (F) in **Figure 5-8(b)**). The observation of the FE pattern confirmed that the tip shape only slightly changed during the temperature lowering steps. By this way it was shown that the sharp (111) apex can be a stable configuration at 1720 K, even though this shape could not be reached by a simple low temperature treatment. Then, the remolding cycle was resumed at the low temperature by increasing the remolding voltage again (i.e., (F) to (L) in **Figure 5-8(b)**). At 5400 V, the extraction voltage dropped discontinuously and the corresponding FE pattern took on a triangular structure. It can be inferred that the sharpest (111) apex, i.e., the SAT nanotip, was formed at stage (H). Further increase of the remolding voltage resulted in gradual increase of the extraction voltage. The FE pattern finally became somewhat random at the end, i.e., the over-remolding state was reached. Fujita and Shimoyama designate the remolding process that changes the treatment temperature at some stage as the “nanotip sequence”.⁴⁹³

The improved angular confinement is definitely due to the morphological change of the tip.

Figure 5-9A illustrates that the field emission from the tip dramatically changes as the tip shape evolves from the A phase, with (211) planes surrounding the (111) apex, to the B phase after the plane collapse. **Figure 5-9B** shows the SEM images of two emitters that have been TF treated by the nanotip sequence. It is clearly seen that the emitter tips are taking a well-defined polyhedral shape dominated by (110) and (100) planes.

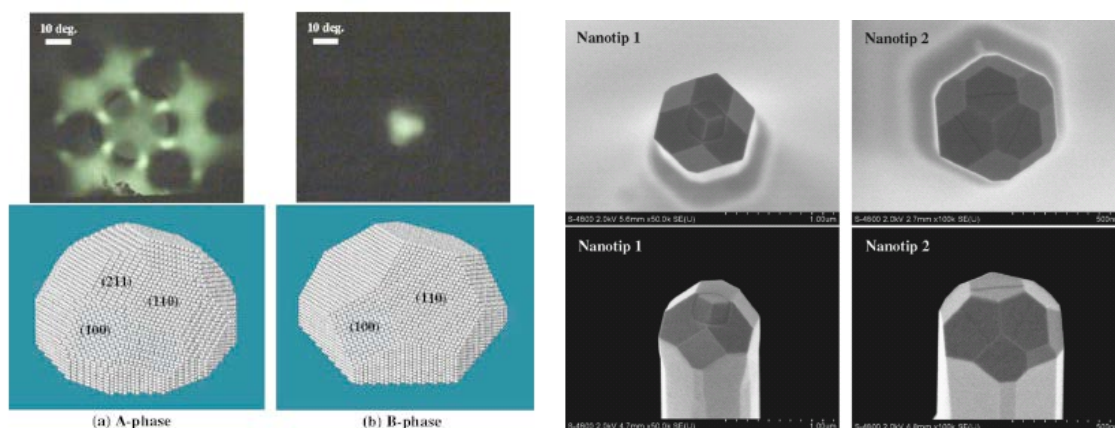
Figure 5-8. Nanotip fabrication sequence of the (111) oriented single-crystal tungsten emitter. (a) The reduction of the extraction voltage to give a fixed screen current with the progress of the sequence. (b) The evolution of the FE pattern. In nanotip sequence the TF treatment is first conducted at a relatively high temperature until the (211) plane collapse takes place. Then the temperature is lowered and the increase of the remolding voltage is resumed. The sequence should be terminated at the stage “(H)”, when the (111) apex becomes the sharpest.⁴⁹⁴



⁴⁹³ S. Fujita, H. Shimoyama, Japanese Patent No. 2007-79736, 26 March 2007.

⁴⁹⁴ Shin Fujita, Hiroshi Shimoyama, “Thermal-field treatment for creating single-crystal tungsten tips with ultimate sharpness,” J. Vac. Sci. Technol. B 26(March 2008):738-744.

Figure 5-9. (A) At left: Comparison of the two tip morphologies of (111) oriented single-crystal tungsten obtained by the TF treatment. (a) Usually, the apex is formed by (211) planes and the FE pattern shows divergent electron emission (A phase). (b) The (111) apex made by the (110) planes (B phase) can be produced by the nanotip sequence. The angular confinement of the field emission is dramatically improved. **(B) At right:** SEM images of two (111) oriented tungsten tips TF treated by the nanotip sequence. It is clearly seen that the emitter tips are taking a well-defined polyhedral shape dominated by (110) and (100) planes.⁴⁹⁵



5.2 Palladium-Coated Tungsten SATs

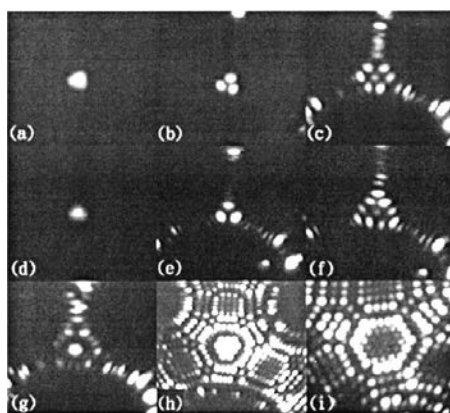
Single-atom sharp pyramidal W tips, wrapped in a Pd overlayer, having atom-perfect wedges can be routinely and repeatedly created using surface-science techniques⁴⁹⁶ (Figure 5-10) and are

⁴⁹⁵ Shin Fujita, Hiroshi Shimoyama, "Thermal-field treatment for creating single-crystal tungsten tips with ultimate sharpness," J. Vac. Sci. Technol. B 26(March 2008):738-744.

⁴⁹⁶ H.S. Kuo, I.S. Hwang, T.-Y. Fu, J.Y. Wu, C.C. Chang, T.T. Tsong, "Preparation and characterization of single-atom tips," Nano Lett. 4(December 2004):2379-2382; http://aao.sinica.edu.tw/download/publication_e/Year2005/math04.pdf, http://dns.ntu-ccms.ntu.edu.tw/references/NANO_LETT-4-2379-2004.pdf. C. Dong, L. Zhang, U. Diebold, T.E. Madey, "A Search For Surface Alloy Formation in Faceting Induced by Monolayer Metal Films: Pd/W(111) and Ni/W(111)," Surface Science 322(1995):221-229. T.-Y. Fu, L.C. Cheng, C.H. Nien, T.T. Tsong, "Method of creating a Pd-covered single-atom sharp W pyramidal tip: Mechanism and energetics of its formation," Phys. Rev. B 64(15 September 2001):113401; <http://www.phys.sinica.edu.tw/~nano/publication/223.pdf>. Theodore E. Madey, Kalman Pelhos, Qifei Wu, Robin Barnes, Ivan Ermanoski, Wenhua Chen, Jacek J. Kolodziej, John E. Rowe, "Nanoscale surface chemistry," Proc. Nat. Acad. Sci. USA 99(2002):6503-6508; http://www.physics.rutgers.edu/~wchen/Madey_page/Full_Publications/PDF/madey_PNAS_2002.pdf. Tsuyoshi Ishikawa, Keisuke Tagawa, Tomohiro Urata, Chuhei Oshima, Boklae Cho, Eiji Rokuta, "Fluctuations of Electron Beams Emitted from Single-Atom Electron Sources Prepared with Different Techniques," e-J. Surf. Sci. Nanotech. 6(2008):11-14; <http://www.jstage.jst.go.jp/article/ejsnt/6/0/11/> pdf. T. Itagaki, E. Rokuta, H.-S. Kuo, K. Nomura, T.

thermally stable up to 1000 K because of the exceptionally large surface-energy anisotropy of the Pd covered W(111) surface; the W tip (apical ~50 nm radius of curvature) is covered with only one physical monolayer of Pd.⁴⁹⁷ The trap barrier for the top Pd atom on a Pd trimer is much greater than 2.8 eV.⁴⁹⁸ The deep trap is due to the formation of an exceptionally stable four-atom Pd cluster at the pyramid tip driven by the large surface-energy anisotropy of the Pd-covered W surfaces. From the original paper:⁴⁹⁹

Figure 5-10. FIM images showing the structure of a single-atom tip: (a) the top layer consists of only one atom; (b) the second layer consists of three atoms; (c) the third layer consists of seven atoms; (d) a regenerated single-atom tip by annealing to 1000 K for 3 min, again only one atom is in the first layer; (e) the second layer consists of three atoms; (f) the third layer now consists of ten atoms; (g) one field-evaporation-resistive atom is left on the third layer, which should be W atom; (h) we can observe the size of (211) facets increase after field evaporating many layers for comparing with (i) a clean W tip without extra treatment of forming a single-atom tip.⁵⁰⁰



Ishikawa, B.-L. Cho, I.-S. Hwang, T.T. Tsong, C. Oshima, "Stabilities in field electron emissions from noble-metal covered W nano-tips: apex structure dependence," *Surface and Interface Analysis* 39(2006):299-303.

⁴⁹⁷ T.-Y. Fu, L.C. Cheng, C.H. Nien, T.T. Tsong, "Method of creating a Pd-covered single-atom sharp W pyramidal tip: Mechanism and energetics of its formation," *Phys. Rev. B* 64(15 September 2001):113401; <http://www.phys.sinica.edu.tw/~nano/publication/223.pdf>.

⁴⁹⁸ Roland Stumpf, Matthias Scheffler, "Theory of self-diffusion at and growth of Al(111)," *Phys. Rev. Lett.* 72(1994):254-257. Erratum: *Phys. Rev. Lett.* 73(1994):508.

⁴⁹⁹ T.-Y. Fu, L.C. Cheng, C.H. Nien, T.T. Tsong, "Method of creating a Pd-covered single-atom sharp W pyramidal tip: Mechanism and energetics of its formation," *Phys. Rev. B* 64(15 September 2001):113401; <http://www.phys.sinica.edu.tw/~nano/publication/223.pdf>.

⁵⁰⁰ T.-Y. Fu, L.C. Cheng, C.H. Nien, T.T. Tsong, "Method of creating a Pd-covered single-atom sharp W pyramidal tip: Mechanism and energetics of its formation," *Phys. Rev. B* 64(15 September 2001):113401; <http://www.phys.sinica.edu.tw/~nano/publication/223.pdf>.

“Here we report a simple method of creating atomically perfect, single-atom pyramidal tips based on impurity and thermal-induced faceting of a crystal face. (The late⁵⁰¹) T.E. Madey and co-workers found and observed with scanning-tunneling microscopy⁵⁰² that three-sided pyramids of a few nanometers size with either {112} or {011} facets can be formed on the W(111) surface by annealing the surface covered with a few monolayers of thermally deposited Pd. The driving force of the pyramidal faceting is attributed to the enhanced anisotropy of the surface free energy of the Pd-covered W surfaces. By taking into account the accompanied increase in the total surface area in this faceting process, along with the involved kinetic factor for the significant mass transport, they also explained why the resultant surface morphology is dominated by {112} facets instead of {011} ones (having a steeper shape of pyramids). We have succeeded in using this surface-science method to create a Pd-layer-covered single-atom sharp pyramidal W tip with atom-perfect wedges on the (111) face of a W field-emitter tip, and to confirm the facets to be the {112} (Figure 5-11). The procedure is very simple and the tip can also be easily regenerated after the top few layers are removed by field evaporation.”

“The W tips are prepared by electrochemical polishing with saturated KOH (aq.) of a piece of thin W wire of 0.1 mm diameter. After careful degassing and low-temperature field evaporation, about 1–2 monolayers of Pd is deposited on the clean W tip. Immediately after the tip is annealed to about 1000 K for 3 min, a single-atom pyramidal tip can be observed at the (111) face as shown in Figure 5-10a. Field evaporation of this atom reveals the second layer to consist of three atoms as seen in Figure 5-10b. If field evaporation is continued, the third layer consisting of seven atoms is seen as in Figure 5-10c. Keeping on field evaporating, we can desorb layer after layer and observe the structure of the next layer. Of course, the single-atom tip is destroyed. Interestingly, the tip can be regenerated after it is annealed again without a new Pd deposition. Figures 5-10(c-f) show the structures of the top three layers of the regenerated single-atom tip. In this case, the third layer consists of ten atoms, now having additional three corner atoms, or the pyramid is now atom perfect without any missing corner atom. During the field evaporation, some special features are noticeable. There is always one atom left on the fourth layer when the third layer is field evaporated as shown in Figure 5-10g. This atom is much harder to be field desorbed than other atoms of the third layer. It can be removed only when the field is high enough to desorb the fourth layer. This field-evaporation-resistive atom is obviously a W atom rather than a Pd atom. A W atom appearing in the third layer of the single-atom tip is clear evidence that only one Pd physical layer covers up the W pyramidal tip, or only one Pd layer is needed to induce the faceting of the W(111) surface. This is the reason we can regenerate the single-atom tip without a new deposition of Pd since only a few Pd atoms need to be supplied from the surrounding surface to regenerate the single-atom pyramid again.”

⁵⁰¹ Ulrike Diebold, “In memoriam of Theodore Eugene Madey: October 24, 1937–July 27, 2008,” *Surface Science Reports* 64(28 February 2009):iii-iv.

⁵⁰² C.H. Nien, T.E. Madey, “Atomic structures on faceted W(111) surfaces induced by ultrathin films of Pd,” *Surf. Sci. Lett.* 380(15 May 1997):L527-L532;
http://www.physics.rutgers.edu/~madey/Publications/Full_Publications/PDF/madey_SS_1997_N.pdf. C.H. Nien, T.E. Madey, Y.W. Tai, T.C. Leung, J.G. Che, C.T. Chan, “Coexistence of {011} facets with {112} facets on W(111) induced by ultrathin films of Pd,” *Phys. Rev. B* 59(1999):10335-10340. K.J. Song, R.A. Demmin, C. Dong, E. Garfunkel, T.E. Madey, “Faceting Induced by an Ultrathin Film: Pt on W(111),” *Surf. Sci. Lett.* 227(1990):L79.

“Theoretical studies⁵⁰³ from both embedded-atom and first-principles calculations find that the bcc (211) surface covered by a certain metal film has lower surface free energy than the film-covered bcc (111) surface. In fact impurity-induced faceting has been phenomenon of great interest for many years. The thermodynamic driving force is attributed to the surface-energy anisotropy.⁵⁰⁴ In Pd covered W(111), the energetic advantage is so large that it can compensate for the accompanied increase in total surface area of the forming {112} face pyramid. The other reason is that it is kinetically favorable. Characteristic behavior is found when one of the kinetic processes becomes rate limiting.⁵⁰⁵ The activation energies of terrace diffusion for W on W(110), W(211), W(111), and Pd on W(110), W(211), W(111) are 0.8660.09, 0.7660.07, 1.78 eV, and 0.51, 0.3460.01, 1.0260.06 eV, respectively.⁵⁰⁶ Pd atoms with the much lower diffusion barriers are much more mobile than W atoms. In other words, they can approach the stable state at a much lower temperature. These smaller barriers turn out to be a critical factor for forming pyramidal facets and the single-atom tip for two reasons. First, Pd atoms can desorb already at ~1100 K.⁵⁰⁷ Second, the surface energy anisotropy, which is the thermodynamic driving force, generally decreases with increasing temperature.⁵⁰⁸ From the diffusion data, we also notice that Pd atoms diffuse along the (112) surface channel with the smallest barrier. One can easily see from the structure model shown in **Figure 5-11** that Pd atoms can easily move to the upper (111) layers along the (112) surface channels to form a single-atom tip. But, even before the (112) channels are formed, Pd atoms can move toward the W(111) facet and can step up the (111) layers

⁵⁰³ J.G. Che, C.T. Chan, C.H. Kuo, T.C. Leung, “Faceting Induced by Ultrathin Metal Films: A First Principles Study,” *Phys. Rev. Lett.* 79(24 November 1997):4230-4233; <http://www.physics.fudan.edu.cn/tps/people/jgche/paper/prl79-4230.pdf>. S.P. Chen, “Theoretical studies of ultrathin film-induced faceting on W(111) surfaces,” *Surf. Sci.* 274(15 August 1992):L619-L626.

⁵⁰⁴ G. Wulff, “Zur frage der Geschwindigkeit des Wachstums und der Aufiosung der Krystalflächen,” *Z. Kristallogr. Mineral.* 34(1901):499-531. Conyers Herring, “Some Theorems on the Free Energies of Crystal Surfaces,” *Phys. Rev.* 82(1951):87-93. Ellen D. Williams, Norman C. Bartelt, “Surface faceting and the equilibrium crystal shape,” *Ultramicroscopy* 31(September 1989):36-48.

⁵⁰⁵ M. Ozdemir, A. Zangwill, “Morphological equilibration of a faceted crystal,” *Phys. Rev. B* 45(1992):3718-3729.

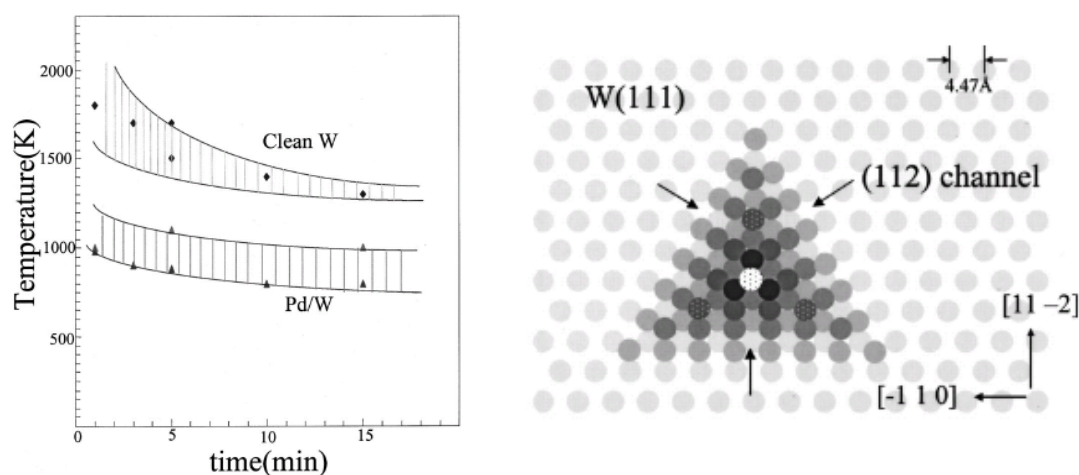
⁵⁰⁶ D.W. Bassett, M.J. Parsley, “Field ion microscope studies of transition metal adatom diffusion on (110), (211) and (321) tungsten surfaces,” *J. Phys. D: Appl. Phys.* 3(1970):707-716. W.R. Graham, G. Ehrlich, “Surface Self-Diffusion of Single Atoms,” *Thin Solid Films* 25(January 1975):85-96; William R. Graham, Gert Ehrlich, “Direct identification of atomic binding sites on a crystal,” *Surf. Sci.* 45(October 1974):530-552. D.W. Bassett, “Field ion microscope studies of submonolayer films of nickel, palladium and platinum on (110) tungsten surfaces,” *Thin Solid Films* 48(1978):237-246. D. Cowell Senft, G. Ehrlich, “Long Jumps in Surface Diffusion: One-Dimensional Migration of Isolated Adatoms,” *Phys. Rev. Lett.* 74(1995):294-297.

⁵⁰⁷ K.J. Song, C.Z. Dong, T.E. Madey, “Faceting of tungsten(111) Induced by Ultrathin Palladium Films,” *Langmuir* 7(December 1991):3019-3026; <http://pubs.acs.org/doi/abs/10.1021/la00060a019>.

⁵⁰⁸ J.C. Heyraud, J.J. Metois, “Equilibrium shape and temperature: Lead on graphite,” *Surf. Sci.* 128(1983):334-342.

already.⁵⁰⁹ The measured extra reflective barrier for Pd diffusion on the W(110), W(211), W(111) are 0.2860.03, 0.3060.03, 0.6460.03 eV, respectively.⁵¹⁰ Although the reflective barriers are quite high, they are not rate limiting above 500 K. Thus Pd atoms can move across different faces toward the (111) face from any part of the W-tip surface. Another kinetic factor of the mass transport favoring a {112} pyramid more than a steeper {011} one is that the latter involves rearrangements of many more atoms from the original surface morphology than the former.”

Figure 5-11. Left: Diagram showing the temperature and time needed in facet formation for clean W tips and Pd-covered W tips. **Right:** Top view of a hard-sphere model showing the atomic structures near the top of the single-atom tip. The single atom sits on a pyramid with three {211} facets. Atoms can move to upper layers along the (112) surface channel as the arrows indicate. The gray spheres with white dots are corner atoms that are missing sometimes as in **Figure 5-10c**.⁵¹¹



“An important question is the stability of the single-atom tip. We find that the top atom routinely appears after annealing at 1000 K for 3 min and will not disappear by further annealing. The trap barrier for the top Pd atom on Pd trimer is therefore much greater than 2.8 eV.⁵¹² This trapping

⁵⁰⁹ T.-Y. Fu, Y.R. Tzeng, T.T. Tsong, “Atomic View of the Upward Movement of Step-Edge and In-Layer Atoms of Ir Surfaces,” *Phys. Rev. Lett.* 76(1996):2539-2542.

⁵¹⁰ T.-Y. Fu, L.C. Cheng, C.H. Nien, T.T. Tsong, “Method of creating a Pd-covered single-atom sharp W pyramidal tip: Mechanism and energetics of its formation,” *Phys. Rev. B* 64(15 September 2001):113401; <http://www.phys.sinica.edu.tw/~nano/publication/223.pdf>.

⁵¹¹ T.-Y. Fu, L.C. Cheng, C.H. Nien, T.T. Tsong, “Method of creating a Pd-covered single-atom sharp W pyramidal tip: Mechanism and energetics of its formation,” *Phys. Rev. B* 64(15 September 2001):113401; <http://www.phys.sinica.edu.tw/~nano/publication/223.pdf>.

⁵¹² T.-Y. Fu, L.C. Cheng, C.H. Nien, T.T. Tsong, “Method of creating a Pd-covered single-atom sharp W pyramidal tip: Mechanism and energetics of its formation,” *Phys. Rev. B* 64(15 September 2001):113401; <http://www.phys.sinica.edu.tw/~nano/publication/223.pdf>.

barrier is much larger than either the diffusion barrier or the extra-reflective barrier of Pd on the W(111). The deep trap is due to the formation of an exceptionally stable four-atom Pd cluster at the pyramid tip driven by the large surface-energy anisotropy of the Pd-covered W surfaces. The formation of a single-atom tip is promoted by a directional walk of Pd adatoms toward the apex position as in a directional-walk experiment.⁵¹³ We estimate with a measurement the potential-energy difference toward and away from the tip to be 0.013 eV. This tilt in the surface potential toward the upper (111) layer arises also from the surface-free-energy anisotropy.”

Szczepkowicz and Ciszewski⁵¹⁴ also tested thermally-annealed Pd faceting on the apex of a tungsten needle having a radius of curvature of ~200 nm (Figure 5-12). Massive faceting occurred at annealing temperatures of ~1100 K, and the number density and size of facets were observed to be a function of temperature. A surprising result was that the faceting was independent of the amount of deposited adsorbate Pd atoms – depositions from 3-15 nm thickness always produced the same amount of Pd on the surface within the FIM field of view. This was attributed primarily to the surface diffusion of Pd towards the regions outside the field of view of the microscope.

Figure 5-12. Left: Schematic model of the tungsten crystal faceted by the presence of Pd, viewed in cross-section. **Right:** Schematic drawing illustrating Pd distribution on a tungsten needle crystal at (a) 600 K and (b) 1100 K.⁵¹⁵



Ishikawa et al.⁵¹⁶ produced Pd on tungsten SATs by two methods, both starting by sharpening one end of a single-crystalline (111)-oriented W wire with a diameter of 0.127 mm by

⁵¹³ T.T. Tsong, Gary Kellogg, “Direct observation of the directional walk of single adatoms and the adatom polarizability,” *Phys. Rev. B* 12(1975):1343-1353.

⁵¹⁴ Stu Borman, “A Science Academy Like No Other,” *C&EN* 87(5 January 2009):27-29; <http://pubs.acs.org/cen/science/87/8701sci1.html>

⁵¹⁵ Andrzej Szczepkowicz, Antoni Ciszewski, “Faceting of curved tungsten surface induced by palladium,” *Surf. Sci.* 515(2002):441-452; http://www.zmp.ifd.uni.wroc.pl/asz/Pd_W_faceting_preprint.pdf.

⁵¹⁶ Tsuyoshi Ishikawa, Keisuke Tagawa, Tomohiro Urata, Chuhei Oshima, Boklae Cho, Eiji Rokuta, “Fluctuations of Electron Beams Emitted from Single-Atom Electron Sources Prepared with Different Techniques,” *e-J. Surf. Sci. Nanotech.* 6(2008):11-14; http://www.jstage.jst.go.jp/article/ejssnt/6/0/11/_pdf. Tsuyoshi Ishikawa, Tomohiro Urata, Boklae Cho, Eiji Rokuta, Chuhei Oshima, Yoshinori Terui, Hidekazu Saito, “Highly efficient electron gun with a single-atom electron source,” *Appl. Phys. Lett.* 90(6 April 2007):143120.

electrochemical etching with KOH (aq). Using the vacuum deposition technique the tip surface was cleaned in UHV by flash heating up to ~2000 K, then Pd was deposited in a few atomic layers on the tip surface. The Pd-covered W tip was then heated at 1000 K in UHV for fabrication of the single-atom electron source, causing facet formation at the tip apex which was confirmed by using FEM and Fowler-Nordheim (FN) plot measurements. The FEM pattern of the clean tip exhibited a three-fold rotational symmetry determined mainly by the anisotropic work functions of the hemispherical (111) tip apex. Using the electroplating deposition technique, metal deposition was carried out in a few atomic layers thickness on the W(111) tip surface by electroplating in electrolyte just after the electrochemical etching. Then the metal-covered tip was mounted in the vacuum chamber and heated to fabricate the single-atom electron source.

5.3 Other Noble-Metal-On-Tungsten SATs

Kuo et al.⁵¹⁷ note that single-atom tips (SATs) used in SPM can achieve good spatial resolution and allow manipulation of single atoms, but such tips have proven very difficult to prepare. Traditional methods⁵¹⁸ for preparing single-atom tips required special equipment and tedious procedures in ultra-high vacuum (UHV), and the tips could not be produced reliably. Even if a single-atom tip was obtained, the tip usually did not last long because its structure was not thermodynamically or chemically stable. It has long been known that ultrathin Pd, Pt, Au, Ir, or Rh films grown on a W(111) surface could form three-sided pyramids with (211) facets upon annealing in UHV.⁵¹⁹ (The bcc W(111) and Mo(111) surfaces are morphologically unstable

⁵¹⁷ Ing-shouh Hwang, Hong-shi Kuo, Tien T. Tsong, Tsu-yi Fu, "Single-atom tip and preparation method thereof," United States Patent 7507320, filing date 10/09/2004, publication date 03/24/2009; <http://www.freepatentsonline.com/7507320.pdf>. H.S. Kuo, I.S. Hwang, T.-Y. Fu, J.Y. Wu, C.C. Chang, T.T. Tsong, "Preparation and characterization of single-atom tips," Nano Lett. 4(December 2004):2379-2382; http://aao.sinica.edu.tw/download/publication_e/Year2005/math04.pdf, http://dns.ntu-cems.ntu.edu.tw/references/NANO_LETT-4-2379-2004.pdf.

⁵¹⁸ H.W. Fink, "Mono-atomic tips for scanning tunneling microscopy," IBM J. Res. Develop. 30(1986):460-465. H.W. Fink, "Point Source for Ions and Electrons," Physica Scripta 38(1988):260-263. Vu Thien Binh, S.T. Purcell, N. Garcia, J. Doglioni, "Field-emission electron spectroscopy of single-atom tips," Phys. Rev. Lett. 69(1992):2527-2530. See also: N. Ernst, J. Unger, H.W. Fink, M. Grunze, C. Wöll, "Comment on 'Field-emission spectroscopy of single-atom tips'," Phys. Rev. Lett. 70(1993):2503. V.T. Binh, N. Garcia, "On the electron and metallic ion emission from nanotips fabricated by field-surface-melting technique – experiments on W and Au tips," Ultramicroscopy 42-44(1992):80-90. K. Nagaoka, H. Fujii, K. Matsuda, M. Komaki, Y. Murata, C. Oshima, T. Sakurai, "Field emission spectroscopy from field-enhanced diffusion-growth nano-tips," Appl. Surf. Sci. 182(5 October 2001):12-19.

⁵¹⁹ K.J. Song, R.A. Demmin, C. Dong, E. Garfunkel, T.E. Madey, "Faceting Induced by an Ultrathin Film: Pt on W(111)," Surf. Sci. Lett. 227(1990):L79. K.J. Song, C.Z. Dong, T.E. Madey, "Faceting of tungsten(111) Induced by Ultrathin Palladium Films," Langmuir 7(December 1991):3019-3026; <http://pubs.acs.org/doi/abs/10.1021/la00060a019>. T.E. Madey, J. Guan, C.H. Nien, C.Z. Dong, H.S. Tao, R.A. Campbell, "Faceting Induced by Ultrathin Metal Films on W(111) and Mo(111): Structure, Reactivity, and Electronic Properties," Surf. Rev. Lett. 3(1996):1315-1328. T.E. Madey, C.H. Nien, K. Pelhos, J.J. Kolodziej, I.M. Abdelrehim, H.S. Tao, "Faceting induced by ultrathin metal films: structure, electronic properties and reactivity," Surface Science 438(1999):191-206;

when covered by monolayer films of certain metals (including Rh, Pd, Ir, Pt, Au), and they become “nanotextured” upon annealing at $T > 700$ K: the surface becomes covered by nanoscale three-sided pyramids with mainly (211) facets.⁵²⁰ Kuo notes that the elements that are observed to induce faceting have Pauling electronegativities >2.0 .)

As already noted in [Section 5.2](#), Fu and Tsong⁵²¹ in 2001 demonstrated that Pd-covered W(111) single-atom tips could be created by the same faceting process – i.e., by evaporating a Pd monolayer on a tungsten tip and then annealing the tip in ultra-high vacuum (UHV). The major advantage of this method is that the faceting is a thermodynamic process, so that when the tip is destroyed it could be regenerated through simple annealing. Most importantly, the stacking of the single-atom tip remains the same after each regeneration, ensuring a long operating lifetime. This success also implies that other noble metals (such as Pt, Ir, Rh, and Au) grown on W(111) tips may also form single-atom tips through a similar procedure.

However, two requirements in this preparation procedure made its application less convenient. First, prior to the noble metal deposition a clean W surface had to be prepared in UHV, which requires applying a very high electric field or a very high temperature to remove surface impurity atoms. Second, an evaporator has to be installed inside the UHV chamber to evaporate a noble metal film onto the clean W tip, and most laboratory setups don’t have room for an evaporator.

In 2004, Kuo et al.⁵²² demonstrated a new, simple, and easily reproducible method of preparing single-atom tips in which both the preparation of a clean W tip surface and the deposition of a noble metal film are carried out in an electrochemical cell. (Their group has filed a patent on the process.)⁵²³ This tip can be stored in ambient conditions for a long time. After the tip is

http://www.isr.umd.edu/gwrubloff/teaching/enma490fall03/resources/current/final_report/120203_Anne/ref_11.pdf.

⁵²⁰ T.E. Madey, C.H. Nien, K. Pelhos, J.J. Kolodziej, I.M. Abdelrehim, H.S. Tao, “Faceting induced by ultrathin metal films: structure, electronic properties and reactivity,” *Surface Science* 438(1999):191-206; http://www.isr.umd.edu/gwrubloff/teaching/enma490fall03/resources/current/final_report/120203_Anne/ref_11.pdf.

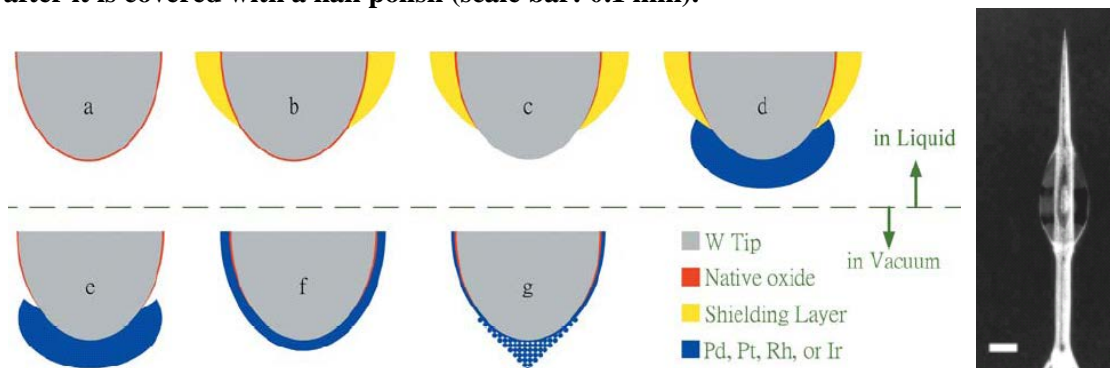
⁵²¹ T.-Y. Fu, L.C. Cheng, C.H. Nien, T.T. Tsong, “Method of creating a Pd-covered single-atom sharp W pyramidal tip: Mechanism and energetics of its formation,” *Phys. Rev. B* 64(15 September 2001):113401; <http://www.phys.sinica.edu.tw/~nano/publication/223.pdf>

⁵²² Hong-Shi Kuo, Ing-Shouh Hwang, Tsu-Yi Fu, Yu-Chun Lin, Che-Cheng Chang, Tien T. Tsong, “Noble Metal/W(111) Single-Atom Tips and Their Field Electron and Ion Emission Characteristics,” *Japanese Journal of Applied Physics* 45(2006):8972-8983; [http://www.phys.sinica.edu.tw/~nano/publication/Ing-Shouh%20HWANG/Noble%20MetalW\(111\)%20Single-Atom%20Tips%20and%20Their%20Field%20Electron.pdf](http://www.phys.sinica.edu.tw/~nano/publication/Ing-Shouh%20HWANG/Noble%20MetalW(111)%20Single-Atom%20Tips%20and%20Their%20Field%20Electron.pdf). H.S. Kuo, I.S. Hwang, T.-Y. Fu, J.Y. Wu, C.C. Chang, T.T. Tsong, “Preparation and characterization of single-atom tips,” *Nano Lett.* 4(December 2004):2379-2382; http://aao.sinica.edu.tw/download/publication_e/Year2005/math04.pdf, http://dns.ntu-ccms.ntu.edu.tw/references/NANO_LETT-4-2379-2004.pdf.

⁵²³ Ing-shouh Hwang, Hong-shi Kuo, Tien T. Tsong, Tsu-yi Fu, “Single-atom tip and preparation method thereof,” United States Patent 7507320, filing date 10/09/2004, publication date 03/24/2009; <http://www.freepatentsonline.com/7507320.pdf>.

transferred into a vacuum chamber and following a gentle annealing, a single-atom tip with the atomic structure identical to the one prepared by vacuum evaporation can be obtained (Figure 5-13).

Figure 5-13. Left: Procedure for preparation of single-atom tips: (a) A single crystal W(111) tip is prepared through electrochemical etching; (b) the tip is covered with nail polish except for the tip apex; (c) the native oxide at the tip apex is reduced through cathodic cleaning in an electrochemical cell; (d) a noble metal film is electroplated on the tip; (e) the nail polish is removed though cleaning in acetone; (f) after being transferred into vacuum, the tip is annealed and the plated noble metal atoms diffuse to other parts of the tip; (g) when the tip is covered by only one physical layer of a noble metal, a pyramidal single-atom tip builds up spontaneously.⁵²⁴ **Right:** Optical micrograph of a W(111) tip after it is covered with a nail polish (scale bar: 0.1 mm).⁵²⁵



Kuo et al.⁵²⁶ detail their process as follows: “The procedure for preparing SATs using our new method can be divided into two parts: the liquid and vacuum processes.”

⁵²⁴ H.S. Kuo, I.S. Hwang, T.-Y. Fu, J.Y. Wu, C.C. Chang, T.T. Tsong, “Preparation and characterization of single-atom tips,” *Nano Lett.* 4(December 2004):2379-2382; http://ao.sinica.edu.tw/download/publication_e/Year2005/math04.pdf, http://dns.ntu-ccms.ntu.edu.tw/references/NANO_LETT-4-2379-2004.pdf.

⁵²⁵ Hong-Shi Kuo, Ing-Shouh Hwang, Tsu-Yi Fu, Yu-Chun Lin, Che-Cheng Chang, Tien T. Tsong, “Preparation of Single-Atom Tips and Their Field Emission Behaviors,” *e-J. Surf. Sci. Nanotech.* 4(2006):233-238; <http://www.phys.sinica.edu.tw/~nano/publication/Ing-Shouh%20HWANG/Preparation%20of%20Single-Atom%20Tips%20and%20Their%20Field%20Emission%20Behaviors.pdf>.

⁵²⁶ Hong-Shi Kuo, Ing-Shouh Hwang, Tsu-Yi Fu, Yu-Chun Lin, Che-Cheng Chang, Tien T. Tsong, “Noble Metal/W(111) Single-Atom Tips and Their Field Electron and Ion Emission Characteristics,” *Japanese Journal of Applied Physics* 45(2006):8972-8983; [http://www.phys.sinica.edu.tw/~nano/publication/Ing-Shouh%20HWANG/Noble%20MetalW\(111\)%20Single-Atom%20Tips%20and%20Their%20Field%20Electron.pdf](http://www.phys.sinica.edu.tw/~nano/publication/Ing-Shouh%20HWANG/Noble%20MetalW(111)%20Single-Atom%20Tips%20and%20Their%20Field%20Electron.pdf).

“In the liquid process, a (111) orientated single crystal W wire of 0.13 mm diameter (purity 99.999%, FEI Co.) is electrochemically polished to a needle shape in KOH solution with an AC voltage. The tip is inspected using either an optical microscope or an electron microscope to ensure sharpness. The apex of the needle is approximately hemispherical with an average radius of curvature of 50 nm. After polishing, the tip surface is covered with a thin native oxide layer, which has to be removed before the plating of a noble metal film. To decrease the total amount of the material to be deposited (plating metal), we use nail polish to shield the tip from the electrolyte except for the apex part. The shielded tip is immersed into 0.1M HCl (15 mL) and held at -0.6V (SCE) to reduce the surface oxide for about 3 min. Subsequently, a small amount of the plating electrolyte (15 mL) is introduced into the electrochemical cell under the same cathodic polarization conditions. Faradic current is in situ monitored during the electrochemical process, and the deposition time is controlled to within 10-15 s. At $t \sim 195$ s, the tip is removed from the plating bath, and the current drops to zero, indicating the end of the electrochemical reaction.”

“Before transferring the electroplated tip into our laboratory-built UHV FIM/FEM chamber, we use acetone to remove the nail polish covering on the tip. The chamber has a base pressure of about 1×10^{-10} torr. Only heat treatments are used for degassing the tip as well as for faceting. The temperature of the tip is measured with an optical pyrometer. After a proper heat treatment (~ 1000 K), a He-Ne gas mixture with a pressure of 2×10^{-5} torr is utilized as an image gas for FIM observations. By FIM, we can examine the atomic structure of the tip surface. Typically, a positive high voltage is applied to the tip and carefully and slowly increased for observing atomic images as well as for field evaporating surface atoms.”

“After degassing a Pd-plated tip in UHV at 700 K for 5 min, we obtain an FIM image of the tip. Since the tip apex is covered with a Pd multilayer, a longer period of annealing than that for the vacuum evaporation of Pd is required for extra Pd atoms to diffuse to the tip shank. After annealing at 1000 K for 20 min, an ordered atomic structure starts to appear. If the tip is annealed for additional 5 min, a perfect bcc atomic structure centered around (111) can be clearly identified, suggesting that a Pd pseudomorphic overlayer is formed on the W(111) tip surface. The tip is further annealed to 1000 K for 5 min, and the image of a single-atom tip is observed. This topmost atom can be field-ionized and field-evaporated by further increasing the positive voltage of the tip, known as field evaporation. Once the top-layer atom is removed, the atomic structure of the second atomic layer is revealed. With field evaporation, the atomic structure of the tip can be examined layer by layer.”

Kuo et al. used a field ion microscope (FIM) to study the atomic stacking of single-atom tips. **Figure 5-14** shows FIM images of Pd-covered W(111) single-atom tips. Only one atom is seen on the topmost layer (**Figure 5-14a**). The second atomic layer was studied by applying a stronger electric field to remove the topmost atom (field evaporation), causing the second layer consisting of three atoms to be exposed (**Figure 5-14b**). With another field evaporation, the third layer consisting of 10 atoms was observed (**Figure 5-14c**). **Figure 5-14d** and **Figure 5-14e** show the next two layers, and a hard sphere model for this pyramidal tip is drawn in **Figure 5-14f**. After several field evaporations the tip apex was destroyed, but a single-atom tip with the same stacking could be regenerated simply by annealing to 1000 K, as shown in **Figure 5-14(g-i)**. Kuo's experiments indicated that this process could be repeated tens of times.

Figure 5-14. (a)-(e) FIM images showing the structure of a Pd-covered W(111) single-atom tip: (a) the top layer; (b) the second layer; (c) the third layer; (d) the fourth layer; and in (e) the pyramidal structure is destroyed; (f) a 3-D hard-sphere model of the pyramidal nanotip; (g)-(i) FIM images showing the structure of a regenerated Pd-covered W(111) single-atom tip: (g) the top layer; (h) the second layer; (i) the third layer.⁵²⁷

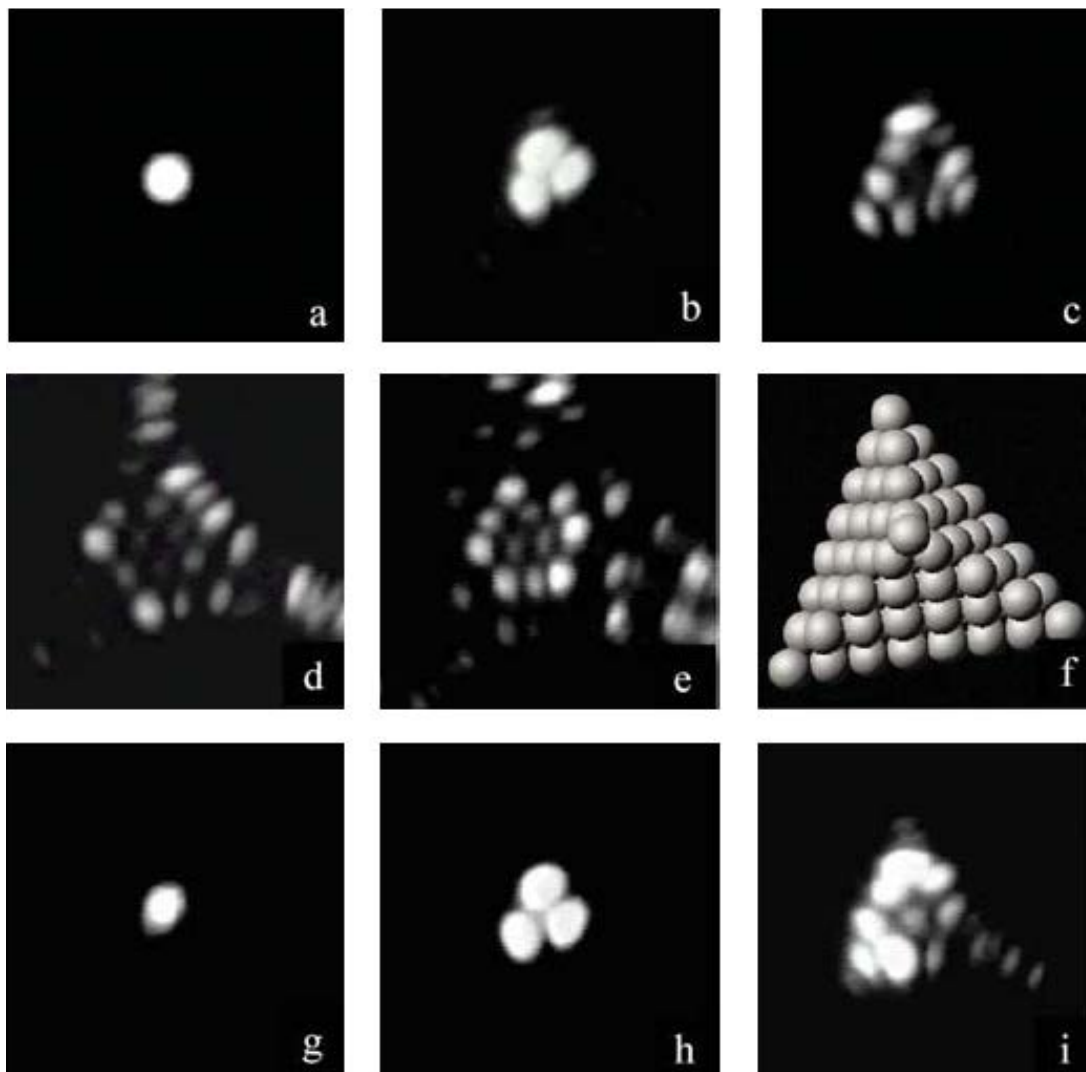
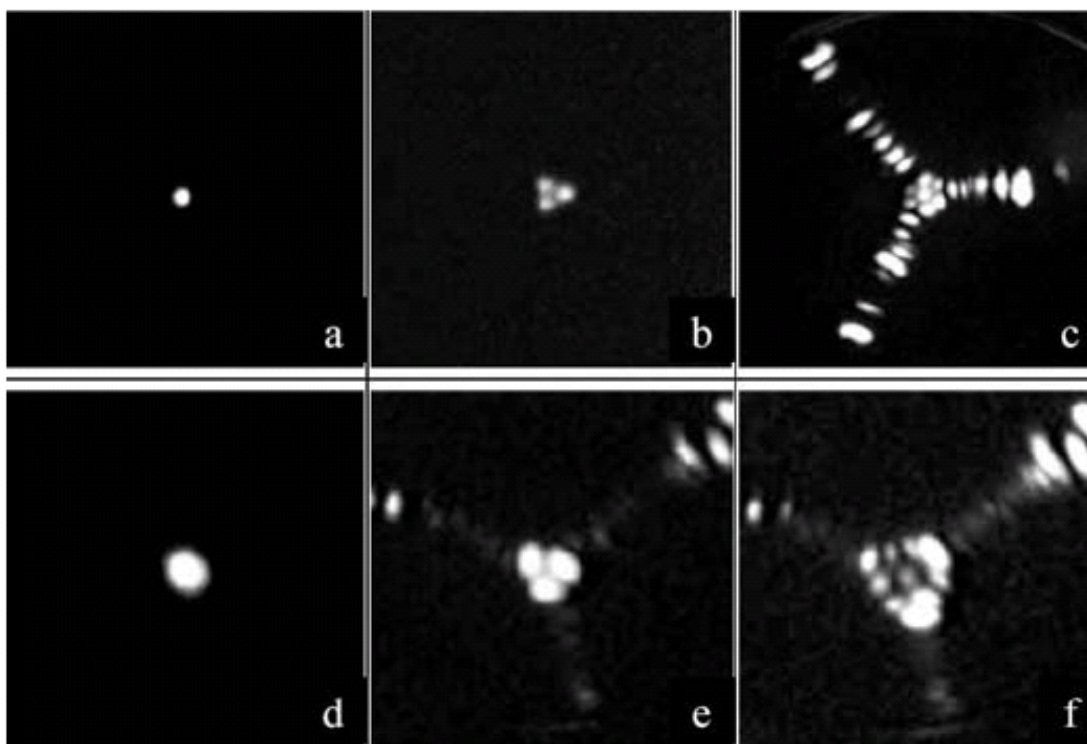


Figure 5-15 shows FIM images of Pt-covered W(111) and Rh-covered W(111) single-atom tips prepared by a similar procedure. The atomic structures are very similar to that of the Pd-covered

⁵²⁷ H.S. Kuo, I.S. Hwang, T.-Y. Fu, J.Y. Wu, C.C. Chang, T.T. Tsong, "Preparation and characterization of single-atom tips," *Nano Lett.* 4(December 2004):2379-2382; http://ao.sinica.edu.tw/download/publication_e/Year2005/math04.pdf , http://dns.ntu-ccms.ntu.edu.tw/references/NANO_LETT-4-2379-2004.pdf.

W(111) single-atom tip, and they all are regenerable. These results further indicate that Kuo's electroplating approach can be applied to other faceting systems to produce single-atom tips. A few preliminary experimental studies have been done on the temperature sensitivity of W atom migrations⁵²⁸ on W(111) and Ir atom migrations⁵²⁹ on Ir (111) surfaces, to begin understanding what paths the atoms might be taking during their migrations (e.g., terrace diffusion and ascending, descending, or detachment motions).

Figure 5-15. (a)-(c) FIM images showing the structure of a Pt-covered W(111) single-atom tip: (a) the top layer; (b) the second layer; (c) the third layer; and (d)-(f) FIM images showing the structure of a Rh-covered W(111) single-atom tip: (d) the top layer; (e) the second layer; (f) the third layer.⁵³⁰



⁵²⁸ T.Y. Fu, W.J. Weng, T.T. Tsong, "Dynamic study of W atoms and clusters on W(111) surfaces," *Applied Surface Science* 254(30 September 2008):7831-7834.

⁵²⁹ Tsu-Yi Fu, T. Tien, Tsong, "The Role of the Lattice Step in Epitaxial Growth," *Mater. Res. Soc. Symp. Proc.* 570(1999):33.

⁵³⁰ H.S. Kuo, I.S. Hwang, T.-Y. Fu, J.Y. Wu, C.C. Chang, T.T. Tsong, "Preparation and characterization of single-atom tips," *Nano Lett.* 4(December 2004):2379-2382; http://aao.sinica.edu.tw/download/publication_e/Year2005/math04.pdf , http://dns.ntu-cms.ntu.edu.tw/references/NANO_LETT-4-2379-2004.pdf.

According to Kuo et al.,⁵³¹ for a Pt-plated W(111) tip, a SAT can also be obtained simply by annealing at 1100 K in vacuum. The atomic stacking of the Pt/W(111) tip is the same as that of the Pd/W(111) tip, and both SATs can be regenerated. For Pd- and Pt-covered SATs, this is a major stacking sequence with 1, 3, and 10 atoms from the top to the deeper layer. However, there is a second stacking sequence with 1, 6, and 15 atoms. This sequence is seldom observed (<10%) for Pd/W(111) and Pt/W(111) SATs, but it is more often observed for Rh/W(111) and Ir/W(111) SATs. An example is shown in Figure 5-16. After annealing, a Rh electroplated tip at 1100 K for 30 min, we obtain a Rh-covered SAT with a stacking sequence of 1, 3, and 10 atoms, as shown in Figure 5-16(a-c). After the field evaporations, the tip is annealed at 1100 K again to recover the single-atom sharpness. The barriers blocking transition between the two stacking sequences are higher than most energies commonly encountered in DMS, e.g., ~3 eV for pyramidal Rh-coated W tips and ~2.7 eV for pyramidal Ir-coated W tips (Figure 5-17).⁵³²

The stacking sequence can be controlled to some degree by choice of annealing temperature. In the case of a Rh/W(111) tip (Figure 5-16), annealing at 1100 K after electroplating produces a 1-3-10 tip, but after field evaporation of this tip the SAT apex is recovered by re-annealing to 1100K, whereupon a 1-6-15 tip is obtained.⁵³³ Both pyramidal structures are terminated with one atom and bounded with the same {211} faceting. The probability for either sequence is a function of annealing temperature – in general, a 1-3-10 stacking sequence is favored for a high annealing temperature. With Rh-covered tips, the probability of 1-3-10 stacking is only 35% at 1100 K but increases to 72.5% at 1300 K.⁵³⁴

⁵³¹ Hong-Shi Kuo, Ing-Shouh Hwang, Tsu-Yi Fu, Yu-Chun Lin, Che-Cheng Chang, Tien T. Tsong, “Noble Metal/W(111) Single-Atom Tips and Their Field Electron and Ion Emission Characteristics,” Japanese Journal of Applied Physics 45(2006):8972-8983; [http://www.phys.sinica.edu.tw/~nano/publication/Ing-Shouh%20HWANG/Noble%20MetalW\(111\)%20Single-Atom%20Tips%20and%20Their%20Field%20Electron.pdf](http://www.phys.sinica.edu.tw/~nano/publication/Ing-Shouh%20HWANG/Noble%20MetalW(111)%20Single-Atom%20Tips%20and%20Their%20Field%20Electron.pdf).

⁵³² Tsu-Yi Fu, Yu-Chun Lin, Hong-Shi Kuo, Ing-Shouh Hwang, Tien T. Tsong, “Study of two types of Ir or Rh covered single atom pyramidal W tips,” Surface Science 601(2007):3992-3995; <http://www.phys.sinica.edu.tw/~nano/eng/publication/Fu-2007.pdf>.

⁵³³ Hong-Shi Kuo, Ing-Shouh Hwang, Tsu-Yi Fu, Yu-Chun Lin, Che-Cheng Chang, Tien T. Tsong, “Noble Metal/W(111) Single-Atom Tips and Their Field Electron and Ion Emission Characteristics,” Japanese Journal of Applied Physics 45(2006):8972-8983; [http://www.phys.sinica.edu.tw/~nano/publication/Ing-Shouh%20HWANG/Noble%20MetalW\(111\)%20Single-Atom%20Tips%20and%20Their%20Field%20Electron.pdf](http://www.phys.sinica.edu.tw/~nano/publication/Ing-Shouh%20HWANG/Noble%20MetalW(111)%20Single-Atom%20Tips%20and%20Their%20Field%20Electron.pdf).

⁵³⁴ P.J. Berlowitz, D.W. Goodman, “Chemisorption of ultrathin Pd layers on W(110) and W(100): adsorption of H₂ and CO,” Langmuir 4(September 1988):1091-1095; <http://pubs.acs.org/doi/abs/10.1021/la00083a004>.

Figure 5-16. FIM images showing two types of Rh-covered W(111) single-atom tip: (a) The first layer consists of 1 atom. (b) The second layer consists of 3 atoms. (c) The third layer consists of 10 atoms. (d) Top view model of tip with 1-3-10 stacking sequence. (e) The first layer consists of 1 atom. (f) The second layer consists of 6 atoms. (g) The third layer consists of 15 atoms; (h) Top view model of tip with 1-6-15 stacking sequence.⁵³⁵

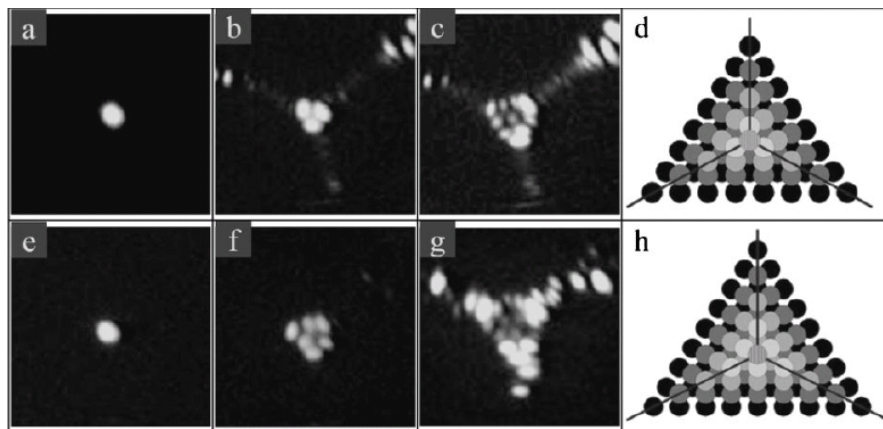
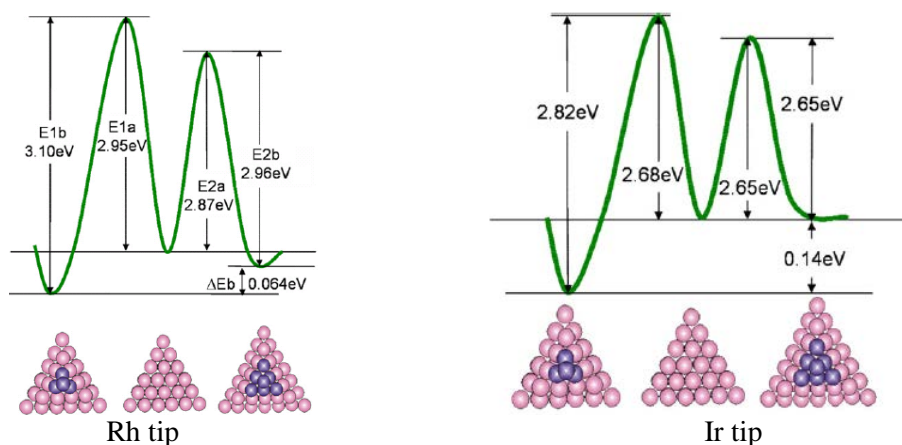


Figure 5-17. Potential energy diagram showing calculated activation barriers for different structures of Rh-covered (left) and Ir-covered (right) single-atom W pyramidal tips.⁵³⁶

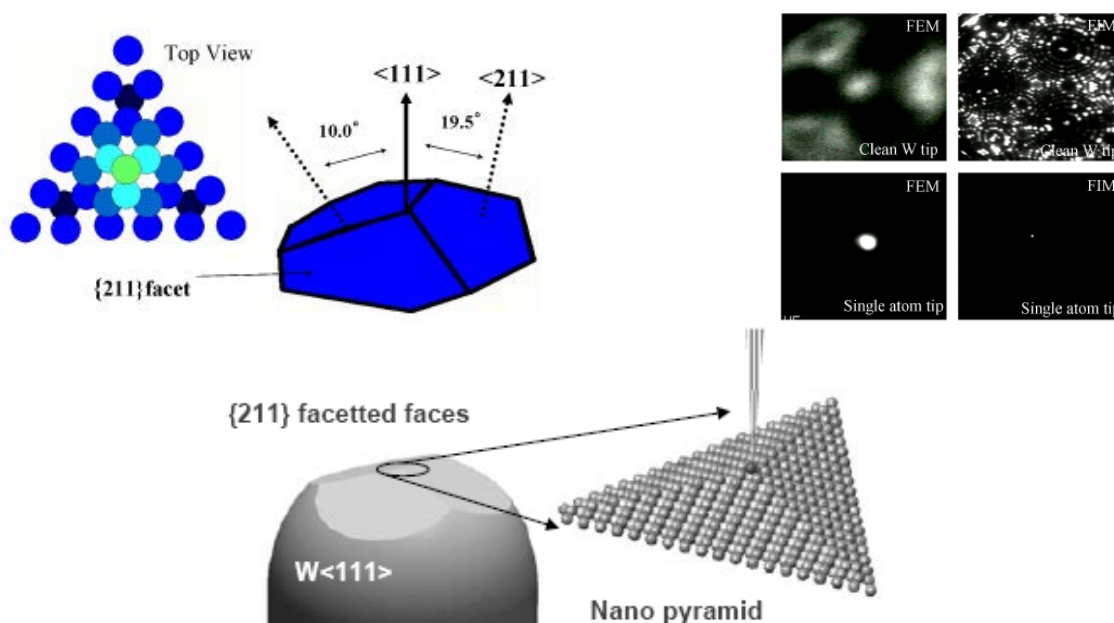


⁵³⁵ Hong-Shi Kuo, Ing-Shouh Hwang, Tsu-Yi Fu, Yu-Chun Lin, Che-Cheng Chang, Tien T. Tsong, "Noble Metal/W(111) Single-Atom Tips and Their Field Electron and Ion Emission Characteristics," Japanese Journal of Applied Physics 45(2006):8972-8983; [http://www.phys.sinica.edu.tw/~nano/publication/Ing-Shouh%20HWANG/Noble%20MetalW\(111\)%20Single-Atom%20Tips%20and%20Their%20Field%20Electron.pdf](http://www.phys.sinica.edu.tw/~nano/publication/Ing-Shouh%20HWANG/Noble%20MetalW(111)%20Single-Atom%20Tips%20and%20Their%20Field%20Electron.pdf).

⁵³⁶ Tsu-Yi Fu, Yu-Chun Lin, Hong-Shi Kuo, Ing-Shouh Hwang, Tien T. Tsong, "Study of two types of Ir or Rh covered single atom pyramidal W tips," Surface Science 601(2007):3992-3995; <http://www.phys.sinica.edu.tw/~nano/eng/publication/Fu-2007.pdf>.

One limitation on these tips is that their aspect ratio is not uniform – the metal pyramids are very sharp, but these lie atop tip termini that have much large radii of curvature (Figure 5-18).⁵³⁷ Thus it would be ideal if all two-tip reactions and high-angle approaches to the workpiece could be eliminated from our DMS reaction sequence schedule to avoid steric congestion at the worksite.

Figure 5-18. Left: Schematic view of nano-pyramids terminated with a single atom of Pd, Pt, Au and Rh grown on the W<111> tip. The {211} facet face covers the pyramid. The angle between the <111> tip orientation and the direction normal to the {211} face is 19.5° and the angle between the tip orientation and the directions normal to the ridge lines is 10°. **Right:** Typical FEM and FIM patterns of the clean W<111> tip, and the single-atom tip of Rh. The clean <111> tip with a hemi-spherical shape shows a wide-spread FEM pattern, and the single-atom tip exhibits a collimated spot.⁵³⁸ **Bottom:** Electron emission from a single atom at the top of a nanopillar grown on the (111) face of a W tip.⁵³⁹



⁵³⁷ Chuhei Oshima, Eiji Rokuta, Takahiro Itagaki, Tsuyosi Ishikawa, Bokurai Cho, Hong-Shi Kuo, Ing-Shouh Hwang, Tien T. Tsong, "Demountable Single-Atom Electron Source," e-J. Surf. Sci. Nanotech. 3(9 December 2005):412-416; <http://www.jstage.jst.go.jp/article/ejsnt/3/0/412/pdf>.

⁵³⁸ Chuhei Oshima, Eiji Rokuta, Takahiro Itagaki, Tsuyosi Ishikawa, Bokurai Cho, Hong-Shi Kuo, Ing-Shouh Hwang, Tien T. Tsong, "Demountable Single-Atom Electron Source," e-J. Surf. Sci. Nanotech. 3(9 December 2005):412-416; <http://www.jstage.jst.go.jp/article/ejsnt/3/0/412/pdf>.

⁵³⁹ Tsuyoshi Ishikawa, Keisuke Tagawa, Tomohiro Urata, Chuhei Oshima, Boklae Cho, Eiji Rokuta, "Fluctuations of Electron Beams Emitted from Single-Atom Electron Sources Prepared with Different Techniques," e-J. Surf. Sci. Nanotech. 6(2008):11-14; <http://www.jstage.jst.go.jp/article/ejsnt/6/0/11/pdf>.

Says one news report:⁵⁴⁰ “A few years ago, Hong-Shi Kuo, Ing-Shouh Hwang, and Tien T. Tsong of the Nanoscience & Nanotechnology Core Facility at Academia Sinica’s Institute of Physics and coworkers developed a quick electrochemical method for making single-atom tips for electron microscopy (Nano Lett. 4(2004):2379). ‘It used to be very difficult to make stable and robust single-atom tips,’ institute professor Ting-Kuo Lee said. With the new electrochemical plating and thermal faceting process, ‘tips can now be made into a stable pyramidal shape, usually in less than an hour, and are also very easy to repair,’ he said.” (Another group claims to be able to make the same tips but without using the nail polish.)⁵⁴¹

In summary, the collaboration of Kuo et al.⁵⁴² (with participants at Academia Sinica, National Tsing Hua University, and National Taiwan Normal University, all in Taiwan) has developed a new, simple, and easily reproducible method of preparing single-atom tips. By electroplating a thin noble metal film onto a single-crystal W(111) tip, a single-atom tip can be obtained after a simple annealing in vacuum, that can be used as single-atom field emitters.⁵⁴³ These noble metal-plated W(111) tips can survive in ambient conditions for months before transfer into a vacuum system, are both thermally and chemically stable, can be regenerated when accidentally damaged, and maintain a small extension angle and the same atomic stacking each time they are regenerated. By 2006-8,⁵⁴⁴ the group had succeeded in preparing Pd/W(111), Pt/W(111),

⁵⁴⁰ Stu Borman, “A Science Academy Like No Other,” C&EN 87(5 January 2009):27-29; <http://pubs.acs.org/cen/science/87/8701sci1.html>.

⁵⁴¹ Ito Wataru, Katsuta Hiroshi, Matsumura Tomokazu, Oshima Chuhei, “Preparation and Characterization of single-atom tips by an electroplating method without nail polish,” Paper 7, 7.7 Micro-Field Emitter, 10 September 2009, The Japan Society of Applied Physics, 70th Autumn Meeting, 8-11 September 2009, Toyama University, Toyama, Japan; http://secure1.gakkai-web.net/gakkai/jsap_pro/english/pro/bunrui7.html.

⁵⁴² H.S. Kuo, I.S. Hwang, T.-Y. Fu, J.Y. Wu, C.C. Chang, T.T. Tsong, “Preparation and characterization of single-atom tips,” Nano Lett. 4(December 2004):2379-2382; http://aao.sinica.edu.tw/download/publication_e/Year2005/math04.pdf, http://dns.ntu-ccms.ntu.edu.tw/references/NANO_LETT-4-2379-2004.pdf.

⁵⁴³ T. Itagaki, E. Rokuta, H.-S. Kuo, K. Nomura, T. Ishikawa, B.-L. Cho, I.-S. Hwang, T.T. Tsong, C. Oshima, “Stabilities in field electron emissions from noble-metal covered W nano-tips: apex structure dependence,” Surface and Interface Analysis 39(2006):299-303. E. Rokuta, T. Itagaki, D. Miura, T. Moriyama, T. Ishikawa, B.-L. Cho, T.Y. Fu, T.T. Tsong, C. Oshima, “Atomic-scale field emitter with self-repairable function and thermodynamically stable structure: FEM study on Pd-covered nanopyramids on W<111> tips,” Applied Surface Science 251(15 September 2005):205-209. E. Rokuta, H.-S. Kuo, T. Itagaki, K. Nomura, T. Ishikawa, B.-L. Cho, I.-S. Hwang, T.T. Tsong, C. Oshima, “Field emission spectra of single-atom tips with thermodynamically stable structures,” Surface Science 602(2008):2508-2512; <http://www.phys.sinica.edu.tw/~nano/publication/Rokuta-SS-2008.pdf>.

⁵⁴⁴ Hong-Shi Kuo, Ing-Shouh Hwang, Tsu-Yi Fu, Yu-Chun Lin, Che-Cheng Chang, Tien T. Tsong, “Preparation of Single-Atom Tips and Their Field Emission Behaviors,” e-J. Surf. Sci. Nanotech. 4(2006):233-238; <http://www.phys.sinica.edu.tw/~nano/publication/Ing-Shouh%20HWANG/Preparation%20of%20Single-Atom%20Tips%20and%20Their%20Field%20Emission%20Behaviors.pdf>. Tsu-Yi Fu, Yu-Chun Lin, Hong-Shi Kuo, Ing-Shouh Hwang, Tien T. Tsong, “Study of two types of Ir or Rh covered single atom pyramidal W tips,” Surface Science 601(2007):3992-3995;

Rh/W(111), Au/W(111), and Ir/W(111) single-atom tips, and they believed that their method could also be used for the preparation of noble-metal/Mo(111) pyramidal tips, as one physical monolayer of a noble metal also induces a similar faceting transition on a Mo(111) substrate.⁵⁴⁵ Nomura et al.⁵⁴⁶ have fabricated Au nanopyramids on flat Mo(111) substrate via thermal annealing of a gold monolayer – FIM does not show single-atom termination, but energy spectra of the tip-emission electrons strongly suggest the realization of a single-atom termination just after annealing.

Nomura et al.⁵⁴⁷ also fabricated Au-covered W(111) nanotips also using an electroplating method, and found that the stable nanotips possessed a three-sided pyramid structure terminated with three atoms, differing from the nanotips covered with the other noble metals such as Pd, Pt, Rh, and Ir, of which all the final structures are terminated with a single atom.⁵⁴⁸ The self-repairing function and the demountable characteristic were confirmed for this tip.

Winkler et al.⁵⁴⁹ filed a related patent in 2010 which appears to describe a similar process in which noble metals are deposited onto a sharp W tip, and then high voltage is applied to the tip to induce field emission, resulting in the formation of a single-atom pyramidal tip apex. Purcell and

<http://www.phys.sinica.edu.tw/~nano/eng/publication/Fu-2007.pdf>. Yu-Wen Liao, L.H. Chen, K.C. Kao, C.-H. Nien, Minn-Tsong Lin, Ker-Jar Song, “Faceting and defaceting phase transitions of Pd/W(111),” Phys. Rev. B 75(2007):125428; <http://web.phys.ntu.edu.tw/nanomagnetism/eng/pdf/060-PRB75-125428-2007.pdf>. Hong-Shi Kuo, Ing-Shouh Hwang, Tsu-Yi Fu, Yu-Chun Lin, Che-Cheng Chang, Tien T. Tsong, “Noble Metal/W(111) Single-Atom Tips and Their Field Electron and Ion Emission Characteristics,” Japanese Journal of Applied Physics 45(2006):8972-8983; [http://www.phys.sinica.edu.tw/~nano/publication/Ing-Shouh%20HWANG/Noble%20MetalW\(111\)%20Single-Atom%20Tips%20and%20Their%20Field%20Electron.pdf](http://www.phys.sinica.edu.tw/~nano/publication/Ing-Shouh%20HWANG/Noble%20MetalW(111)%20Single-Atom%20Tips%20and%20Their%20Field%20Electron.pdf).

⁵⁴⁵ K.J. Song, J.C. Lin, M.Y. Lai, Y.L. Wang, “Faceting Phase Transitions of Mo(111) Induced by Pd, Au, and Oxygen Overlayers,” Surf. Sci. 327(1995):17-32.

⁵⁴⁶ K. Nomura, T. Nagao, B.L. Cho, H. Katsuda, T. Matsumura, C. Oshima, “Thermodynamically stable nanotips of Au-Mo alloy,” J. Vac. Sci. Technol. B 27(November 2009):2432-2434.

⁵⁴⁷ K. Nomura, E. Rokuta, T. Itagaki, C. Oshima, Hong-shi Kuo, T.T. Tsong, “Electron Emission Characteristics of Au-covered Tungsten<111> Nanotips,” e-Journal of Surface Science and Nanotechnology 6(2008):25-28.

⁵⁴⁸ E. Rokuta, T. Itagaki, D. Miura, T. Moriyama, T. Ishikawa, B.-L. Cho, T.Y. Fu, T.T. Tsong, C. Oshima, “Atomic-scale field emitter with self-repairable function and thermodynamically stable structure: FEM study on Pd-covered nanopyramids on W<111> tips,” Applied Surface Science 251(15 September 2005):205-209.

⁵⁴⁹ Dieter Winkler, Udo Weigel, Stefan Grimm, “Method Of Preparing An Ultra Sharp Tip, Apparatus For Preparing An Ultra Sharp Tip, And Use Of An Apparatus,” IPC8 Class: AC25D534FI, USPC Class: 205205, Patent application number: 20100006447; <http://www.faqs.org/patents/app/20100006447>.

Binh⁵⁵⁰ used a field-emission process to create a single-atom Au nanotip on a tungsten base tip substrate.

5.4 Other Metal-On-Metal SATs

In 2010, Hong et al.⁵⁵¹ in Taiwan reported at a Chinese-language nanotech conference the growth of cobalt-on-platinum pyramidal SATs formed by surface faceting. After depositing 4-5 monolayers of Co atoms on a Pt(111) surface, Co islands formed in an fcc structure and formed a pyramidal nanotip having single, dimer or trimer cobalt atoms at both room temperature and at 20 K. The CoPt nanopyramid is grown on Pt {531} and Pt {210} planes – the {531} pyramidal site is formed by expanded {111}, {110} and {311} faces, while the {210} pyramidal site is formed by expanded {110} and {311} faces. The formation of Co islands on Pt(111) via Stranski-Krastanov (SK)⁵⁵² growth mode yields yet another kind of single atom tip. Schmid et al.⁵⁵³ had earlier reported the growth of irregular Co nanopyramids on Pt(111) under UHV room temperature conditions (Figure 5-19).

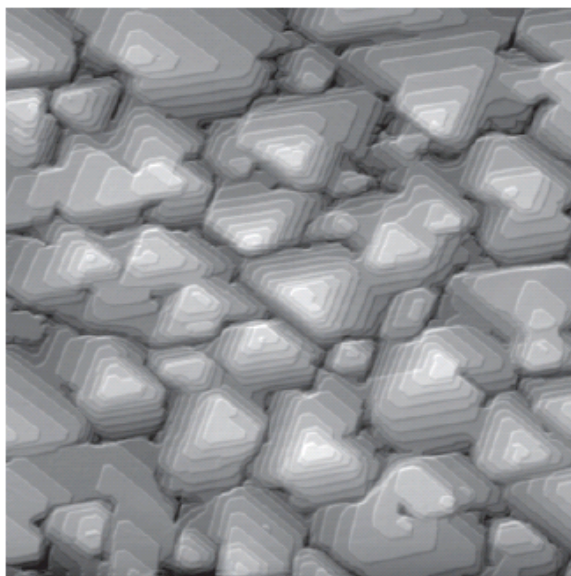
⁵⁵⁰ S.T. Purcell, Vu Thien Binh, “Realization of an axially aligned Au-ion source of atomic size,” Appl. Phys. Lett. 75(30 August 1999):1332.

⁵⁵¹ S.J. Hong, C.L. Chiang, Y.J. Chen, T.Y. Fu, “Formation of Pt based cobalt magnetic ultra-sharp nano tip,” Poster Presentation FP-018 (Surface Science), 2010 Annual Meeting of the Physical Society of ROC in Tainan, Taiwan-Argonne Workshop on Nano-structured Materials, 1-4 February 2010; <http://psroc2010.ncku.edu.tw/pdf/FP-018.pdf>

⁵⁵² Most epitaxial growth occurs via a vapor phase technique such as molecular beam epitaxy (MBE). In Volmer-Weber (VW) growth, adatom-adatom interactions are stronger than those of the adatom with the surface, leading to the formation of three-dimensional adatom clusters or islands. Growth of these clusters, along with coarsening, will cause rough multi-layer films to grow on the substrate surface. Antithetically, during Frank-van der Merwe (FM) growth, adatoms attach preferentially to surface sites resulting in atomically smooth, fully formed layers. This layer-by-layer growth is two dimensional, indicating that complete films form prior to growth of subsequent layers. Stranski-Krastanov (SK) growth is an intermediary process characterized by both 2D layer and 3D island growth. Transition from the layer-by-layer to island-based growth occurs at a critical layer thickness which is highly dependent on the chemical and physical properties, such as surface energies and lattice parameters, of the substrate and film.

⁵⁵³ M. Schmid, E. Lundgren, G. Leonardelli, A. Hammerschmid, B. Stanka, P. Varga, “Exchange processes in interlayer diffusion – kinks, corners and the growth mode,” Appl. Phys. A 72(2001):405-412; <http://202.127.1.11/applied%20physics%20a/72/72403.pdf>.

Figure 5-19. STM constant-current topographs ($300 \times 300 \text{ nm}^2$) cobalt nanopramids resulting from 8 monolayers of Co deposited on Pt(111) at room temperature in UHV conditions.⁵⁵⁴



Zhao et al.⁵⁵⁵ have observed field emission from a thermally cleaned Mo(110) single tip in UHV – the narrow energy distribution is attributed to a nanotip spontaneously formed on the $\sim 75 \text{ nm}$ radius Mo tip from in situ buildup by field-induced surface diffusion. Auger electron spectroscopy showed that residual surface Ca (an interstitial impurity in the Mo rods) segregated from the bulk during thermal cleaning and is likely the source of mobile atoms that formed the nanotip, which might be a single-atom calcium-on-Mo(110) tip (i.e., in the form of a disordered Ca pyramid).

McClelland and Watanabe⁵⁵⁶ have observed field emission from a single sodium metal atom adsorbed on a tungsten tip.

⁵⁵⁴ M. Schmid, E. Lundgren, G. Leonardelli, A. Hammerschmid, B. Stanka, P. Varga, “Exchange processes in interlayer diffusion – kinks, corners and the growth mode,” Appl. Phys. A 72(2001):405-412; <http://202.127.1.11/applied%20physics%20a/72/72403.pdf>.

⁵⁵⁵ Xin Zhao, R.A. Outlaw, R.L. Champion, J.J. Wang, D.M. Manos, B.C. Holloway, “Field emission from a Ca nanotip grown on a Mo<110> microtip,” Applied Physics Letters 85(August 2004):1415-1417.

⁵⁵⁶ G.M. McClelland, F. Watanabe, “Field Emission Switch,” Appl. Phys. Lett. 67(1995):3200-3202.

5.5 Pure Noble Metal Wire SATs

In 2009, Kuo et al.⁵⁵⁷ reported a reliable new method for preparing a pure Ir metal single-atom tip by thermal treatment in oxygen. This tip can easily be maintained and regenerated in vacuum, ensuring it has sufficient lifetime for practical applications. The method, as further elucidated in their patent,⁵⁵⁸ has been experimentally demonstrated with iridium but is claimed (in the patent) also to be workable using Pt, Pd and Rh. The method is very simple and proceeds in three steps: etching, surface cleaning, and SAT formation.

In the first step (etching), a polycrystalline Ir wire having a diameter of 100 microns and a length of about 5 mm was electrochemically etched to form a sharp end. This was accomplished by mixing NaNO_3 and KOH by weight ratio of 1:1 in a platinum crucible and heating the contents to form a molten salt mixture, then dipping the iridium wire into the molten salt mixture with an AC voltage of 7-9 V (rms) applied between the wire and a counterelectrode with the frequency set from 60 to 300 Hz. After etching, the Ir wire was rinsed in water and acetone, whereupon SEM measurement revealed that the etched Ir wire had a sharp end with a radius of about 200 nm.

In the second step (surface cleaning), according to the patent⁵⁵⁹ the etched Ir wire was loaded into a chamber and heated at 500 °C for 2 sec or less, then at 1500 °C for 2 seconds or less, in both cases in an oxygen atmosphere at an oxygen partial pressure of $P_{\text{O}_2} = 2 \times 10^{-7}$ Torr. According to the published paper,⁵⁶⁰ “the needle is thermally flashed at 1500 °C for several times, and then cooled down to 20 K with a closed-cycle cryostat for FIM imaging” using helium as the imaging gas.

In the third step (SAT formation), and at the same oxygen pressure as before (2×10^{-7} Torr), the wire was annealed at 400-600 °C for 5 minutes. The atomic structure of the Ir tip as well as the apical pyramid (i.e., the pyramidal structure) was then characterized using an FIM. The FIM picture generated from the topmost layer of the pyramid, in which only one iridium atom was detected, confirmed the formation of an iridium SAT after the aforementioned treatments. The topmost atom was then removed via field evaporation to expose the second layer. Three Ir atoms were detected from the second layer of the pyramid. Then the second layer was also removed by field evaporation. Three atomic ridges were detected, confirming that a three-sided pyramid had been formed on the sharp end of the Ir wire. An atomic hardball model of the pyramid with a

⁵⁵⁷ Hong-Shi Kuo, Ing-Shouh Hwang, Tsu-Yi Fu, Ying-Siang Hwang, Yi-Hsien Lu, Chun-Yueh Lin, Jin-Long Hou, Tien T. Tsong, “A single-atom sharp iridium tip as an emitter of gas field ion sources,” *Nanotechnology* 20(19 August 2009):335701.

⁵⁵⁸ Hong-Shi Kuo, Ing-shouh Hwang, Tien T. Tsong, Tsu-Yi Fu, “Atomically Sharp Iridium Tip,” IPC8 Class: AB21G100FI, USPC Class: 428600, 2009; <http://www.faqs.org/patents/app/20090110951>.

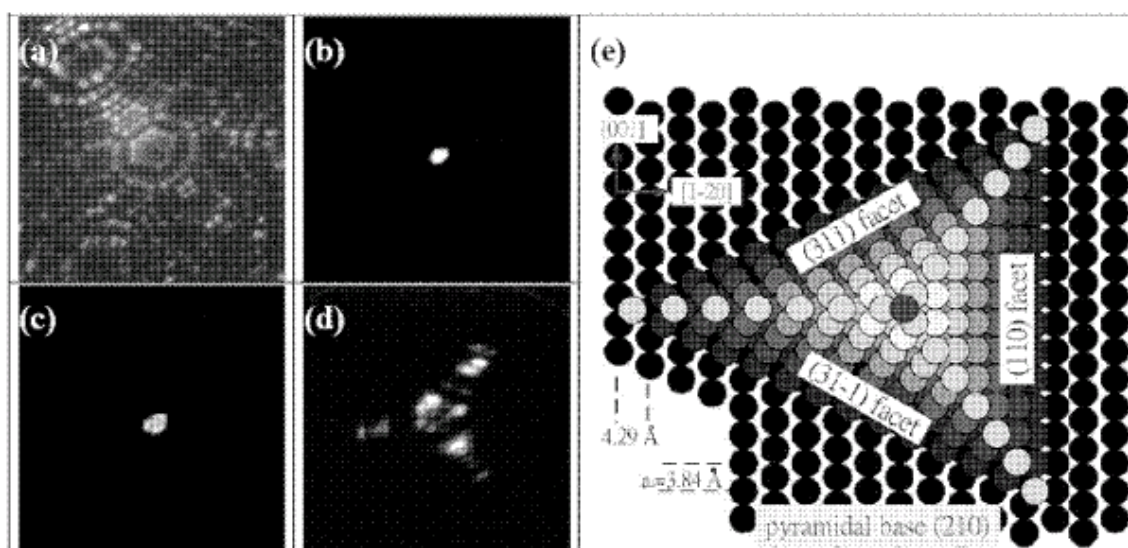
⁵⁵⁹ Hong-Shi Kuo, Ing-shouh Hwang, Tien T. Tsong, Tsu-Yi Fu, “Atomically Sharp Iridium Tip,” IPC8 Class: AB21G100FI, USPC Class: 428600, 2009; <http://www.faqs.org/patents/app/20090110951>.

⁵⁶⁰ Hong-Shi Kuo, Ing-Shouh Hwang, Tsu-Yi Fu, Ying-Siang Hwang, Yi-Hsien Lu, Chun-Yueh Lin, Jin-Long Hou, Tien T. Tsong, “A single-atom sharp iridium tip as an emitter of gas field ion sources,” *Nanotechnology* 20(19 August 2009):335701.

single-atom tip, which matches the FIM results nicely, further verifies the well-defined atomic structure of the pyramid (Figure 5-20).

A damaged pyramid can be recovered just by repeating the procedures described in the “SAT formation” step once again. The regenerated pyramid has the same atomic stacking structure. In addition, only one pyramid is formed on the sharp end of the Ir wire. It is believed that the area of the {210} plane on the sharp end of the iridium wire is so small that only one nanopyramid is generated. Multiple pyramids or a planar truncated pyramid may be formed when the sharp end of the wire following the first step has a radius larger than 200 nm. While apparently not yet demonstrated experimentally at the time of the patent filing, the method was believed to be applicable to other metals such as platinum, palladium, and rhodium to generate atomically sharp tips.

Figure 5-20. (a)-(d) FIM images with He as the image gas showing the atomic structure of an Ir(210) tip: (a) pristine Ir surface obtained by repeated thermal flash and field evaporation ($V_{\text{ext}} = 10.2$ kV); (b) after a thermal treatment in oxygen, the tip apex ends with only one atom ($V_{\text{ext}} = 7.1$ kV); (c) the second layer of the tip apex consists of three atoms ($V_{\text{ext}} = 7.9$ kV); (d) the third layer and the three ridges showing a pyramidal structure ($V_{\text{ext}} = 8.7$ kV); (e) a hardball model of the nano-pyramid.⁵⁶¹



⁵⁶¹ Hong-Shi Kuo, Ing-Shouh Hwang, Tsu-Yi Fu, Ying-Siang Hwang, Yi-Hsien Lu, Chun-Yueh Lin, Jin-Long Hou, Tien T. Tsong, “A single-atom sharp iridium tip as an emitter of gas field ion sources,” *Nanotechnology* 20(19 August 2009):335701.

Bryl and Szczepkowicz⁵⁶² have reported that a macroscopic W(111) tip will develop facets and form a truncated three-sided pyramid when annealed at 1400-1600 K after being exposed to about 1.3 Langmuir of oxygen. Further annealing of the tip in the 1000-1060 K temperature range leads to significant sharpening of the tip apex, with FIM observations revealing that the apex consists of several atoms at most and FEM images suggesting that these prepared tips can be used as point sources of electrons.

In 2009, Govind et al.⁵⁶³ studied the formation of oxygen-induced nanopyramids on the atomically rough and morphological unstable Rh(210) surface using Auger electron spectroscopy (AES), low energy electron diffraction (LEED), and UHV-scanning tunneling microscopy (STM). The researchers found that ~18 nm pyramids could be formed upon annealing the oxygen-covered Rh(210) surface at ≥ 550 K in the presence of oxygen (10^{-8} Torr) and the pyramidal facets were identified as two (731) faces and a (110) face. The study suggests that the oxygen overlayer can be removed from the surface via catalytic reaction at low temperature using CO oxidation while preserving (“freezing”) the pyramidal facet structure. The resulting clean faceted surface remains stable for $T \sim 600$ K. For temperatures above this value, the surface irreversibly relaxes to the planar state.

Another possible way to make noble metal wire SATs is to pull apart atomic sized wires (ASWs) (Figure 5-21). To do this, in 2009 Kizuka and Monna⁵⁶⁴ first prepared platinum nanotips by evaporating Pt in a vacuum chamber and deposited the metal on a Si cantilever with a nanotip for AFM. The cantilever tip was attached to the front of a tube piezoelement on a cantilever holder for HRTEM. A Pt plate 0.2 mm in thickness was attached to a plate holder and the contact edge of the plate was thinned to 5-20 nm by argon ion milling. The cantilever and plate holders were inserted into the transmission electron microscope under a modest vacuum (10^{-5} Pa). The cantilever tip was brought into contact with the edge surface of the opposing plate by piezomanipulation while applying a bias voltage of 13-30 mV at 20 Hz between the cantilever tip and the plate. The cantilever tip was next pressed into the plate edge to prepare nanocontacts (NCs) and then retracted to elongate them, at room temperature. The force acting on the contacts was measured by optical detection of cantilever deflection and ranged from 0 to 1.5 nN for the ASWs.

⁵⁶² Robert Bryl, Andrzej Szczepkowicz, “A method of microtip fabrication based on oxygen induced faceting,” *Applied Surface Science* 241(15 March 2005):431-434.

⁵⁶³ G. Govind, Wenhua Chen, Hao Wang, T.E. Madey, “Formation of Oxygen Induced Nanopyramids on Rh(210) Surface,” *Transport and Optical Properties of Nanomaterials: Proceedings of the International Conference-ICTOPON-2009*, AIP Conference Proceedings 1147(29 June 2009):521-527.

⁵⁶⁴ Tokushi Kizuka, Kosuke Monna, “Atomic configuration, conductance, and tensile force of platinum wires of single-atom width,” *Phys. Rev.* 80(2009):205406;
http://www.tulips.tsukuba.ac.jp/dspace/bitstream/2241/104213/1/PRB_80-20.pdf.

Figure 5-21. Observation of SAT formation in situ using HRTEM lattice imaging. (A) Time-sequence series of high-resolution images of thinning from a Pt nanocontact to a single-atom-width wire by retraction while applying an alternate-current voltage of 30 mV with a frequency of 20 Hz. The cantilever tip was separated from the plate with a speed of ~ 0.5 nm/s. The nanocontact and wire are located between the tip in the upper region of each frame and the plate in the lower region. The image contrast was increased to show the contact and wire clearly; as a result, the tip and plate regions appeared with lower intensities. The brighter area corresponds to the vacuum. **(B)** The configuration of atoms along the observation direction, corresponding to the high-resolution images in (A). **(C)** The line intensity of the high-resolution images in (A) along the minimum width of the constriction region. Broken lines represent three darkness levels, i.e., the vacuum level and two equally spaced levels. **(D)** Models of the atomic configuration of the cross-section at the minimum width.⁵⁶⁵

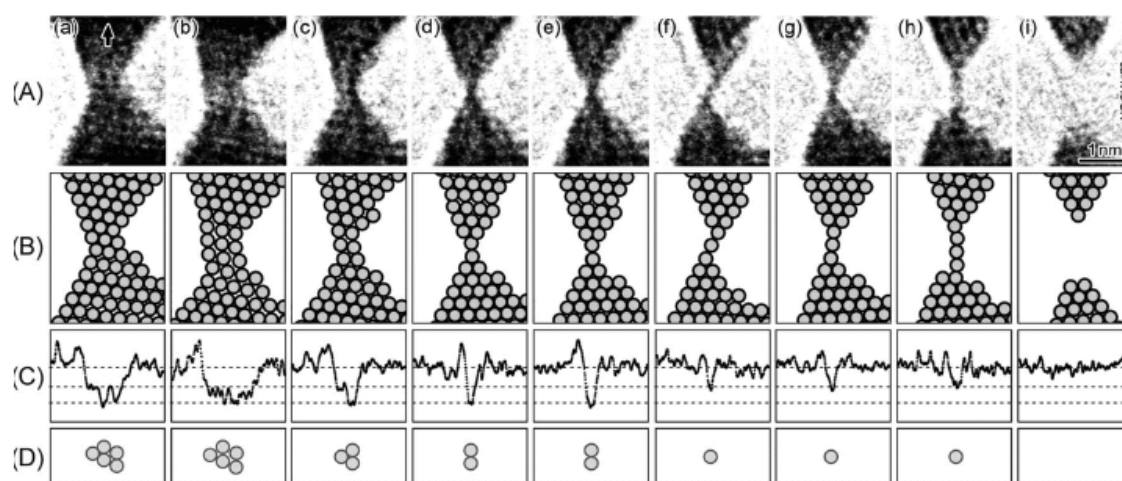


Figure 5-21 shows a time-sequence series of high-resolution images of thinning from Pt nanocontact to ASW by simple retraction with a speed of ~ 0.5 nm/s without using the conductance feedback system. The NC and ASW are observed between the tip in the upper region and the plate in the lower region of each frame in the figure, with the nanocontact becoming thinner during retraction until the ASW finally breaks, leaving a single-atom Pt tip in the last frame.

Similar results have been obtained for Au⁵⁶⁶ and Pd⁵⁶⁷ ASWs, though these papers do not indicate whether a SAT is formed at the moment when tip retraction breaks the single-atom wire.

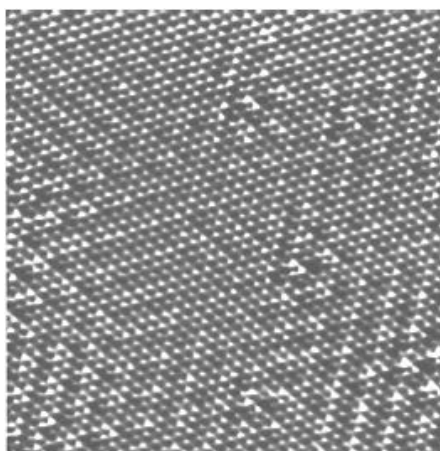
⁵⁶⁵ Tokushi Kizuka, Kosuke Monna, "Atomic configuration, conductance, and tensile force of platinum wires of single-atom width," Phys. Rev. 80(2009):205406; http://www.tulips.tsukuba.ac.jp/dspace/bitstream/2241/104213/1/PRB_80-20.pdf.

⁵⁶⁶ Tomoko Matsuda, Tokushi Kizuka, "Structure and Tensile Force of Nanometer- and Atomic-Sized Gold Contacts during Conductance Feedback Control," Jpn. J. Appl. Phys. 48(2009):125007. Tokushi Kizuka, "Atomic configuration and mechanical and electrical properties of stable gold wires of single-atom width,"

Pan et al.⁵⁶⁸ have described another method of producing an “atomically sharp” (defined as “having one or a few atoms at the end”) superconducting niobium metal tip:

“The superconducting tips are made from 0.2 mm diameter niobium (Nb) wire by mechanical sharpening. The tip installation is carried out with the STM open to air at room temperature. The STM chamber is then sealed, evacuated to 10^{-6} Torr, and cooled to 4.2 K. The natural oxide of Nb at the apex of the tip is removed, and the tip is further sharpened by field emission against an Au target in cryogenic ultrahigh vacuum at 4.2 K. After this process, the sharpness of the tip is verified by identification of atomic scale features on Au and NbSe₂ (Figure 5-22) surfaces.”

Figure 5-22. Topographic image (150 Å square) of a NbSe₂ surface acquired at 4.2 K in constant current mode with the Nb superconducting tip; a charge density wave pattern is clearly visible, but the atomic resolution of the image indicates that this superconducting tip is atomically sharp.⁵⁶⁹



Phys. Rev. B 77(2008):155401; https://www.tulips.tsukuba.ac.jp/dspace/bitstream/2241/99261/1/PRB-77_15.pdf.

⁵⁶⁷ Tomoko Matsuda, Tokushi Kizuka, “Palladium Wires of Single Atom Width as Mechanically Controlled Switching Devices,” Jpn. J. Appl. Phys. 45(2006):L1337-L1339. Tomoko Matsuda, Tokushi Kizuka, “Structure of Nanometer-Sized Palladium Contacts and Their Mechanical and Electrical Properties,” Jpn. J. Appl. Phys. 46(2007):4370-4374. Tomoko Matsuda, Tokushi Kizuka, “Slip Sequences during Tensile Deformation of Palladium Nanocontacts,” Jpn. J. Appl. Phys. 48(2009):115003.

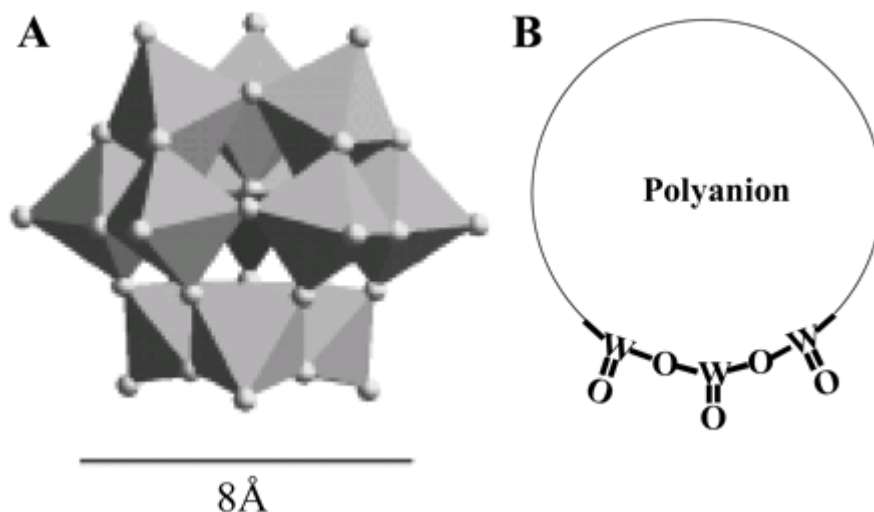
⁵⁶⁸ S.H. Pan, E.W. Hudson, J.C. Davis, “Vacuum tunneling of superconducting quasiparticles from atomically sharp scanning tunneling microscope tips,” Appl. Phys. Lett. 73(16 November 1998):2992-2994; <http://web.mit.edu/physics/hudson/Assets/Papers/Berkeley/SCTip.pdf>.

⁵⁶⁹ S.H. Pan, E.W. Hudson, J.C. Davis, “Vacuum tunneling of superconducting quasiparticles from atomically sharp scanning tunneling microscope tips,” Appl. Phys. Lett. 73(16 November 1998):2992-2994; <http://web.mit.edu/physics/hudson/Assets/Papers/Berkeley/SCTip.pdf>.

5.6 Metal Cluster SATs

Another metal-based single-atom tip employs more complex metal-containing structures such as Pt/Ir- $\text{H}_3\text{PW}_{12}\text{O}_{40}$.⁵⁷⁰ In this scheme, the complex shown in **Figure 5-23** is attached to a mechanically formed Pt/Ir tip to functionalize the metal tip as an STM probe. Note that the frontier atom in this case is an oxygen atom.

Figure 5-23. Molecular structure of the pseudospherical Keggin-type $[\text{PW}_{12}\text{O}_{40}]^{3-}$ heteropolyanion. Oxygen atoms are represented as spheres. A sphere projecting outward in each WO_6 octahedron represents terminal oxygen species.⁵⁷¹



The field emission characteristics of a single 1-nm-diameter Au cluster supported on a W(110) field-emission tip has been studied as well.⁵⁷²

⁵⁷⁰ In K. Song, John R. Kitchin, Mark A. Barteau, “ $\text{H}_3\text{PW}_{12}\text{O}_{40}$ -functionalized tip for scanning tunneling microscopy,” PNAS 99(30 April 2002):6471-6475; <http://www.pnas.org/content/99/suppl.2/6471.full>.

⁵⁷¹ In K. Song, John R. Kitchin, Mark A. Barteau, “ $\text{H}_3\text{PW}_{12}\text{O}_{40}$ -functionalized tip for scanning tunneling microscopy,” PNAS 99(30 April 2002):6471-6475; <http://www.pnas.org/content/99/suppl.2/6471.full>.

⁵⁷² M.E. Lin, R.P. Andres, R. Reifenberger, “Observation of the discrete electron energy states of an individual nanometer-size supported gold cluster,” Phys. Rev. Lett. 67(1991):477-480.

5.7 Accreted Metal-Atom SATs

Another method for making atomically sharp tips, also using metals, was demonstrated in 2009 by Gross et al.⁵⁷³ at IBM Zurich, who prepared metal tips to which a single CO molecule was bonded and then employed to produce images of a surface-bound pentacene molecule with atomic resolution.

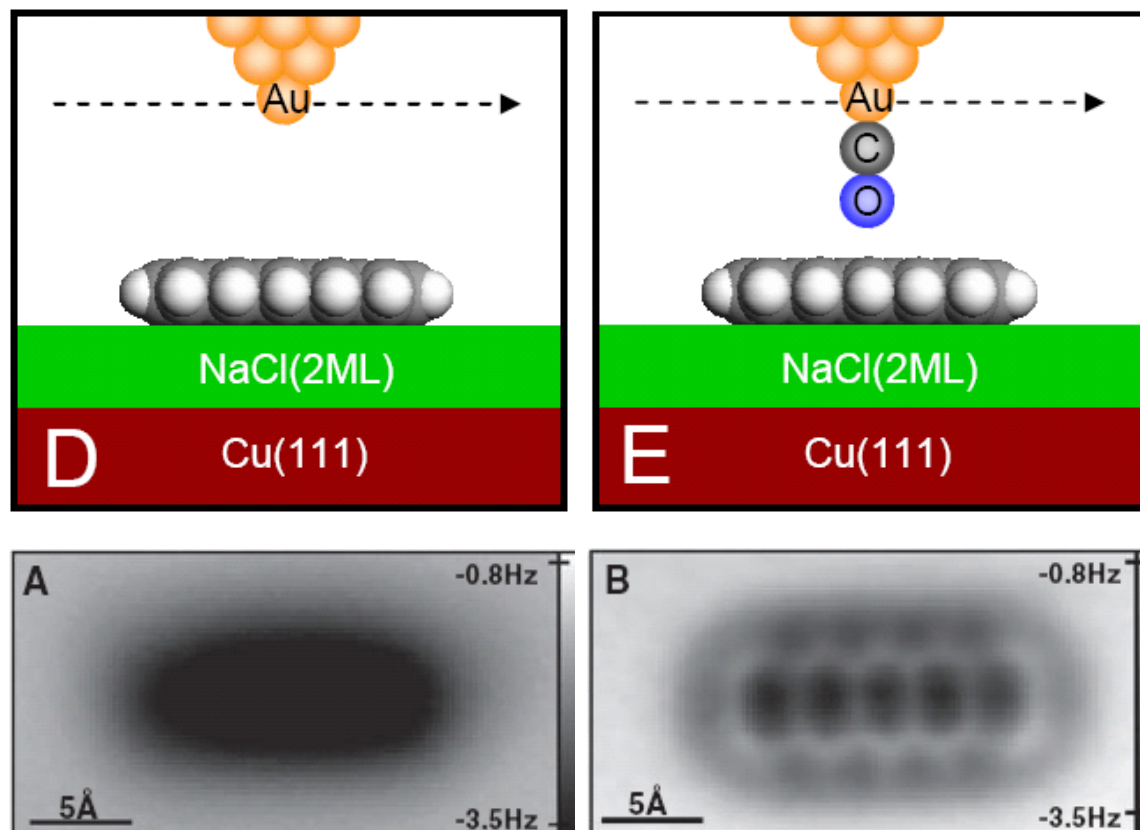
In this work, tip fabrication began with a cut 50- μm -thick PtIr wire whose apex was coated with copper by means of controlled indentations into a Cu substrate, producing an atomically-imprecise Cu coating at the tip apex. An atomically sharp silver or gold tip was then obtained by accreting Ag or Au atoms, one by one, to the tip. To pick up a Au or Ag atom,⁵⁷⁴ the tip was first positioned above a single Au or Ag adatom from a population of such atoms previously sputtered onto a NaCl(2 ML)/Cu(111) surface. Then, starting from a typical set point of $I = 2 \text{ pA}$, $V = 200 \text{ mV}$, the tip was approached to the adatom by about 4 Å, and the event of picking up the atom was observed as a sudden jump in the tunneling current. Multiple numbers of Au or Ag adatoms were picked up deliberately with the tip by repeating this process a number of times until a stable and atomically sharp metallic tip was obtained (Figure 5-24). Such tips can be characterized by imaging single Au or Ag adatoms as circular protrusions that exhibit a comparably small frequency shift of about $\Delta f = (2 \pm 1) \text{ Hz}$ at a tunneling set point of $I = 2 \text{ pA}$, $V = 200 \text{ mV}$ above NaCl(2 ML)/Cu(111).

It is unstated (and perhaps unknown to the authors) whether the Ag or Au metal atoms self-assemble to form a neat pyramidal geometry at the tip, but apparently these tips can be fabricated on an ad hoc basis with at least one prominent atomically sharp protrusion. Imaging scans using the plain metal tips produces images with very poor resolution, but the subsequent pickup of a CO molecule by the atomically sharp metal tip permits good-quality atomic resolution images to be obtained, with oxygen as the frontier atom of the compound tip. An oxygen tip is not ideal for DMS applications. However, the ability of these metal-CO structures to survive use as scanning tips for significant periods of time suggests that the stability of the Ag or Au tips might be sufficient for DMS. Perhaps the operating characteristics of these tips can be improved by high-temperature annealing. Further investigation of these possibilities appears warranted.

⁵⁷³ Leo Gross, Fabian Mohn, Nikolaj Moll, Peter Liljeroth, Gerhard Meyer, “The Chemical Structure of a Molecule Resolved by Atomic Force Microscopy,” *Science* 325(28 August 2009):1110-1114; <http://www.sciencemag.org/cgi/content/full/325/5944/1110>.

⁵⁷⁴ Jascha Repp, Gerhard Meyer, Fredrik E. Olsson, Mats Persson, “Controlling the Charge State of Individual Gold Adatoms,” *Science* 305(23 July 2004):493-495.

Figure 5-24. Idealized structure of an atomically sharp gold tip (top left), and the same Au tip after pickup of a CO molecule to obtain atomically precise imaging (top right). AFM (qPlus, 20 pm amplitude) images of a pentacene molecule (a chain of 5 benzene rings) using a plain Ag tip (bottom left) and a metal tip with CO attached (bottom right) are also shown.⁵⁷⁵



5.8 Cleaved Si, NiO, and Be Crystallite SATs

The preparation of AFM tips with a specified front-atom symmetry and chemical identity is instrumental for performing well defined experiments.

Silicon is our first example. Commercial silicon cantilever tips are oriented in a (001) direction, but in silicon the natural cleavage planes are (111) planes. If a macroscopic tip crystallite is limited by natural cleavage planes, a (001) oriented tip will in general not end in a single atom tip,

⁵⁷⁵ Leo Gross, Fabian Mohn, Nikolaj Moll, Peter Liljeroth, Gerhard Meyer, "The Chemical Structure of a Molecule Resolved by Atomic Force Microscopy," *Science* 325(28 August 2009):1110-1114; <http://www.sciencemag.org/cgi/content/full/325/5944/1110>.

but in a rooftop type of symmetry. However, a tip which points into a (111) direction will end in a single atom if we assume bulk termination. Moreover, the front atom of this tip is expected to be particularly stable because it is bonded to the rest of the tip by three bonds and exposes a single dangling bond towards the sample. In 2001, Giessibl et al.⁵⁷⁶ cleaved single crystalline silicon so as to obtain Si crystallites which were limited by (111) planes likely ending in a single atom tip.⁵⁷⁷ The silicon crystallite was cleaved in air, causing an oxide layer of typical thickness $\sim 20\text{\AA}$ to develop at the surface, then affixed to one tine of a qPlus tuning fork AFM sensor (Figure 5-25A). As expected, these tips did not yield good STM images after bringing them into vacuum. However, after exposing them to electron bombardment (the same procedure as used for preparing the silicon 7×7 surface) the tips worked excellently in STM mode and also in AFM mode.⁵⁷⁸ It was expected that the (111) oriented sidewalls of the tip would reconstruct just like a flat silicon surface, but that even then the front atom would still be bonded to three next neighbors and would expose a single dangling bond. Figure 5-25B shows an AFM image obtained with such a (111) oriented single-atom tip.

Huang et al.⁵⁷⁹ have done a density-of-states calculation for an atomically sharp Si tip (terminating in a single atom) using a tight-binding model.

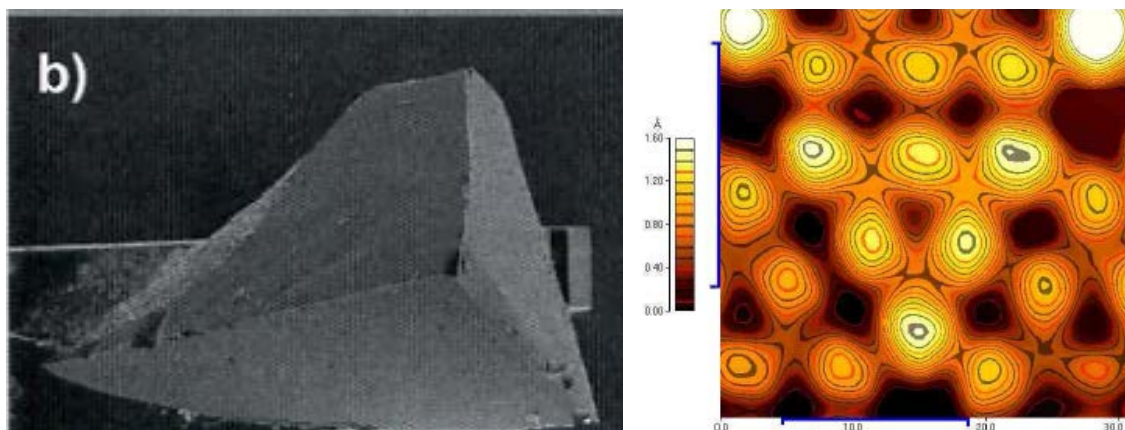
⁵⁷⁶ F.J. Giessibl, H. Bielefeldt, S. Hembacher, J. Mannhart, "Imaging of atomic orbitals with the atomic force microscope – experiments and simulations," *Ann. Phys. (Leipzig)* 10(2001):887-910; <http://arxiv.org/abs/cond-mat/0107195v1>.

⁵⁷⁷ F.J. Giessibl, S. Hembacher, H. Bielefeldt, J. Mannhart, "Imaging silicon by atomic force microscopy with crystallographically oriented tips," *Appl. Phys. A* 72(2001):S15-S17.

⁵⁷⁸ F.J. Giessibl, S. Hembacher, H. Bielefeldt, J. Mannhart, "Imaging silicon by atomic force microscopy with crystallographically oriented tips," *Appl. Phys. A* 72(2001):S15-S17.

⁵⁷⁹ Z.-H. Huang, P.H. Cutler, N.M. Miskovsky, T.E. Sullivan, "Calculation of local density of states at an atomically sharp Si tip," *J. Vac. Sci. Technol. B* 13(1995):522.

Figure 5-25. (A) Left: A single-crystal Si tip terminated by three (111) faces cleaved *ex situ* from a silicon crystallite, then mounted on a qPlus sensor tine.⁵⁸⁰ **(B) Right:** Topographic image of a Si(111)-(7x7) surface observed by FM-AFM, imaged with a single crystal silicon tip roughly oriented in a (111) direction, with imaging parameters $k = 1800$ N/m, amplitude $A = 2.5$ Å, $f_0 = 20531$ Hz, $\Delta f = +85$ Hz, thus $\gamma = +30$ fNm^{1/2} with rms frequency error $\delta\Delta f = 0.09$ Hz at a scanning speed of 20 nm/s.⁵⁸¹



Nickel oxide (NiO) tips that are bound by (001) planes cleaved *ex situ*⁵⁸² and *in situ*⁵⁸³ have been created as well (Figure 5-26A). NiO crystallizes in the rock salt structure ($a = 417$ pm), exhibits a nearly perfect bulk terminated (001) surface⁵⁸⁴ with a (1x1) chemical surface unit cell, and is a collinear antiferromagnet below 525 K. NiO tips were prepared by cleaving larger crystals *ex situ*

⁵⁸⁰ F.J. Giessibl, H. Bielefeldt, S. Hembacher, J. Mannhart, “Imaging of atomic orbitals with the atomic force microscope – experiments and simulations,” Ann. Phys. (Leipzig) 10(2001):887-910; <http://arxiv.org/abs/cond-mat/0107195v1>. Franz J. Giessibl, “Principles and Applications of the qPlus Sensor,” in S. Morita et al., eds., Noncontact Atomic Force Microscopy, Springer-Verlag Berlin Heidelberg, 2009, pp. 121-142.

⁵⁸¹ F.J. Giessibl, H. Bielefeldt, S. Hembacher, J. Mannhart, “Imaging of atomic orbitals with the atomic force microscope – experiments and simulations,” Ann. Phys. (Leipzig) 10(2001):887-910; <http://arxiv.org/abs/cond-mat/0107195v1>.

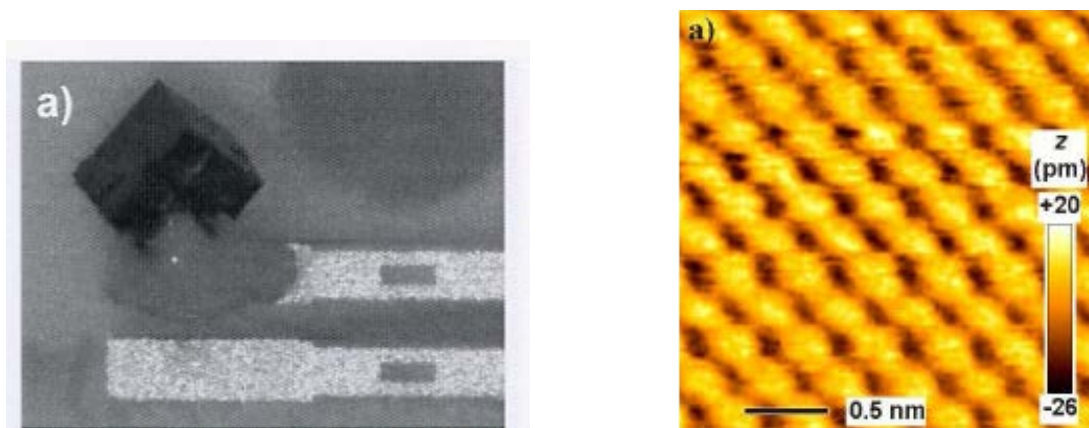
⁵⁸² M. Schmid, F.J. Giessibl, J. Mannhart, “Searching atomic spin contrast on nickel oxide (001) by force microscopy,” Phys. Rev. B 77(2008):045402. See also: M. Schmid, A. Renner, F.J. Giessibl, “Device for in situ cleaving of hard crystals,” Rev. Sci. Instrum. 77(16 March 2006):036101.

⁵⁸³ T. Wutscher, Einkristalline spitzen fuer die rasterkraftmikroskopie, Diploma thesis, Universitaet Regensburg, Germany, 2007.

⁵⁸⁴ Tetsuaki Okazawa, Yoshihiro Yagi, Yoshiaki Kido, “Rumpled surface structure and lattice dynamics of NiO(001),” Phys. Rev. B 67(2003):195406.

and searching for sharply pointed crystallites with sizes of roughly $50\text{ }\mu\text{m} \times 50\text{ }\mu\text{m} \times 250\text{ }\mu\text{m}$.⁵⁸⁵ Annealing by electron bombardment in UHV is difficult for an insulator like NiO, so Schmid et al. cleaned the tips *in situ* by scratching along the NiO surface.⁵⁸⁶ The NiO SAT can be used to obtain atomic resolution images of an NiO surface (Figure 5-26B). A repetition of the experiment at lower temperature would be required to determine whether the SAT apex consisted of a single Ni or O atom.

Figure 5-26. (A) Left: Single-crystal NiO tip mounted on a qPlus sensor. The cuts in the crystal are designed to facilitate cleaving so as to create a tip with three freshly cleaved NiO(001) surfaces.⁵⁸⁷ (B) Right: Atomic resolution topographical image of an NiO(001) surface obtained with FM-AFM in the repulsive mode, taken with an NiO tip oscillating with amplitude $A \sim 1\text{ }\text{\AA}$ at $\Delta f = +66\text{ Hz}$.⁵⁸⁸



⁵⁸⁵ M. Schmid, F.J. Giessibl, J. Mannhart, "Searching atomic spin contrast on nickel oxide (001) by force microscopy," *Phys. Rev. B* 77(2008):045402. See also: M. Schmid, A. Renner, F.J. Giessibl, "Device for in situ cleaving of hard crystals," *Rev. Sci. Instrum.* 77(16 March 2006):036101.

⁵⁸⁶ M. Schmid, F.J. Giessibl, J. Mannhart, "Searching atomic spin contrast on nickel oxide (001) by force microscopy," *Phys. Rev. B* 77(2008):045402. See also: M. Schmid, A. Renner, F.J. Giessibl, "Device for in situ cleaving of hard crystals," *Rev. Sci. Instrum.* 77(16 March 2006):036101.

⁵⁸⁷ M. Schmid, F.J. Giessibl, J. Mannhart, "Searching atomic spin contrast on nickel oxide (001) by force microscopy," *Phys. Rev. B* 77(2008):045402. See also: M. Schmid, A. Renner, F.J. Giessibl, "Device for in situ cleaving of hard crystals," *Rev. Sci. Instrum.* 77(16 March 2006):036101. Franz J. Giessibl, "Principles and Applications of the qPlus Sensor," in S. Morita et al., eds., *Noncontact Atomic Force Microscopy*, Springer-Verlag Berlin Heidelberg, 2009, pp. 121-142.

⁵⁸⁸ M. Schmid, F.J. Giessibl, J. Mannhart, "Searching atomic spin contrast on nickel oxide (001) by force microscopy," *Phys. Rev. B* 77(2008):045402. See also: M. Schmid, A. Renner, F.J. Giessibl, "Device for in situ cleaving of hard crystals," *Rev. Sci. Instrum.* 77(16 March 2006):036101.

Beryllium metal is another possible candidate tip material for enhanced resolution because a beryllium atom has just four electrons, leading to a small covalent radius of only 96 pm. Be is conductive, but also has a high elastic modulus and a high binding energy compared to other light metals, a necessity for a stable tip apex. However beryllium tips that are prepared *ex situ* are covered with a robust oxide layer that cannot be removed by just heating the tip. Hofmann et al.⁵⁸⁹ have demonstrated a successful preparation method that combines the heating of the tip by field emission and a mild collision with a clean metal plate – a technique that yields a clean, oxide-free tip surface as proven by a work function of $\Phi_{\text{exp}} = 5.5$ eV as deduced from a current-distance curve.

The researchers⁵⁹⁰ used beryllium tips produced by crushing a polycrystalline beryllium lump (purity of 99.5%) with a gripper. The procedure was conducted in a liquid environment to meet safety regulations. Possible tips are selected from the resulting fragments under an optical microscope. Most of the fragments show macroscopically flat cleavage planes due to the brittle fracture behavior of beryllium. In an SEM image of one such fragment (**Figure 5-27A**), the front region of a selected beryllium piece is shown and indicates that the surfaces of the cleavage planes exhibit many small protrusions. The selected beryllium fragments are glued conductively onto a gold wire, which is attached to the front side of the free prong of a qPlus tuning fork using non conductive glue.

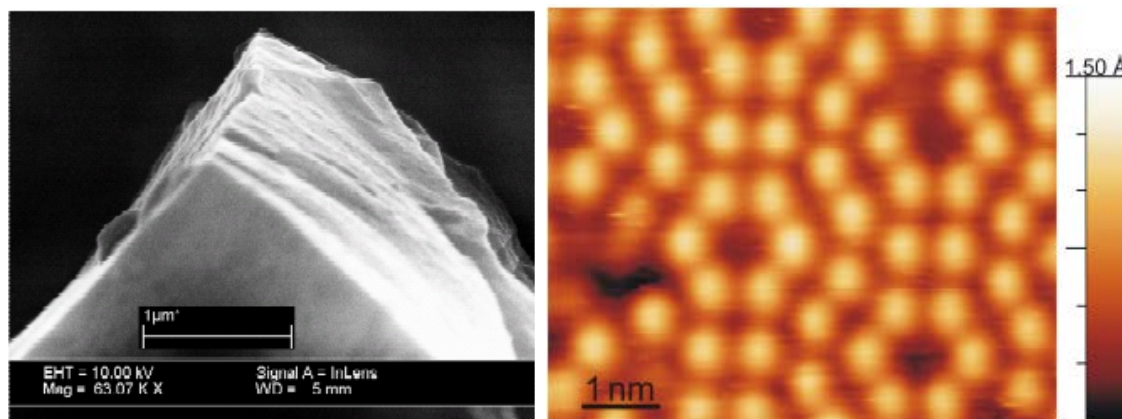
The sensor is transferred to a room temperature UHV chamber (base pressure 5×10^{-11} mbar). The Be tip must then be cleaned to achieve stable tunneling operation. For the preparation of beryllium tips, it is not enough to just heat the tip apex because the oxide layer has a higher melting (~ 2600 °C) and boiling point (~ 3200 °C) than the covered beryllium (~ 1300 °C) and also the oxide layer is very rigid. Therefore it is necessary to melt the tip apex and additionally to break the oxide mechanically. For this purpose, the Be tip is brought into contact with a metal plate while a voltage of 1 kV is applied. Shortly before mechanical contact, visible arcing occurs between tip and sample. At contact of the tip to the metal plate, the oxide breaks open and the tip is melted to the plate. By retracting the tip for a few micrometers it is torn off the metal plate and again a vacuum arc is generated due to high field emission current.

The Be tip is then used as an STM probe to image the Si (111)-(7x7) surface and demonstrably achieves atomic resolution (**Figure 5-27B**), proving the single-atom termination of the beryllium tip. Because beryllium is very reactive, the tip has to be prepared again after a few hours at room temperature. However, the researchers expect that the tip lifetime would be at least weeks in an LHe (liquid helium)-temperature UHV environment.

⁵⁸⁹ T. Hofmann, J. Welker, F.J. Giessibl, “Preparation of light-atom tips for Scanning Probe Microscopy by explosive delamination,” JVST B (May/June 2010), in press;
<http://arxiv.org/ftp/arxiv/papers/1001/1001.1321.pdf>.

⁵⁹⁰ T. Hofmann, J. Welker, F.J. Giessibl, “Preparation of light-atom tips for Scanning Probe Microscopy by explosive delamination,” JVST B (May/June 2010), in press;
<http://arxiv.org/ftp/arxiv/papers/1001/1001.1321.pdf>.

Figure 5-27. (A) Left: SEM image of a cleaved beryllium fragment used as scanning probe tip; on the macroscopically flat cleavage planes many small protrusions are visible. **(B) Right:** STM image of the Si-(111)-(7x7) surface recorded with a beryllium tip after tip preparation; image size is $5.4 \times 6.5 \text{ nm}^2$, imaging parameters $V = -1.5 \text{ V}$, $I_t = 69 \text{ pA}$.⁵⁹¹



5.9 Other Studies of SATs

A few other SATs have been investigated experimentally. Much of the interest since at least the 1980s⁵⁹² is due to their possible use as very high quality field emission tips.

5.9.1 Diamond SAT Theory Studies

Diamond SATs have not yet been fabricated experimentally, although improved CVD diamond film nucleation on (100)-oriented iridium surfaces has been demonstrated by diamond-MEMS researchers at Sandia,⁵⁹³ which may suggest future possibilities.

On the theory side, Miskovsky and Cutler⁵⁹⁴ have computed the local density of states for a diamond SAT, modeled as a pyramidal cluster of 159 carbon atoms surmounted by a single

⁵⁹¹ T. Hofmann, J. Welker, F.J. Giessibl, "Preparation of light-atom tips for Scanning Probe Microscopy by explosive delamination," *JVST B* (May/June 2010), in press;
<http://arxiv.org/ftp/arxiv/papers/1001/1001.1321.pdf>.

⁵⁹² N.D. Lang, A. Yacoby, Y. Imry, "Theory of a single-atom point source for electrons," *Phys. Rev. Lett.* 63(1989):1499-1502.

⁵⁹³ Thomas A. Friedmann, John P. Sullivan, Subhash L Shinde, Ed S. Piekos, "Nucleation, Growth, and Processing of Oriented Diamond Films for MEMS Applications," 9:00 AM GG1.2, Session GG1: Materials and Processes for MEMS, Symposium GG: Microelectromechanical Systems--Materials and Devices II, 1-2 December 2008.

carbon atom – even though no such tip has yet been fabricated and the DLC asperity tip shown in **Table 2-1** has a handful of C atoms at its atomically-imprecise apex. The stick-slip behavior of a diamond SAT on crystalline copper surface has been simulated using MD,⁵⁹⁵ there has been a theoretical simulation of AFM images as performed with a model of a diamond single-atom tip or two kinds of multiple-atom diamond tips scanned on a graphite substrate surface,⁵⁹⁶ and a diamond SAT is calculated able to sustain forces >30 nN against C(110) surface during contact mode AFM.⁵⁹⁷

5.9.2 Single-Atom Metal Carbide Tips

Refractory-metal carbides are metallic conductors. They are mechanically hard and have very high melting temperatures, with high thermal and mechanical stability that apparently translates into lower atomic mobility.⁵⁹⁸

Yu and Chang⁵⁹⁹ at IBM Yorkshire Heights have fabricated atomically sharp tungsten carbide (WC) coated single-atom W(111) and W(100) tips and atomically sharp hafnium carbide

⁵⁹⁴ N.M. Miskovsky, P.H. Cutler, “Local density of states calculation for a discrete model of a diamond single atom tip,” Eleventh International Vacuum Microelectronics Conference, 19-24 July 1998, pp. 275-276. N.M. Miskovsky, Paul H. Cutler, “Local density of states calculation for a discrete model of a diamond single atom tip,” Appl. Phys. Lett. 74(22 February 1999):1093. N.M. Miskovsky, P.H. Cutler, “Calculation of the local density of states for a discrete pyramidal model of a diamond tip surmounted by a single atom,” Surf. Sci. 439(1999):173-180; [http://cms.kist.re.kr/informations/papers/Science%20Direct/Surface%20Science%20439%20173-180%20\(1999\).pdf](http://cms.kist.re.kr/informations/papers/Science%20Direct/Surface%20Science%20439%20173-180%20(1999).pdf).

⁵⁹⁵ Jun Shimizu, Hiroshi Eda, Libo Zhou, “Molecular Dynamics Simulation on Dependence of Atomic-scale Stick-slip Phenomenon upon Probe Tip Shape,” Initiatives of Precision Engineering at the Beginning of a Millennium, 10th International Conference on Precision Engineering (ICPE), 18-20 July 2001, Yokohama, Japan, Springer US, 2001, pp. 759-763; <http://www.springerlink.com/content/v78763g34662v302/>.

⁵⁹⁶ Naruo Sasaki, Masaru Tsukada, “Effect of the tip structure on atomic-force microscopy,” Phys. Rev. B 52(1995):8471-8482.

⁵⁹⁷ “Mechanical Response of Diamond at Nanometer Scales: Diamond Polishing and Atomic Force Microscopy,” MRS Proceedings, Fall 2000 Symposium Q, Q8.6.1.

⁵⁹⁸ Ming L. Yu, Ho-Seob Kim, Brian W. Hussey, T.H. Philip Chang, William A. Mackie, “Energy distributions of field emitted electrons from carbide tips and tungsten tips with diamondlike carbon coatings,” J. Vac. Sci. Technol. B 14(November 1996):3797-3801.

⁵⁹⁹ Ming L. Yu, Brian W. Hussey, Ernst Kratschmer, T. H. Philip Chang, William A. Mackie, “Improved emission stability of carburized HfC<100> and ultrasharp tungsten field emitters,” J. Vac. Sci. Technol. B 13(November/December 1995):2436-2440. Ming L. Yu, Norton D. Lang, Brian W. Hussey, T.H. Philip Chang, William A. Mackie, “New Evidence for Localized Electronic States on Atomically Sharp Field Emitters,” Phys. Rev. Lett. 77(1996):1636-1639. Ming L. Yu, T.H. Philip Chang, “Properties and stability of single-atom field emitters,” Appl. Surf. Sci. 146(May 1999):334-340.

HfC(100) and zirconium carbide ZrC(100) tips, from which they measured field emission, e.g., of 10 $\mu\text{A}/\text{sr}$ for over 1 hour with angular confinement to a 3° semicone angle.⁶⁰⁰ Their “carburized” nanotips were formed at room temperature using modest electric fields ($\leq 100 \text{ V}/\mu\text{m}$) and currents (a few μA) after acetylene processing at 1×10^{-6} Torr (see below for details). The tungsten-carbon bond is stronger than the tungsten-tungsten bond, which should have the effect of limiting the mobility of tungsten atoms on the tip apex by increasing the activation energy of diffusion.⁶⁰¹

In the Yu-Chang work,⁶⁰² the tungsten-carbide-coated W(111) tips were formed by heating sharpened W(111) tips in 4×10^{-6} Torr of acetylene at 1100 K for 5 minutes to form a thin tungsten carbide layer.⁶⁰³ Sharp ZrC(100) and HfC(100) emitters were prepared first by the electrochemical etching of single crystal ZrC and HfC rods. The tips (having curvature radius $< 50 \text{ nm}$) were cleaned by 2000 K thermal annealing and field evaporation in a VG FIM-100 ultrahigh vacuum (UHV) analysis chamber. The tips were then “carburized” by heating in 4×10^{-6} Torr of acetylene at 1100 K to replenish carbon lost in thermal annealing.⁶⁰⁴ To obtain single-atom tips the researchers followed Binh et al.⁶⁰⁵ and used the buildup process⁶⁰⁶ (see [Section 3.10](#) and [Section 5.1](#)). It is known that the buildup process causes the growth of nanoprotusions with the apex atom at the tip end.⁶⁰⁷ A strong electric field is applied at elevated temperature to the

⁶⁰⁰ Ming L. Yu, Brian W. Hussey, Ernst Kratschmer, T. H. Philip Chang, William A. Mackie, “Improved emission stability of carburized HfC<100> and ultrasharp tungsten field emitters,” J. Vac. Sci. Technol. B 13(November/December 1995):2436-2440.

⁶⁰¹ J.P. Barbour, F.M. Charbonnier, W.W. Donald, W.P. Dyke, E.E. Martin, L.K. Trolan, “Determination of the Surface Tension and Surface Migration Constants for Tungsten,” Phys. Rev. 117(March 1960):1452-1459.

⁶⁰² Ming L. Yu, Norton D. Lang, Brian W. Hussey, T.H. Philip Chang, William A. Mackie, “New Evidence for Localized Electronic States on Atomically Sharp Field Emitters,” Phys. Rev. Lett. 77(1996):1636-1639.

⁶⁰³ Ming L. Yu, Brian W. Hussey, Ernst Kratschmer, T. H. Philip Chang, William A. Mackie, “Improved emission stability of carburized HfC<100> and ultrasharp tungsten field emitters,” J. Vac. Sci. Technol. B 13(November/December 1995):2436-2440.

⁶⁰⁴ Ming L. Yu, Brian W. Hussey, Ernst Kratschmer, T. H. Philip Chang, William A. Mackie, “Improved emission stability of carburized HfC<100> and ultrasharp tungsten field emitters,” J. Vac. Sci. Technol. B 13(November/December 1995):2436-2440.

⁶⁰⁵ V.T. Binh, “In Situ Fabrication and Regeneration of Microtips for Scanning Tunnelling Microscopy,” J. Microsc. 152(November 1988):355-361. Vu Thien Binh, S.T. Purcell, N. Garcia, J. Doglioni, “Field-emission electron spectroscopy of single-atom tips,” Phys. Rev. Lett. 69(1992):2527-2530. See also: N. Ernst, J. Unger, H.W. Fink, M. Grunze, C. Wöll, “Comment on ‘Field-emission spectroscopy of single-atom tips’,” Phys. Rev. Lett. 70(1993):2503.

⁶⁰⁶ P.C. Bettler, F.M. Charbonnier, “Activation Energy for the Surface Migration of Tungsten in the Presence of a High-Electric Field,” Phys. Rev. 119(1960):85-93. Yu. A. Vlasov, V.G. Pavlov, V.N. Shrednik, Sov. Tech. Phys. Lett. 12(1986):224.

⁶⁰⁷ V.T. Binh, “In Situ Fabrication and Regeneration of Microtips for Scanning Tunnelling Microscopy,” J. Microsc. 152(November 1988):355-361.

apex of a field emission tip, generating a driving force that moves the tip atoms toward the local field maximum with the elevated temperature promoting atomic mobility. A nanostructure is formed at the tip apex that can end with a single atom, i.e., a single-atom tip. Since the driving force is independent of the direction of the electric field, built-up tips can be produced using either positive or negative bias. The typical procedure was to apply several kV positive bias at the tip at 1500 K for a few seconds, or apply a negative bias on the tip to give a large emission current (a few mA) at room temperature until buildup occurred. The second technique was preferred because the buildup process could then be watched by field-emission microscopy (FEM). The field emission at the buildup site would increase suddenly, giving intense emission within a semicone angle of a few degrees. The crystalline direction of the buildup varied from one experiment to the other, occasionally producing more than one buildup site on the same tip. The researchers were not successful in preparing built-up tips (SATs) on clean carbide tips without the acetylene treatment, and they were unable to establish sufficient process control to form the various types of built-up sites reproducibly.

Is the single atom at the tip a metal atom or a carbon atom? Given that the atom at the tip apex behaves like an adsorbed atom, Yu and Chang⁶⁰⁸ concluded that the tip apex atoms are metal atoms. (Resonant levels can only weakly couple to the bulk metal; carbon has low lying valence states a few volts below the Fermi level,⁶⁰⁹ and the observation of energy distributions quite close to the Fermi level suggests the apex atoms might be metallic.⁶¹⁰) What about the atoms immediately below the apex atom? The apex atom appears to be only weakly interacting with the bulk of the tip, so it was further suggested⁶¹¹ that the apex atom has to be on top of a small protrusion of certain height,⁶¹² with the spacer a single carbon atom or an aggregate of carbon atoms. (The fact that carbon deposition by acetylene was necessary in all cases suggested that the protrusion could be mostly carbon; the low density of states of carbon close to the Fermi level would effectively reduce the coupling of the valence band electrons with the electrons of the apex atom.⁶¹³) Hence the overall picture that emerges, albeit very uncertain, is of a single metal atom

⁶⁰⁸ Ming L. Yu, Norton D. Lang, Brian W. Hussey, T.H. Philip Chang, William A. Mackie, "New Evidence for Localized Electronic States on Atomically Sharp Field Emitters," *Phys. Rev. Lett.* 77(1996):1636-1639.

⁶⁰⁹ E.W. Plummer, B.J. Wacławski, T.V. Vorburger, "Photoelectron spectra of the decomposition of ethylene on (110) tungsten," *Chem. Phys. Lett.* 28(October 1974):510-515. See also E.W. Plummer, in R. Gomer, ed., *Interactions on Metal Surfaces: Topics in Applied Physics*, Vol. 4, Springer-Verlag, New York, 1975, p. 144.

⁶¹⁰ Ming L. Yu, T.H. Philip Chang, "Properties and stability of single-atom field emitters," *Appl. Surf. Sci.* 146(May 1999):334-340.

⁶¹¹ Ming L. Yu, T.H. Philip Chang, "Properties and stability of single-atom field emitters," *Appl. Surf. Sci.* 146(May 1999):334-340.

⁶¹² François Gautier, Hervé Ness, Daniel Stoeffler, "Electronic structure of transition metal tips and tip-surface interactions," *Ultramicroscopy* 42-44(July 1992):91-96.

⁶¹³ Ming L. Yu, T.H. Philip Chang, "Properties and stability of single-atom field emitters," *Appl. Surf. Sci.* 146(May 1999):334-340.

at the apex position bonded immediately below to one or more carbon atoms in the metal carbide lattice structure.

Other refractory transition metal carbides such as tantalum carbide TaC,⁶¹⁴ titanium carbide TiC,⁶¹⁵ hafnium carbide HfC,⁶¹⁶ and niobium carbide NbC⁶¹⁷ have also been investigated as possible field emission cathodes (and thus are potentially useful for attempting to make single atom tips), along with similar metal carbide coatings on Mo field emitter tips.⁶¹⁸ Carbide emitters can be made by carburizing metal emitters (e.g., TaC)⁶¹⁹ or by etching bulk carbide (e.g., from bulk ZrC⁶²⁰ and surface-processed TiC(110)⁶²¹ and NbC(110)⁶²²). There have been a few theory

⁶¹⁴ N.A. Gorbatiy, E.M. Ryabchenko, "The behavior of adsorbed Cs films on single-crystal spikes of Ta and Ta₂C," *Sov. Phys. Solid State* 7(1 October 1965): 921-926. E.G. Shirokov, "Increasing the total field-emission current," *Sov. Phys. Tech. Phys.* 14(1970):1134. William A. Mackie, Jennifer L. Morrissey, Clarence H. Hinrichs, Paul R. Davis, "Field emission from hafnium carbide," *J. Vac. Sci. Technol. A* 10(July 1992):2852-2856. W.A. Mackie, R.L. Hartman, P.R. Davis, "High current density field emission from transition metal carbides," *Appl. Surf. Sci.* 67(1993):29-35. William A. Mackie, Robert L. Hartman, Mark A. Anderson, Paul R. Davis, "Transition metal carbides for use as field emission cathodes," *J. Vac. Sci. Technol. B* 12(March 1994):722-726. W.A. Mackie, Tianbao Xie, P.R. Davis, "Transition metal carbide field emitters for field-emitter array devices and high current applications," *J. Vac. Sci. Technol. B* 17(March 1999):613-619.

⁶¹⁵ Hiroshi Adachi, Kiyoshi Fujii, Shigeaki Zaima, Yukio Shibata, Chuhei Oshima, Shigeaki Otani, Yoshio Ishizawa, "Stable carbide field emitter," *Appl. Phys. Lett.* 43(1 October 1983):702-703. Y. Ishizawa, "Field-emission properties of surface-processed TiC tips," *J. Phys. D* 22(14 November 1989):1763-1767. W.A. Mackie, L.A. Southall, Tianbao Xie, G.L. Cabe, F.M. Charbonnier, P.H. McClelland, "Emission fluctuation and slope-intercept plot characterization of Pt and transition metal carbide field-emission cathodes in limited current regimes," *J. Vac. Sci. Technol. B* 21(31 July 2003):1574-1580.

⁶¹⁶ William A. Mackie, Jennifer L. Morrissey, Clarence H. Hinrichs, Paul R. Davis, "Field emission from hafnium carbide," *J. Vac. Sci. Technol. A* 10(July 1992):2852-2856.

⁶¹⁷ W.A. Mackie, L.A. Southall, Tianbao Xie, G.L. Cabe, F.M. Charbonnier, P.H. McClelland, "Emission fluctuation and slope-intercept plot characterization of Pt and transition metal carbide field-emission cathodes in limited current regimes," *J. Vac. Sci. Technol. B* 21(31 July 2003):1574-1580. Y. Ishizawa, T. Aizawa, S. Otani, "Stable field emission and surface evaluation of surface-processed NbC<110> tips," *Appl. Surf. Sci.* 67(2 April 1993):36-42.

⁶¹⁸ W.A. Mackie, Tianbao Xie, M.R. Matthews, B.P. Routh, Jr., P.R. Davis, "Field emission from ZrC and ZrC films on Mo field emitters," *J. Vac. Sci. Technol. B* 16(July 1998):2057-2062.

⁶¹⁹ N.A. Gorbatiy, E.M. Ryabchenko, "The behavior of adsorbed Cs films on single-crystal spikes of Ta and Ta₂C," *Sov. Phys. Solid State* 7(1 October 1965): 921-926. E.G. Shirokov, "Increasing the total field-emission current," *Sov. Phys. Tech. Phys.* 14(1970):1134.

⁶²⁰ M.I. Elinson, G.A. Kudintseva, *Radiotekhn. Elektron.* 7(1962):1511.

⁶²¹ Hiroshi Adachi, Kiyoshi Fujii, Shigeaki Zaima, Yukio Shibata, Chuhei Oshima, Shigeaki Otani, Yoshio Ishizawa, "Stable carbide field emitter," *Appl. Phys. Lett.* 43(1 October 1983):702-703. Y. Ishizawa, "Field-emission properties of surface-processed TiC tips," *J. Phys. D* 22(14 November 1989):1763-1767.

studies⁶²³ of the field emission properties of a single-atom carbon protrusion standing on a metal surface.

Yu et al.⁶²⁴ examined tungsten field emitters with diamondlike carbon coatings, but the coating all proved to be polycrystalline and no evidence for single-atom (carbon) terminations could be found. Single-crystal diamond was grown on “sharp” silicon field emission tips via CVD⁶²⁵ but also produced no SATs.

Silicon carbide (SiC) surfaces show atomically stepped slopes (nanofacets)⁶²⁶ but no pyramidal faceting.

5.9.3 Single-Atom Aluminum Tips

Gohda and Watanabe⁶²⁷ have used DFT to analyze theoretically the electron emission characteristics of an aluminum Al(100) single-atom tip structure. They model a clean Al(100) surface using a slab consisting of four Al layers, upon which is attached a single-atom terminated

⁶²² Y. Ishizawa, T. Aizawa, S. Otani, “Stable field emission and surface evaluation of surface-processed NbC<110> tips,” Appl. Surf. Sci. 67(2 April 1993):36-42.

⁶²³ N.D. Lang, A. Yacoby, Y. Imry, “Theory of a single-atom point source for electrons,” Phys. Rev. Lett. 63(1989):1499-1502. A. Mayer, N.M. Miskovsky, P.H. Cutler, “Theoretical comparison between field-emission properties of carbon protrusions ranging from an isolated atom to multi-wall nanotubes,” J. Phys.: Condens. Matter 15(2003):R177-R191; <http://perso.fundp.ac.be/~amayer/Papers/paper31.pdf>.

⁶²⁴ Ming L. Yu, Ho-Seob Kim, Brian W. Hussey, T.H. Philip Chang, William A. Mackie, “Energy distributions of field emitted electrons from carbide tips and tungsten tips with diamondlike carbon coatings,” J. Vac. Sci. Technol. B 14(November 1996):3797-3801.

⁶²⁵ E.I. Givargizov, V.V. Zhimov, A.L. Stepanova, P.S. Plekhanov, R.I. Kozlov, “Field emission characteristics of polycrystalline and single-crystalline diamond grown on Si tips,” Appl. Surf. Sci. 94/95(2 March 1996):117-122.

⁶²⁶ S. Odaka, H. Miyazaki, S.-L. Li, A. Kanda, K. Morita, S. Tanaka, Y. Miyata, H. Kataura, K. Tsukagoshi, Y. Aoyagi, “Anisotropic transport in graphene on SiC substrate with periodic nanofacets,” Appl. Phys. Lett. 96(9 February 2010):062111.

⁶²⁷ Y. Gohda, S. Watanabe, “Total Energy Distribution of Field-Emitted Electrons from Al(100) Surface with Single-Atom Terminated Protrusion,” Phys. Rev. Lett. 87(2001):177601. Y. Gohda, S. Watanabe, “Theoretical analysis of field emission from atomically sharp aluminum tips,” Surf. Sci. 516(20 September 2002):265-271; <http://202.127.1.11/surface%20science/516/516306.pdf>. Y. Gohda, S. Watanabe, “Tunneling barrier for field emission from atomically sharp aluminum tips,” American Physical Society, Annual APS March Meeting, 18-22 March 2002, Indiana Convention Center, Indianapolis, Indiana Meeting ID: MAR02, abstract #W10.004; <http://adsabs.harvard.edu/abs/2002APS..MARW10004G>. Y. Gohda, S. Watanabe, “Theoretical analysis of field emission from metallic nanostructures on Si(100) surfaces,” J. Phys.: Condens. Matter 16(2004):4685-4696; http://www.iop.org/EJ/article/0953-8984/16/26/004/cm4_26_004.pdf?request-id=088a5fa8-43cd-40a4-8878-02a7f271d597.

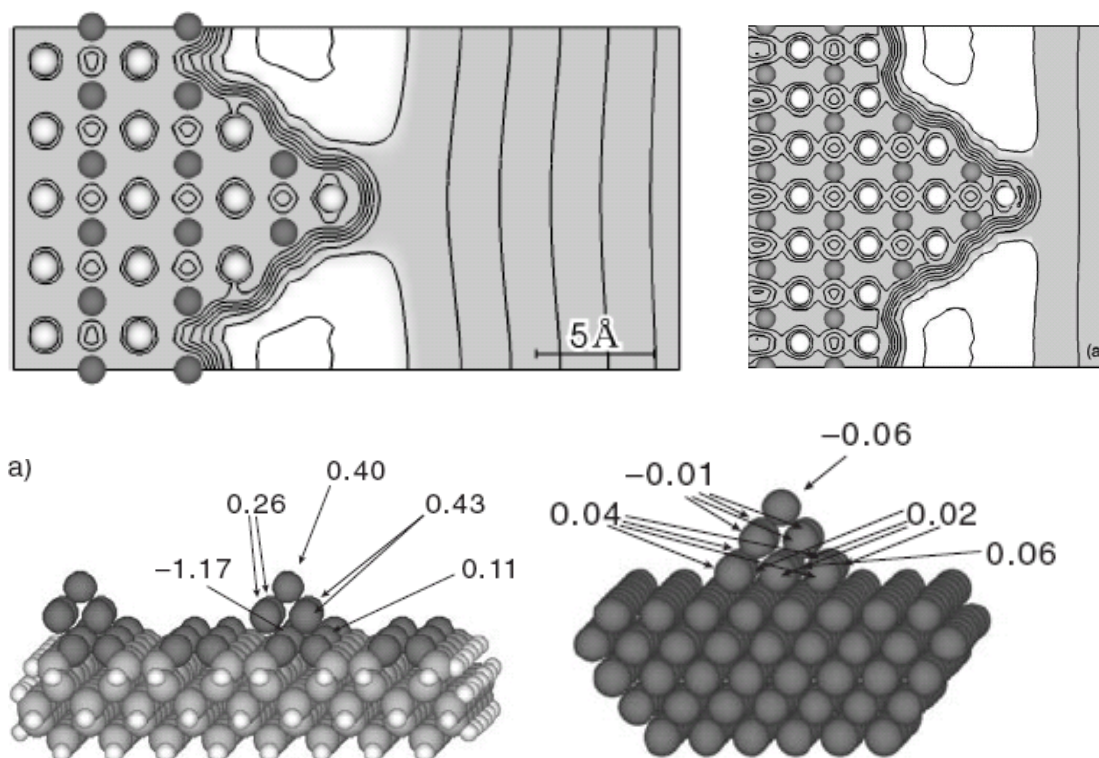
pyramidal protrusion consisting of 14 Al atoms (one, four, and nine atoms in the topmost, second, and third layers, respectively) (Figure 5-28A). The height of this protrusion is 0.7 nm and the radius of the apex is 0.15 nm, as estimated from the electron density distribution obtained from their calculation. In a second model, they model a larger aluminum SAT having 30 metal atoms, where the topmost, second, third, and fourth layer is composed of one, four, nine, and 16 aluminum atoms, respectively, in which case 226 Al atoms are included in a two-dimensional unit cell with the protrusion having a height of 0.9 nm and an apex radius of 0.15 nm (Figure 5-28B). In yet another paper⁶²⁸ the authors modeled two 5-atom Al pyramids on a silicon surface (Figure 5-28C) and a 14-atom SAT protrusion on a 5-layer pure metal surface (Figure 5-28D).

Snow et al.⁶²⁹ hint at a possible approach for making aluminum SATs. In their experimental work, they fabricate atomic point contacts by using anodic oxidation of thin Al films with an atomic force microscope. In situ electrical measurements are used as feedback to control the fabrication of Al nanowires that are subsequently anodized through their cross section to form the point contacts; in some devices, conductance stabilizes near $2e^2/h$ corresponding to a single atomic-sized conducting channel. Gently pulling apart the single-atom point contact may produce an aluminum SAT at the tip apex.

⁶²⁸ Y. Gohda, S. Watanabe, "Theoretical analysis of field emission from metallic nanostructures on Si(100) surfaces," J. Phys.: Condens. Matter 16(2004):4685-4696; http://www.iop.org/EJ/article/0953-8984/16/26/004/cm4_26_004.pdf?request-id=088a5fa8-43cd-40a4-8878-02a7f271d597.

⁶²⁹ E.S. Snow, D. Park, P.M. Campbell, "Single-atom point contact devices fabricated with an atomic force microscope," Appl. Phys. Lett. 69(8 July 1996):269.

Figure 5-28. Effective potential around single-atom protrusion on Al(100) surface for a (A) 14-atom SAT (top left)⁶³⁰ and a (B) 30-atom SAT (top right).⁶³¹ Other models used for DFT calculations⁶³² include (C) an $\text{Al}_{34}\text{Si}_{269}\text{H}_{168}$ cluster (bottom left) and (D) an Al_{304} cluster (bottom right).



⁶³⁰ Y. Gohda, S. Watanabe, "Total Energy Distribution of Field-Emitted Electrons from Al(100) Surface with Single-Atom Terminated Protrusion," *Phys. Rev. Lett.* 87(2001):177601.

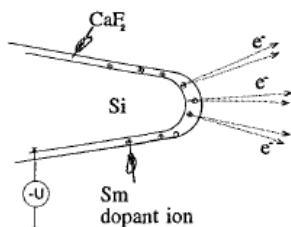
⁶³¹ Y. Gohda, S. Watanabe, "Theoretical analysis of field emission from atomically sharp aluminum tips," *Surf. Sci.* 516(20 September 2002):265-271; <http://202.127.1.11/surface%20science/516/516306.pdf>.

⁶³² Y. Gohda, S. Watanabe, "Theoretical analysis of field emission from metallic nanostructures on Si(100) surfaces," *J. Phys.: Condens. Matter* 16(2004):4685-4696; http://www.iop.org/EJ/article/0953-8984/16/26/004/cm4_26_004.pdf?request-id=088a5fa8-43cd-40a4-8878-02a7f271d597.

5.9.4 Metal-Atom Doped-Coating SATs

One group at the Institute of Spectroscopy (Russia) claims to have tentatively demonstrated electron emission through a single-atom source which is present as a dopant in a dielectric coating on a sharp semiconductor tip.⁶³³ In these experiments, high conductivity n-type single crystal Si whiskers were grown on one end of a Si rod with dimensions of 1 x 1 x 10 mm. As-grown whiskers were sharpened by wet etching (Vapor-Liquid-Solid growth technique), followed by repeated thermal oxidation with HF etching for oxide removal. Prepared tips were 100 μm in height with a curvature radius < 25 nm. Next, CaF_2 films were grown on the Si tips via molecular beam epitaxy (MBE) at 500-600 $^\circ\text{C}$ with a base pressure in the growth chamber of 0.5×10^{-11} Torr. CaF_2 containing samarium metal atoms in the necessary concentration was evaporated from a Knudsen cell,⁶³⁴ yielding a ~ 3 nm thick $\text{CaF}_2:\text{Sm}^{2+}$ coating with a concentration of Sm dopant ions in the coating of 0.2 mol. % (Figure 5-29). The field electron emission images produced using these tips suggest a possible experimental observation of a single-atom electron source due to the resonant tunneling of electrons through the energy states of a single Sm dopant ion embedded in the dielectric coating.

Figure 5-29. Illustrating the resonant tunneling process from Si tip through dopant Sm^{2+} ion in CaF_2 coating on the tip surface.⁶³⁵



However, this method seems unlikely to be useful as a single-atom tip for DMS because: (1) the position of the dopant metal atom relative to the curve of the coated tip is poorly controlled, (2) the dopant atom is an electrically charged ion, and (3) the dopant metal atom may be embedded at uncontrolled depths below the surface of the ~ 3 nm thick CaF_2 coating, which would render it useless for DMS work.

⁶³³ V.N. Konopsky, S.K. Sekatskii, V.S. Letokhov, "Single Atom Electron Emission from the Silicon Tip Coated by Calcium Fluoride with Samarium Dopant Ions," Journal de Physique IV Colloque C5, suppldment au Journal de Physique III, Volume 6, September 1996, pp. C5-125 - C5-128.

⁶³⁴ N.S. Sokolov, J.C. Alvarez, N.L. Yakovlev, "Fluoride layers and superlattices grown by MBE on Si(111): dynamic RHEED and Sm^{2+} photoluminescence studies," Appl. Surf. Sci. 60/61(1992):421-425.

⁶³⁵ V.N. Konopsky, S.K. Sekatskii, V.S. Letokhov, "Single Atom Electron Emission from the Silicon Tip Coated by Calcium Fluoride with Samarium Dopant Ions," Journal de Physique IV Colloque C5, suppldment au Journal de Physique III, Volume 6, September 1996, pp. C5-125 - C5-128.

6. Single-Atom Tip Systems

In this final Section, we review several proposals for making a complete single-atom tip system that is ready for use in a metrologically-driven AFM manipulation device, i.e., the molecular workstation. We start in [Section 6.1](#) with a general review of the physical structure of the qPlus sensor, the most popular alternative to the standard cantilever approach, as we believe it is most likely that this is the system that we'll be using for the workstation.

Next, we present what we currently believe to be the leading approaches (in terms of simplicity of manufacture and repeatable quality of the result) for incorporating a SAT into a qPlus sensor, including, in descending order of our current extremely tentative preference, the Iridium qPlus Tip System ([Section 6.2](#)), the Tungsten-Iridium qPlus Tip System ([Section 6.3](#)), the EBID/Field-Sharpens qPlus System ([Section 6.4](#)), and the MEMS-Based qPlus Tip System ([Section 6.5](#)). In most of these cases there are two or more alternative techniques to choose from, that involve different technical tradeoffs. Various combinations of these approaches are also readily imagined.

It is believed that the roadmap presented here and elsewhere in this report provides a basis for developing a specific experimental R&D program to develop an AFM-ready SAT tip system for the molecular workstation.

6.1 qPlus-Based AFM Tip System

One major practical challenge of DMS is the relocation of a single atomic site on a sample which may be several mm^2 in area – e.g., after abstracting an H atom from a passivated surface, we must revisit this same atomic lattice site to add, say, a methyl group, after moving the tip a significant distance or in some cases exchanging tips. This requires a viable methodology for relocating atomic sites on a macroscopic sample. Some existing techniques for tip registration, usually involving identification of surface landmarks, have been described at length elsewhere⁶³⁶ so we will not repeat that discussion here.

Assuming we use a qPlus sensor of some kind in the workstation design, the vibratory-sensing qPlus feature may be actively employed during a tip registration operation (i.e., looking for a known surface feature). The sensing feature may also be used during broad-area surface scans, as for example when mapping a presentation surface, a release surface, or a disposal surface, or when mapping a workpiece in progress. For the rest of the time, the qPlus resonator may be turned off and the sensor used only as a rigid tip that is moved around the workspace using dead

⁶³⁶ “Molecular Workstation Roadmap: Survey of Key Technologies Needed to Perform Positionally Controlled Diamondoid Mechanosynthesis using a Molecular Workstation,” V2.2, Nanofactory Corporation, 24 November 2009.

reckoning provided by the high-precision metrology system,⁶³⁷ to perform DMS operations. The qPlus system is thus expected to be used in two modes: active (during periodic tip registrations and during workpiece or surface scans) and passive (during DMS operations).

As reviewed by Giessibl,⁶³⁸ the inventor of the qPlus sensor, the first atomic force microscope utilized a cantilever that was built by hand in the laboratory from gold foil and a small piece of diamond acting as a tip.⁶³⁹ Soon after, MEMS (microelectromechanical systems) capabilities offered by the semiconductor industry were used to mass-fabricate cantilevers from silicon. Initially, Si-based cantilevers were built from SiO₂ and Si₃N₄.⁶⁴⁰ Later, cantilevers with integrated tips were machined from silicon-on-insulator wafers.⁶⁴¹ The most common cantilevers in use today are built from all-silicon with integrated tips pointing in a (001) crystal direction and go back to Wolter et al.,⁶⁴² followed by a number of companies that offer Si cantilevers with integrated sharp tips on wafers, including a few hundred cantilevers each. By contrast, the qPlus sensor still requires manual assembly – even two decades after the introduction of AFM, manual assembly of its key component is still practiced.

As Giessibl⁶⁴³ explains, the qPlus sensor is based on the quartz tuning fork, a wonderful invention that allows the very-low-cost manufacture of wristwatches that can keep time much more precisely than mechanical watches that are priced orders of magnitude higher.⁶⁴⁴ Quartz tuning forks are etched from single crystal quartz⁶⁴⁵ that is oriented in an X+5° orientation.⁶⁴⁶ This

⁶³⁷ “Molecular Workstation Roadmap: Survey of Key Technologies Needed to Perform Positionally Controlled Diamondoid Mechanosynthesis using a Molecular Workstation,” V2.2, Nanofactory Corporation, 24 November 2009.

⁶³⁸ Franz J. Giessibl, “Principles and Applications of the qPlus Sensor,” in S. Morita et al. (eds.), *Nanocontact Atomic Force Microscopy*, Springer-Verlag Berlin Heidelberg, 2009, pp. 121-142.

⁶³⁹ G. Binnig, C.F. Quate, Ch. Gerber, “Atomic Force Microscopy,” *Phys. Rev. Lett.* 56(3 March 1986):930-933.

⁶⁴⁰ T.R. Albrecht, S. Akamine, T.E. Carver, C.F. Quate, “Microfabrication of cantilever styli for the atomic force microscope,” *J. Vac. Sci. Technol. A* 8(1990):3386-3396.

⁶⁴¹ S. Akamine, R.C. Barrett, C.F. Quate, “Improved atomic force microscope images using microcantilevers with sharp tips,” *Appl. Phys. Lett.* 57(1990):316-318.

⁶⁴² O. Wolter, Th. Bayer, J. Greschner, “Micromachined silicon sensors for scanning force microscopy,” *J. Vac. Sci. Technol. B* 9(1991):1353-1357.

⁶⁴³ Franz J. Giessibl, “Principles and Applications of the qPlus Sensor,” in S. Morita et al. (eds.), *Nanocontact Atomic Force Microscopy*, Springer-Verlag Berlin Heidelberg, 2009, pp. 121-142.

⁶⁴⁴ E. Momosaki, *Proc. 1997 IEEE Intl. Freq. Contr. Symp.* 56(1997):552.

⁶⁴⁵ When a crystal of quartz is properly cut and mounted, it can be made to distort in an electric field by applying a voltage to an electrode near or on the crystal. This property is known as piezoelectricity. When the field is removed, the quartz will generate an electric field as it returns to its previous shape, and this can generate a voltage. The result is that a quartz crystal behaves like a circuit composed of an inductor, capacitor and resistor, with a precise resonant frequency. The crystal oscillator circuit sustains oscillation

orientation ensures that the frequency variation with temperature is almost zero at 28 °C – the typical temperature of a watch mounted on a wrist. (Note: We should investigate the possibility of using different cuts, ones that minimize frequency variation with temperature at 80 K (LN2) or at 5-20 K (LHe), the temperatures at which the molecular workstation is mostly likely going to be operating.) The piezoelectricity of quartz allows for a simple transformation of the mechanical oscillation of the quartz fork to an electrical signal. Frequency stability is excellent and power consumption is very low (ideal for watch applications). Quartz oscillators can be manufactured lithographically: the reproducible precision etching of a quartz wafer into an array of tuning forks is well-known.⁶⁴⁷ Processes exist for negative photoresist photolithography in an additive process and for positive photoresist photolithography in a subtractive process, to etch an array of quartz tuning forks.

Figure 6-1A shows a quartz tuning fork as used in Swatch watches, that has not yet been trimmed. The prongs are rectangular and are entirely surrounded by gold electrodes – two vertical and two horizontal layers of gold (**Figure 6-1B**). **Figure 6-1C** shows a similar tuning fork in which the metal case of the device has been opened and one can see the transparent quartz fork as well as the gold electrodes. The gold electrodes have been removed partially at the ends of the prongs to adjust the eigenfrequency to exactly 2^{15} Hz (32.768 kHz). **Figure 6-1D** is a mechanical analogue to the tuning fork. When both prongs have exactly the same mass and stiffness, an oscillation mode evolves in which both prongs oscillate opposite to each other with extremely small losses and thus giving a sensor with a very high quality or Q value.⁶⁴⁸

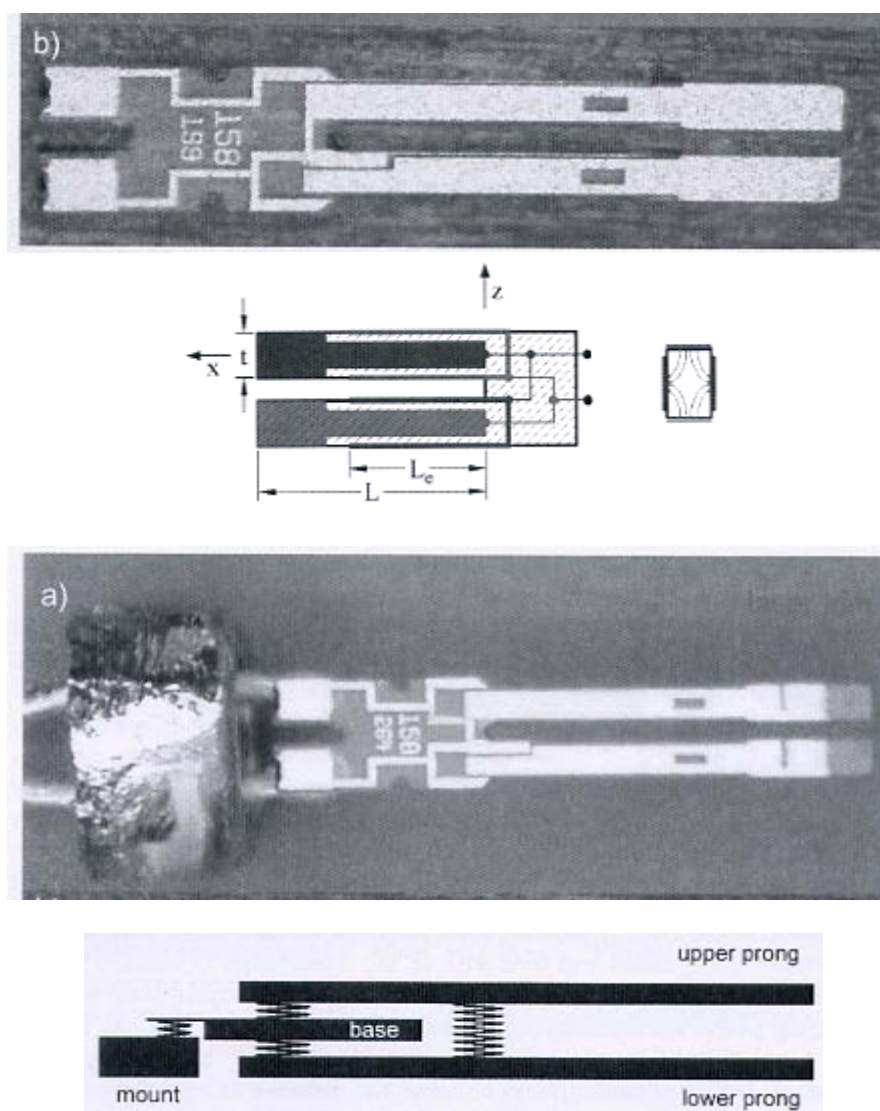
by taking a voltage signal from the quartz resonator, amplifying it, and feeding it back to the resonator. The rate of expansion and contraction of the quartz is the resonant frequency, and is determined by the cut and size of the crystal. When the energy of the generated output frequencies matches the losses in the circuit, an oscillation can be sustained. An oscillator crystal has two electrically conductive plates, with a slice or tuning fork of quartz crystal sandwiched between them. During startup, the circuit around the crystal applies a random noise AC signal to it, and purely by chance, a tiny fraction of the noise will be at the resonant frequency of the crystal. The crystal will therefore start oscillating in synchrony with that signal. As the oscillator amplifies the signals coming out of the crystal, the signals in the crystal's frequency band will become stronger, eventually dominating the output of the oscillator. The narrow resonance band of the quartz crystal filters out all the unwanted frequencies. The output frequency of a quartz oscillator can be either the fundamental resonance or a multiple of the resonance, called an overtone frequency.

⁶⁴⁶ F.L. Walls, in Eduard A. Gerber, Arthur Ballato, eds., *Precision Frequency Control*, Academic Press, Orlando FL, 1985, pp. 276-279.

⁶⁴⁷ Sungkyu Lee, "Photolithography and Selective Etching of an Array of Quartz Tuning Fork Resonators with Improved Impact Resistance Characteristics," *Jpn. J. Appl. Phys.* 40(2001):5164-5167.

⁶⁴⁸ Franz J. Giessibl, "Principles and Applications of the qPlus Sensor," in S. Morita et al. (eds.), *Nanocontact Atomic Force Microscopy*, Springer-Verlag Berlin Heidelberg, 2009, pp. 121-142.


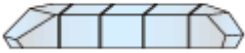
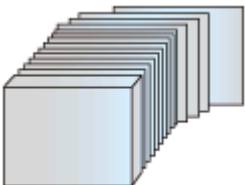
Figure 6-1. Quartz tuning forks,⁶⁴⁹ top to bottom: (A) Untrimmed tuning fork as used in watches, as taken out of a wafer. The trimming procedure has not been done on this fork as can be seen by the undamaged gold plating at the end of the fork at far right. (B) Electrode configuration of the quartz tuning fork. (C) A tuning fork with an opened metal case; the gold plating has been partially removed at far right to trim the mass of the prongs to produce an eigenfrequency of exactly 32.768 Hz. (D) Mechanical analogue of the tuning fork. In principle, the fork is a quite complex mechanical system with many oscillation modes and eigenfrequencies. When both prongs are symmetric, the antiparallel mode where one prong oscillates opposite to the other one has a very high Q value.



⁶⁴⁹ Franz J. Giessibl, "Principles and Applications of the qPlus Sensor," in S. Morita et al. (eds.), Nanocontact Atomic Force Microscopy, Springer-Verlag Berlin Heidelberg, 2009, pp. 121-142.

How are these tuning forks manufactured in the first place? The manufacturing of a quartz tuning fork begins with growing a synthetic quartz crystal using a hydrothermal synthesis process.⁶⁵⁰ Hydrothermal synthesis can be defined as a method of synthesis of single crystals which depends on the solubility of minerals in hot water under high pressure. The crystal growth is performed in an apparatus consisting of a steel pressure vessel called autoclave, in which a nutrient is supplied along with water. A gradient of temperature is maintained at the opposite ends of the growth chamber so that the hotter end dissolves the nutrient and the cooler end causes seeds to take additional growth. The further steps in the process used to manufacture tuning-fork crystal units from a synthetic crystal are illustrated in **Table 6-1**. Over 600 quartz tuning fork manufacturers from around the world are listed in **Appendix A**.⁶⁵¹

Table 6-1. How a synthetic quartz crystal becomes a tuning-fork crystal unit.⁶⁵²




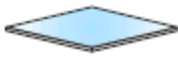


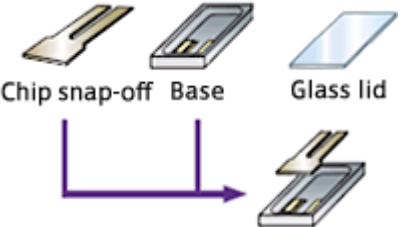
Image	Title of Step	Description of Step
	Grow monocrystalline quartz crystal using hydrothermal synthesis ⁶⁵³	Grow a synthetic monocrystalline quartz crystal using the hydrothermal synthesis process, producing a crystal that is about 19 cm long and weighs about 127 grams.
	1. From rough synthetic crystal to block cutting	Synthetic crystals grown for tuning-fork crystal units are cut into blocks.
	2. Wafer slicing	The blocks are sliced into thin wafers.

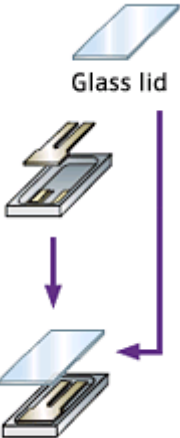

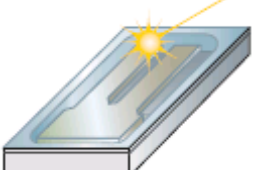

⁶⁵⁰ “Hydrothermal synthesis,” http://en.wikipedia.org/wiki/Hydrothermal_synthesis.

⁶⁵¹ “Crystal Oscillator Directory”; http://homepage.ntlworld.com/jan.ooijman/crystal_oscillator_directory.htm.

⁶⁵² “Factory Tour: Process for manufacturing tuning-fork crystal units,” Epsom Toyocom, 2010; <http://www.epsontoyocom.co.jp/english/special/crystal/enjoy/plant/timing.html>.

⁶⁵³ “Hydrothermal synthesis,” http://en.wikipedia.org/wiki/Hydrothermal_synthesis.

 <p>1. Lapping Surface hills and valleys are removed with a grinding fluid.</p>  <p>2. Etching The wafer surface is etched to remove roughness.</p>  <p>3. Polishing The wafer is polished to a mirror finish with an abrasive compound.</p>	3. Wafer polishing	The quartz crystal wafers are polished.
 <p>1. Sputtering The wafer is coated with gold and chrome.</p>  <p>2. Contour etching The gold and chrome is removed.</p>  <p>3. Electrode processing Electrodes are added and circuits are patterned by a photolithographic process.</p>	4. Photoetching	A photolithographic process is used to form the tuning-fork shape.
 <p>Chip snap-off Base Glass lid</p>	5. Mounting	The crystal chip is connected to a base with a conductive adhesive.

 <p>Glass lid</p>	6. Lid sealing	The low-melting-point glass is melted to bond the glass lid to the base.
	7. Vacuum sealing	A ball of gold and germanium is melted to seal the device in a vacuum state.
	8. Frequency adjusting	The frequency of the crystal chip is fine-tuned by shaving off part of the electrodes on the tips of the crystal chip with a laser.
	9. Marking	The products are marked with the designated number.
	10. Completion	The process from rough synthetic crystal to finished tuning-fork crystal unit takes about one month to complete.

Frequency adjustment is a vital point in the tuning-fork crystal unit manufacturing process in terms of quality control,⁶⁵⁴ but these adjustments are not made until the final step of the manufacturing process, after the crystal has been packaged and is ready for marking with a product number. This is accomplished via the glass lid. The frequency of the crystal can be fine-tuned by using a laser to shave off bits of the electrodes on the tips of the crystal chip through the glass. The ability to precisely adjust the frequency of a crystal chip after it has been packed in a vacuum state makes it possible to mass-produce crystal devices of higher accuracy.

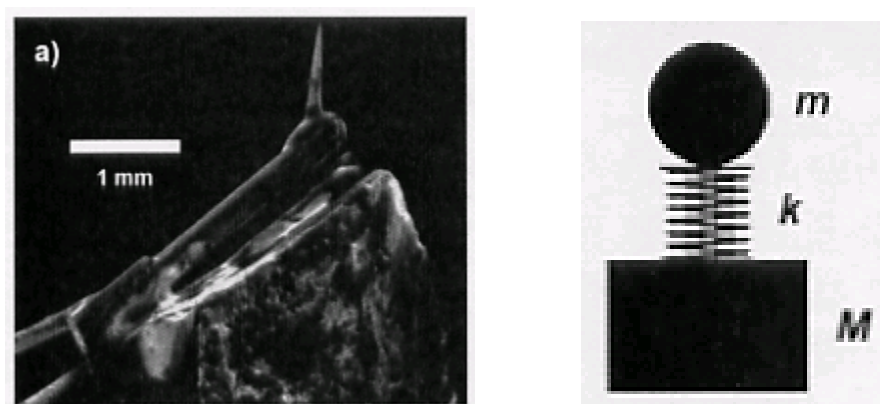
Quartz tuning forks were applied to SPMs quite early because of their useful properties. However, the high symmetry of tuning forks has to be given up when a probe is attached to one

⁶⁵⁴ “Factory Tour: Process for manufacturing tuning-fork crystal units,” Epsom Toyocom, 2010; <http://www.epsontoyocom.co.jp/english/special/crystal/enjoy/plant/timing.html>.

of the prongs as is required for using the fork as a sensor. Even when the mass of a tip attached to one of the prongs is compensated by attaching a counterweight of similar mass to the other prong, the asymmetry that affects the prong that interacts with a surface cannot be lifted easily. Giessibl was the first to attach one prong to a heavy substrate so as to produce a quartz cantilever instead of a quartz tuning fork, allowing the use even of heavy tips or in situations involving a strong interaction with a surface bond without reducing the Q factor – an arrangement called the qPlus sensor configuration, as opposed to a tuning fork configuration.⁶⁵⁵

In the first-generation qPlus sensor device circa 1998 (Figure 6-2), used for high speed imaging in ambient conditions,⁶⁵⁶ the electrical connections of the fork were wired to an instrumentation amplifier with a high gain. The charges that are collected on the electrodes when the sensor is deflected cause a voltage change in the input of an instrumentation amplifier, making the device self-sensing. In this first prototype of a qPlus sensor, the free prong of the tuning fork is glued to a piece of Pyrex glass. The tip is an etched tungsten wire with a wire diameter of ~200 microns. The mechanical analogue to the qPlus sensor is much simpler than in the case of the tuning fork (Figure 6-1D) because only the free prong is allowed to oscillate. The mass of the mount M_{mount} should be large compared to the effective mass M_{fork} of the fork, where $M_{\text{mount}} > 1000 M_{\text{fork}}$ is a reasonable value.⁶⁵⁷

Figure 6-2. A quartz tuning fork is glued onto a heavy substrate, turning the tuning fork into a qPlus sensor; the mechanical analogue to the qPlus sensor is shown at right.⁶⁵⁸



⁶⁵⁵ F.J. Giessibl, German Patent p. DE 196 33 546 (1996); F.J. Giessibl, US Patent No. 6,240,771 (2001).

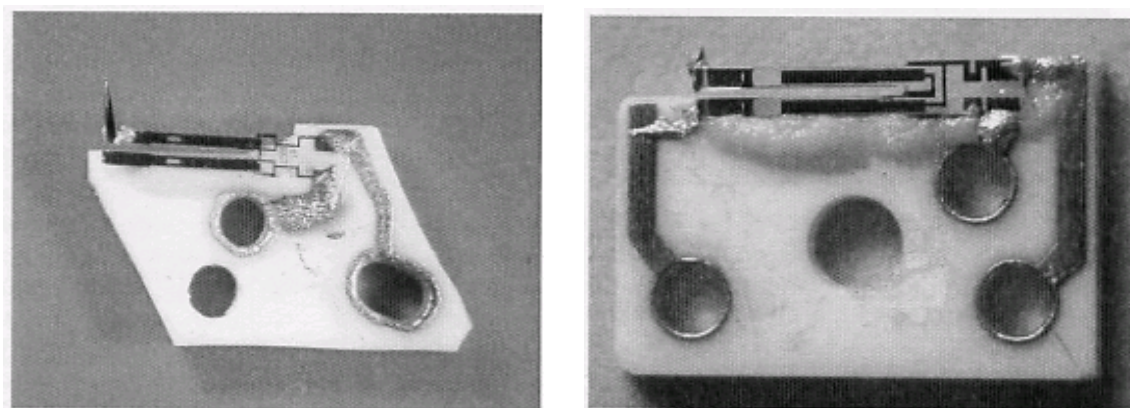
⁶⁵⁶ F.J. Giessibl, "High-Speed Force Sensor for Force Microscopy and Profilometry Utilizing a Quartz Tuning Fork", *Applied Physics Letters* 73(1998):3956-3958.

⁶⁵⁷ Franz J. Giessibl, "Principles and Applications of the qPlus Sensor," in S. Morita et al. (eds.), *Nanocontact Atomic Force Microscopy*, Springer-Verlag Berlin Heidelberg, 2009, pp. 121-142.

⁶⁵⁸ Franz J. Giessibl, "Principles and Applications of the qPlus Sensor," in S. Morita et al. (eds.), *Nanocontact Atomic Force Microscopy*, Springer-Verlag Berlin Heidelberg, 2009, pp. 121-142.

In the second-generation qPlus sensor device circa mid-2000s (**Figure 6-3A**), the manufacture of the sensor was simplified by designing a ceramic substrate made of alumina with vias and conductive leads as well as mounting holes. Substrates of this kind are used in hybrid electronics design and can be ordered as custom designs.⁶⁵⁹ To obtain a sensor with a high Q-value, it is important to create a very stiff bond between the fork and the substrate. This can be achieved by using a very thin layer of glue and by taking care that the area where the free prong meets the base part of the fork remains free of glue. This sensor design can also be used to build a lateral force sensor by rotating the tip by 90° and oscillating the tip parallel to the surface.⁶⁶⁰ In the third-generation qPlus sensor device circa 2009 (**Figure 6-3B**), the tip is connected via a dedicated terminal. This allows application of high voltages for tip annealing or field emission without affecting the deflection sensor's amplifiers. Both electrodes of the fork are fed into a current-to-voltage amplifier and the difference between the two signals has much less interference noise than a single deflection electrode.⁶⁶¹

Figure 6-3. (A) Left: Second-generation qPlus sensor. The sensor consists of three parts: the tuning fork, a ceramic substrate, and the tip. Electrical connections are made using conductive epoxy.⁶⁶² (B) Right: Third-generation qPlus sensor. A different ceramic substrate is used that allows the tip potential to be isolated from the electrodes of the sensor. The tip is contacted with a squeezed gold wire (diameter 10 microns). The Q-value still remains on the order of a few thousand. The two electrodes of the tuning fork are fed into a single amplifier.⁶⁶³



⁶⁵⁹ CeramTec, CeramTec AG, Marktreidwitz, Germany (2008).

⁶⁶⁰ EpoTek, Norwood, MA 02062-9106, USA (2008).

⁶⁶¹ Franz J. Giessibl, Markus Herz, Jochen Mannhart, "Friction traced to the single atom," PNAS 99(2002):12006-12010.

⁶⁶² M. Smolka, Rasterkraftmikroskopie, Diploma Thesis, Universitaet Regensburg, Germany, 2008.

⁶⁶³ Franz J. Giessibl, "Principles and Applications of the qPlus Sensor," in S. Morita et al. (eds.), Nanocontact Atomic Force Microscopy, Springer-Verlag Berlin Heidelberg, 2009, pp. 121-142.

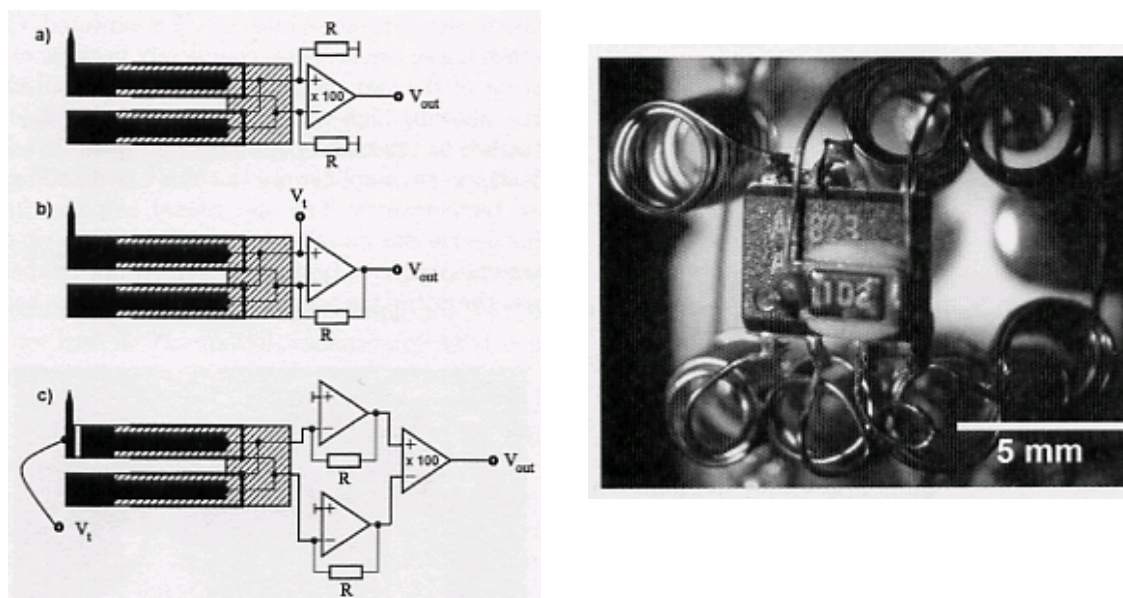
The qPlus sensor needs only one more component to produce an electrical deflection signal: a current-to-voltage converter that converts the flowing charges generated by the oscillating prongs into a voltage. Because cable capacity has an adverse effect on the noise performance of the deflection measurement, the amplifier should be located as close as possible to the sensor. For vacuum and low temperature applications, it is challenging to design an amplifier that is compatible with these demanding environments.

Figure 6-4 shows the evolution of amplifiers during the three generations of qPlus sensors created by Giessibl.⁶⁶⁴ An instrumentation amplifier (Figure 6-4a) was used in the first-generation qPlus experiments in ambient environments. Here, when the qPlus sensor is deflected, charges accumulate on the electrodes which cause a voltage increase in the capacitor (qPlus electrodes plus cable capacitance) and the voltage differential is measured with the instrumentation amplifier. To define the input potentials of the instrumentation amplifier and to avoid long-term charging effects, the inputs need to be connected to ground with a very large resistivity (at least 100 MΩ). The second-generation type (Figure 6-4b) is a traditional transimpedance amplifier as used in current amplifiers of STMs. To obtain a high bandwidth, it is important to use a resistor that has little stray capacitance – surface-mount-device (SMD) resistor work well here. The case of the amplifier should be vacuum compatible – e.g., the amplifier should be available in a metallic or ceramic case, though Giessibl has used plastic cases in UHV without apparent additional outgassing or adverse effects on vacuum pressure. Proper heat sinking is important if the amplifier operates in a vacuum, especially if small cases are used, and operating the amplifiers close to the lower threshold of operating voltage minimizes heating due to the electrical power consumed in the amplifier. The third-generation preamplifier type (Figure 6-4c) uses two channels for the deflection measurement. Thus the signal becomes twice as large and the signal/noise ratio rises by $2^{1/2}$; correlated noise such as interference noise cancels completely. Also, the tip bias is completely free, allowing high-voltage tip treatment or field emission while the sensor is attached to the microscope.⁶⁶⁵ Figure 6-4d shows an amplifier for the most demanding environments: vacuum and low temperatures.

⁶⁶⁴ Franz J. Giessibl, “Principles and Applications of the qPlus Sensor,” in S. Morita et al. (eds.), *Nanocontact Atomic Force Microscopy*, Springer-Verlag Berlin Heidelberg, 2009, pp. 121-142.

⁶⁶⁵ Franz J. Giessibl, Markus Herz, Jochen Mannhart, “Friction traced to the single atom,” *PNAS* 99(2002):12006-12010.

Figure 6-4. At left: Three types of preamplifiers for qPlus sensor. (a) First generation, and instrumentation amplifier with two resistors. (b) Second generation, a current-to-voltage converter or transimpedance amplifier, similar to the ones used in STM current amplification. (c) Third generation, a dual current-to-voltage converter with an instrumentation amplifier. Resistor values are all $\sim 100\text{ M}\Omega$, with a small and low capacity SMD design.⁶⁶⁶ At right: (d) A low-temperature preamplifier⁶⁶⁷ with an attached heating resistor.⁶⁶⁸



Heyde et al.⁶⁶⁹ use a slightly different version of the qPlus sensor in their LHe-temperature apparatus (Figure 6-5A). For their device,⁶⁷⁰ they use a quartz tuning fork upon which is mounted a cut $\text{Pt}_{90}/\text{Ir}_{10}$ wire that serves as an NC-AFM/STM tip. Tip preparation is performed in

⁶⁶⁶ Franz J. Giessibl, "Principles and Applications of the qPlus Sensor," in S. Morita et al. (eds.), *Nanocontact Atomic Force Microscopy*, Springer-Verlag Berlin Heidelberg, 2009, pp. 121-142.

⁶⁶⁷ Analog Devices, One Technology Way, P.O. Box 9106, Norwood, MA 02062-9106, USA, 2008.

⁶⁶⁸ Franz J. Giessibl, "Principles and Applications of the qPlus Sensor," in S. Morita et al. (eds.), *Nanocontact Atomic Force Microscopy*, Springer-Verlag Berlin Heidelberg, 2009, pp. 121-142.

⁶⁶⁹ M. Heyde, G.H. Simon, T. Konig, "Study of Thin Oxide Films with NC-AFM: Atomically Resolved Imaging and Beyond," in S. Morita et al. (eds.), *Nanocontact Atomic Force Microscopy*, Springer-Verlag Berlin Heidelberg, 2009, pp. 143-167.

⁶⁷⁰ H.-P. Rust, M. Heyde, H.-J. Freund, "Signal electronics for an atomic force microscope equipped with a double quartz tuning fork sensor," *Rev. Sci. Instrum.* 77(2006):043710. M. Heyde, G.H. Simon, H.-P. Rust, H.-J. Freund, "Probing Adsorption Sites on Thin Oxide Films by Dynamic Force Microscopy," *Appl. Phys. Lett.* 89(2006):263107.

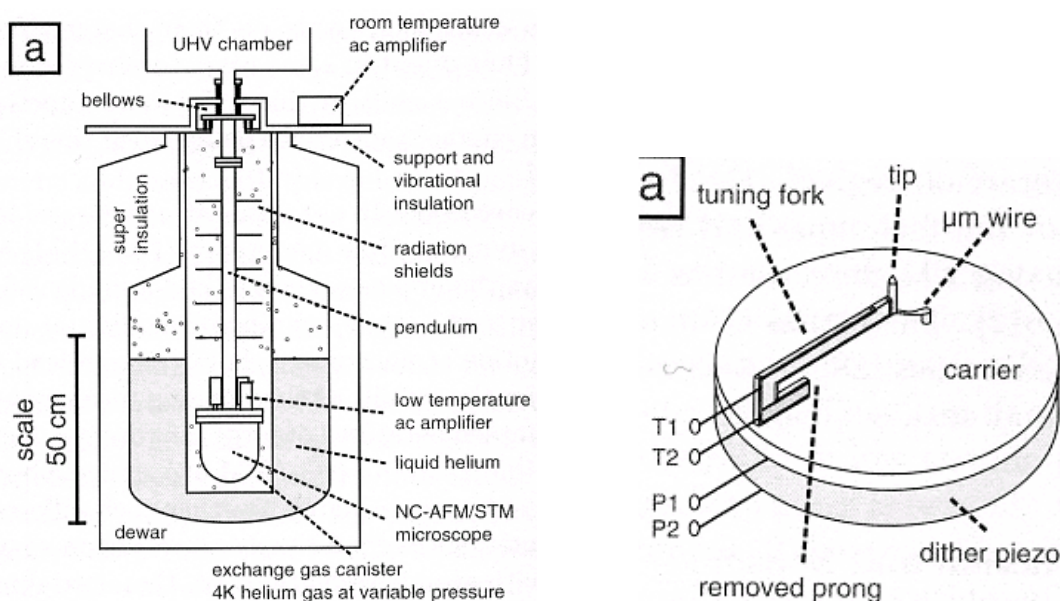
situ by field emission and/or by dipping the tip into and pulling necks from the sample surface, which removes residual oxide contaminants and produces adequate tip configurations for conventional SPM work. The tip wire has a diameter of 250 μm and is electrically connected to the signal electronics through a thin Pt/Rh wire with a diameter of 50 μm . Both tip and contact wire are electrically insulated from the tuning fork and its electrodes. The frequency shift is directly recorded via the tuning fork electrodes while the tunneling current is taken independently from the contact wire of the tip (Figure 6-5B). Excitation of the tuning fork along the tip axis is done with a separate slice of piezo crystal (the “dither piezo”) on top of the z-piezo. The contacting prong of the tuning fork that is attached to the ceramic carrier plate has been cut short, increasing the spring constant from the more typical 1,800 N/m value for an intact fork up to a much larger $k \sim 22,000$ N/m value. This spring constant is significantly higher than typical interatomic force constants and thus prevents a sudden “jump-to-contact” of the cantilever even at very small tip-sample distances and oscillation amplitudes (typically 100-2000 pm for their work). Using this apparatus, the authors have obtained atomic resolution of metal oxide surfaces.

The IBM group that includes Andreas Heinrich at IBM Almaden has used a low-temperature NC-AFM/STM apparatus with a qPlus sensor with a spring constant $k = 1800$ N/m and using a sub-Angstrom oscillation amplitude (25-30 pm) to measure the vertical and lateral forces exerted by the probe tip on an adsorbed cobalt metal atom on a Pt(111) metal surface before and during a controlled manipulation process.⁶⁷¹ (Breaking a Co-Pt bond apparently requires ~ 1.4 nN, vs. ~ 4 nN for an Ir-Pt point contact bond.⁶⁷²) The stability and spatial resolution of the instrument is on the order of ~ 1 pm. In this work, a “metallic iridium” tip is mounted on one leg of a cantilever made from a quartz tuning fork, while the other leg is fixed on a three-axis piezoelectric scanner. However, this metallic iridium tip is atomically imprecise and might not be a stable SAT: “Iridium was chosen as the tip material based on its hardness....The tip was fabricated by mechanically fragmenting an Ir wire and selecting a small sharp fragment. The iridium tip was initially cleaned in vacuum by locally heating the apex at an applied voltage of ~ 600 V and by gently touching the tip to the sample surface. Thus, the actual chemical composition of the tip apex is unknown and might contain metal atoms from the sample metal.”

⁶⁷¹ Markus Ternes, Christopher P. Lutz, Andreas J. Heinrich, “Atomic Manipulation on Metal Surfaces,” in S. Morita et al. (eds.), *Nanocontact Atomic Force Microscopy*, Springer-Verlag Berlin Heidelberg, 2009, pp. 191-215.

⁶⁷² Markus Ternes, Christopher P. Lutz, Andreas J. Heinrich, “Atomic Manipulation on Metal Surfaces,” in S. Morita et al. (eds.), *Nanocontact Atomic Force Microscopy*, Springer-Verlag Berlin Heidelberg, 2009, pp. 191-215. S.R. Bahn, K.W. Jacobsen, “Chain Formation of Metal Atoms,” *Phys. Rev. Lett.* 87(2001):266101.

Figure 6-5. (A) Left: The LHe experimental setup: An evacuated pendulum of about 1 meter length suspended with steel bellows from the main UHV chamber is the central design feature providing mechanical vibration insulation; at its end, the NC-AFM/STM head is mounted in a UHV environment; the pendulum is placed inside an exchange gas canister filled with helium gas, surrounded by a liquid helium bath; the helium gas chamber prevents acoustic noise from perturbing the microscope which permitting thermal coupling to the liquid cryogen (He or N₂); the low temperature AC amplifier is situated near the NC-AFM/STM head while the room temperature AC amplifier is mounted outside the dewar. **(B) Right:** The sensor setup for NC-AFM/STM low-temperature UHV operation: Dither piezo with connections P1 & P2 for mechanical excitation in the z-direction along the tip axis; the quartz tuning fork is attached to a ceramic carrier plate, with electrically separated signal wires for force (T1 & T2 contacts of the tuning fork) and current detection (μm wire); the same tip senses both signals.⁶⁷³



6.2 Iridium qPlus Tip System

We need single-atom tips for the molecular workstation bootstrap system. Ideally, these single-atom tips would be manufactured directly onto a qPlus AFM sensor apparatus, forming a single-unit device (via unitary fabrication) that can be inserted, as is, into the workstation metrology system. This would allow the tip system to be developed, fabricated, and tested as an effort entirely separate from the metrology system development effort, and also may allow us to build

⁶⁷³ M. Heyde, G.H. Simon, T. König, “Study of Thin Oxide Films with NC-AFM: Atomically Resolved Imaging and Beyond,” in S. Morita et al. (eds.), *Nanocontact Atomic Force Microscopy*, Springer-Verlag Berlin Heidelberg, 2009, pp. 143-167.

fairly uniform qPlus SAT systems in a repeatable manner (an improvement over existing one-off fabrication techniques, though not quite as good as mass-production). Two methods for producing SATs, known as field-assisted tip sharpening ([Section 3.10](#)) and oxygen-induced sharpening ([Section 3.11](#)), have been available for several decades but produce inconsistent tips that are relatively difficult to remediate in situ if the tip becomes damaged during use.

6.2.1 Brief EBID Primer

The approach proposed in this section would employ FIB (focused ion beam induced deposition) aka. ion beam-induced deposition (IBID), or FEB (focused electron beam) aka. electron-beam-induced deposition (EBID) processes ([Figure 6-6](#)) to achieve unitary fabrication of SAT qPlus tip systems. Generally in these processes, a precursor gas is “cracked” by the energy provided from a focused beam of electrons or ions, causing a localized deposition of some heavy element or metal atom. (By switching between a deposition gas and an etching gas ([Figure 6-6B](#)), one can also use the technique as an attach-and-release tool to/from a nanomanipulator or sensor.) The proposed method starts with a (macroscale) quartz tuning fork ([Section 6.1](#)), ideally still residing on a lithographically-produced wafer ([Table 6-1](#)) or, alternatively, acquired from a wristwatch ([Figure 6-1A](#)). The fork is then placed in a vacuum chamber and 4 fabrication steps are performed, as described in the following three subsections. The result would be a finished EBID-built qPlus quartz tuning-fork-mounted pure iridium SAT tip, ready to go into the molecular workstation metrology apparatus. It is claimed⁶⁷⁴ that the method relied upon here may also be workable using the alternative noble metals Pt, Pd and Rh.⁶⁷⁵

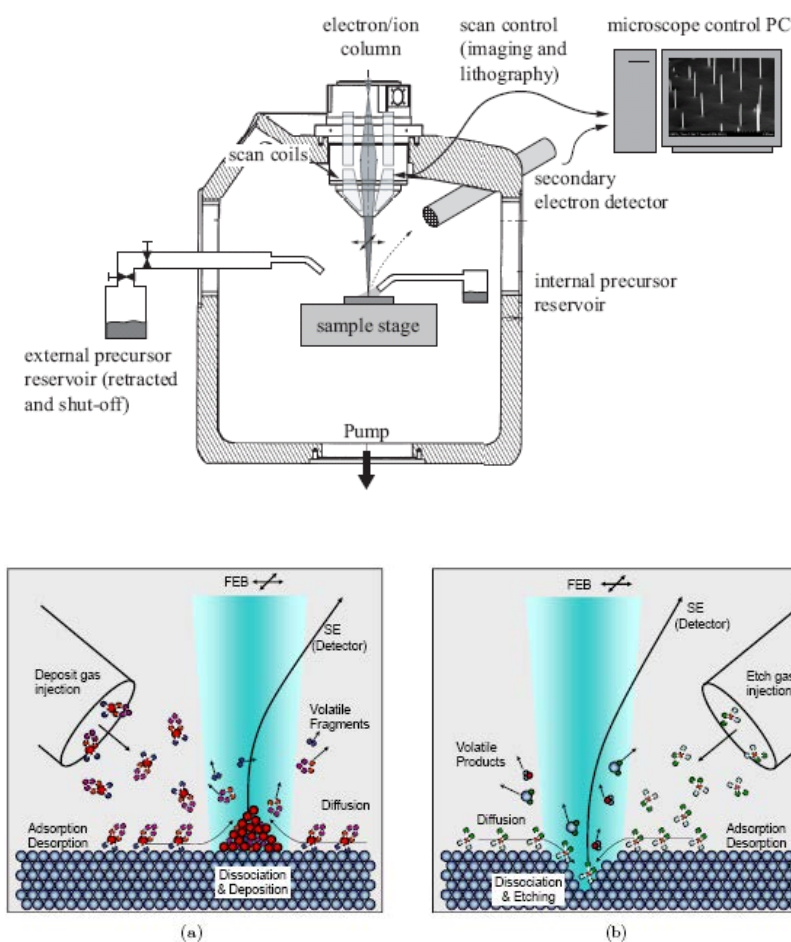
In the EBID process, a gas precursor adsorbs to the surface and is decomposed into volatile and nonvolatile components by electron bombardment. Ideally, the nonvolatile component remains “deposited” on the substrate, while the volatile byproducts are desorbed from the surface and pumped from the vacuum chamber. EBID was initially observed in the context of carbon contamination or “staining” during electron microscopy as a result of residual carbonaceous gas species.⁶⁷⁶

⁶⁷⁴ Hong-Shi Kuo, Ing-shouh Hwang, Tien T. Tsong, Tsu-Yi Fu, “Atomically Sharp Iridium Tip,” IPC8 Class: AB21G100FI, USPC Class: 428600, 2009; <http://www.faqs.org/patents/app/20090110951>.

⁶⁷⁵ Note that iridium, like the other platinum metals, does not (when solid) react with carbon or graphite, but unlike platinum, palladium or rhodium, it is unaffected by molten tin, lead, copper or most base metals and can be heated unchanged in contact with such refractory metals as tungsten, molybdenum, tantalum, and zirconium.

⁶⁷⁶ K.L. Klein, S.J. Randolph, J.D. Fowlkes, L.F. Allard, H.M. Meyer III, M.L. Simpson, P.D. Rack, “Single-crystal nanowires grown via electron-beam-induced deposition,” *Nanotechnology* 19(27 August 2008):345705.

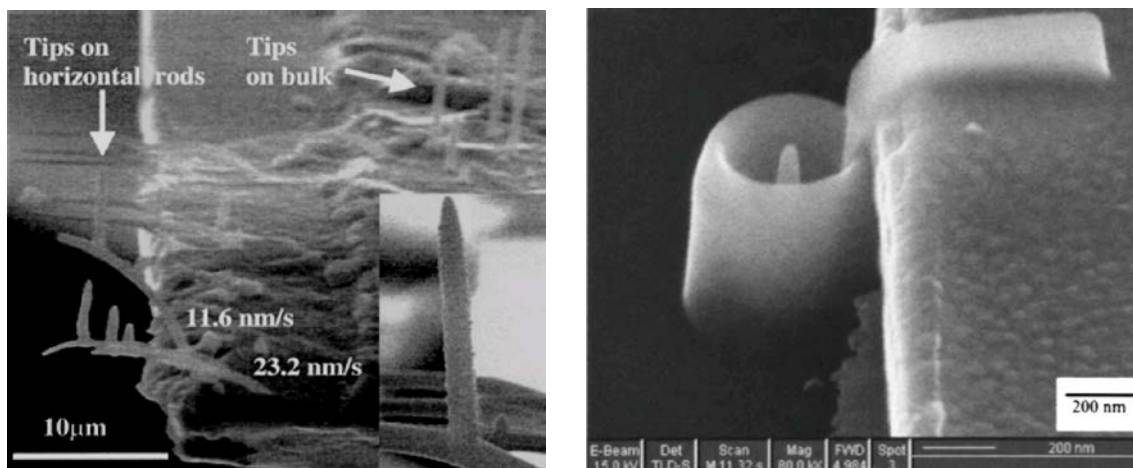
Figure 6-6. (A) Above: Schematics of FEB and FIB nanofabrication systems; precursor supply with external and internal precursor reservoirs are shown; the computer monitor shows FEB deposited pillars in tilt view. (B) Below: (a) Principle of FEB induced deposition: Molecules adsorb at the surface of the solid substrate and are dissociated under electron impact; volatile fragments are pumped away and a deposit grows coaxially to the beam; here, molecules are injected by a tube nozzle-based gas injection system. (b) Principle of FEB induced etching: The surface adsorbed molecules dissociate under electron impact into reactive species and form volatile compounds with the substrate material.⁶⁷⁷



⁶⁷⁷ Ivo Utke, Patrik Hoffmann, John Melngailis, "Gas-assisted focused electron beam and ion beam processing and fabrication," J. Vac. Sci. Technol. B 26(July 2008):1197-1276.

Electron-beam-induced deposition (EBID),⁶⁷⁸ is capable of synthesizing complex three-dimensional structures (Figure 6-7) and has recently realized 1 nm resolution (Figure 6-8)⁶⁷⁹ with measurements of electrical current used to monitor the EBID deposit height (Figure 6-9). Beams of electrons and ions are now fairly routinely focused to dimensions in the nanometer range.* Since the beams can be used to locally alter material at the point where they are incident on a surface, they represent direct nanofabrication tools.⁶⁸⁰

Figure 6-7. Left: Electron micrographs of three-dimensional copper nanostructures. These structures consisted of a vertical fiber deposited on the flanks of a horizontal fiber.⁶⁸¹
Right: An electron micrograph of a completed field emission (FE) device fully fabricated by EBID.⁶⁸²



⁶⁷⁸ Ivo Utke, Patrik Hoffmann, John Melngailis, "Gas-assisted focused electron beam and ion beam processing and fabrication," J. Vac. Sci. Technol. B 26(July 2008):1197-1276. S.J. Randolph, J.D. Fowlkes, P.D. Rack, "Focused, Nanoscale Electron-Beam-Induced Deposition and Etching," Critical Reviews in Solid State and Materials Sciences 31(September 2006):55-89; <http://www.informaworld.com/smpp/section?content=a768444964&fulltext=713240928>.

⁶⁷⁹ Willem F. van Dorp, Bob van Someren, Cornelis W. Hagen, Pieter Kruit, "Approaching the Resolution Limit of Nanometer-Scale Electron Beam-Induced Deposition," Nano Lett. 5(July 2005):1303-1307.

⁶⁸⁰ Ivo Utke, Patrik Hoffmann, John Melngailis, "Gas-assisted focused electron beam and ion beam processing and fabrication," J. Vac. Sci. Technol. B 26(July 2008):1197-1276.

⁶⁸¹ I. Utke, A. Luisier, P. Hoffmann, D. Laub, P.A. Buffat, "Focused-electron-beam-induced deposition of freestanding three-dimensional nanostructures of pure coalesced copper crystals," Applied Physics Letters 81(2002):3245-3247; <http://dx.doi.org/10.1063/1.1517180>.

⁶⁸² Katsuhisa Murakami, Mikio Takai, "Characteristics of nano electron source fabricated using beam assisted process," Journal of Vacuum Science & Technology B 22(May 2004):1266-1268.

Figure 6-8. Tungsten-containing dots written in regular arrays by electron beam-induced deposition (EBID) had an mean size (averaged over 100 dots) of 1.0 nm. Large and small dots are present in the arrays because of the statistical spread in the dot size, with the smallest having a diameter of only 0.7 nm; lines with the smallest width 1.9 nm at a 3.2 nm spacing have also been fabricated.⁶⁸³

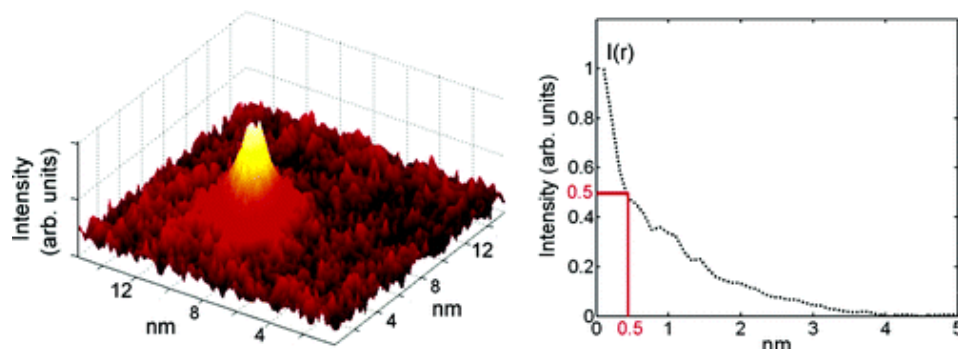
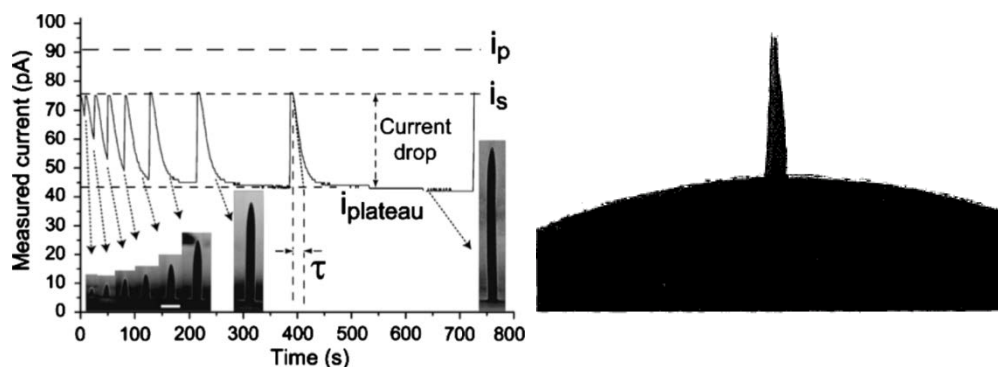


Figure 6-9. (A) Left: A plot showing the use of in-situ sample current measurements to monitor the EBID deposit height, providing in-situ control of the focused-electron-beam-induced deposition process with precursors used for Au, Cu, Rh, and SiO₂ deposition. A picoamperemeter monitors the electron current flowing through the sample, which reproducibly drops at a characteristic rate to a plateau value during deposition.⁶⁸⁴ **(B)** Right: Rhenium tip for testing as field electron emitter deposited on the apex of a microscale-sharpened tungsten wire (tip is ~200 nm wide at base, ~70 nm at apex).⁶⁸⁵



⁶⁸³ Willem F. van Dorp, Bob van Someren, Cornelis W. Hagen, Pieter Kruit, "Approaching the Resolution Limit of Nanometer-Scale Electron Beam-Induced Deposition," *Nano Lett.* 5(July 2005):1303-1307.

⁶⁸⁴ T. Bret, I. Utke, A. Bachmann, P. Hoffmann, "In situ control of the focused-electron-beam-induced deposition process," *Appl. Phys. Lett.* 83(2003):4005-4007.

⁶⁸⁵ N.A. Kislov, I.I. Khodos, E.D. Ivanov, J. Barthel, "Electron-beam-induced fabrication of metal-containing nanostructures," *Scanning* 18(1996):114-118; http://www.mpi-halle.de/mpi/publi/pdf/1749_96.pdf.

In certain respects FEB fabrication and FIB fabrication are complimentary. The situation for gas-assisted processing can be summarized as follows:⁶⁸⁶

FIB has generally a higher yield in deposition and etching but generally damages the area addressed and contaminates it with gallium. Also selectivity is difficult to achieve. FEB on the other hand produces no – or substantially less – damage or contamination and can have high selectivity, but is slower, produces low metal content deposits, and cannot be used to remove inert materials such as gold.

How inherent are the disadvantages? For FEB it was shown that smart chemistry can improve the metal content close to 100% by using inorganic precursors and additional reactive gases. The same approach should allow finding etchants for most materials. In how far the yield can be improved with this concept remains an open question, but clearly the exposure dwell time of the electron or ion beams has to be reduced to a minimum. Especially, for small structures the throughput is often limited by gas replenishment and not by the yield. It can be concluded that for FEB the disadvantages are not inherent but rather represent the present state of the art of precursor research. For Ga⁺-based FIB the disadvantages are coupled to the heavy mass of ions and are thus inherent. However, replacing the predominantly-used Ga⁺ ions by lighter ions such as protons or helium or other noble gases might diminish the extent of damage and contamination, where they prove detrimental in nanofabrication.⁶⁸⁷

Perhaps the most important single factor in the EBID process is the chemistry of the deposition precursor.⁶⁸⁸ The precursor must produce a solid deposit and volatile byproducts as a result of an electron-stimulated dissociation reaction. A wide array of precursor materials that meet these criteria have already been investigated and found to be useful in the study of EBID. For ease of reference, **Table 6-2** lists many of the materials that have been successfully deposited by EBID and their corresponding precursors, and other important experimental parameters.⁶⁸⁹ Note that the list includes not just metals but also semiconductors like Si and Ge, and also insulators like silicon oxides and carbon. In the case of carbon, lateral growth of a carbon nanopillar using electron beam-induced chemical vapor deposition (EB-CVD) is dominated by forward scattering of the electron beam (**Figure 6-10**), reducing the minimum diameter of the carbon nanopillar to 5 nm; in contrast, vertical growth with EB-CVD produces thicker pillars ~50 nm in diameter with a shape that evidences forward scattering of the primary electrons – and the amorphous carbon

⁶⁸⁶ Ivo Utke, Patrik Hoffmann, John Melngailis, “Gas-assisted focused electron beam and ion beam processing and fabrication,” *J. Vac. Sci. Technol. B* 26(July 2008):1197-1276.

⁶⁸⁷ Ivo Utke, Patrik Hoffmann, John Melngailis, “Gas-assisted focused electron beam and ion beam processing and fabrication,” *J. Vac. Sci. Technol. B* 26(July 2008):1197-1276.

⁶⁸⁸ S.J. Randolph, J.D. Fowlkes, P.D. Rack, “Focused, Nanoscale Electron-Beam-Induced Deposition and Etching,” *Critical Reviews in Solid State and Materials Sciences* 31(September 2006):55-89; <http://www.informaworld.com/smpp/section?content=a768444964&fulltext=713240928>.

⁶⁸⁹ Ivo Utke, Patrik Hoffmann, John Melngailis, “Gas-assisted focused electron beam and ion beam processing and fabrication,” *J. Vac. Sci. Technol. B* 26(July 2008):1197-1276. 510.

nanopillars are graphitized by annealing.⁶⁹⁰ (Pretty much any hydrocarbon can serve as an EBID precursor for carbon deposition, including alkanes, alkenes, camphor, menthol, DMSO, acetone, methanol, acetic acid, etc.⁶⁹¹

Figure 6-10. FEB deposition events on the surface of the deposit or substrate.⁶⁹²

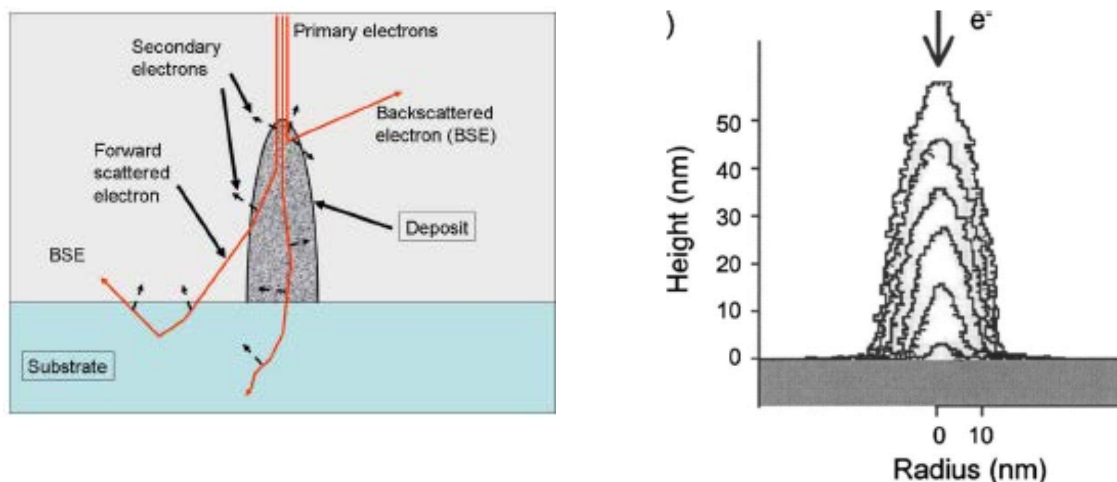


Table 6-2. Representative list of EBID materials and precursors.

Material	Precursor	References	Comments
----------	-----------	------------	----------

⁶⁹⁰ J. Fujita, M. Ishida, T. Ichihashi, Y. Ochiai, T. Kaito, S. Matsui, "Carbon nanopillar laterally grown with electron beam-induced chemical vapor deposition," *Journal of Vacuum Science & Technology B* 21(November 2003):2990-2993; <http://dx.doi.org/10.1116/1.1624259>.

⁶⁹¹ Ivo Utke, Patrik Hoffmann, John Melngailis, "Gas-assisted focused electron beam and ion beam processing and fabrication," *J. Vac. Sci. Technol. B* 26(July 2008):1197-1276.

⁶⁹² Ivo Utke, Patrik Hoffmann, John Melngailis, "Gas-assisted focused electron beam and ion beam processing and fabrication," *J. Vac. Sci. Technol. B* 26(July 2008):1197-1276.

Ag	Ag(I)-SC ₁₂	REF. ⁶⁹³	silver dodecanethiolate
Al	Al(CH ₃) ₃	REF. ⁶⁹⁴	Al with some C, not quantified
Al	AlH ₃ -N(CH ₃) ₃	REF. ⁶⁹⁵	Al:Ga:C:N :: 29:12:31:28
Au	AuCIPF ₃	REF. ⁶⁹⁶	>95 at.% Au
Au	Me ₂ Au(tfac)	REF. ⁶⁹⁷	dimethyl-gold-trifluoro-acetylacetonate
Au	Au ₅₅ (PPh ₃) ₁₂ Cl ₆	REF. ⁶⁹⁸	makes conductive lines (IBID)
Au	Au-contain. inks	REF. ⁶⁹⁹	makes conductive lines (IBID)
C	C ₁₄ H ₁₀	REF. ⁷⁰⁰	phenanthrene
C	AuCl ₃ or AlCl ₃	REF. ⁷⁰¹	on C substrate, forms CCl ₄ , makes C pillars
Co	Co ₂ (CO) ₈	REF. ⁷⁰²	12-80 at.% Co
Cr	CrO ₂ Cl ₂	REF. ⁷⁰³	Cr:O:Cl :: 1:2.2:1.1
Cr	Cr(C ₆ H ₆) ₂	REF. ⁷⁰⁴	---
Cr	Cr(CO) ₆	REF. ⁷⁰⁵	---
Cu	hfac-Cu-TMVS	REF. ⁷⁰⁶	hexafluoroacetylacetonato-Cu(I)-trimethylvinyl-silane; makes "pure" Cu
Fe	Fe(CO) ₅	REF. ⁷⁰⁷	---
Fe	Fe ₃ (CO) ₁₂	REF. ⁷⁰⁸	---
GaAs	TMG and AsH ₃	REF. ⁷⁰⁹	tri-methyl-gallium; AsH ₃ cracked at 1273 K
GaN	D ₂ GaN ₃	REF. ⁷¹⁰	perdeuterated gallium azide
GaN	GaH ₃ :NC ₇ H ₁₄	REF. ⁷¹¹	requires 600 °C substrate
Ge	Ge ₂ H ₆	REF. ⁷¹²	deposition on Si ₃ N ₄ membrane
Ir	[IrCl(PF ₃) ₂] ₂	REF. ⁷¹³	Ir:Cl:P :: 1:1:1
Ir	[Ir ₄ (CO) ₁₁ Br]NEt ₄	REF. ⁷¹⁴	makes conductive lines (IBID)
Mo	Mo(CO) ₆	REF. ⁷¹⁵	---
Ni	Ni(CO) ₄	REF. ⁷¹⁶	---
Ni	Ni(PF ₃) ₄	REF. ⁷¹⁷	---
Os	Os ₃ (CO) ₁₂	REF. ⁷¹⁸	---
Pd	Pd(OOCCH ₃) ₂	REF. ⁷¹⁹	palladium acetate (liquid)
Pt	Pt(PF ₃) ₄	REF. ⁷²⁰	81% Pt, 17%P, 1%F
Pt	H ₂ PtCl ₆ + H ₂ O	REF. ⁷²¹	~90% Pt, 10%Cl; chloroplatinic acid in aq. soln.
Rh	Rh ₂ Cl ₂ (CO) ₄	REF. ⁷²²	56 at.% Rh, 34 at.% C, 5 at.% Cl
Rh	[RhCl(PF ₃) ₂] ₂	REF. ⁷²³	Rh _{0.66} P _{0.33}
Ru	Ru ₃ (CO) ₁₂	REF. ⁷²⁴	---
Re	Re ₂ (CO) ₁₀	REF. ⁷²⁵	---
Si	SiH ₂ Cl ₂	REF. ⁷²⁶	89 at.% Si, 2% Cl and 9% O
Si	Si ₂ H ₆	REF. ⁷²⁷	makes crystalline Si on Si and Ge substrates
Si	AuCl ₃ or AlCl ₃	REF. ⁷²⁸	on Si substrate, forms SiCl ₄ , makes Si pillars
Si ₃ N ₄	N ₂	REF. ⁷²⁹	nitrogen on Si(100)
SiO ₂	Si ₂ H ₆ + O ₂	REF. ⁷³⁰	---
SiO ₂	Si(OMe) ₄ + O ₂	REF. ⁷³¹	SiO _{2.5} C _{3.2} (no added O ₂ gas)
SiO _x	TEOS	REF. ⁷³²	silicon alkoxide tetraethoxysilane; Si _{0.15} C _{0.45} O _{0.4}
Sn	SnCl ₄	REF. ⁷³³	52 at. % Sn, 48 at. % Cl; poor adhesion to Si
Sn	Sn(CH ₃) ₄	REF. ⁷³⁴	tetramethyl tin
TaO _x	Ta(OEt) ₅	REF. ⁷³⁵	tantalum pentaethoxide; Ta:C:O :: 10:3:5
TiO _x	Ti(-OC ₃ H ₇) ₄	REF. ⁷³⁶	---
TiO _x	Ti(NO ₃) ₄	REF. ⁷³⁷	titanium tetranitrate; 35% Ti; 57% O; 8.5% N
W	W(CO) ₆	REF. ⁷³⁸	75 at.% W (best)
W	WF ₆	REF. ⁷³⁹	W:F:C :: 93.3:4.4:2.3
W	WCl ₆	REF. ⁷⁴⁰	58 at.% W; 16 at.%Cl; 8 at.% C; 18 at.% O
ZrO ₂	e-beam resist	REF. ⁷⁴¹	zirconium n-butoxide + benzoyl acetone

⁶⁹³ Seong-Eun Kim, Young-Hwan Han, Byung cheol Lee, Jong-Chan Lee, "One-pot fabrication of various

silver nanostructures on substrates using electron beam irradiation,” *Nanotechnology* 21(19 February 2010):075302.

⁶⁹⁴ Akira Ishibashi, Kenji Funato, Yoshifumi Mori, “Electron-beam-induced resist and aluminum formation,” *J. Vac. Sci. Technol. B* 9(January 1991):169-172; <http://dx.doi.org/10.1116/1.585281>.

⁶⁹⁵ M.E. Gross, L.R. Harriott, R.L. Opila, “Focused ion beam stimulated deposition of aluminum from trialkylamine alanes,” *J. Appl. Phys.* 68(1 November 1990):4820-4824.

⁶⁹⁶ I. Utke, P. Hoffmann, B. Dwir, K. Leifer, E. Kapon, P. Doppelt, “Focused electron beam induced deposition of gold,” *J. Vac. Sci. Technol. B* 18(November 2000):3168-3171. T. Brintlinger, M.S. Fuhrer, J. Melngailis, I. Utke, T. Bret, A. Perentes, P. Hoffmann, M. Abourida, P. Doppelt, “Electrodes for carbon nanotube devices by focused electron beam induced deposition of gold,” *J. Vac. Sci. Technol. B* 23(November 2005):3174-3177; <http://www.physics.umd.edu/mfuhrer/publications/FEBID.pdf>.

⁶⁹⁷ H.W.P. Koops, R. Weiel, D.P. Kern, T.H. Baum, “High-resolution electron-beam induced deposition,” *J. Vac. Sci. Technol. B* 6(January 1988):477-481. <http://dx.doi.org/10.1116/1.584045>.

⁶⁹⁸ P. Hoffmann, H. Vandenbergh, J. Flicstein, G. Benassayag, J. Gierak, J.F. Bresse, “Direct Writing of Iridium Lines with a Focused Ion-Beam,” *Journal of Vacuum Science & Technology B* 9(November 1991):3483-3486.

⁶⁹⁹ H.G. Craighead, L.M. Schiavone, “Metal deposition by electron beam exposure of an organometallic film,” *Appl. Phys. Lett.* 48(23 June 1986):1748-1750.

⁷⁰⁰ J. Fujita, M. Ishida, T. Ichihashi, Y. Ochiai, T. Kaito, S. Matsui, “Carbon nanopillar laterally grown with electron beam-induced chemical vapor deposition,” *Journal of Vacuum Science & Technology B* 21(November 2003):2990-2993; <http://dx.doi.org/10.1116/1.1624259>.

⁷⁰¹ M. Shimojo, S. Bysakh, K. Mitsuishi, M. Tanaka, M. Song, K. Furuya, “Selective growth and characterization of nanostructures with transmission electron microscopes,” *Appl. Surf. Sci.* 241(2005):56-60.

⁷⁰² Y.M. Lau, P.C. Chee, J.T.L. Thong, V. Ng, “Properties and applications of cobalt-based material produced by electron-beam-induced deposition,” *Journal of Vacuum Science & Technology A* 20(July 2002):1295-1302. <http://dx.doi.org/10.1116/1.1481040>. I. Utke, T. Bret, D. Laub, Ph. Buffat, L. Scandella, P. Hoffmann, “Thermal effects during focused electron beam induced deposition of nanocomposite magnetic-cobalt-containing tips,” *Microelectron. Eng.* 73-74(June 2004):553-558. I. Utke, J. Michler, Ph. Gasser, C. Santschi, D. Laub, M. Cantoni, P. A. Buffat, C. Jiao, P. Hoffmann, “Cross Section Investigations of Compositions and Sub-Structures of Tips Obtained by Focused Electron Beam Induced Deposition,” *Adv. Eng. Mater.* 7(May 2005):323-331.

⁷⁰³ S. Wang, Y.M. Sun, J.M. White, “Electron induced deposition and in situ etching of CrO_xCl_y films,” *Appl. Surf. Sci.* 249(2005):110-114.

⁷⁰⁴ Shinji Matsui, Katsumi Mori, “New selective deposition technology by electron-beam induced surface reaction,” *Journal of Vacuum Science & Technology B* 4(1986):299-304; <http://dx.doi.org/10.1116/1.583317>.

⁷⁰⁵ R.R. Kunz, T.M. Mayer, “Electron beam induced surface nucleation and low-temperature decomposition of metal carbonyls,” *J. Vac. Sci. Technol. B* 6(September 1988):1557-1564. N.A. Kislov,

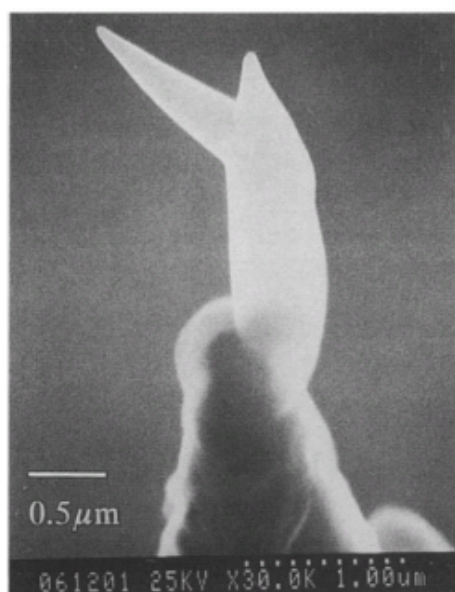
-
- I.I. Khodos, E.D. Ivanov, J. Barthel, "Electron-beam-induced fabrication of metal-containing nanostructures," *Scanning* 18(1996):114-118; http://www.mpi-halle.de/mpi/publi/pdf/1749_96.pdf.
- ⁷⁰⁶ I. Utke, A. Luisier, P. Hoffmann, D. Laub, P.A. Buffat, "Focused-electron-beam-induced deposition of freestanding three-dimensional nanostructures of pure coalesced copper crystals," *Applied Physics Letters* 81(2002):3245-3247; <http://dx.doi.org/10.1063/1.1517180>.
- ⁷⁰⁷ R.R. Kunz, T.E. Allen, T.M. Mayer, "Selective area deposition of metals using low-energy electron beams," *J. Vac. Sci. Technol. B* 5(September 1987):1427-1431; <http://dx.doi.org/10.1116/1.583629>.
- ⁷⁰⁸ M.A. Bruk, E.N. Zhikharev, E.I. Grigorrsquoev, A.V. Spirin, V.A. Kalrsquonov, I.E. Kardash, "Focused electron beam-induced deposition of iron- and carbon-containing nanostructures from triiron dodecacarbonyl vapor," *High Energy Chem.* 39(March 2005):65-68. Translated from *Khimiya Vysokikh Energii*, Vol. 39, No. 2, 2005, pp. 93-96.
- ⁷⁰⁹ T. Takahashi, Y. Arakawa, M. Nishioka, T. Ikoma, "Selective growth of GaAs wire structures by electron beam induced metalorganic chemical vapor deposition," *Applied Physics Letters* 60(1992):68-70; <http://dx.doi.org/10.1063/1.107376>.
- ⁷¹⁰ P.A. Crozier, J. Tolle, J. Kouvetakis, Cole Ritter, "Synthesis of uniform GaN quantum dot arrays via electron nanolithography of D_2GaN_3 ," *Applied Physics Letters* 84(2004):3441-3443; <http://dx.doi.org/10.1063/1.1736314>.
- ⁷¹¹ T. Nagata, P. Ahmet, Y. Sakuma, T. Sekiguchi, T. Chikyow, "GaN nanostructure fabrication by focused-ion-beam-assisted chemical vapor deposition," *Appl. Phys. Lett.* 87(July 2005):013103.
- ⁷¹² Sutharsan Ketharanathan, Renu Sharma, P.A. Crozier, Jeff Drucker, "Electron beam induced deposition of pure, nanoscale Ge," *J. Vac. Sci. Technol. B* 24(March 2006):678-681.
- ⁷¹³ Tristan Bret, Ivo Utke, Patrik Hoffmann, Maurice Abourida, Pascal Doppelt, "Electron range effects in focused electron beam induced deposition of 3D nanostructures," *Microelectron. Eng.* 83(April-September 2006):1482-1486.
- ⁷¹⁴ P. Hoffmann, H. Vandenbergh, J. Flicstein, G. Benassayag, J. Gierak, J.F. Bresse, "Direct Writing of Iridium Lines with a Focused Ion-Beam," *Journal of Vacuum Science & Technology B* 9(November 1991):3483-3486.
- ⁷¹⁵ M. Weber, H.W.P. Koops, M. Rudolph, J. Kretz, G. Schmidt, "New compound quantum dot materials produced by electron-beam induced deposition," *J. Vac. Sci. Technol. B* 13(May 1995):1364-1368; <http://dx.doi.org/10.1116/1.587854>.
- ⁷¹⁶ S. Rubel, M. Trochet, E.E. Ehrichs, W.F. Smith, A.L. de Lozanne, "Nanofabrication and rapid imaging with a scanning tunneling microscope," *J. Vac. Sci. Technol. B* 12(May 1994):1894-1897; <http://dx.doi.org/10.1116/1.587664>.
- ⁷¹⁷ A. Perentes, G. Sinicco, G. Boero, B. Dwir, P. Hoffmann, "Focused electron beam induced deposition of nickel," *J. Vac. Sci. Technol. B* 25(November 2007):2228-2232.
- ⁷¹⁸ V. Scheurer, H.W.P. Koops, T. Tschudi, "Electron beam decomposition of carbonyls on silicon," *Microelectronic Engineering* 5(December 1986):423-430; <http://dx.doi.org/10.1016/0167-9317%2886%2990072-9>.

-
- ⁷¹⁹ T.J. Stark, T.M. Mayer, D.P. Griffis, P.E. Russell, "Formation of Complex Features using Electron-Beam Direct-Write Decomposition of Palladium Acetate," *Journal of Vacuum Science & Technology B* 10(November 1992):2685-2690. T.J. Stark, T.M. Mayer, D.P. Griffis, P.E. Russell, "Electron Beam Induced Metallization of Palladium Acetate," *J. Vac. Sci. Technol. B* 9(November 1991):3475-3478; <http://dx.doi.org/10.1116/1.585826>.
- ⁷²⁰ S. Wang, Y.-M. Sun, Q. Wang, J.M. White, "Electron-beam induced initial growth of platinum films using $\text{Pt}(\text{PF}_3)_4$," *Journal of Vacuum Science & Technology B* 22(July 2004):1803-1806; <http://dx.doi.org/10.1116/1.1761266>.
- ⁷²¹ Eugenii U. Donev, J. Todd Hastings, "Electron-Beam-Induced Deposition of Platinum from a Liquid Precursor," *Nano Lett.* 9(2009):2715-2718.
- ⁷²² F. Cicoira, P. Hoffmann, C.O.A. Olsson, N. Xanthopoulos, H.J. Mathieu, P. Doppelt, "Auger electron spectroscopy analysis of high metal content micro-structures grown by electron beam induced deposition," *Appl. Surf. Sci.* 242(2005):107; <http://www.nanofemtolab.qc.ca/Pubblicazioni%20Fabio/15.pdf>.
- ⁷²³ P. Hoffmann, I. Utke, F. Cicoira, B. Dwir, K. Leifer, E. Kapon, P. Doppelt, "Focused electron beam induced deposition of gold and rhodium," *Materials Research Society Symposium - Proceedings* 624(2000):171-177. Fabio Cicoira, "Electron Beam Induced Deposition Of Rhodium Nanostructures," Thèse No. 2528, École Polytechnique Fédérale De Lausanne, 2002; http://biblion.epfl.ch/EPFL/theses/2002/2528/EPFL_TH2528.pdf. F. Cicoira, K. Leifer, P. Hoffmann, I. Utke, B. Dwir, D. Laub, P.A. Buffat, E. Kapon, P. Doppelt, "Electron beam induced deposition of rhodium from the precursor $[\text{RhCl}(\text{PF}_3)_2]_2$: Morphology, structure and chemical composition," *Journal of Crystal Growth* 265(2004):619-626; <http://dx.doi.org/10.1016/j.jcrysgro.2004.02.006>.
- ⁷²⁴ V. Scheurer, H.W.P. Koops, T. Tschudi, "Electron beam decomposition of carbonyls on silicon," *Microelectronic Engineering* 5(December 1986):423-430; <http://dx.doi.org/10.1016/0167-9317%2886%2990072-9>.
- ⁷²⁵ N.A. Kislov, I.I. Khodos, E.D. Ivanov, J. Barthel, "Electron-beam-induced fabrication of metal-containing nanostructures," *Scanning* 18(1996):114-118; http://www.mpi-halle.de/mpi/publi/pdf/1749_96.pdf.
- ⁷²⁶ Shinji Matsui, Masanobu Mito, "Si deposition by electron beam induced surface reaction," *Appl. Phys. Lett.* 53(17 October 1988):1492; <http://dx.doi.org/10.1063/1.100465>.
- ⁷²⁷ F. Bozso, P. Avouris, "Thermal and electron-beam-induced reaction of disilane on $\text{Si}(100)-(2 \times 1)$," *Phys. Rev. B* 38(15 August 1988):3943-3947. F. Hirose, H. Sakamoto, "Low-Temperature Si Selective Epitaxial Growth Using Electron-Beam-Induced Reaction," *Jpn. J. Appl. Phys.* 34(1995):5904-5907.
- ⁷²⁸ M. Shimojo, S. Bysakh, K. Mitsuishi, M. Tanaka, M. Song, K. Furuya, "Selective growth and characterization of nanostructures with transmission electron microscopes," *Appl. Surf. Sci.* 241(2005):56-60.
- ⁷²⁹ Brymer H. Chin, Gert Ehrlich, "Formation of silicon nitride structures by direct electron beam writing," *Applied Physics Letters* 38(1981):253-255; <http://dx.doi.org/10.1063/1.92334>.

-
- ⁷³⁰ Koji Nakano, Tetsuhiro Horie, Hitoshi Sakamoto, "Low-Temperature Growth of SiO₂ Films by Electron-Induced Ultrahigh Vacuum Chemical Vapor Deposition," *Jpn. J. Appl. Phys.* 35(1996):6570-6573.
- ⁷³¹ A. Perentes, P. Hoffmann, "Focused Electron Beam Induced Deposition of Si-Based Materials From SiO_xC_y to Stoichiometric SiO₂: Chemical Compositions, Chemical-Etch Rates, and Deep Ultraviolet Optical Transmissions," *Chem. Vap. Deposition* 13(2007):176-184. A. Perentes, P. Hoffmann, "Oxygen assisted focused electron beam induced deposition of Si-containing materials: Growth dynamics," *J. Vac. Sci. Technol. B* 25(November 2007):2233-2238.
- ⁷³² S. Lipp, L. Frey, C. Lehrer, B. Frank, E. Demm, S. Pauthner, H. Ryssel, "Tetramethoxysilane as a precursor for focused ion beam and electron beam assisted insulator (SiO_x) deposition," *Journal of Vacuum Science & Technology B* 14(November 1996):3920-3923; <http://dx.doi.org/10.1116/1.588695>
- ⁷³³ H.O. Funsten, J.W. Boring, R.E. Johnson, "Low-temperature beam-induced deposition of thin tin films," *J. Appl. Phys.* 71(1 February 1992):1475-1484; <http://people.virginia.edu/~rej/papers-scan/Funstenetal-JAppPhy92.pdf>.
- ⁷³⁴ Herbert O. Funsten, "Model for beam-induced deposition of thin metallic films," *Nucl. Instrum. Methods Phys. Res. B* 72(November 1992):183-196.
- ⁷³⁵ Kenji Gamo, D. Takehara, Y. Hamamura, M. Tomita, S. Namba, "Maskless ion beam assisted deposition of W and Ta films," *Microelectron. Eng.* 5(December 1986):163-170.
- ⁷³⁶ William J. Mitchell, Evelyn L. Hu, "Selective area chemical vapor deposition of titanium oxide films: Characterization of Ti(OC₃H₇)₄ as an electron beam resist," *J. Vac. Sci. Technol. B* 17(July 1999):1622-1626; <http://dx.doi.org/10.1116/1.590801>.
- ⁷³⁷ A. Perentes, T. Bret, I. Utke, P. Hoffmann, M. Vaupel, "Real-time reflectometry-controlled focused-electron-beam-induced deposition of transparent materials," *J. Vac. Sci. Technol. B* 24(March 2006):587-591.
- ⁷³⁸ H.W.P. Koops, R. Weiel, D.P. Kern, T.H. Baum, "High-resolution electron-beam induced deposition," *J. Vac. Sci. Technol. B* 6(January 1988):477-481. <http://dx.doi.org/10.1116/1.584045>. P.C. Hoyle, J.R.A. Cleaver, H. Ahmed, "Ultralow-energy focused electron beam induced deposition," *Applied Physics Letters* 64(1994):1448-1450; <http://dx.doi.org/10.1063/1.111912>. D. Beaulieu, Yong Ding, Z.L. Wang, W.J. Lackey, "Influence of process variables on electron beam chemical vapor deposition of platinum," *Journal of Vacuum Science and Technology B: Microelectronics and Nanometer Structures* 23(September 2005):2151-2159; <http://dx.doi.org/10.1116/1.2050672>.
- ⁷³⁹ Shinji Matsui, Katsumi Mori, "New selective deposition technology by electron-beam induced surface reaction," *Journal of Vacuum Science & Technology B* 4(1986):299-304; <http://dx.doi.org/10.1116/1.583317>. Z. Xu, T. Kosugi, K. Gamo, S. Namba, "An x-ray photoelectron spectroscopy study on ion beam induced deposition of tungsten using WF₆," *J. Vac. Sci. Technol. B* 7(November 1989):1959-1962. K. Gamo, S. Namba, *Mater. Res. Soc. Symp. Proc.* 131(1989):531.
- ⁷⁴⁰ Shinji Matsui, Katsumi Mori, "New selective deposition technology by electron-beam induced surface reaction," *Journal of Vacuum Science & Technology B* 4(1986):299-304; <http://dx.doi.org/10.1116/1.583317>.

EBID-made tips have been fabricated for use in scanning probe (STM) work out of tungsten and carbon.⁷⁴² For example, Matsui et al.⁷⁴³ fabricated an STM tip for use in measuring sidewall roughness of deep grooves that has two directional tips perpendicular to sidewall and bottom surfaces (**Figure 6-11**). Here, a mechanical-polished Pt/Ir wire tip was set into the SEM and an electron beam focused for ~1 hr, causing a needlelike carbonaceous contamination tip to grow at the rate of ~1 $\mu\text{m}/\text{hour}$ at 25 kV; a 50-nm thick Au coating was rf-sputtered onto the tip surfaces to increase conductivity, yielding two tips with an average surface roughness of 11 nm. (See [Section 3.8](#) for further discussion of the EBID fabrication of SPM tips.)

Figure 6-11. An STM tip for measuring sidewall roughness, made by EB deposition.⁷⁴⁴



⁷⁴¹ K.R.V. Subramanian, M.S.M. Saifullah, E. Tapley, D.-J. Kang, M.E. Welland, M. Butler, "Direct writing of ZrO_2 on a sub-10 nm scale using an electron beam," *Nanotechnology* 15(January 2004):158-162.

⁷⁴² Y. Akama, E. Nishimura, A. Sakai, "New scanning tunneling microscopy tip for measuring surface topography," *J. Vac. Sci. Technol. A* 8(January 1990):429-433. Shinji Matsui, Toshinori Ichihashi, Masakazu Baba, Akinobu Satoh, "Electron beam induced selective etching and deposition technology," *Superlattices and Microstructures* 7(1990):295-301.

⁷⁴³ Shinji Matsui, Toshinori Ichihashi, Masakazu Baba, Akinobu Satoh, "Electron beam induced selective etching and deposition technology," *Superlattices and Microstructures* 7(1990):295-301.

⁷⁴⁴ Shinji Matsui, Toshinori Ichihashi, Masakazu Baba, Akinobu Satoh, "Electron beam induced selective etching and deposition technology," *Superlattices and Microstructures* 7(1990):295-301.

6.2.2 Step 1: Attach Iridium Nanowire to Quartz Fork

Plan A. The very simplest way to perform this step would be to mount the “polycrystalline Ir wire having a diameter of 100 microns and a length of about 5 mm” described in the Kuo et al. patent⁷⁴⁵ directly onto the quartz fork. To do this, we first position the iridium wire atop the prong in an appropriate position and orientation, then IBID- or EBID-solder the wire to the prong – the EBID layers act as a binder as the deposited amorphous material “welds” the wire to the prong (Figure 6-12).⁷⁴⁶ (Gas-assisted FEB and FIB are often used as attachment tools for carbon nanotubes or nanowires onto AFM tips or microelectromechanical system structures.⁷⁴⁷) After that, ion or electrochemical etching (Section 3.12) or other means of tip sharpening is used to produce a tapered geometry at the distal end of the already-attached wire so that the tapered tip has a curvature radius of 200 nm or less, as required by the Kuo et al.⁷⁴⁸ SAT-fabrication process.

⁷⁴⁵ Hong-Shi Kuo, Ing-shouh Hwang, Tien T. Tsong, Tsu-Yi Fu, “Atomically Sharp Iridium Tip,” IPC8 Class: AB21G100FI, USPC Class: 428600, 2009; <http://www.faqs.org/patents/app/20090110951>.

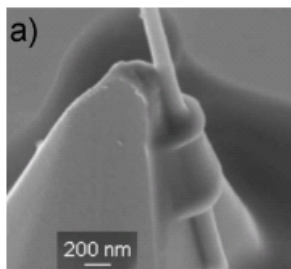
⁷⁴⁶ MinFeng Yu, Mark J. Dyer, George D. Skidmore, Henry W. Rohrs, Xue Kun Lu, Kevin D. Ausman, James Von Ehr, Rodney S. Ruoff, “3 Dimensional Manipulation of Carbon Nanotubes under a Scanning Electron Microscope,” Sixth Foresight Nanotechnology Conference, November 1998; <http://www.foresight.org/Conferences/MNT6/Papers/Yu/index.html>. See also: Robert F. Service, “AFMs Weld Parts for Nanoconstruction,” *Science* 282(27 November 1998):1620-1621. H.W.P. Koops, R. Weiel, D.P. Kern, T.H. Baum, “High-resolution electron-beam induced deposition,” *J. Vac. Sci. Technol. B* 6(January 1988):477-481. <http://dx.doi.org/10.1116/1.584045>.

⁷⁴⁷ Min-Feng Yu, Oleg Lourie, Mark J. Dyer, Katerina Moloni, Thomas F. Kelly, Rodney S. Ruoff, “Strength and Breaking Mechanism of Multiwalled Carbon Nanotubes Under Tensile Load,” *Science* 287(28 January 2000):637-640; http://www.bimat.org/assets/pdf/00_287yu.pdf. Lixin Dong, Fumihito Arai, Toshio Fukuda, “Electron-beam-induced deposition with carbon nanotube emitters,” *Appl. Phys. Lett.* 81(2002):1919-1921; http://www.egr.msu.edu/~ldong/Publication/JP200203_APL_81_1919_Dong.pdf. P.A. Williams, S.J. Papadakis, M.R. Falvo, A.M. Patel, M. Sinclair, A. Seeger, A. Helser, R.M. Taylor, S. Washburn, R. Superfine, “Controlled placement of an individual carbon nanotube onto a microelectromechanical structure,” *Appl. Phys. Lett.* 80(2002):2574-2576; <http://www.cs.unc.edu/~seeger/publications/2002Williams.CNTMEMS.APL2002.pdf>. W. Ding, D.A. Dikin, X. Chen, R.D. Piner, R.S. Ruoff, E. Zussman, X. Wang, X. Li, “Mechanics of hydrogenated amorphous carbon deposits from electron-beam-induced deposition of a paraffin precursor,” *J. Appl. Phys.* 98(2005):014905; http://bimat.org/assets/pdf/nu_05_98ding.pdf. S. Orso, U.G.K. Wegst, C. Eberl, E. Arzt, “Micrometer-scale tensile testing of biological attachment devices,” *Adv. Mater.* 18(2006):874-877. S. Hoffmann, F. Östlund, J. Michler, H.J. Fan, M. Zacharias, S.H. Christiansen, C. Ballif, “Fracture strength and Young’s modulus of ZnO nanowires,” *Nanotechnology* 18(23 May 2007):205503. M. Becker, V. Sivakov, G. Andrä, R. Geiger, J. Schreiber, S. Hoffmann, J. Michler, A. P. Milenin, P. Werner, S.H. Christiansen, “The SERS and TERS Effects Obtained by Gold Droplets on Top of Si Nanowires,” *Nano Lett.* 7(2007):75-80; http://www.mpi-halle.de/mpi/publi/pdf/7247_07.pdf.

⁷⁴⁸ Hong-Shi Kuo, Ing-Shouh Hwang, Tsu-Yi Fu, Ying-Siang Hwang, Yi-Hsien Lu, Chun-Yueh Lin, Jin-Long Hou, Tien T. Tsong, “A single-atom sharp iridium tip as an emitter of gas field ion sources,” *Nanotechnology* 20(19 August 2009):335701. Hong-Shi Kuo, Ing-shouh Hwang, Tien T. Tsong, Tsu-Yi Fu, “Atomically Sharp Iridium Tip,” IPC8 Class: AB21G100FI, USPC Class: 428600, 2009; <http://www.faqs.org/patents/app/20090110951>.

Alternatively, the polycrystalline Ir wire could be sharpened first, then welded to the quartz fork prong via EBID. Further analysis is required to determine the ideal order of these operations.

Figure 6-12. FEB-deposited clamp to fix a nanowire to an AFM cantilever pyramid.⁷⁴⁹



After the tapered nanowire is attached, FEB-induced etching (**Figure 6-6B(b)**) can be used to trim excess wire from the shank end nearest to the prong, resulting in a clean attachment.

Nanowires made from Pt, Pd, or Rh feedstock wire also could presumably be used in place of Ir, if this will produce a SAT with superior mechanochemical performance for DMS operations, given that Kuo et al.⁷⁵⁰ have alleged that these three metals should also facetize at a nanowire apex when thermally annealed.

Plan B. To avoid having to manually mount a preformed wire on a quartz fork prong, in Plan B we grow the wire onto the prong instead. In this first step, IBID or EBID is used to deposit a pure iridium metal column or “nanowire” onto the appropriate flat face of the quartz (SiO_2) tuning fork. This nanowire can be deposited vertically or horizontally out from the quartz surface, whichever may be the most convenient for the particular instrumentation (since IBID and EBID are versatile processes that can draw out virtually any continuous 3D shape). The assumption is that the wire will be oriented normal to the surface, though that is not an essential requirement for the apparatus.

The nanowire should be fabricated lengthy enough to avoid geometric congestion at the worksite (in case two tooltips must be juxtaposed during DMS operations), perhaps in the 50-100 micron range, but not so lengthy that troublesome mechanical vibrations might arise that could reduce the accuracy of the metrological positioning system to which the tip system will be attached (a factor that will require further analysis). The shank of the iridium column can be cylindrical near the attachment site at the quartz surface, but the nanowire should taper to a more pointed apex with a

⁷⁴⁹ W. Ding, D.A. Dikin, X. Chen, R.D. Piner, R.S. Ruoff, E. Zussman, X. Wang, X. Li, “Mechanics of hydrogenated amorphous carbon deposits from electron-beam-induced deposition of a paraffin precursor,” J. Appl. Phys. 98(2005):014905; http://bimat.org/assets/pdf/nu_05_98ding.pdf.

⁷⁵⁰ Hong-Shi Kuo, Ing-shouh Hwang, Tien T. Tsong, Tsu-Yi Fu, “Atomically Sharp Iridium Tip,” IPC8 Class: AB21G100FI, USPC Class: 428600, 2009; <http://www.faqs.org/patents/app/20090110951>.

curvature radius as small as conveniently possible without heroic efforts (e.g., in the 10-50 nm range); but in no case should the curvature be larger than 200 nm.

To our knowledge, there are no published accounts of vertically-deposited iridium nanowires onto SiO₂ substrate for the purpose of fabricating a scanning probe tip, as we require for our application here. However, there are at least two papers that describe beam-assisted deposition of iridium metal onto a flat SiO₂ substrate. In both cases the silicon dioxide substrate is an oxide coating on a high-purity silicon wafer, rather than a quartz surface, but the two surfaces are chemically similar which is why we believe these process could also work on quartz. Note that the iridium-SiO₂ interface has been found to be stable during annealing up to 900 °C.⁷⁵¹ A third paper describes the EBID of vertical Ir nanowires onto Si surface.⁷⁵²

In the first paper by Hoffmann et al.,⁷⁵³ a complex Ir-containing precursor chemical is spread on a 1-micron-thick SiO₂ surface, irradiated by gallium ion beam (an example of a IBID process), then washed and heated, leaving pure Ir metal nanowires written onto the surface. This is an example of Ir metal being laid down and adhered to a SiO₂ surface. (Ir metal apparently is also very difficult to oxidize: “After 15 minutes at 580 °C in air, no oxide formation is observed.”⁷⁵⁴) The abstract of the paper reads, in part, as follows:

“Direct writing of metal features narrower than 100 nm is accomplished by scanning a focused ion beam over a substrate covered with a thin solid metalorganic film. A metalorganic cluster coordination compound [Ir₄(CO)₁₁Br][N(C₂H₅)₄] is spun on an oxidized silicon wafer from acetone solution and the resulting layer is irradiated with a focused 20 keV Ga-ion beam. The partially decomposed irradiated film regions show a marked decrease of solubility in acetone. Developing by dissolving the nonirradiated parts of the surface hence leaves narrow lines of partially reacted metalorganic precursor. High temperature treatment of these lines, either in vacuum or in a reactive gas stream, completes the decomposition to quite pure iridium, as is confirmed by micro-Auger analysis. In these preliminary experiments we obtained lines (**Figure 6-13**) with room temperature electrical resistivities as low as 400 μΩ-cm, at direct writing speeds of 40 μm/sec to 0.8 mm/sec, which correspond to ion doses of 3.1 x 10¹⁶ ions/cm² to 1.6 x 10¹⁵ ions/cm², respectively. The width of the metal lines decreases with decreasing ion dose in this range from 180 nm down to 90 nm. The adhesion to the substrate increases with increasing ion dose. The thickness of the resulting iridium lines depends mainly on the thickness of the

⁷⁵¹ M.A. Pawlak, T. Schram, K. Maex, A. Vantomme, “Investigation of iridium as a gate electrode for deep sub-micron CMOS technology,” *Microelectron. Eng.* 70(2003):373-376.

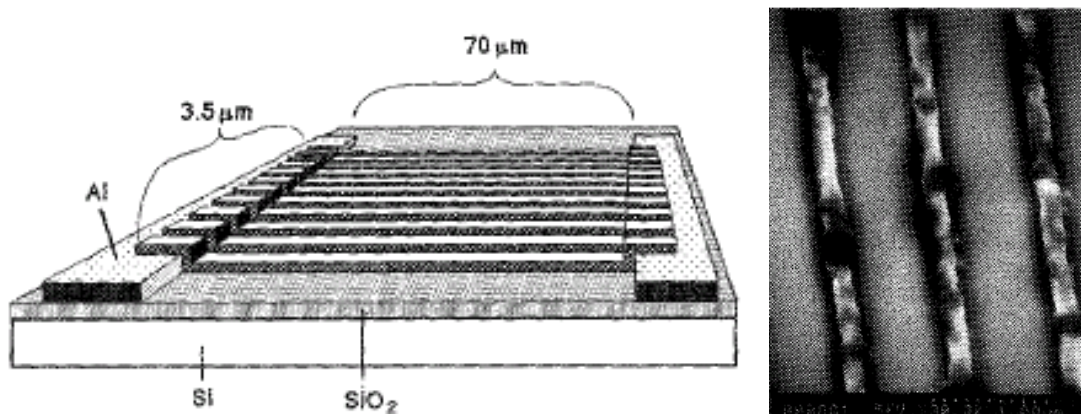
⁷⁵² Tristan Bret, Ivo Utke, Patrik Hoffmann, Maurice Abourida, Pascal Doppelt, “Electron range effects in focused electron beam induced deposition of 3D nanostructures,” *Microelectron. Eng.* 83(April-September 2006):1482-1486.

⁷⁵³ P. Hoffmann, H. Vandenbergh, J. Flicstein, G. Benassayag, J. Gierak, J.F. Bresse, “Direct Writing of Iridium Lines with a Focused Ion-Beam,” *Journal of Vacuum Science & Technology B* 9(November 1991):3483-3486.

⁷⁵⁴ K. Swars, ed., *Gmelin Handbook of Inorganic Chemistry, Iridium, Ergänzungsband 2, Verbindungen*, Springer, Berlin, 1978.

metalorganic precursor layer. The maximum possible thickness of the $[\text{Ir}_4(\text{CO})_{11}\text{Br}][\text{N}(\text{C}_2\text{H}_5)_4]$ layer that can be used depends on the effective penetration depth of the ions in this layer.”

Figure 6-13. (A) Left: Schematic demonstration of the iridium lines written (using FIB) with a pitch of 300 nm and 100 μm length resulting in a 3.5 μm wide multiline rectangle interconnecting two aluminum lines which serve as electrical contacts. (B) Right: SEM picture of iridium stripes obtained with a focused Ga-ion beam on a thermally oxidized silicon wafer; beam parameters: 1 ms dwell time, 60 pA current intensity, 20 kV accelerating voltage, 35 nm beam size, 3.1×10^{16} ions/ cm^2 , 40 $\mu\text{m}/\text{sec}$ writing speed producing stripes of 200 nm width and 30 nm thickness with sharp borders and steep walls.⁷⁵⁵



The iridium line-writing process is illustrated schematically in **Figure 6-13A**, and **Figure 6-13B** shows the actual patterns obtained experimentally as observed using high resolution SEM with the chemical composition of the structures determined by micro-Auger analysis. The resulting iridium metal lines are about 30 nm thick, using a solid precursor layer thickness of 50 nm. We presume that subsequent cycles of the same process could extend the Ir nanowire thickness to much greater depths, and higher ion doses also produce thicker lines.⁷⁵⁶ The iridium cluster salt precursor used here is easily synthesized⁷⁵⁷ but is a yellow solid that must be dissolved in acetone

⁷⁵⁵ P. Hoffmann, H. Vandenberg, J. Flicstein, G. Benassayag, J. Gierak, J.F. Bresse, “Direct Writing of Iridium Lines with a Focused Ion-Beam,” *Journal of Vacuum Science & Technology B* 9(November 1991):3483-3486.

⁷⁵⁶ P. Hoffmann, H. Vandenberg, J. Flicstein, G. Benassayag, J. Gierak, J.F. Bresse, “Direct Writing of Iridium Lines with a Focused Ion-Beam,” *Journal of Vacuum Science & Technology B* 9(November 1991):3483-3486.

⁷⁵⁷ P. Chini, G. Ciani, L. Garlaschelli, S. Manassero, S. Martinengo, A. Sironi, F. Canziani, “New tetrahedral cluster compounds of iridium. Synthesis of the anions $[\text{Ir}_4(\text{CO})_{11}\text{X}]^-$ ($\text{X} = \text{Cl}, \text{Br}, \text{I}, \text{CN}, \text{SCN}$) and x-ray structure of $[\text{PPh}_4][\text{Ir}_4(\text{CO})_{11}\text{Br}]$,” *J. Organometal. Chem.* 152(30 May 1978):C35-C38.

and stored in the dark to prevent photodecomposition; regarding thermal degradation, the decomposition reaction in air starts at 200 °C and goes to completion at 500 °C.

Hoffmann et al.⁷⁵⁸ note that an alternative to their approach is the irradiation with charged particle beams of metalorganic gases adsorbed on the deposition surface,⁷⁵⁹ but point out that their approach involving the charged-particle irradiation of a solid metalorganic precursor adsorbed on the deposition surface gives faster writing speeds. (Melngailis and Blauner⁷⁶⁰ used a scanned focused ion beam to deposit gold from dimethyl gold hexafluoro acetylacetonate and achieved linewidths down to 0.1 µm, and reviewed the work of others who have similarly deposited lines of Al, W, Ta, and Cr.)

In the second paper by Lee et al.⁷⁶¹ (incorporating by reference two related papers⁷⁶² that are cited as describing the IBID deposition methodology that was used), an electron beam vaporizes a pure iridium metal source while an Ar ion beam is simultaneously focused on the silicon wafer surface to assist deposition. Using this process, deposited material layers are amorphous regardless of the current level of the ion beam.⁷⁶³ During this experiment the iridium metal was deposited to a thickness of 370 nm on the silicon wafer. **Figure 6-14A** is a TEM cross-sectional image of the resulting film, which appears to show a pure silicon base layer with perhaps a thin SiO₂ coating, above which lies the pure Ir metal with a broken layer of iridium oxide on the topmost surface after electrochemical cycling in a solvent environment (for intended use as a chemical sensor); **Figure 6-14B** shows a SEM micrograph of the broken oxide surface. Since this method uses evaporated pure metal vapor atoms, it's not clear if this procedure can be used to deposit either a well-defined free-standing column of pure metal, or alternatively a sufficiently conical mound of iridium to meet the requirements for an SAT fabrication method.

⁷⁵⁸ P. Hoffmann, H. Vandenberg, J. Flicstein, G. Benassayag, J. Gierak, J.F. Bresse, "Direct Writing of Iridium Lines with a Focused Ion-Beam," *Journal of Vacuum Science & Technology B* 9(November 1991):3483-3486.

⁷⁵⁹ John Melngailis, P.G. Blauner, "Focused Ion Beam Induced Deposition," *MRS Proc.* 147(Spring 1989):127.

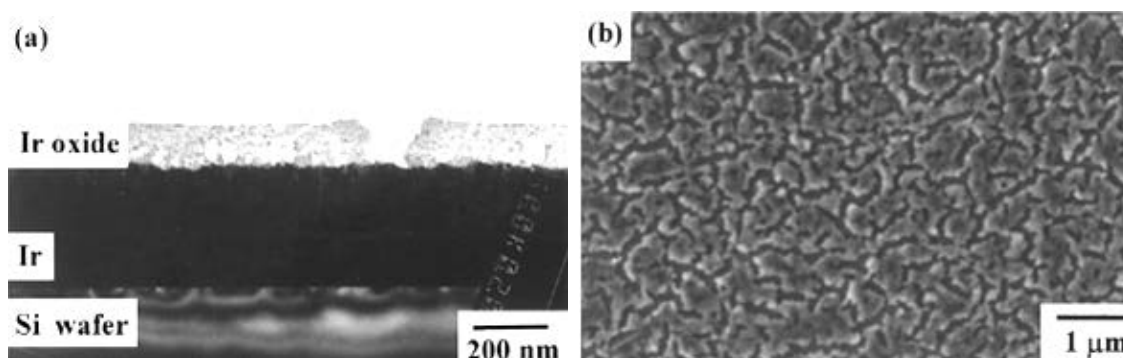
⁷⁶⁰ John Melngailis, P.G. Blauner, "Focused Ion Beam Induced Deposition," *MRS Proc.* 147(Spring 1989):127.

⁷⁶¹ In-Seop Lee, R.A. Buchanan, Young-Hee Lee, "Charge injection properties of iridium films formed by ion beam assisted deposition," *J. Mater. Sci. Lett.* 21(2002):1859-1861; [http://yhlee.yonsei.ac.kr/PDF/Ir\(letter\).pdf](http://yhlee.yonsei.ac.kr/PDF/Ir(letter).pdf).

⁷⁶² Jae-Man Choi, Young-Min Kong, Sona Kim, Hyoun-Ee Kim, Cheol Seong Hwang, In-Seop Lee, "Formation and characterization of hydroxyapatite coating layer on Ti-based metal implant by electron-beam deposition," *J. Mater. Res.* 14 (July 1999):2980-2985; http://til.catalysis.nsk.su/Materials_Research/1999/JMR86_99/VOL14/ISSUE07/P02980.PDF. Jae-Man Choi, Hyoun-Ee Kim, In-Seop Lee, "Ion-beam-assisted deposition (IBAD) of hydroxyapatite coating layer on Ti-based metal substrate," *Biomaterials* 21(March 2000):469-473.

⁷⁶³ Jae-Man Choi, Hyoun-Ee Kim, In-Seop Lee, "Ion-beam-assisted deposition (IBAD) of hydroxyapatite coating layer on Ti-based metal substrate," *Biomaterials* 21(March 2000):469-473.

Figure 6-14. (A) Left: Cross-section TEM of Ir after 600 electrochemical cycles in a solvent environment. (B) Right: SEM micrograph of “activated” Ir surface.⁷⁶⁴

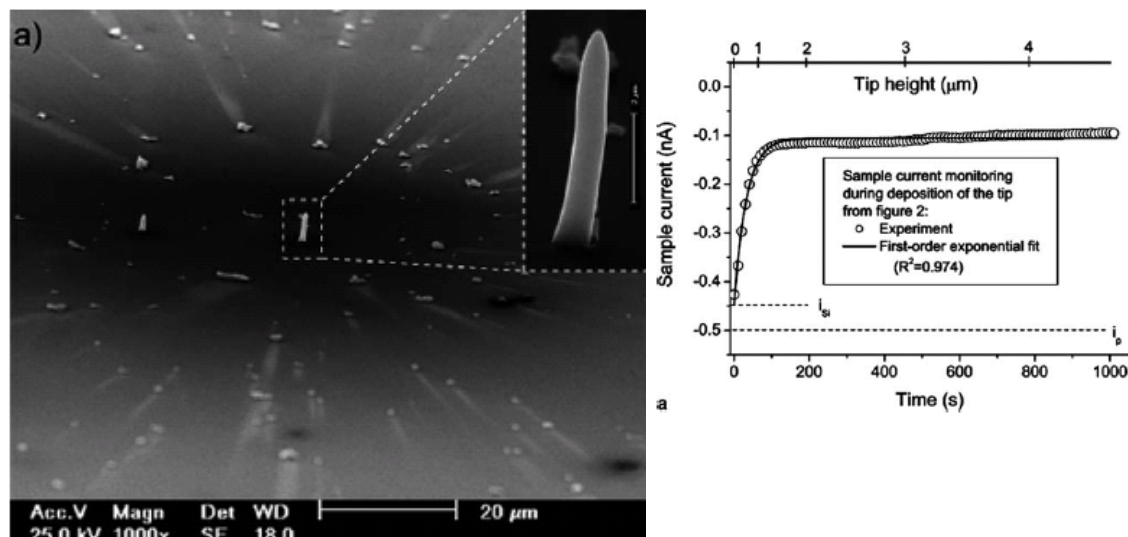


In the third paper by Bret et al.,⁷⁶⁵ a tapered vertical pillar of iridium metal (Figure 6-15) is deposited on a “naturally oxidized” silicon surface (i.e., SiO_2) using an $[\text{IrCl}(\text{PF}_3)_2]_2$ precursor and a beam voltage of 25 kV (500 pA current). (A rhodium nanowire was similarly deposited, though not in a columnar shape, using $[\text{RhCl}(\text{PF}_3)_2]_2$ precursor.) The tip has a curvature radius of ~ 150 nm (just small enough), but unfortunately is not very pure – electron-dispersive X-ray microanalysis suggests an average composition of IrClP, with a density of only 13.4 kg/m^3 (vs. 22.4 kg/m^3 for pure Ir metal). It is currently unknown whether or not the addition of a co-dosing gas such as H_2 or O_2 to the precursor gas might produce a higher-purity noble metal nanowire, but such a prospect seems plausible and this issue could be resolved by further experimental work.

⁷⁶⁴ In-Seop Lee, R.A. Buchanan, Young-Hee Lee, “Charge injection properties of iridium films formed by ion beam assisted deposition,” J. Mater. Sci. Lett. 21(2002):1859-1861; [http://yhlee.yonsei.ac.kr/PDF/Ir\(letter\).pdf](http://yhlee.yonsei.ac.kr/PDF/Ir(letter).pdf).

⁷⁶⁵ Tristan Bret, Ivo Utke, Patrik Hoffmann, Maurice Abourida, Pascal Doppelt, “Electron range effects in focused electron beam induced deposition of 3D nanostructures,” Microelectron. Eng. 83(April-September 2006):1482-1486.

Figure 6-15. (A) Left: SEM tilted views of an experimentally-obtained iridium tip deposited at 25 kV and 500 pA with a 16 ms dwell time and a 30 nm/sec lateral speed, on a SiO_2 surface, from $[\text{IrCl}(\text{PF}_3)_2]_2$. (B) Right: In-situ sample electrical current evolution during deposition of the iridium ($\sim\text{IrCIP}$) tip.⁷⁶⁶



Gong et al.⁷⁶⁷ have also deposited extremely smooth iridium (Ir) thin films on Si(100) substrate at relatively low temperature ($< 300\text{ }^{\circ}\text{C}$) by a pulsed laser deposition (PLD) technique using an iridium target (metal source) in a vacuum atmosphere. PLD produced well-crystallized and single-phase Ir thin films with (111) preferred orientation at a silicon substrate temperature of $200\text{--}300\text{ }^{\circ}\text{C}$, with surface roughness increasing and room-temperature resistivity decreasing when higher substrate temperatures are used. A metalorganic chemical vapor deposition (MOCVD) method using $\text{Ir}(\text{EtCp})(1,5\text{COD})$ [iridium(ethylcyclopentadienyl)(1,5-cyclooctadiene)] precursor has been demonstrated⁷⁶⁸ for depositing Ir thin films on SiO_2 substrate and it was found that growth rates ($0.05\text{--}4.6\text{ nm/min}$) were highly influenced by oxygen flow; perhaps a focused oxygen beam might encourage growth of a metallic column, similar to EBID. Various methods of depositing Ir thin films directly onto fused SiO_2 have “spalled over the entire sample surface, likely due to residual stress between the $\{\text{SiO}_2\}$ substrate and the depositing $\{\text{Ir}\}$ film”;⁷⁶⁹

⁷⁶⁶ Tristan Bret, Ivo Utke, Patrik Hoffmann, Maurice Abourida, Pascal Doppelt, “Electron range effects in focused electron beam induced deposition of 3D nanostructures,” *Microelectron. Eng.* 83(April-September 2006):1482-1486.

⁷⁶⁷ Yansheng Gong, Chuanbin Wang, Qiang Shen, Lianmeng Zhang, “Low-temperature deposition of iridium thin films by pulsed laser deposition,” *Vacuum* 82(19 February 2008):594-598.

⁷⁶⁸ Yves Ritterhaus, Tetyana Hur'yeva, Marco Lisker, Edmund Paul Burte, “Iridium Electrodes for Ferroelectric Capacitors Deposited by Liquid-Delivery MOCVD,” *MRS Proc.* (Fall 2005).

⁷⁶⁹ M.R. Behfrooz, “Study of Iridium (Ir) Thin Films Deposited on to SiO_2 Substrates,” *Journal of Sciences, Islamic Republic of Iran* 16(2005):175-182; http://www.sid.ir/En/VEWSSID/J_pdf/97320050203.pdf.

predepositing a thin intermediate layer of chromium (Cr) between the SiO₂ and Ir layers apparently “decreases residual stress and enhances film adhesion,” producing a film with surface roughness less than 1 nm.⁷⁷⁰ (EBID processes for Cr are known.⁷⁷¹)

In addition, we note that the pure-metal nanowire with pyramidal tip method described by Kuo et al.⁷⁷² (Section 5.5) may also be workable using Pt, Pd and Rh metals, as well as Ir. Conveniently, positionally-controlled EBID has been demonstrated for Pt using Pt(PF₃)₄ precursor on a Cr-coated Si(100) substrate,⁷⁷³ for Pd using Pd(OOCCH₃)₂ (liquid palladium acetate) precursor to write 50 nm features,⁷⁷⁴ and for Rh⁷⁷⁵ using [RhCl(PF₃)₂]₂ precursor.⁷⁷⁶ (A chemically similar precursor for Ir exists⁷⁷⁷ and has been used to write pillars via EBID,⁷⁷⁸ as noted earlier.)

⁷⁷⁰ M.R. Behfroz, “Study of Iridium (Ir) Thin Films Deposited on to SiO₂ Substrates,” Journal of Sciences, Islamic Republic of Iran 16(2005):175-182; http://www.sid.ir/En/VEWSSID/J_pdf/97320050203.pdf.

⁷⁷¹ Shinji Matsui, Katsumi Mori, “New selective deposition technology by electron-beam induced surface reaction,” Journal of Vacuum Science & Technology B 4(1986):299-304; <http://dx.doi.org/10.1116/1.583317>.

⁷⁷² Hong-Shi Kuo, Ing-Shouh Hwang, Tsu-Yi Fu, Ying-Siang Hwang, Yi-Hsien Lu, Chun-Yueh Lin, Jin-Long Hou, Tien T. Tsong, “A single-atom sharp iridium tip as an emitter of gas field ion sources,” Nanotechnology 20(19 August 2009):335701. Hong-Shi Kuo, Ing-shouh Hwang, Tien T. Tsong, Tsu-Yi Fu, “Atomically Sharp Iridium Tip,” IPC8 Class: AB21G100FI, USPC Class: 428600, 2009; <http://www.faqs.org/patents/app/20090110951>.

⁷⁷³ S. Wang, Y.-M. Sun, Q. Wang, J.M. White, “Electron-beam induced initial growth of platinum films using Pt(PF₃)₄,” Journal of Vacuum Science & Technology B 22(July 2004):1803-1806; <http://dx.doi.org/10.1116/1.1761266>.

⁷⁷⁴ T.J. Stark, T.M. Mayer, D.P. Griffis, P.E. Russell, “Formation of Complex Features using Electron-Beam Direct-Write Decomposition of Palladium Acetate,” Journal of Vacuum Science & Technology B 10(November 1992):2685-2690. T.J. Stark, T.M. Mayer, D.P. Griffis, P.E. Russell, “Electron Beam Induced Metallization of Palladium Acetate,” J. Vac. Sci. Technol. B 9(November 1991):3475-3478; <http://dx.doi.org/10.1116/1.585826>.

⁷⁷⁵ T. Bret, I. Utke, A. Bachmann, P. Hoffmann, “In situ control of the focused-electron-beam-induced deposition process,” Applied Physics Letters 83(2003):4005-4007.

⁷⁷⁶ P. Hoffmann, I. Utke, F. Cicoira, B. Dwir, K. Leifer, E. Kapon, P. Doppelt, “Focused electron beam induced deposition of gold and rhodium,” Materials Research Society Symposium - Proceedings 624(2000):171-177. Fabio Cicoira, “Electron Beam Induced Deposition Of Rhodium Nanostructures,” Thèse No. 2528, École Polytechnique Fédérale De Lausanne, 2002; http://biblion.epfl.ch/EPFL/theses/2002/2528/EPFL_TH2528.pdf. F. Cicoira, K. Leifer, P. Hoffmann, I. Utke, B. Dwir, D. Laub, P.A. Buffat, E. Kapon, P. Doppelt, “Electron beam induced deposition of rhodium from the precursor [RhCl(PF₃)₂]₂: Morphology, structure and chemical composition,” Journal of Crystal Growth 265(2004):619-626; <http://dx.doi.org/10.1016/j.jcrysgro.2004.02.006>.

⁷⁷⁷ M.A. Bennett, J. Patmore, “Four and Five-Coordinate complexes of Rhodium and Iridium Containing Trifluorophosphine,” Inorg. Chem. 10(November 1971):2387-2395.

One potential problem is that EBID often produces deposits of low purity; e.g., during EBID of Rh, only 60% Rh is found in the deposit.⁷⁷⁹ IBID processes often produce structures with higher purity and a higher deposition rate. Fortunately, it appears that 95% purity for EBID can at least sometimes be achieved by using ultraclean conditions in 10^{-10} mbar UHV which minimizes contamination from the residual gas.⁷⁸⁰

Presently, there are three conceptual approaches⁷⁸¹ followed for obtaining pure deposit material with kV beams. They comprise the use of (1) inorganic molecules, (2) additional reactive gases, and (3) UHV systems:

(1) Inorganic molecules are presently limited in variety to a few metal hydrides, metal halides, and metal trifluorophosphines. The stability and the handling of these precursors are delicate and it would be desirable for the future to have less sensitive (moisture, light, and spontaneous decomposition) and less toxic molecules at hand. As simple rule of thumb, the precursor with highest probability of obtaining the desired product is a poorly stable compound, which decomposes thermally at a temperature slightly above the substrate temperature to the wanted product. This precursor should not contain polymerizable ligand atoms such as C, S, and, to a lower extent, P.

(2) Adding reactive gases forms volatile reaction products with unwanted codeposits, mostly hydrocarbons. Using an oxidizing reactive gas additionally removes oxygen deficiencies of the deposited material and worked very well for oxide deposition. A reducing reactive gas should be used if metal oxides must be avoided.

(3) The use of UHV systems for pure metal deposition proved very recently successful for iron. It will be the issue of further research if this is the case also for other molecules.

Iridium thin films have also been grown by atomic layer deposition (ALD),⁷⁸² e.g., using $\text{Ir}(\text{acac})_3$ (acac = acetylacetonato), ozone, and molecular hydrogen as precursors at low

⁷⁷⁸ Tristan Bret, Ivo Utke, Patrik Hoffmann, Maurice Abourida, Pascal Doppelt, "Electron range effects in focused electron beam induced deposition of 3D nanostructures," *Microelectron. Eng.* 83(April-September 2006):1482-1486.

⁷⁷⁹ Fabio Cicoira, "Electron Beam Induced Deposition Of Rhodium Nanostructures," Thèse No. 2528, École Polytechnique Fédérale De Lausanne, 2002; http://biblion.epfl.ch/EPFL/theses/2002/2528/EPFL_TH2528.pdf.

⁷⁸⁰ Hans-Peter Steinrück, "Electron beam induced deposition of nanostructures," Research Profile, Page 3; http://www.chemie.uni-erlangen.de/img/uploaded/1241450875_HPS_Research.pdf.

⁷⁸¹ Ivo Utke, Patrik Hoffmann, John Melngailis, "Gas-assisted focused electron beam and ion beam processing and fabrication," *J. Vac. Sci. Technol. B* 26(July 2008):1197-1276.

⁷⁸² O. Jylhä, R. Saarinen, M. Lindblad, O. Krause, "Iridium on porous supports prepared by ALD for heterogeneous catalysis applications," ALD 2004, Helsinki, 16-18 August 2004. Titta Aaltonen, Mikko Ritala, Väino Sammelselg, Markku Leskela, "Atomic Layer Deposition of Iridium Thin Films," *J. Electrochem. Soc.* 151(2004):G489-G492. Jani Hmlinen, Esa Puukilainen, Marianna Kemell, Leila Costelle, Mikko Ritala, Markku Leskel, "Atomic Layer Deposition of Iridium Thin Films by Consecutive Oxidation and Reduction Steps," *Chem. Mater.* 21(2009):4868-4872.

temperatures between 165 and 200 °C.⁷⁸³ (At this temperature range, iridium oxide film results in a process without H₂, therefore H₂ has a reducing effect on the film after the oxidizing ozone pulse.) Iridium metal films were successfully deposited on Al₂O₃ nucleation layers but also directly on bare soda lime glasses and native oxide covered silicon substrates. About 60 nm thick films had resistivities and roughnesses less than 12 μΩ cm and 1.4 nm, respectively; the films contained ≤ 2 atom % hydrogen, ≤ 1 atom % carbon, and 4–7 atom % oxygen as impurities. The iridium films had a preferred (111) crystal orientation even at the lowest growth temperatures.⁷⁸⁴ Other noble metals can also be grown via ALD.⁷⁸⁵ Growing an Ir nanowire using ALD might require coating the quartz fork with a coating that resists deposition except at the desired spot (which is clear of the resist), followed by ALD and the subsequent removal of the resist, in order to establish positional control over the site of deposition. Fairly pure iridium metal CVD thin films have been deposited on various ceramic substrates using complex metallorganic precursors such as ((methylcyclopentadienyl) (1,5-cyclooctadiene))iridium,⁷⁸⁶ iridium acetylacetonate co-dosed with O₂,⁷⁸⁷ dicarbonylacetylacetonate iridium co-dosed with O₂,⁷⁸⁸ and iridium carbonyl (tetrakisiridium dodecacarbonyl)⁷⁸⁹ or iridium(I) carbonyl⁷⁹⁰ (measurements of electron beam

⁷⁸³ Jani Hmlinen, Esa Puukilainen, Marianna Kemell, Leila Costelle, Mikko Ritala, Markku Leskel, "Atomic Layer Deposition of Iridium Thin Films by Consecutive Oxidation and Reduction Steps," *Chem. Mater.* 21(2009):4868-4872.

⁷⁸⁴ T. Aaltonen, M. Ritala, Y.-L. Tung, Y. Chi, K. Arstila, K. Meinander, M. Leskelä, "Atomic Layer Deposition of Noble Metals: Exploration of the Low Limit of the Deposition Temperature," *J. Mater. Res.* 19(2004):3353-3358. O. Jylhä, R. Saarinen, M. Lindblad, O. Krause, "Iridium on porous supports prepared by ALD for heterogeneous catalysis applications," ALD 2004, Helsinki, 16-18 August 2004. Titta Aaltonen, Mikko Ritala, Väino Sammelselg, Markku Leskela. "Atomic Layer Deposition of Iridium Thin Films," *J. Electrochem. Soc.* 151(2004):G489-G492.

⁷⁸⁵ Titta Aaltonen, "Atomic Layer Deposition of Noble Metal Thin Films," PhD thesis, University of Helsinki, Helsinki, Finland, 2005;
<http://www.cambridgenanotech.com/theses/Atomic%20Layer%20Deposition%20of%20Noble%20Metal%20Thin%20Films.pdf>.

⁷⁸⁶ Y.-M. Sun, X.-M. Yan, N. Mettlach, J. P. Endle, P. D. Kirsch, J. G. Ekerdt, S. Madhukar, R. L. Hance, J. M. White, "Precursor chemistry and film growth with (methylcyclopentadienyl) (1,5-cyclooctadiene)iridium," *J. Vac. Sci. Technol. A* 18(January 2000):10-16.

⁷⁸⁷ Y-M. Sun, J. Endle, K. Smith, J. G. Ekerdt, R. L. Hance, P. Alluri, J. M. White, "Metallorganic Chemical Vapor Deposition of Ir Films With Iridium Acetylacetonate and Carbonyl Precursors," *Ferroelectric Thin Films VII*, 30 Nov.-3 Dec. 1998, Boston, MA; *Proceedings of the Symposium*, 1999, pp. 101-106.

⁷⁸⁸ Y-M. Sun, J. Endle, K. Smith, J. G. Ekerdt, R. L. Hance, P. Alluri, J. M. White, "Metallorganic Chemical Vapor Deposition of Ir Films With Iridium Acetylacetonate and Carbonyl Precursors," *Ferroelectric Thin Films VII*, 30 Nov.-3 Dec. 1998, Boston, MA; *Proceedings of the Symposium*, 1999, pp. 101-106.

⁷⁸⁹ Y-M. Sun, J. Endle, K. Smith, J. G. Ekerdt, R. L. Hance, P. Alluri, J. M. White, "Metallorganic Chemical Vapor Deposition of Ir Films With Iridium Acetylacetonate and Carbonyl Precursors," *Ferroelectric Thin Films VII*, 30 Nov.-3 Dec. 1998, Boston, MA; *Proceedings of the Symposium*, 1999, pp. 101-106.

induced perturbations of CO chemisorbed on Ir(111) found that electron-stimulated dissociation occurs at only 1-2% of the rate of stimulated desorption).⁷⁹¹

Finally, iridium cannot easily be electroplated from aqueous solutions⁷⁹² but it can be electrodeposited from molten salts,⁷⁹³ a process that might be useful if a sub-micron-size electrode surrounded by insulator could be fabricated at the desired position on the quartz tuning fork surface.

6.2.3 Step 2: Surface Cleaning and Annealing

In the second step, described by Kuo et al.⁷⁹⁴ as “surface cleaning”, the iridium nanowire is placed in a vacuum chamber containing an oxygen atmosphere at an oxygen partial pressure of $P_{O_2} = 2 \times 10^{-7}$ Torr, then is thermally flashed several times at 1500 °C for 2 seconds or less each time. This has the effect of dislodging and eliminating any surface impurities.

Because it has already been demonstrated experimentally, we know that the Plan A (wire attachment) process described in Step 1 will produce a clean noble metal apex surface after thermal flashing. The Kuo et al. patent⁷⁹⁵ describes the original iridium feedstock wire from

⁷⁹⁰ Y.-L. Chen, C.-C. Hsu, Y.-H. Song, Y. Chi, A. J. Carty, S.-M. Peng, G.-H. Lee, “Iridium Metal Thin Films and Patterned IrO₂ Nanowires Deposited Using Iridium(I) Carbonyl Precursors,” *Chemical Vapor Deposition* 12(2006):442-447.

⁷⁹¹ M.L. Shek, S.P. Withrow, W.H. Weinberg, “Electron beam induced desorption and dissociation of CO chemisorbed on Ir(111),” *Surf. Sci.* 72(April 1978):678-692.

⁷⁹² “Electrodeposition of Iridium: Progress In Deposition From Aqueous Solutions,” *Platinum Metals Rev.* 10(1966):59; <http://www.platinummetalsreview.com/pdf/pmr-v10-i2-059-059.pdf>. “Vapour Phase Deposition of Iridium: New Techniques For Applying Coatings On Graphite,” *Platinum Metals Rev.* 12(1968):62-63; <http://www.platinummetalsreview.com/pdf/pmr-v12-i2-062-063.pdf>. N.A. Saltykova, O.V. Portnyagin, “Electrodeposition of Iridium–Ruthenium Alloys from Chloride Melts: the Structure of the Deposits,” *Russian Journal of Electrochemistry* 37(September 2001):924-930.

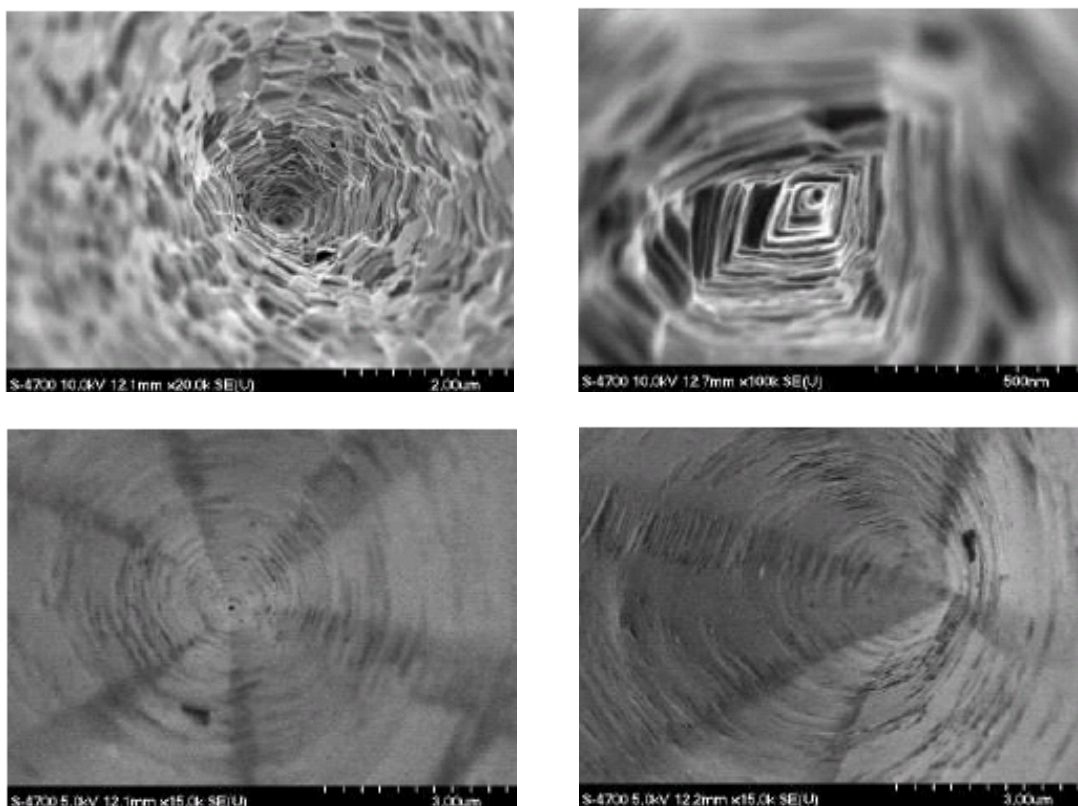
⁷⁹³ N.A. Saltykova, O.V. Portnyagin, “Electrodeposition of Iridium–Ruthenium Alloys from Chloride Melts: the Structure of the Deposits,” *Russian Journal of Electrochemistry* 37(September 2001):924-930. David Schlain, Frank X. McCawley, Gerald R. Smith, “Electrodeposition of Platinum Metals from Molten Cyanides: A Technique Applicable to Electroforming,” *Platinum Metals Rev.* 21(1977):38-42; <http://www.platinummetalsreview.com/pdf/pmr-v21-i2-038-042.pdf>.

⁷⁹⁴ Hong-Shi Kuo, Ing-Shouh Hwang, Tsu-Yi Fu, Ying-Siang Hwang, Yi-Hsien Lu, Chun-Yueh Lin, Jin-Long Hou, Tien T. Tsong, “A single-atom sharp iridium tip as an emitter of gas field ion sources,” *Nanotechnology* 20(19 August 2009):335701. Hong-Shi Kuo, Ing-shouh Hwang, Tien T. Tsong, Tsu-Yi Fu, “Atomically Sharp Iridium Tip,” IPC8 Class: AB21G100FI, USPC Class: 428600, 2009; <http://www.faqs.org/patents/app/20090110951>.

⁷⁹⁵ Hong-Shi Kuo, Ing-shouh Hwang, Tien T. Tsong, Tsu-Yi Fu, “Atomically Sharp Iridium Tip,” IPC8 Class: AB21G100FI, USPC Class: 428600, 2009; <http://www.faqs.org/patents/app/20090110951>.

which the nanowire is etched (in their process) as “a polycrystalline Ir wire having a diameter of 100 microns and a length of about 5 mm” (Figure 6-16A).

Figure 6-16. (A) Top: SEM images showing a top view of two polycrystalline tungsten tips; the tip surface is very rough because the tip is composed of differently oriented crystallites. (B) Bottom: SEM images showing top views of a single-crystal (111)-oriented tungsten tip; the surface is smooth and uniform due to the constant orientation of the wire, and a clear three-fold symmetry can be observed about the (111) direction.⁷⁹⁶



This means that the feedstock wire most likely consists of randomly- or semirandomly-oriented metal nanocrystals or nanoscale metal single-crystal domains, with the result that the tip of the metal does not consist of a single preferred crystallographic plane but rather consists of some

⁷⁹⁶ Anne-Sophie Lucier, “Preparation and Characterization of Tungsten Tips Suitable for Molecular Electronics Studies,” M.S. Thesis, Center for the Physics of Materials, Department of Physics, McGill University, Montreal, Quebec, Canada, February 2004; <http://www.physics.mcgill.ca/~peter/theses/lucier.pdf>. See also: Anne-Sophie Lucier, Henrik Mortensen, Yan Sun, and Peter Grütter, “Determination of the atomic structure of scanning probe microscopy tungsten tips by field ion microscopy,” Phys. Rev. B 72, 235420 (2005).

mixture of such planes. Following the tip-sharpening etch process recommended by Kuo et al.,⁷⁹⁷ it seems likely that the randomized crystal plane character of the nanowire apex would persist. Similarly, any iridium metal nanowires produced via IBID or EBID are likely to be largely amorphous though probably with some embedded nanocrystals. For example, in the case of Rh cited earlier, structural analysis and TEM revealed that, independently of the deposition conditions, the EBID-deposited material was made up of Rh nanocrystals immersed in a lighter amorphous matrix.⁷⁹⁸

On the other hand, if a beam-assisted deposition (Plan B) is chosen in Step 1 ([Section 6.2.1](#)), the nanowire metal is unlikely to be as pure as if a bulk-manufactured wire is attached as in Plan A. Because it apparently has not yet been reported experimentally, we don't know if the Plan B (beam deposition) approach as described in Step 1 will produce a clean noble metal apex surface after thermal flashing, nor do we know if such a surface will facetize under thermal annealing as required in Step 3. The answer to these questions must be resolved by future experimental work. If the chemical and crystallographic differences at the nanowire apex present a problem for Step 3 ([Section 6.2.3](#)) of the tip-system fabrication method proposed here, there are two possible solutions.

First, it may be possible to increase the purity of the deposited iridium nanowire via thermal or laser annealing, possibly in a special atmosphere such as hydrogen which could help carry off the liberated contaminants. Such annealing could also convert more of the amorphous material into polycrystalline material, moving the atomic structure of the beam-deposited nanowire somewhat closer to the structure of the bulk-produced nanowire that has been demonstrated, experimentally, to work.

Second, a source of pure iridium metal could be vaporized and applied via IBID as a thin coating (perhaps 10 nm thick) to overlay the entire relatively-impure beam-deposited nanowire. The immediate vicinity of the attachment site of the nanowire to the quartz fork might also receive a thin coating of pure Ir due to “splattering” or “overspray” (e.g., see the darkened region on the SiO₂ surface around the grown Ir nanowire shown in [Figure 6-15A](#); [Section 6.2.2](#)), but there is a good chance that this would not impair the function of the tuning fork sensor – another unknown that could be firmly resolved by experimental work.

⁷⁹⁷ Hong-Shi Kuo, Ing-Shouh Hwang, Tsu-Yi Fu, Ying-Siang Hwang, Yi-Hsien Lu, Chun-Yueh Lin, Jin-Long Hou, Tien T. Tsong, “A single-atom sharp iridium tip as an emitter of gas field ion sources,” *Nanotechnology* 20(19 August 2009):335701. Hong-Shi Kuo, Ing-shouh Hwang, Tien T. Tsong, Tsu-Yi Fu, “Atomically Sharp Iridium Tip,” IPC8 Class: AB21G100FI, USPC Class: 428600, 2009; <http://www.faqs.org/patents/app/20090110951>.

⁷⁹⁸ Fabio Cicoira, “Electron Beam Induced Deposition Of Rhodium Nanostructures,” Thèse No. 2528, École Polytechnique Fédérale De Lausanne, 2002; http://biblion.epfl.ch/EPFL/theses/2002/2528/EPFL_TH2528.pdf.

6.2.4 Step 3: Formation of Pyramidal SAT at the Apex

In the third step (SAT formation) using the process demonstrated experimentally by Kuo et al.,⁷⁹⁹ and at the same oxygen pressure (2×10^{-7} Torr) as for the surface cleaning in Step 2 ([Section 6.2.2](#)), the iridium nanowire would be annealed at 400-600 °C for 5 minutes. The atomic structure of the Ir tip should then reorganize into an apical pyramid (i.e., the three-sided pyramidal structure) with a single metal atom in the top position, resulting in the formation of an iridium SAT on the sharp end of the Ir nanowire (resembling the atomic hardball model; [Figure 5-20](#)) after the aforementioned treatments. If the pyramidal SAT is damaged during use, the original SAT can be recovered just by repeating the Step 3 procedure once again. The regenerated pyramid will have the same atomic stacking structure. In addition, only one SAT nanopyramid is formed on the sharp end of the Ir wire as long as the sharp end of the wire has a radius less than 200 nm after Steps 1 and 2 have been completed.

Note that the heating required for thermal annealing might more conveniently be applied via focused laser heating or focused electron beam bombardment of the tip. (Single-atom tips are not destroyed when irradiated with 150-MHz optical laser pulses.)⁸⁰⁰ This would eliminate the need either (1) to move the tip assembly from the vacuum chamber into a baking furnace or (2) to heat the entire vacuum chamber, during DMS operations that will most likely be taking place at cryogenic temperatures.

6.2.5 Step 4: Formation of Electrical Contacts

After Step 3 is complete, the macroscale quartz tuning fork must be affixed to a larger (possibly ceramic) qPlus sensor handle structure, and electrical connections must be made between that handle structure and the quartz fork. IBID or EBID processes could be used for both tasks – both to attach the fork to the handle and to coat the tuning fork surfaces with conductive metals to provide the necessary electrical contacts.

Besides conductivity and adequate wetting of quartz and metal surfaces, the primary constraint on EBID materials to be used in Step 4 is thermal lability. More specifically, to induce the Ir pyramidal facets to self-assemble (or to re-form the pyramids by subsequent annealing, if the SAT tip gets damaged during use), it must be possible to bake the whole qPlus device at an annealing temperature of 400-600 °C (673-873 K) for the iridium qPlus tip system fabrication process described in [Section 6.2](#) (and Step 3 described in [Section 6.2.3](#), in particular); and for some of the processes described in [Section 6.3](#) for the tungsten-iridium qPlus tip system

⁷⁹⁹ Hong-Shi Kuo, Ing-Shouh Hwang, Tsu-Yi Fu, Ying-Siang Hwang, Yi-Hsien Lu, Chun-Yueh Lin, Jin-Long Hou, Tien T. Tsong, “A single-atom sharp iridium tip as an emitter of gas field ion sources,” *Nanotechnology* 20(19 August 2009):335701. Hong-Shi Kuo, Ing-shouh Hwang, Tien T. Tsong, Tsu-Yi Fu, “Atomically Sharp Iridium Tip,” IPC8 Class: AB21G100FI, USPC Class: 428600, 2009; <http://www.faqs.org/patents/app/20090110951>.

⁸⁰⁰ Peter Hommelhoff, Catherine Kealhofer, Anoush Aghajani-Talesh, Yvan R.P. Sortais, Seth M. Foreman, Mark A. Kasevich, “Extreme localization of electrons in space and time,” *Ultramicroscopy* 109(2009):423-429.

fabrication and operation, even higher baking temperatures up to 1000-1300 K may be required. The “device” certainly includes the pyramidal formed tip, the quartz fork, the ceramic handle structure, and any electrical contacts on the handle structure, but perhaps not the associated preamplifier electronics (**Figure 6-4**) if these can be designed as an easily detached module.

The melting point for quartz is 1883 K, well above all proposed SAT-baking temperatures, and most ceramics (that might be used in the large qPlus handle structure) are thermally stable to even higher temperatures. So the thermal lability issue pertains mainly to the choice of metal for making electrical connections. Some obvious alternatives, listed in descending order of electrical conductivity and all experimentally demonstrated to be capable of beam-induced or beam-assisted deposition (**Table 6-2**), are as follows:

(1) **Silver.** Ag is the best known conductor ($k = 6.3 \times 10^7 \text{ ohm}^{-1}\text{m}^{-1}$) and has a melting point of 1234 K, which is fine for the iridium qPlus tip system but might not be quite high enough for the tungsten-iridium qPlus tip system.

(2) **Copper.** Cu is the second-best conductor ($k = 5.9 \times 10^7 \text{ ohm}^{-1}\text{m}^{-1}$) and has a melting point of 1356 K, which is in the same rank as gold. However, copper metal in contact with SiO_2 may oxidize.

(3) **Gold.** In commercial qPlus tips, and in tuning forks used in wristwatches, the usual soldering metal is gold. Au has a good volume conductivity of $k = 4.1 \times 10^7 \text{ ohm}^{-1}\text{m}^{-1}$ and melts at 1336 K which is close to the maximum SAT-cooking temperature that we need to use, but probably high enough for most purposes. Gold metal in contact with SiO_2 is unlikely to oxidize. Since gold can be beam-deposited to >95% purity,⁸⁰¹ this metal may be the best choice if the relatively modest melting point temperature is acceptable.

(4) **Aluminum.** Al is a very good conductor ($k = 3.6 \times 10^7 \text{ ohm}^{-1}\text{m}^{-1}$) but has a melting point of only 933 K, which may be fine for the iridium qPlus tip system but is probably unusable for the tungsten-iridium qPlus tip system.

(5) **Iridium.** Ir is a good conductive metal ($k = 2.0 \times 10^7 \text{ ohm}^{-1}\text{m}^{-1}$) with a high melting point of 2683 K. The metal can be beam-deposited on SiO_2 ,⁸⁰² and probably on other ceramics as well. Iridium may be the all-around safest alternative if the metal is already being beam-deposited in the tip-system fabrication method of choice.

⁸⁰¹ I. Utke, P. Hoffmann, B. Dwir, K. Leifer, E. Kapon, P. Doppelt, “Focused electron beam induced deposition of gold,” J. Vac. Sci. Technol. B 18(November 2000):3168-3171. T. Brintlinger, M.S. Fuhrer, J. Melngailis, I. Utke, T. Bret, A. Perentes, P. Hoffmann, M. Abourida, P. Doppelt, “Electrodes for carbon nanotube devices by focused electron beam induced deposition of gold,” J. Vac. Sci. Technol. B 23(November 2005):3174-3177; <http://www.physics.umd.edu/mfuhrer/publications/FEBID.pdf>.

⁸⁰² P. Hoffmann, H. Vandenbergh, J. Flicstein, G. Benassayag, J. Gierak, J.F. Bresse, “Direct Writing of Iridium Lines with a Focused Ion-Beam,” Journal of Vacuum Science & Technology B 9(November 1991):3483-3486. Tristan Bret, Ivo Utke, Patrik Hoffmann, Maurice Abourida, Pascal Doppelt, “Electron range effects in focused electron beam induced deposition of 3D nanostructures,” Microelectron. Eng. 83(April-September 2006):1482-1486.

(6) **Tungsten.** W is a good conductive metal ($k = 1.8 \times 10^7 \text{ ohm}^{-1}\text{m}^{-1}$), about one-third as conductive as silver or copper, with one of the highest melting points of any metal at 3683 K. In the case of the tungsten-iridium qPlus tip system, a facility to EBID the metal will already be in place. One potential problem is oxidation on an SiO_2 surface (and perhaps on other ceramic oxides, if they are used for the sensor handle structure. If W is deposited on SiO_2 some oxide contamination of the pure metal might be anticipated, and further study would be required to determine if the amount of such contamination would seriously affect the conductivity of the electrical connections formed by this metal.

(7) **Chromium.** Cr is a fairly conductive metal ($k = 7.8 \times 10^6 \text{ ohm}^{-1}\text{m}^{-1}$) with a sufficiently high melting point of 2163 K, and is capable of EBID deposition.

(8) **Rhenium.** Re metal is only a fair electrical conductor ($k = 5.4 \times 10^6 \text{ ohm}^{-1}\text{m}^{-1}$). It can be deposited using $\text{Re}_2(\text{CO})_{10}$ gas “consists of a single pure rhenium phase” after annealing at 1073 K, which could be used “to produce highly conductive nanowires and tips for application in nanoelectronics, emission electronics (Figure 6-9B), and STM”.⁸⁰³ Rhenium has a very high melting point of 3453 K.

6.3 Tungsten-Iridium qPlus Tip System

The approach proposed in this section also employs electron-beam-induced deposition (EBID) processes to achieve unitary fabrication of SAT qPlus tip systems. The proposed method again starts with a (macroscale) quartz tuning fork (Section 6.1), ideally still residing on a lithographically-produced wafer (Table 6-1) or, alternatively, acquired from a wristwatch (Figure 6-1A). The fork is then placed in a vacuum chamber and 3 fabrication steps are performed, as described in the following subsections. The result is a finished qPlus quartz tuning-fork-mounted noble-metal-based SAT tip, ready to go into the molecular workstation metrology apparatus.

6.3.1 Step 1: Attach Tungsten Nanowire to Quartz Fork

Plan A. The very simplest way to perform this step would be to mount a single-crystal tungsten wire oriented to expose the W(111) surface at the apex (Figure 6-16B). Such wires can be purchased commercially, and the flat W(111) crystal face has been demonstrated to induce pyramidal faceting by a number of noble metals including Au, Ir, Pd, Pt and Rh (Section 5.3).

In Plan A, we first position the tungsten wire atop the prong in an appropriate position and orientation, then IBID- or EBID-solder the wire to the prong – the EBID layers act as a binder as the deposited amorphous material “welds” the wire to the prong (Figure 6-12).⁸⁰⁴ (Gas-assisted

⁸⁰³ N.A. Kislov, I.I. Khodos, E.D. Ivanov, J. Barthel, “Electron-beam-induced fabrication of metal-containing nanostructures,” *Scanning* 18(1996):114-118; http://www.mpi-halle.de/mpi/publi/pdf/1749_96.pdf.

⁸⁰⁴ MinFeng Yu, Mark J. Dyer, George D. Skidmore, Henry W. Rohrs, Xue Kun Lu, Kevin D. Ausman, James Von Ehr, Rodney S. Ruoff, “3 Dimensional Manipulation of Carbon Nanotubes under a Scanning

FEB and FIB are often used as attachment tools for carbon nanotubes or nanowires onto AFM tips or microelectromechanical system structures.)⁸⁰⁵ After that, ion or electrochemical etching (Section 3.12) or other means of tip sharpening is used to produce a tapered geometry at the distal end of the already-attached wire so that the tapered tip has a curvature radius on the order of 50 nm, a tip size that has been demonstrated to work by Kuo et al..⁸⁰⁶ Alternatively, the single-crystal W wire could be sharpened first, then welded to the quartz fork prong via EBID. Further analysis is required to determine the ideal order of these operations.

After the tapered nanowire is attached, FEB-induced etching can be used to trim excess wire from the shank end nearest to the prong, resulting in a clean attachment to the qPlus sensor assembly.

Electron Microscope,” Sixth Foresight Nanotechnology Conference, November 1998; <http://www.foresight.org/Conferences/MNT6/Papers/Yu/index.html> . See also: Robert F. Service, “AFMs Weld Parts for Nanoconstruction,” *Science* 282(27 November 1998):1620-1621. H.W.P. Koops, R. Weiel, D.P. Kern, T.H. Baum, “High-resolution electron-beam induced deposition,” *J. Vac. Sci. Technol. B* 6(January 1988):477-481. <http://dx.doi.org/10.1116/1.584045>.

⁸⁰⁵ Min-Feng Yu, Oleg Lourie, Mark J. Dyer, Katerina Moloni, Thomas F. Kelly, Rodney S. Ruoff, “Strength and Breaking Mechanism of Multiwalled Carbon Nanotubes Under Tensile Load,” *Science* 287(28 January 2000):637-640; http://www.bimat.org/assets/pdf/00_287yu.pdf. Lixin Dong, Fumihito Arai, Toshio Fukuda, “Electron-beam-induced deposition with carbon nanotube emitters,” *Appl. Phys. Lett.* 81(2002):1919-1921; http://www.egr.msu.edu/~ldong/Publication/JP200203_APL_81_1919_Dong.pdf. P.A. Williams, S.J. Papadakis, M.R. Falvo, A.M. Patel, M. Sinclair, A. Seeger, A. Helser, R.M. Taylor, S. Washburn, R. Superfine, “Controlled placement of an individual carbon nanotube onto a microelectromechanical structure,” *Appl. Phys. Lett.* 80(2002):2574-2576; <http://www.cs.unc.edu/~seeger/publications/2002Williams.CNTMEMS.APL2002.pdf>. W. Ding, D.A. Dikin, X. Chen, R.D. Piner, R.S. Ruoff, E. Zussman, X. Wang, X. Li, “Mechanics of hydrogenated amorphous carbon deposits from electron-beam-induced deposition of a paraffin precursor,” *J. Appl. Phys.* 98(2005):014905; http://bimat.org/assets/pdf/nu_05_98ding.pdf. S. Orso, U.G.K. Wegst, C. Eberl, E. Arzt, “Micrometer-scale tensile testing of biological attachment devices,” *Adv. Mater.* 18(2006):874-877. S. Hoffmann, F. Östlund, J. Michler, H.J. Fan, M. Zacharias, S.H. Christiansen, C. Ballif, “Fracture strength and Young’s modulus of ZnO nanowires,” *Nanotechnology* 18(23 May 2007):205503. M. Becker, V. Sivakov, G. Andrä, R. Geiger, J. Schreiber, S. Hoffmann, J. Michler, A. P. Milenin, P. Werner, S.H. Christiansen, “The SERS and TERS Effects Obtained by Gold Droplets on Top of Si Nanowires,” *Nano Lett.* 7(2007):75-80; http://www.mpi-halle.de/mpi/publi/pdf/7247_07.pdf.

⁸⁰⁶ Hong-Shi Kuo, Ing-Shouh Hwang, Tsu-Yi Fu, Yu-Chun Lin, Che-Cheng Chang, Tien T. Tsong, “Noble Metal/W(111) Single-Atom Tips and Their Field Electron and Ion Emission Characteristics,” *Japanese Journal of Applied Physics* 45(2006):8972-8983; [http://www.phys.sinica.edu.tw/~nano/publication/Ing-Shouh%20HWANG/Noble%20MetalW\(111\)%20Single-Atom%20Tips%20and%20Their%20Field%20Electron.pdf](http://www.phys.sinica.edu.tw/~nano/publication/Ing-Shouh%20HWANG/Noble%20MetalW(111)%20Single-Atom%20Tips%20and%20Their%20Field%20Electron.pdf). Ing-shouh Hwang, Hong-shi Kuo, Tien T. Tsong, Tsu-yi Fu, “Single-atom tip and preparation method thereof,” United States Patent 7507320, filing date 10/09/2004, publication date 03/24/2009; <http://www.freepatentsonline.com/7507320.pdf>. H.S. Kuo, I.S. Hwang, T.-Y. Fu, J.Y. Wu, C.C. Chang, T.T. Tsong, “Preparation and characterization of single-atom tips,” *Nano Lett.* 4(December 2004):2379-2382; http://aao.sinica.edu.tw/download/publication_e/Year2005/math04.pdf , http://dns.ntu-cems.ntu.edu.tw/references/NANO_LETT-4-2379-2004.pdf.

Plan B. To avoid the necessity of manually mounting a preformed wire on a quartz fork prong, in Plan B we grow a nanowire onto the prong instead. In this first step, IBID or EBID is used to deposit a pure tungsten metal nanoscale column or “nanowire” onto the appropriate flat face of the quartz (SiO_2) tuning fork as outlined in the following subsections of [Section 6.3.1](#).

The principal process design uncertainty here is whether a W(111) face is absolutely required for noble metal faceting to occur on that surface, or if faceting can occur on other crystallographic faces as well. Three possible outcomes may be distinguished:

(1) In the event that the W(111) or some other face is an absolute requirement, then it becomes necessary to ensure that the tungsten nanowire produced by beam-induced deposition yields a tip apex that consists exclusively or predominantly of the required crystallographic face.

(2) If a crystal face of some kind (possibly mixed orientation, as in polycrystalline materials) is required to induce noble metal faceting, then the beam deposition process must yield an exclusively or predominantly crystalline or polycrystalline tip apex.

(3) If a crystalline or polycrystalline tip apex is not required to induce noble metal faceting, then beam deposition of predominantly or exclusively amorphous tungsten metal may suffice.

The apex of the resulting tungsten metal rod or nanowire can then be cleaned or annealed as previously described in [Section 6.2.2](#).

6.3.1.1 Which Tungsten Surfaces are Facetogenic?

As previously noted in [Section 3.5](#), metal adsorbates can induce faceting and other morphological changes on a metal crystal surface ([Figure 3-9](#)).⁸⁰⁷ Reversible surface-step coalescence into facets can be described in terms of equilibrium thermodynamics – Herring⁸⁰⁸ first quantified the requirements on the variation of the surface free energy with orientation for such a phase separation to occur. The great majority of studies of this phenomenon have involved the bcc tungsten W(111) or molybdenum Mo(111) crystallographic faces, but other surfaces have also been observed to induce faceting including the fcc surfaces Ir(210), Pt(210), Ni(210), Cu(210) and Cu(100), the hcp metal surfaces Re($12\bar{3}1$) and Re($11\bar{2}1$), and also Ta(111), Nb(111) and Pd(100). All of these are atomically rough, non-close-packed surfaces with relatively high surface free energies. The presence of adsorbate increases the anisotropy in surface free energy, as well as lowering the average surface free energy. The increased anisotropy means that the faceted surface with its higher exposed surface area has a lower energy than the initially planar

⁸⁰⁷ A. Cetronio, J.P. Jones, “Reconstruction at a metallic interface studied by field ion and field emission microscopy,” *Surf. Sci.* 40(November 1973):227-248. E.D. Williams, N.C. Bartelt, “Thermodynamics of Surface Morphology,” *Science* 251(25 January 1991):393-400.

⁸⁰⁸ C. Herring, “Some Theorems on the Free Energies of Crystal Surfaces,” *Phys. Rev.* 82(1951):87-93.

surface. Thus, faceting is driven by thermodynamics – the minimization of total surface free energy – but is controlled by the kinetics of diffusion, nucleation and growth.⁸⁰⁹

A preliminary survey of the literature has revealed no explicit reports of pyramidal facet formation on tungsten crystallographic faces other than W(111). However, an interesting series of papers published during 1991-1997 by Kołaczkiwicz and Bauer⁸¹⁰ reported work in which the noble metals Ir, Pd, Pt and Rh were evaporated onto a single-crystal W(110) surface. The authors observed Frank-van der Merwe-type growth (Figure 6-17B) at 300 K and Stranski-Krastanov-type growth (Figure 6-17C) at 600-800 K⁸¹¹ along with “metastable structures” in all of the adsorbates⁸¹² including the formation at high temperatures of “large pseudomorphic Rh and Pt islands” that “develop domain walls during cooling”.⁸¹³ In their last paper⁸¹⁴ the authors reported:

“Rh, Ir and Pt form a few metastable LEED structures in the submonolayer range on the W(110) face. The structural transformations in the adsorption layers, which have been observed, are connected with work-function changes represented by successive steps I, II and III in the $\Delta\phi(T)$ curves. The structural changes are associated with mass transport. The behavior of Ir and Pt is similar. The series of steps observed in the $\Delta\phi(T)$ curves is attributed to transitions of the adsorbate from the (3x1) chain structure, which consists of close-packed atomic chains along the (111) crystallographic directions of the substrate and separated by two unoccupied parallel (111) substrate rows, to another structure that consists of small 2D islands elongated in one of the (111) directions, to 2D pseudomorphic islands with domain walls (step II) and finally to islands without domain walls (step III). Formation of the narrow islands or of the pseudomorphic islands is possible either by the displacement of whole chains (or narrow islands) or by the movement of individual atoms.”

⁸⁰⁹ Andrzej Szczepkiewicz, Antoni Ciszewski, Robert Bryl, Czesław Oleksy, Cheng-Hsun Nien, Qifei Wu, Theodore E. Madey, “A comparison of adsorbate-induced faceting on flat and curved crystal surfaces,” *Surf. Sci.* 599(2005):55-68; <http://www.zmp.ifd.uni.wroc.pl/asz/joint-paper-published.pdf>.

⁸¹⁰ J. Kołaczkiwicz, E. Bauer, “Metastable atomic configurations of Rh, Ir, and Pt on W(110),” *Phys. Rev. B* 44(1991):5779-5785. J. Kołaczkiwicz, E. Bauer, “Ultrathin films of Rh, Ir and Pt on tungsten (110),” *Surface Science* 314(20 July 1994):221-242. J. Kołaczkiwicz, E. Bauer, “Behaviour of Rh, Pd, Ir and Pt on the W(110) face above room temperature,” *Surface Science* 366(10 October 1996):71-84. J. Kołaczkiwicz, E. Bauer, “Desorption energy and lateral interaction energy in the adsorption systems of Rh, Pd, Ir and Pt on W(110),” *Surface Science* 374(10 March 1997):95-103.

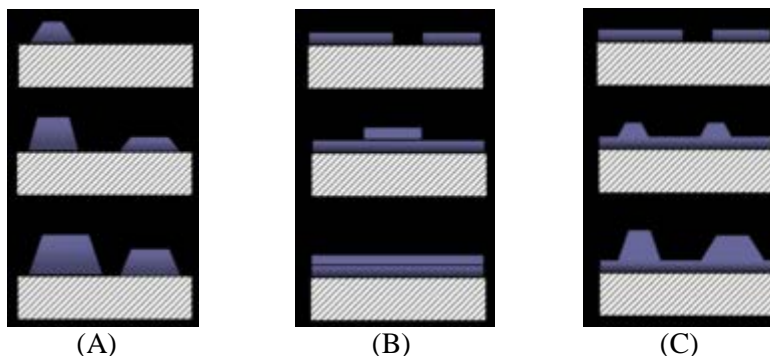
⁸¹¹ J. Kołaczkiwicz, E. Bauer, “Ultrathin films of Rh, Ir and Pt on tungsten (110),” *Surface Science* 314(20 July 1994):221-242.

⁸¹² J. Kołaczkiwicz, E. Bauer, “Ultrathin films of Rh, Ir and Pt on tungsten (110),” *Surface Science* 314(20 July 1994):221-242.

⁸¹³ J. Kołaczkiwicz, E. Bauer, “Behaviour of Rh, Pd, Ir and Pt on the W(110) face above room temperature,” *Surface Science* 366(10 October 1996):71-84.

⁸¹⁴ J. Kołaczkiwicz, E. Bauer, “Desorption energy and lateral interaction energy in the adsorption systems of Rh, Pd, Ir and Pt on W(110),” *Surface Science* 374(10 March 1997):95-103.

Figure 6-17. Cross-section views of the three primary modes of thin film growth including (A) Volmer-Weber (island formation), (B) Frank-van der Merwe (layer-by-layer), and (C) Stranski-Krastanov (layer-plus-island), with each mode shown for <1 monolayer (top), 1-2 monolayer (middle), and >2 monolayer (bottom) of surface coverage.⁸¹⁵



We can conclude that noble metals have high mobility on W(110) surface at high temperature, and do exhibit mass transport as a function of temperature on W(110) – but it's not clear if the "islands" are "pyramids". Note that this work predates much of the noble metal pyramidal faceting work, most of which appeared in the late 1990s and beyond. Also, the methods used by these authors did not include direct SEM/TEM or related imaging techniques, so it's unlikely they could have distinguished pyramids from flat islands, if pyramids were present – and thus it is possible that their observed "large 2D islands without domain walls" could be as yet unidentified pyramids.

There appears to be no information in the literature about the facetogenicity of tungsten single-crystal surfaces other than W(111) (Figure 6-16B) and W(110). It may be possible to perform calculations to ascertain whether or not other surfaces may be facetogenic (i.e., a thermodynamically favored process), but those calculations have not yet been made. Also, until a successful experiment is done there can be no confidence that such a calculation is giving reliable results.

Regarding surfaces that are not single-crystal, Kuo et al.⁸¹⁶ have observed iridium metal pyramidal facetization of a polycrystalline iridium metal wire surface. However, no reports of noble metal facetization on polycrystalline tungsten surface (Figure 6-16A) have been found. Also, no reports have yet been found of noble metal pyramidal facetization on an amorphous metal surface.

⁸¹⁵ "Stranski-Krastanov growth," http://en.wikipedia.org/wiki/Stranski-Krastanov_growth.

⁸¹⁶ Hong-Shi Kuo, Ing-Shouh Hwang, Tsu-Yi Fu, Ying-Siang Hwang, Yi-Hsien Lu, Chun-Yueh Lin, Jin-Long Hou, Tien T. Tsong, "A single-atom sharp iridium tip as an emitter of gas field ion sources," *Nanotechnology* 20(19 August 2009):335701. Hong-Shi Kuo, Ing-shouh Hwang, Tien T. Tsong, Tsu-Yi Fu, "Atomically Sharp Iridium Tip," IPC8 Class: AB21G100FI, USPC Class: 428600, 2009; <http://www.faqs.org/patents/app/20090110951>.

The conservative working assumption is that for noble metal pyramidal facetization to occur, we will probably require an exclusively or predominantly W(111), or perhaps W(110), single-crystal surface. A polycrystalline tip apex exposing one or the other of these two surfaces exclusively or predominantly might also enable noble metal pyramidal facetization. The related possibilities using Mo(111) and related facetizable surfaces might also be explored further, both in the literature and experimentally.

6.3.1.2 Crystal Structure of Beam-Deposited Tungsten

Tungsten nanowires deposited via EBID are typically amorphous metal or nanocrystalline metal embedded in an amorphous metal matrix,⁸¹⁷ but the apex can often be modified ex post (e.g., by high-energy 1 MeV electron-beam irradiation)⁸¹⁸ into polycrystalline bcc tungsten crystallites that might allow noble metal pyramidal facet formation. For example, Kislov et al.⁸¹⁹ report growing tungsten rods from W(CO)₆ precursor via EBID (albeit showing some contamination of the W deposit with tungsten carbide W₂C and tungsten oxide W₃O in addition to pure crystalline tungsten). After annealing at 800 °C for 1 hour the EBID tungsten rods converted into nanocrystals up to 20 nm in size, but the paper doesn't say if the new material is purely polycrystalline material or which crystallographic faces are presented at the tip apex surface. Similarly, Colpo et al.⁸²⁰ describe the plasma enhanced chemical vapor deposition (PECVD) of tungsten using a dual-gas WF₆/H₂ precursor that produces films with a columnar microstructure in a W(111) orientation, but localization to a vertical rod with a consistent diameter in the tens or hundreds of nanometers was not attempted in this work.

Matsui et al.⁸²¹ report that EBID tungsten rods from WF₆ precursor onto a clean Si(100) surface (Figure 6-18) yields material consisting of 85% tungsten, 7.5% fluorine and 7.5% oxygen after a

⁸¹⁷ M. Han, K. Mitsuishi, M. Shimojo, K. Furuya, "Nanostructure characterization of tungsten-containing nanorods deposited by electron-beam-induced chemical vapour decomposition," *Philosophical Magazine* 84(12 April 2004):1281-1289; http://www.informaworld.com/smpp/content%7Edb=all%7Econtent=a713754731%7Ejumtype=ref_intern al%7Efromvnxs=v31n3s1%7Efromtitle=713610945%7Econs.

⁸¹⁸ Ming Hui Song, Kazutaka Mitsuishi, Kazuo Furuya, "Crystallization under 1 MeV electron beam irradiation of nanometer-sized W-dendrites fabricated on alumina substrates with electron-beam-induced deposition," *Materials Science Forum* 475-479(2005):4035-4038, <http://www.scientific.net/MSF.475-479.4035>.

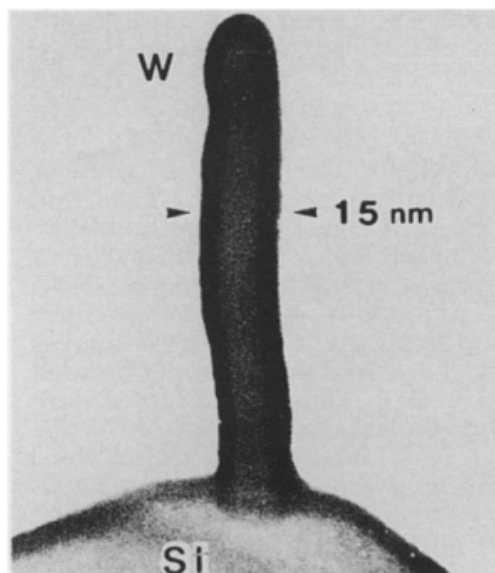
⁸¹⁹ N.A. Kislov, I.I. Khodos, E.D. Ivanov, J. Barthel, "Electron-beam-induced fabrication of metal-containing nanostructures," *Scanning* 18(1996):114-118; http://www.mpi-halle.de/mpi/publi/pdf/1749_96.pdf.

⁸²⁰ Pascal Colpo, François Rossi, Neil Gibson, Douglas Gilliland, "Deposition of tungsten thin films by dual frequency inductively coupled plasma assisted CVD," *Thin Solid Films* 332(2 November 1998):21-24.

⁸²¹ S. Matsui, T. Ichihashi, M. Mito, "Electron beam induced selective etching and deposition technology," *Journal of Vacuum Science & Technology B* 7(September/October 1989):1182 -1190.

15 minute exposure time, forming an exposed surface of β -W clusters. Beta-tungsten is a metastable crystalline form “which possesses the A-15 cubic crystal structure containing eight atoms per unit cell...with a lattice parameter of 5.036 Å”.⁸²² Metastable beta-tungsten transforms to alpha-tungsten at temperatures between 520-625 °C – alpha-tungsten is the stable crystal structure of the metal, a body centered cubic (bcc) form.⁸²³ This transition temperature is very close to the minimum pyramidal facetizing annealing temperature for iridium on tungsten.

Figure 6-18. Tungsten rod with 15 nm diameter fabricated on clean Si(100) substrate using a 120 kV electron beam with 3 nm diameter.⁸²⁴



Similarly, in 2008 Klein et al.⁸²⁵ used high resolution transmission electron microscopy, electron diffraction and electron spectroscopy to determine the effects that electron beam scanning

⁸²² W.R. Morcom, W.L. Worrell, H.G. Sell, H.I. Kaplan, “The preparation and characterization of beta-tungsten, a metastable tungsten phase,” *Metallurgical and Materials Transactions B* 5(January 1974):155-161; <http://resources.metapress.com/pdf-preview.axd?code=377109q7l6k68222&size=largest>.

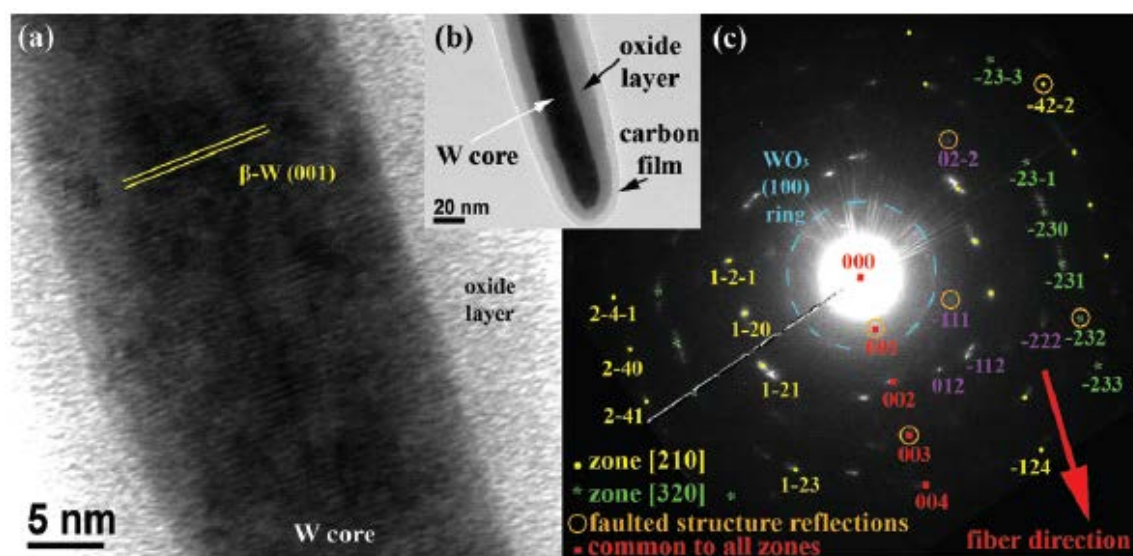
⁸²³ W.R. Morcom, W.L. Worrell, H.G. Sell, H.I. Kaplan, “The preparation and characterization of beta-tungsten, a metastable tungsten phase,” *Metallurgical and Materials Transactions B* 5(January 1974):155-161; <http://resources.metapress.com/pdf-preview.axd?code=377109q7l6k68222&size=largest>.

⁸²⁴ S. Matsui, T. Ichihashi, M. Mito, “Electron beam induced selective etching and deposition technology,” *Journal of Vacuum Science & Technology B* 7(September/October 1989):1182 -1190.

⁸²⁵ K.L. Klein, S.J. Randolph, J.D. Fowlkes, L.F. Allard, H.M. Meyer III, M.L. Simpson, P.D. Rack, “Single-crystal nanowires grown via electron-beam-induced deposition,” *Nanotechnology* 19(27 August 2008):345705.

patterns might have on deposition characteristics using WF_6 precursor. They found that slow, one-dimensional lateral scanning produces textured β -W nanowire cores (a single-crystal (111) A15 type SAD pattern) (Figure 6-19) surrounded by an oxide secondary layer (Figure 6-20), while stationary vertical growth leads to single-crystal (100)-oriented W_3O nanowires.⁸²⁶ Interestingly, the authors⁸²⁷ proudly note: “To our knowledge, this is the first demonstration of single-crystal growth by the EBID process.”⁸²⁸

Figure 6-19. (a) HRTEM image of the core of EBID nanowire #2 showing (001) β -W lattice planes. (b) TEM bright-field image of the wire tip showing a tungsten core surrounded by a tungsten-oxide layer and an amorphous carbon film (contamination layer from imaging). (c) SAD pattern from a ~ 300 nm area about the wire tip, showing β -W reflections for the (210) and (320) zone axes.⁸²⁸

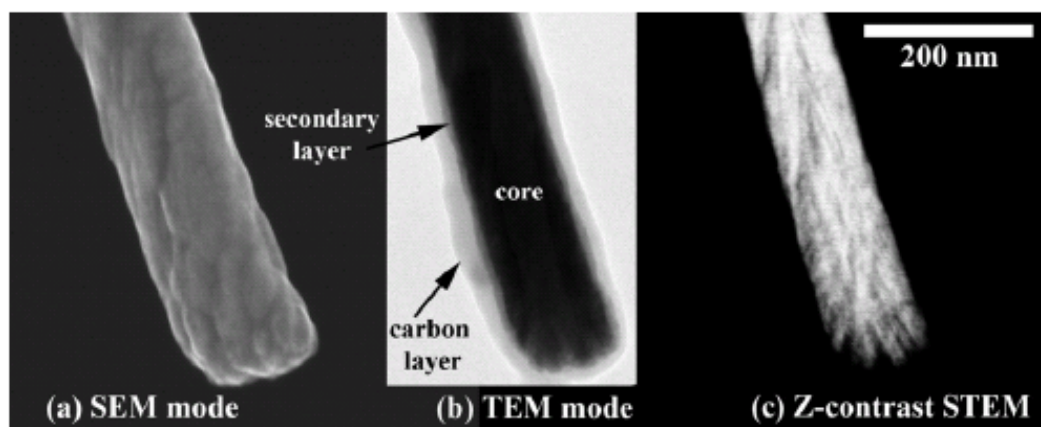


⁸²⁶ K.L. Klein, S.J. Randolph, J.D. Fowlkes, L.F. Allard, H.M. Meyer III, M.L. Simpson, P.D. Rack, “Single-crystal nanowires grown via electron-beam-induced deposition,” *Nanotechnology* 19(27 August 2008):345705.

⁸²⁷ K.L. Klein, S.J. Randolph, J.D. Fowlkes, L.F. Allard, H.M. Meyer III, M.L. Simpson, P.D. Rack, “Single-crystal nanowires grown via electron-beam-induced deposition,” *Nanotechnology* 19(27 August 2008):345705.

⁸²⁸ K.L. Klein, S.J. Randolph, J.D. Fowlkes, L.F. Allard, H.M. Meyer III, M.L. Simpson, P.D. Rack, “Single-crystal nanowires grown via electron-beam-induced deposition,” *Nanotechnology* 19(27 August 2008):345705.

Figure 6-20. Electron micrographs (all at the same scale) of EBID nanowire #4: (a) secondary electron image showing surface roughness; (b) transmitted electron image showing three distinct layers of different contrast due to mass, thickness, and diffraction differences; (c) Z-contrast STEM image showing an internal core of high Z material with density variation. The carbon layer is an artifact of the imaging process.⁸²⁹



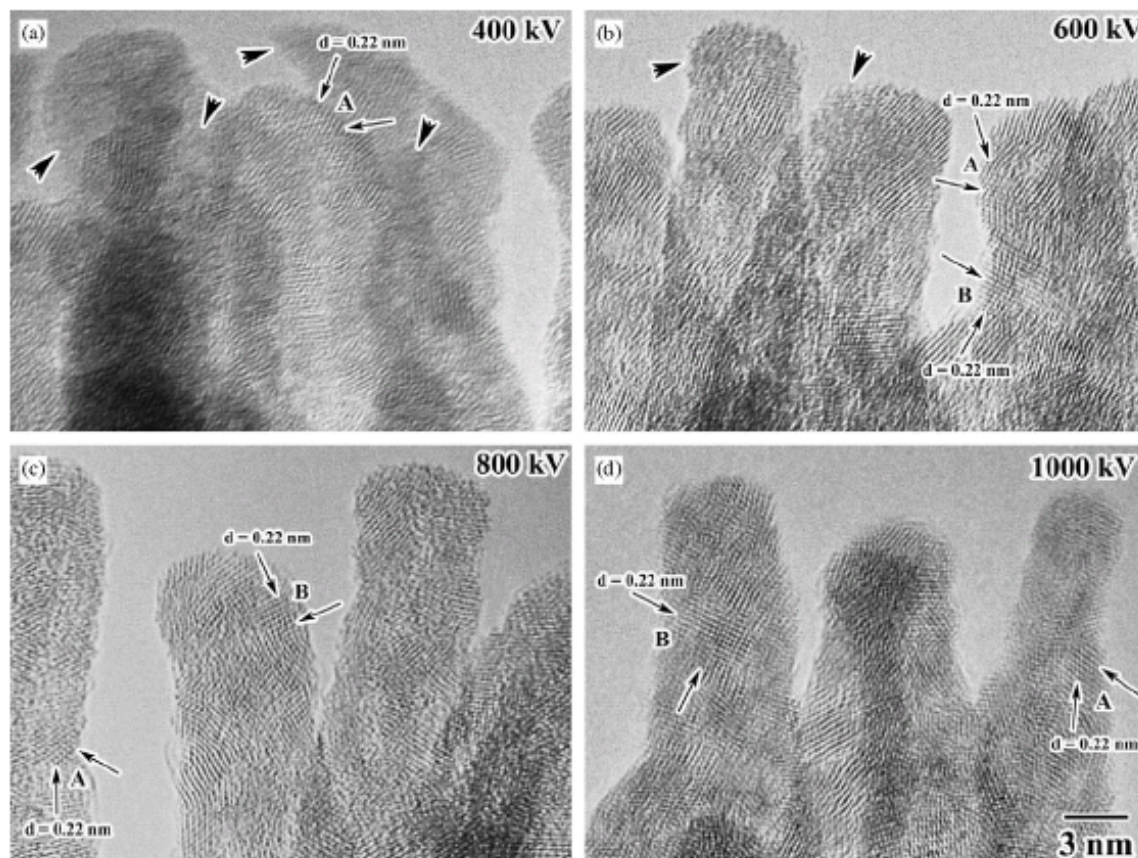
Based on this work, the lateral nanowire with a slow raster pattern has a thin oxide coating and the vertical pattern makes single-crystal W_3O but not W_3W – and Ir might not facetize on W_3O (this could be checked independently, experimentally). However, if oxygen can be rigorously excluded from the EBID chamber then perhaps the oxide coating could be greatly reduced or even eliminated; and if laser or e-beam heating can subsequently anneal the beta-W into alpha-W without loss of lattice orientation, this might produce a single-crystal tungsten nanowire with $W(100)$ lattice planes exposed on the tip apex. (No reports of noble metal facetization on $W(100)$ have yet been found but such facetization at least seems possible.) Laboratory experimental work will probably be required to finally resolve these issues.

Varying the e-beam accelerating voltage might also produce tungsten rods with crystallographic orientations that are useful for pyramidal faceting. Xie et al.⁸³⁰ report that self-standing W-nanodendrite structures were grown on SiO_2 substrate using EBID with various accelerating voltages from 400 to 1000 kV (Figure 6-21), producing nanodendrites consisting of nano-sized grains (determined to be W crystal in bcc structure) and amorphous structures whose degree of crystallinity was found to increase for higher beam energies due to enhanced tungsten atom mobility with higher energy irradiation, thus allowing for rearrangement and crystallization.

⁸²⁹ K.L. Klein, S.J. Randolph, J.D. Fowlkes, L.F. Allard, H.M. Meyer III, M.L. Simpson, P.D. Rack, "Single-crystal nanowires grown via electron-beam-induced deposition," *Nanotechnology* 19(27 August 2008):345705.

⁸³⁰ Guoqiang Xie, Minghui Song, Kazutaka Mitsuishi, Kazuo Furuya, "Effect of accelerating voltage on crystallization of self-standing W-nanodendrites fabricated on SiO_2 substrate with electron-beam-induced deposition," *Physica E: Low-dimensional Systems and Nanostructures* 29(November 2005):564-569.

Figure 6-21. A series of HRTEM micrographs of some branches of nanodendrites grown on SiO_2 substrate irradiated to a fluence of $6.0 \times 10^{21} \text{ e cm}^{-2}$ with different electron beam accelerating voltages. (a) 400 kV; (b) 600 kV; (c) 800 kV; (d) 1000 kV. Arrows indicate lattice fringes in grains A and B, which have inter-fringe angles of 60 (A) and 90 (B) degrees, respectively.⁸³¹



Typical tip thickness was 3 nm. Some relevant information was provided in the paper about the crystallographic orientation at the tip apex:

“Figure 6-21 shows a series of HRTEM micrographs of some branches of nanodendrite structures fabricated with various accelerating voltages to a fluence of $6.0 \times 10^{21} \text{ e cm}^{-2}$. It is revealed that nano-sized W grains in bcc structure are contained in the dendrite structures. Figure 6-21a is an HRTEM micrograph of some branches of nanodendrites grown with an accelerating voltage of 400 kV. Lattice fringes are observed at the most places. This indicates that they are crystal in

⁸³¹ Guoqiang Xie, Minghui Song, Kazutaka Mitsuishi, Kazuo Furuya, “Effect of accelerating voltage on crystallization of self-standing W-nanodendrites fabricated on SiO_2 substrate with electron-beam-induced deposition,” *Physica E: Low-dimensional Systems and Nanostructures* 29(November 2005):564-569.

several nanometers. The largest and also the most frequently observed lattice spacing measured from micrographs is 0.22 nm. It is close to the lattice spacing, 0.224 nm, of W(110) of bcc W crystals with a deviation smaller than 5%. Moreover, lattice fringes with spacing $d \sim 0.22$ nm have inter-fringe angle of 60° (grain A), as well as that of 90° (grain B), as indicated in **Figure 6-21**. They agree to zone axis of (111) and (001) of bcc W structure, respectively. HRTEM micrographs taken from other regions or other dendrites also give similar results. Combined with nanometer-sized area diffraction pattern analyses and EDS analyses, it is clarified that these crystals are W grains in bcc structure. Furthermore, lattice fringes cannot be clearly observed in some places, indicating that a large part of them is in amorphous state, as shown by arrows in **Figure 6-21**. **Figure 6-21b** shows a micrograph of some branches of nanodendrites grown with an accelerating voltage of 600 kV. The fraction of amorphous state in the as-fabricated nanodendrites decreases obviously. For the dendrites fabricated with an accelerating voltage of 800 kV, as shown in **Figure 6-21c**, the amorphous state is observed only in a few places. **Figure 6-21d** shows an HRTEM micrograph of some branches of nanodendrites grown with an accelerating voltage of 1000 kV. Lattice fringes are observed clearly in almost all of the grains except in thick region, where small crystals in random orientations overlapped each other, so that their lattice fringes cannot be clearly observed. Therefore, it is indicated that the fraction of amorphous state in the as-fabricated nanodendrites decreases with an increase in electron beam accelerating voltage.”

The descriptive wording in the paper is not perfectly clear, but it appears that in **Figure 6-21** the regions labeled “A” may be W(111) faces and the regions labeled “B” may be W(100) faces, while all other unlabeled regions are W(110) faces. At 400 kV (**Figure 6-21a**) it looks like the W(111) region lies conveniently at the tip of the structure, so it is possible that Ir placed on these surfaces might pyramidalize selectively off the W(111) faces, albeit possibly at various hard-to-use angles. Note that these tungsten rods are about 4 nm wide, so any iridium nanopyramid(s) should nicely coat the entire apex.

Experiments will probably be required to determine, first, if the isolated tungsten nanodendrites of the kind shown in **Figure 6-21** can be reliably grown at repeatable sizes and orientations on the apex of a tungsten rod on a quartz substrate, and second, if those isolated tungsten nanodendrites, once coated with a noble metal thin film, will induce the noble metal film to rearrange during thermal, laser, or e-beam annealing into the desired pyramidal SATs.

Note that molybdenum nanowires can also be deposited directly onto SiO_2 or quartz surfaces using phase-shifting photolithography (PSP).⁸³²

6.3.1.3 Beam-Deposited Tungsten-Silicon Exchange

If it proves impossible to beam-deposit tungsten nanowires with the desired crystallographic face exposed at the apex, it may be possible to take advantage of a chemical reaction in which EBID

⁸³² C.L. Stender, E.C. Greyson, T.W. Odom, “Patterned MoS_2 -Nanostructures over cm^2 -Areas,” Adv. Mater. 17(2005):2837-2841.

silicon is etched by dual-gas tungsten precursor, depositing tungsten metal in the desired W(111) orientation. This proposed subprocess would proceed in three steps:

- (1) deposit a vertical nanoscale column of pure Si onto the quartz (SiO_2) surface, using positionally-controlled EBID;
- (2) deposit a tungsten pillar into the Si column, mostly consuming the Si and replacing it with W metal, using positionally uncontrolled CVD;
- (3) round off the tungsten pillar apex, via directed e-beam or laser annealing.

It is believed this method might work because WF_6 reacts upon contact with silicon substrate.⁸³³ The deposition occurs selectively on pure Si only, but not on silicon oxide or nitride, thus the reaction is highly sensitive to both contamination deposits and to substrate pre-treatment. The decomposition reaction is fast but saturates when the tungsten layer thickness reaches 10-15 microns. The saturation occurs because the thickening tungsten layer blocks diffusion of WF_6 molecules into the Si substrate which is the only catalyst of molecular decomposition in this process. The deposition process occurs at temperatures between 300-800 °C and results in the formation of hydrofluoric acid vapors. The crystallinity of the produced tungsten layers can be controlled by altering the WF_6/H_2 ratio and the substrate temperature: low ratios and temperatures result in W(100) oriented tungsten crystallites whereas higher values favor the W(111) orientation. Thus a hydrogen-lean dual-gas precursor applied to a pure silicon surface at high temperature should produce predominantly W(111) crystallites. Of course, “if the deposition occurs not in inert but in oxygen containing atmosphere (air) then instead of tungsten, a tungsten oxide layer is produced.”⁸³⁴

According to Lassner and Schubert:⁸³⁵ “CVD tungsten exhibits several advantageous properties, such as high purity, resistivity to grain growth (low energy grain boundaries and absence of stored strain energy), near-theoretical density, and high ductility. Depending on deposition conditions and substrate properties, different types of layers can be produced, such as single crystal layers, layers of a determined crystal orientation, columnar crystallites rectangular to the substrate surface, and so on. The crystal orientation can be influenced by the WF_6/H_2 ratio and the temperature: low temperature and low ratio favor (100) orientation while high values favor (111) orientation. No deposition occurs on insulator surfaces such as SiO_2 or Si_3N_4 .”

Here we also find the authors’ definition of “high” and “low” temperature: “Hydrogen, silicon, and silane are the most common reducing agents for WF_6 in integrated-circuit metallization processes....Reduction with hydrogen or silane allows the deposition of tungsten in the

⁸³³ “Tungsten hexafluoride,” http://en.wikipedia.org/wiki/Tungsten_hexafluoride.

⁸³⁴ Rein U. Kirss, Lamartine Meda, “Chemical vapor deposition of tungsten oxide,” *Applied Organometallic Chemistry* 12(March 1998):155-160; <http://www3.interscience.wiley.com/journal/2700/abstract>.

⁸³⁵ Erik Lassner, Wolf-Dieter Schubert, *Tungsten: Properties, Chemistry, Technology of the Element, Alloys, and Chemical Compounds*, Springer, NY, 1999, pp. 111, 168; <http://books.google.com/books?id=foLRISkt9gcC&pg=PA168#v=onepage&q=&f=false>.

temperature range 300-500 °C. Reduction by silicon is important to deposit tungsten selectively on Si surfaces. In the WF_6 -Si system, two reactions are possible:



Accordingly, twice as much silicon is consumed at higher temperature....The reaction is very fast and stops as soon as a critical tungsten thickness is reached (10-15 microns) {presumably this assumes a surplus of Si is available, and we are not Si-limited}. The thickness depends on the reactor setup, the amount of oxygen on the silicon surface, and pretreatment. It is assumed that a continuous tungsten layer of a certain thickness will inhibit silicon diffusion to the tungsten surface, consequently the penetration of WF_6 to the W/Si interface is stopped.”

To execute the first step of the 3-step process described at the top of this subsection, we will need to produce a well-focused CVD deposition at just the spot we want on the tuning fork surface, which implies some kind of EBID-like process given that CVD generally allows no positional control. According to Lassner and Schubert,⁸³⁶ tungsten deposition will only occur on pure Si, not on SiO_2 (e.g., quartz). As one example, Matsui and Mito⁸³⁷ used EBID to deposit silicon onto a 100 nm thick layer of SiO_2 atop a pure silicon substrate using SiH_2Cl_2 precursor gas; the final film had a composition of 89% Si, 9.1% O, and 1.9% Cl. Regarding the oxygen impurity: “O originates in residual oxygen in the source and sample chambers. If UHV on the order of 10^{-10} Torr is achieved in both chambers, a higher quality film will be deposited.” Regarding the chlorine impurity: “Cl Auger intensity decreases exponentially as the EB exposure time increases....reaches noise level at 10 min exposure. This result indicates that selective desorption is also possible by EB irradiation.” Matsui and Mito don’t report whether the deposited Si is amorphous, crystalline, or other, nor is there any indication of a preferred crystallographic orientation of any deposited crystalline Si. However, it’s not clear that the deposition of W(111) requires any particular crystal face of Si to be present, in order to deposit properly. (An examination of the existing literature on integrated-circuit metallization processes involving WF_6 might provide a more definitive answer to this question.)

Accordingly, we tentatively propose to use EBID to write a small column of pure Si onto the quartz (SiO_2) tuning fork surface. Afterwards, the entire tuning fork assembly can be heated and exposed to the WF_6/H_2 gas, whereupon the silicon in the column will be slowly consumed and replaced by tungsten – the W(111)-oriented tungsten column will grow only on that spot and nowhere else. Lassner and Schubert⁸³⁸ report that the column can be grown as tall as 10-15

⁸³⁶ Erik Lassner, Wolf-Dieter Schubert, *Tungsten: Properties, Chemistry, Technology of the Element, Alloys, and Chemical Compounds*, Springer, NY, 1999, pp. 111, 168; <http://books.google.com/books?id=foLRISkt9gcC&pg=PA168#v=onepage&q=&f=false>.

⁸³⁷ Shinji Matsui, Masanobu Mito, “Si deposition by electron beam induced surface reaction,” *Appl. Phys. Lett.* 53(17 October 1988):1492; <http://dx.doi.org/10.1063/1.100465>.

⁸³⁸ Erik Lassner, Wolf-Dieter Schubert, *Tungsten: Properties, Chemistry, Technology of the Element, Alloys, and Chemical Compounds*, Springer, NY, 1999, pp. 111, 168; <http://books.google.com/books?id=foLRISkt9gcC&pg=PA168#v=onepage&q=&f=false>.

microns if needed, but it is likely that only 100 nm or so may be required for a sufficiently tall rod to provide an adequate aspect ratio for our SAT tip. This rod should be limited in diameter roughly to the width of the original pure silicon spot, since there will be no pure silicon available anywhere else on the quartz surface for the WF_6/H_2 gas to cannibalize. Assuming the apex of the rod has the desired W(111) orientation, EBID or other techniques can be used to deposit a noble metal film onto the tip, allowing us to proceed with the rest of the SAT fabrication process as described below.

6.3.2 Step 2: Formation of Pyramidal Iridium SAT at the Apex

Once a tungsten rod of the appropriate size, shape, and crystallographic orientation at the apex has been deposited onto the SiO_2 surface of the quartz tuning fork prong, the next step is to deposit a bit of iridium (or other pyramid-faceting noble metal such as Pd, Pt, Au, or Rh) onto the tungsten pillar tip, via EBID or by electrochemical or other means, then cook everything at ~ 1100 K to self-assemble (via thermal annealing) the pyramidal iridium single-atom tip (SAT) and to ensure the purity of the Ir at the tip – following the processes demonstrated experimentally by Kuo et al.⁸³⁹ and described at length in [Section 5.3](#). Note that the heating required for thermal annealing might more conveniently be applied via focused laser heating or focused electron beam bombardment of the tip. (Single-atom tips are not destroyed when irradiated with 150-MHz optical laser pulses.)⁸⁴⁰

6.3.3 Step 3: Formation of Electrical Contacts

After Step 2 is complete, the macroscale quartz tuning fork must be affixed to a larger (possibly ceramic) qPlus sensor handle structure, and electrical connections must be made between that handle structure and the quartz fork. IBID or EBID processes could be used for both tasks – both to attach the fork to the handle and to coat the tuning fork surfaces with conductive metals to provide the necessary electrical contacts. See previous discussion in [Section 6.2.4](#) for further details.

⁸³⁹ Ing-shouh Hwang, Hong-shi Kuo, Tien T. Tsong, Tsu-yi Fu, “Single-atom tip and preparation method thereof,” United States Patent 7507320, filing date 10/09/2004, publication date 03/24/2009; <http://www.freepatentsonline.com/7507320.pdf>. H.S. Kuo, I.S. Hwang, T.-Y. Fu, J.Y. Wu, C.C. Chang, T.T. Tsong, “Preparation and characterization of single-atom tips,” Nano Lett. 4(December 2004):2379-2382; http://aao.sinica.edu.tw/download/publication_e/Year2005/math04.pdf, http://dns.ntu-ccms.ntu.edu.tw/references/NANO_LETT-4-2379-2004.pdf.

⁸⁴⁰ Peter Hommelhoff, Catherine Kealhofer, Anoush Aghajani-Talesh, Yvan R.P. Sortais, Seth M. Foreman, Mark A. Kasevich, “Extreme localization of electrons in space and time,” Ultramicroscopy 109(2009):423-429.

6.4 EBID/Field-Sharpened qPlus System

Another conceivable method for producing a qPlus tip system with an SAT at the apex would start by using EBID or the welding of a manually-emplaced nanowire to attach a tungsten rod onto the quartz surface of the qPlus tuning fork prong. After that was done, EBID could again be used to deposit a separate sacrificial conductor path to the rod. Electrical current would then be provided through the conductor to the rod in order to sharpen the apex of the rod to a SAT via field-assisted tip sharpening ([Section 3.10](#)). After an SAT was obtained, the conductor would be removed via positionally-controlled focused-electron-beam (FEB) etching ([Figure 6-6](#)), leaving a finished tungsten SAT sitting on the quartz tuning fork prong. As already noted in [Section 6.2](#), field-assisted tip sharpening has been available for several decades but produces inconsistent results and is relatively difficult to remediate in situ if the tip becomes damaged during use.

The characteristics of such a tip might be improved by adding a noble metal monolayer coating, especially if the noble metal thin film can additionally be thermally induced to rearrange to form a pyramidal noble-metal SAT that could be easily reassembled by simple thermal annealing.

6.5 MEMS-Based qPlus Tip System

Another possibility is that the techniques commonly employed in the fabrication of microelectromechanical system (MEMS) structures could also be used to fabricate a unitary, or near-unitary, qPlus tip system with an SAT at the apex of the tip. Some possibilities might include the following.

6.5.1 Conventional Unitary Lithographic Fabrication

In this method, we would use conventional lithography to fabricate the quartz tuning fork, then lithographically pattern an iridium or tungsten metal column attached to the quartz surface in which the metal column is surrounded and stabilized by a sacrificial material layer that is later dissolved or etched away. This sacrificial material could include a sacrificial conductor to enable field-assisted tip sharpening of the tungsten metal rod, or alternatively the column could include Ir deposited atop a W apex such that it would form an iridium SAT upon thermal annealing.

6.5.2 Two-Component Lithographic Fabrication with Microassembly

In this method, we would use conventional lithography to fabricate the quartz tuning fork, then lithographically pattern a mechanical attachment interface onto the surface. In a separate lithographic process, fabricate or manually assemble an SAT, then use microscale manipulation to manually grab and detach the SAT and mechanically connect it to the mechanical attachment interface that was previously fabricated onto the quartz surface, thus completing the assembly of the qPlus tip system.

One example of this approach is found in the recent graduate work of Kumar et al.,⁸⁴¹ in which AFM probe tips are manually assembled from MEMS-fabricated components called “nanobits”:

“Abstract. We present here a proof-of-principle study of scanning probe tips defined by planar nanolithography and integrated with AFM probes using nanomanipulation. The so-called “nanobits” are 2-4 μm long and 120-150 nm thin flakes of Si_3N_4 or SiO_2 , fabricated by electron beam lithography and standard silicon processing. Using a microgripper they were detached from an array and fixed to a standard pyramidal AFM probe or alternatively inserted into a tipless cantilever equipped with a narrow slit. The nanobit-enhanced probes were used for imaging of deep trenches, without visible deformation, wear or dislocation of the tips of the nanobit after several scans. This approach allows an unprecedented freedom in adapting the shape and size of scanning probe tips to the surface topology or to the specific application.”

Each SAT tip could be grown on a small jig structure that can be processed separately from the qPlus fork, then later mechanically attached to a prong of the qPlus tuning fork – in the event that the MEMS-based qPlus sensor cannot tolerate the moderately high annealing temperatures required to self-assemble the pyramidal single-atom iridium (or other noble metal) tip.

⁸⁴¹ R.T. Rajendra Kumar, S.U. Hassan, O. Sardan Sukas, V. Eichhorn, F. Krohs, S. Fatikow, P. Boggild, “Nanobits: customizable scanning probe tips,” *Nanotechnology* 20(30 September 2009):395703; see video at <http://thefirstmicroscope.org/nanobits-grab-a-piece-of-the-nano-building-kit>.

Appendix A. Directory of Quartz Crystal & Crystal Oscillator Manufacturers

The primary use of quartz crystal components in electronics is to define a frequency: in a watch there is a quartz component which is vibrating at around 32,768 cycles per second (32.768 kHz) and the circuitry in the watch will convert that into a time. The raw material, natural quartz mined in Brazil, is not pure enough to be turned directly into electronic components. It is first melted down, then recrystallized in tall steel columns known as autoclaves. This process takes around 30 days, leaving trace impurities (chiefly aluminum) at a level of around 1 part in a million (a 40-fold improvement).⁸⁴² Ultrapure synthetic monocrystalline quartz is also manufactured⁸⁴³ via the hydrothermal synthesis process.⁸⁴⁴

The faces of blocks of quartz are then machined with great precision to correspond to the atomic planes inside the crystal. The direction of the crystal planes is determined by X-ray diffraction of the blocks and the machining is performed to within 1/12th of a degree. The block (about the size of a small brick) is sawn into thin slices, each of which is then ground to a circular outline and lapped between two abrasive discs until it is at the required thickness – around a couple of millimeters. Intermediate washing and etching stages remove any damaged top surface layers. Electrical connections and mounting plates are then attached and the wafer has become an electronic component.⁸⁴⁵

The following is a list of 629 worldwide manufacturers or distributors of quartz crystals or crystal oscillators for electronics applications.⁸⁴⁶

1. [2B Elettronica s.r.l., Rome, Italy - distributor](#)
2. [4tech Co Ltd, Incheon, Korea - "Frequency Control Products"](#)
3. [A. and T. Trading Co., Hong Kong - no longer active](#)
4. [AATA Japan Co Ltd, Yokohama, Japan - Together with your business!!](#)
5. [Able Tech](#) (South Korea)
6. [Abracon Corporation, Rancho Santa Margarita, CA, USA](#)
7. [Abundance Enterprise Company \(AEC\), Hong Kong](#)

⁸⁴² “Crystal Oscillator Directory”;
http://homepage.ntlworld.com/jan.ooijman/crystal_oscillator_directory.htm.

⁸⁴³ “Factory Tour: Process for manufacturing tuning-fork crystal units,” Epsom Toyocom, 2010;
<http://www.epsontoyocom.co.jp/english/special/crystal/enjoy/plant/timing.html>.

⁸⁴⁴ “Hydrothermal synthesis,” http://en.wikipedia.org/wiki/Hydrothermal_synthesis.

⁸⁴⁵ “Crystal Oscillator Directory”;
http://homepage.ntlworld.com/jan.ooijman/crystal_oscillator_directory.htm.

⁸⁴⁶ “Crystal Oscillator Directory”;
http://homepage.ntlworld.com/jan.ooijman/crystal_oscillator_directory.htm.

8. [Adiva Technology Inc., Lake Forest, CA, USA - "Using Our Technology to Your Advantage"](#)
9. [Advanced Crystal Technology \(ACT, ACT Crystals\), Wokingham, Berks, UK](#)
10. [AEL Crystals Ltd, Crawley, West Sussex, UK - "Global Suppliers of Frequency Control Components"](#)
11. [Aker Technology Co Ltd, Headquarters and Manufacturing in TaiChung Taiwan and factory \(Aker Quartz Crystal Technology Co Ltd\) in GuangDong China - see also aker-usa.com - "As Clear As Crystal"](#)
12. [Amogo Technology Co Ltd see Aker](#)
13. [AnaSem. InC., Funabashi Chiba, Japan - includes "Fine Clock Corporation"](#)
14. [Anderson ECD Inc, San Jose, CA, USA - a specialized multi-franchised stocking distributor of Quartz Crystals, Oscillators, & Resonators - see also andersoncrystal.com](#)
15. [Anderson Electronics, Inc., Hollidaysburg, PA, USA - "Custom Crystals & Crystal Oscillators"](#)
16. [Andhra Electronics Limited \('AEL'\), Kakinada, India](#)
17. [Andy Fleischer, Bremen, Deutschland - Sonderanfertigung von Quarzen für Funkgeräte, Scanner, Pager, Selbstbauschaltungen usw.](#)
18. [Anhui Green Electronical Co., Ltd. \(mainland China\)](#)
19. [Anhui Green Imp. & Exp. Co Ltd](#)
20. [Anhui LanShun Electronic Technology Co Ltd](#)
21. [Anodyne Components, Inc., Costa Mesa, CA, USA - distributor of \(amongst others\) Joyous Crystal Products](#)
22. [Ansen Quartz Co Ltd, Taiwan - "Pulsing Your Frequency"](#)
23. [AOR Ltd, Quartz Crystal Device Division, Tokyo, Japan - worldwide distributor of major Japanese manufacturers of crystal, oscillator and filter devices](#)
24. [AR Electronique \(AR Électronique, AR-E\), Besançon, France - "vibrer d'une même fréquence"](#)
25. [ARGO Technologies Co Ltd, His-Chin, Taiwan](#)
26. [ASC Semiconductors \(H.K.\) Ltd - no longer exists](#)
27. [Ascend Frequency Devices, Newport Beach, CA, USA](#)
28. [ASK The Crystal Technology, Chung Ju, Korea - combines the strength of 4 independent factories - "The Frequency Leader" - 问, 询问, 要求, 邀请](#)
29. [Astor Limited, former name ASC Semiconductors \(Hong Kong\) Limited - no longer exists](#)
30. [Astrium \(a wholly owned subsidiary of EADS\)](#)
31. [AT&T Frequency Control Products, since 1995 part of Vectron International](#)
32. [Auhon Electronic Co. Ltd. \(mainland China\)](#)
33. [auris-GmbH, Hameln, Germany - "we live crystals"](#)
34. [AVX \(A Kyocera Group Company\), Kyoto, Japan](#)
35. [AXTAL GmbH & Co. KG, Lobbach, Germany - Advanced XTAL Products + Consulting - "THE Expert for Frequency Control and Piezo Sensors"](#)
36. [BaoTou HuaZi Electronics Technology Co Ltd, Inner Mongolia, China \(original name: BaoTou Electronics Instrument Factory\) - 包头华资电子科技有限公司 \(原包头市电子仪器厂\)](#)

37. [Baotou Xinhongda Electronic Co Ltd, Baotou, Inner Mongolia China \('XHD'\) - 包头市新宏大电子有限责任公司 - off the radar screen](#)
38. [BBA Electronics Co Ltd, Cheongju-si, Korea - □□□□□□□□□□\(□\)](#)
39. [BeckElec, Phoenix, AZ, USA](#)
40. [Beijing Candor Electronic Co Ltd - "Quartz Crystal & Oscillator Professional"](#)
41. [Beijing Chenjing Electronics Co Ltd \(formerly China 707 state owned factory\) - The pioneer manufacturer of piezoelectric crystal components in China - affiliated with Sevenstar Huachuang Electronics Co., Ltd. \('HCE'\)](#)
42. [Beijing Crystal Electronics Co Ltd, \(formerly bcrystal.com belongs to China Aerospace Corporation\) - 北京科瑞思特电子有限公司 'BCE'](#)
43. [Beijing Crystal Photoelectric Science & Technology Inc](#)
44. [Beijing JingYuXing Technology Co Ltd, \(also www.jfvny.com\) - 北京晶宇兴科技有限公司 - JFVNY®](#)
45. [Beijing Realgiant Technology Co Ltd \(also crystal-bj.com\) - "Yes we do!"](#)
46. [Beijing TACT Electronic Co Ltd](#)
47. [Beijing Tokyo Denpa Electronics Co Ltd \(TEW-B\) - a joint venture of Beijing Sevenstar Science and Technology, Tokyo Denpa \(TEW\) and MEITOKU Trading](#)
48. [Bharat Electronics Limited \(BEL\), Bangalore, India](#)
49. [Bliley Technologies, Inc., Erie, PA, USA - "Low Phase Noise Frequency Generation Products"](#)
50. [BMG PLUS - CJS research-and-production firm "BMG plus" - Закрытое акционерное общество "Научно-производственная фирма "БМГ ПЛЮС", Moscow, Russia](#)
51. [BMG-Quartz, Moscow, Russia - БМГ-КБАПИ](#)
52. [Bomar Crystal Co., Middlesex, NJ, USA - "A World of Quality"](#)
53. [BOWEI Integrated Circuits Co Ltd, Shijiazhuang, China](#)
54. [Brel International, Inc., Sarasota, FL, USA - "Serving The Electronic Industry Since 1952"](#)
55. [Brookdale Frequency Controls, Inc., Bay Shore, NY, USA - "World Class Supplier of Frequency Control Products"](#)
56. [BS Telecommunication Co Ltd \('BSTEL', 'BST' or 'BS'\), Gunpo, Korea - no longer in business](#)
57. [Bubang Techron Co Ltd \('BBT'\), Cheonan-City, Korea - "Customers Delight Through 3B \(Best Quality, Best Price, Best Service\)](#)
58. [Buy cheap temperature compensated quartz crystal oscillator texo oscillators resonator wholesale suppliers voltage controlled circuits oven schematic mhz smd resonator clock programmable oscillator vctcxo ocxo vcxo khz radio xtals](#)
59. [Cal Crystal Lab, Inc. / Comclok, Inc., Anaheim, CA, USA - "Your Source for Crystals and Clock Oscillators"](#)
60. [Caliber Electronics Inc., San Clemente, CA - "When Timing Is Everything.....Specify Caliber Electronics Inc."](#)
61. [Caltron Devices Ltd, Hong Kong / Global Electronics \(Shenzhen\) Co Ltd](#)
62. [Cardinal Components, Inc., Wayne, NJ, USA - "Leaders in Programmable Oscillators, TCXO, VCXO, VC-TCXO Products"](#)
63. [Carriernet Global Ltd. \(Singapore\)](#)

64. [Cathodeon Crystals Limited \('A PYE Group Company'\), Linton, Cambridgeshire, England](#)
65. [Centum Rakon India Pvt Ltd. \(CRIPL\), Bangalore, India \(formerly Centum Frequency Products Pvt Ltd\) - a joint venture of Centum Electronics Ltd and Rakon Ltd - Indigenous Manufacturing + Master Reseller for all Rakon products in India.](#)
66. [CEPE \(Compagnie d'Électronique et de Piézo-Électricité\), Argenteuil, France - set up within Thomson-CSF => C-MAC => Rakon](#)
67. [CETC Deqing Huaying Electronics Co Ltd, Huzhou City, China](#)
68. [Champion Technologies, Inc. => M-Tron => MtronPTI](#)
69. [Changsha Weixi Electronic Technology Co Ltd - out of business?](#)
70. [Changshu Taicheng Crystal Technology, also spelled 'Tricheng' \('BST'\) - out of business](#)
71. [Changzhou Songjing Electronic Co Ltd - synthetic quartz crystal grower](#)
72. [Chelcom - ChungHo Elcom \(formerly Kony Precision Co Ltd\), Incheon, Korea - "Genuine Leadership of high technology"](#)
73. [Chengdu Benyue Technology Co Ltd, Jinniu, China \(also Chengdu Renhe Electronic Co.,Ltd, CREC\) 仁和集团](#)
74. [Chengdu Dayang Kanghong Electronics Ltd Co](#)
75. [Chenmoun Enterprise Ltd, Taipei, Taiwan](#)
76. [Chequers Electronic \(China\) Ltd, Hong Kong \('CQ'\)](#)
77. [China National Scientific Instruments & Materials Corp. \(CSIMC\), Hangzhou, China - "We dedicate ourselves to frequency controls field..."](#)
78. [China Shenzhen Sanshrill Technology Co Ltd](#)
79. [Cinetech Ind Co Ltd \(Huang Cheng Company Ltd. / Meftech Corporation\), Taipei, Taiwan - "Superior quality - high reliability" \('MSC'\)](#)
80. [CINOX,Cincinnati, Ohio was founded as Tedford Crystal Laboratories => Harris Corporation => CINOX => EG&G, Inc. => Vectron \('VI-Cincinnati'\)](#)
81. [Citizen Finetech Miyota Co Ltd, \(formerly Citizen Miyota Co Ltd\) - Crystal Device Department, Kitasaku-gun, Nagano Prefecture, Japan](#)
82. [Citizen Quartz Crystals c/o Citizen Systems America - Component Sales Division, Torrance, CA, USA - "From the maker of precision watches comes a full line of quartz crystals and oscillators"](#)
83. [Citizen Watch Co Ltd - 'Citizen Crystal Devices', Tokyo, Japan - シチズン時計](#)
84. [C-MAC MicroTechnology - Frequency Control Products \('CMAC FCP'\); comprises C-MAC Quartz Crystals Ltd. + C-MAC Frequency Products SAS + C-MAC Frequency Products Ltd. \(sometimes referred to as 'CFP'\) => Rakon](#)
85. [Colorado Crystal Corporation \(CCC\), Loveland, CO, USA manufacturer](#)
86. [Communication Techniques, Inc. \(CTI\) acquired by Herley Industries, Inc.](#)
87. [Commutek Electronics Ltd \(CMT\) headquartered in Hong Kong with manufacturing plants in Beijing and Heibei Province, PRC](#)
88. [Composants Quartz et Electronique \(CQE\) => Temex](#)
89. [Comtec Crystals Group \('CC'\) comprises of Comtec Crystals GmbH, Poing, Germany and Comtec Crystals SARL, Haguenau France](#)
90. [Comways \(H.K.\) Electronics Limited \(Hong Kong SAR\)](#)
91. [Connor-Winfield Corporation, Aurora, IL, USA](#)

92. [Copelec, acquired by Matel-Fordahl in 1995](#)
93. [Core Electronics, Cypress, CA, USA - "Crystals, Oscillators, Resonators"](#)
94. [Corning Frequency Control Inc. => Vectron](#)
95. [CPM Electronics Co Ltd, Shenzhen, China](#)
96. [CQT Group \(China Quartz Technology\) compr. Quartz Crystal Electronics Tianjin, CQT Technology, Jiaying CQT Quartz, Jiaying Chintele Quartz Technology, Shanghai South Ocean Electron, Hangzhou Freq-Control Tech Electronics & CSIMC](#)
97. [CresTech \(S\) Pte Ltd, Singapore - "Towards Partnership Around The World"](#)
98. [Criterion Precision Components Inc., Taiwan - out of business?](#)
99. [Croven Crystals, Wenzel International, Inc., Whitby, Ontario, Canada - "Precision Quartz Crystals"](#)
100. [Crystal China \(China Crystal Oscillator Industry Portal\) - 晶振中国 - 中国晶振行业门户](#)
101. [Crystal Quartz Technology \('CQT'\), Boksburg, South Africa](#)
102. [Crystal Works, Shawnee, OK, USA => Connor-Winfield](#)
103. [Crystal-Manufacturer.com = Taitien Electronics](#)
104. [Crystek Corporation \(Crystek Crystals – Crystek Microwave\), Fort Myers, FL, USA](#)
105. [CT Industries \(Int'l\) Ltd. - out of business?](#)
106. [CTS Corporation, Bloomingdale, IL, USA - "EveryWhere, Every Day"](#)
107. [DaeWon Precision Co Ltd, Incheon, Korea \('DPC'\) □□□□](#)
108. [Daishinku Corp. \(KDS\), Kakogawa, Hyōgo, Japan 大真空 - "Small Size, Global Reach"](#)
109. [Delipro s.r.o., Piešťany, Slovak Republic - former Tesla employees partnered with Tele Quarz in 1996 \(TQ transferred its crystal mass production from Euro Quarz, Austria to Delipro\)](#)
110. [Design Bureau MEGAHERTZ - ООО "КБ МЕГАГЕРЦ", Волгоградская \(Volgograd\), Russia](#)
111. [Digi-Key Corp. \(Thief River Falls MN\)](#)
112. [Dong Jin Electronics Co Ltd, Anyang-City, Kyungki-Do, Korea - "Trust Technology! With Dong Jin Electronics"](#)
113. [Dongguan Dapu Telecom Technology Co Ltd \('D&P' => 'DP'\) - 大普通信](#)
114. [DongGuan Telestar Electronics Co Ltd - 东莞市加隆达实业有限公司 - \('STAR' OR 'TS'\)](#)
115. [Dongguan Yajing Electronic Co Ltd \('YJ', 'Ya Jing'\)](#)
116. [Dongguan Youlian Electronic Group - Dongguan City, China - a factory affiliated with MEC Hong Kong - "'YL" marking](#)
117. [Dongguan Zhuoer Electric Co Ltd - 卓尔电子](#)
118. [Dongyang Sanhe](#)
119. [Dove Electronic Components, Inc., East Setauket, NY, USA - "The Crystal & Oscillator Specialist!"](#)
120. [Dow Enterprise, Seoul, Korea](#)
121. [Dr. Steeg & Reuter Quarz-Electronic GmbH, Bad Homburg, Germany - supplied optical quartz even before Jacques & Pierre Curie discovered piezoelectricity - went bankrupt in 1991](#)

122. [E.C.O. nv \(European Crystal Organization nv\), Herselt, Belgium - "Frequency Technology"](#)
123. [eCERA ComTek Corporation, Jhongli City, Taiwan - "the technology to make a better world!" \(on September 7, 2005 Pericom acquired a 99.9% interest in eCERA Comtek Corporation from Aker Technology Co., Ltd.\)](#)
124. [Ecliptek Corporation, Costa Mesa, CA, USA](#)
125. [ECM Electronics Ltd., Ashington, West Sussex, UK](#)
126. [ECS, Inc. International, "Electronic Component Solutions", Olathe, KS, USA - "World Leader in Piezo Electric Based Frequency Control Products"](#)
127. [EDC - Electro Dynamics Crystal Corporation acquired by INFICON](#)
128. [EG&G Frequency Products Division => Oscillatek => Vectron](#)
129. [E-Jinghe \('JH'\), Shijiazhuang City, China - 石家庄市晶禾科技有限公司](#)
130. [Electrical Material Company \(Hong Kong SAR\)](#)
131. [Electronic Crystal Corp. acquired by EDC in 1988](#)
132. [Electronic Research Company \(ERC\) acquired by EDC in 2001](#)
133. [Electronics Component Co., Ltd. \(mainland China\)](#)
134. [Elemechtec Quartz Crystal Company \('EMT'\), head office in Hong Kong, a branch office in Taiwan and production site in Fogang China - "Your Friend of Quartz Crystal & Silicon Rubber"](#)
135. [EM Microelectronic-Marin SA, Marin, Switzerland - also known as EM-Marin, EM Micro or EM, formerly Ebauches Electroniques Marin \(EEM\) - member of The Swatch Group Ltd.](#)
136. [Epson Electronics America, Inc., San Jose, CA, USA - "Exceed your vision"](#)
137. [Epson Europe Electronics GmbH, Munich, Germany - "Exceed your vision"](#)
138. [Epson Toyocom Corporation \('ETC', エプソントヨコム\), Hineshi, Tokyo Japan - the Quartz Device Operations Division of Seiko Epson Corporation \("Epson"\) integrated with Toyo Communication Equipment Co., Ltd. \("Toyocom"\) - "The leading company of Quartz Devices"](#)
139. [ESKA Crystals, Glostrup, Denmark](#)
140. [E-Spaceon \(Spaceon Electronics\), Chengdu, China](#)
141. [E-Tech Electronics Ltd. \('ETL'\), Hong Kong, China](#)
142. [Etimes Group, Shenzhen, Guangdong, China \(Shenzhen Etimes Electronics / Timemaker Crystal Technology / Quartz Crystal\)](#)
143. [Etna JSC \(ЭТНА\), Moscow, Russia - "The research and production enterprise" - "Designing and production of piezoelectronic devices"](#)
144. [Euro Quarz, Ternitz, Austria \(Tele Quarz daughter, closed in 1996 - production transferred to Delipro, Slovakia\)](#)
145. [Euroquartz Ltd., Crewkerne, Somerset \(incorporating Brookes Crystals, Webster Electronics, Frequency Products Limited & Euroquartz Filters\) - "manufacturer of high-quality frequency-control products"](#)
146. [EZTeck, Seoul, Korea \('Ezt'\) - "Frequency Control Devices"](#)
147. [FanAsia Electronics Technology Ltd., WuZhou, China](#)

148. [Fargo, Hong Kong, China - "Top quality crystal for high performance product"](#)
149. [FCT Co Ltd \(Frequency Control Technology\), Korea - out of business?](#)
150. [Filtronetics, Inc., Kansas City, MO - "the maker of Filters, Clock Oscillators, Quartz Crystals"](#)
151. [Fine Crystal Co Ltd, Muroran-shi, Hokkaido, Japan - a subsidiary of The Japan Steel Works, Ltd.](#)
152. [Fonon \(Phonon\) - ОАО "ЛИТ-ФОНОН" \(previously ОАО "Фонон"\), Москва, Россия \(Moscow, Russia\)](#)
153. [Fordahl-FOQ Group - merger of Fordahl Frequency Control Products \(Bruegg, Switzerland\) and FOQ Piezo Technik \(Bad Rappenau, Germany\)](#)
154. [Fortiming Corporation, Marlboro, MA, USA \(also 4Timing\) - "Providing Comprehensive Frequency Control Products and the Latest Information for Frequency Management and Timing Requirements"](#)
155. [Fox Electronics, Fort Myers, FL, USA - "Fox Rocks..."](#)
156. [FREQTECH OHG, Karlsfeld, Germany - "Your first and second source"](#)
157. [Frequency Electronics, Inc. \(FEI, incl. Gillam & Zyfer-Odetics\) - affiliated with Morion, Russia for supply of quartz oscillators.](#)
158. [Frequency Management International \(FMI\), Huntington Beach, CA, USA - Complete SOLUTIONS in Standard, Custom & Precision Frequency Control Devices](#)
159. [Fronter Electronics Co Ltd, Shenzhen, China \('FT'\) - 深圳市福良电子有限公司 \(factory in Shandong\)](#)
160. [FSUE Omsk Research Institute of Communications and Electronics \(ONIP\) piezo- and microelectronics department \('ОНИИП'\), Omsk Russia](#)
161. [Fujian Xun Da Electron Co Ltd](#)
162. [FujiCom Co Ltd, Japan - 富士コム](#)
163. [GAIN. co. Ltd. \(no longer active\)](#)
164. [GEMMA Quartz & Crystal \(previously SICN\), Annecy, France](#)
165. [GENDA Electronics Co Ltd, ZhuHai & Shenzhen, China](#)
166. [General Electronic Devices \(GED\), San Marcos, CA - "Our Goal Is Your Complete Satisfaction"](#)
167. [Gentech Crystals.Com, Plantation, FL, USA - Inactive](#)
168. [Gen-Worldly Quartz Crystal Co., Hong Kong - 振和石英電子公司](#)
169. [Geyer Electronic, Munich, Germany - "Qualität brilliant. Quarze von Geyer" - 'the professional among the suppliers of quartz products'](#)
170. [Global Co Ltd, Chuo-shi, Yamanashi - manufacturing and sales of Quartz Crystal Blanks for Quartz Crystal Oscillators](#)
171. [Golledge Electronics Ltd., Ilminster, Somerset, England](#)
172. [Grace Electronics \('GE'\), Suwon-City, Korea](#)
173. [Great Marking \(HK\) Industry Co Ltd \('GMK'\), ShenZhen, China](#)
174. [Green International Trading Group Ltd. \(U.K.\)](#)
175. [Greenray Industries, Inc., Mechanicsburg, PA, USA - "Frequency Control Solutions"](#)
176. [Griffon Enterprise Co. \('GEC'\), Hong Kong](#)
177. [Guangzhou Can Xin Electronic Limited \('CXE', 'CANXIN'\)](#)
178. [Guangzhou Dayang Electronic Co Ltd - 'DY'](#)

179. [Guangzhou HiSoft Electronics Co Ltd](#)
180. [Guangzhou Jinghui Electronics Co Ltd.](#)
181. [Guangzhou Ruidejing Electronics Co Ltd](#)
182. [Guangzhou Sandtin Electronic & Technology Co Ltd - products include HC-49/T HC-49/S HC-49/SS HC-49S/SMD HC-49SS/SMD JU-3*8 JU-2*6 JU-2*6/SMD AT-3*9 8038B UM-1 UM-5 3225B 4025B 5032A 5032B 6035A 6035B 7050B DIP08 DIP14 5032B 7050B 7050C DIP SMD/DIP](#)
183. [Guangzhou Shengda Electronic Co Ltd - SANTO - 广州市圣大电子有限公司](#)
184. [Guangzhou Tianma Telecom Technology Co Ltd - 天马电讯](#)
185. [Guanwi Electronics Co Ltd, Shenzhen, China - 深圳冠威电子有限公司](#)
186. [Haining Sanmu Electrons Co Ltd - a specialised manufacturer of piezo components in China](#)
187. [Halloran Electronics Co Ltd, Hachioji, Tokyo, Japan - "Time to think is also the cost"](#)
188. [Han Kyung Telecom Co Ltd \(HKT\), Seoul, Korea - out of business](#)
189. [Hangzhou Hosonic Electronic Co Ltd - a subsidiary of the Hosonic Group Taiwan specialized in producing and selling frequency control products.](#)
190. [Hangzhou Jingpeng electronic Co Ltd \(JPS\)](#)
191. [HaoStar Technology \(HST\), Taipei, Taiwan - "A Bright Star in crystal/oscillator industry" \(HAO STAR\)](#)
192. [Harmony Electronics Corp \(H.ELE\), Kaohsiung, Taiwan](#)
193. [HC electronics s.r.o., Hradec Kralove, Czech Republic](#)
194. [HCD Research Ltd., Burgess Hill, West Sussex, UK - "Experts in precision frequency engineering"](#)
195. [HCJ Quartz \(S\) Pte Ltd, Singapore](#)
196. [Hebei Huayuan Electronic Technology Co Ltd](#)
197. [Hebei Yuandong Communication System Engineering Co Ltd, Time-Frequency Division - an enterprise from the 54th Research Institute of China Electronics Technology Group Corporation \(CETC\) - 'CTI'](#)
198. [HEC, INC. Hooray USA, Westlake Village, CA](#)
199. [Heko Elektronikk AS, Rælingen, Norway](#)
200. [Henan Dali Electronic Co Ltd, China - out of business?](#)
201. [Herley Industries, Inc. \(Herley-CTI, Inc.\), Whippany, NJ](#)
202. [Hertz Technology Inc. ヘルツ株式会社 \(from Oct. 2006: Kyocera Kinseki Hertz Corp.\), Tokyo, Japan](#)
203. [Hewlett-Packard \(HP\) Frequency and Time Division, Santa Clara, CA, USA](#)
204. [Hitone / Raytone \(a joint venture by Tangshan Raytone Electronics Co Ltd and Hong Kong investor, Hitone Electronics Co Ltd\), Tangshan, Hebei, China](#)
205. [HJEC \(Huijing Electronic Technology Co Ltd\) is a marketing center of Tangshan Jingyuan Yufeng Electronic Corp., Shenzhen, China](#)
206. [HM International - Frequency Technology, Herselt, Belgium](#)
207. [Hokuriku Electric Industry Co Ltd \(HDK\), Toyama City, Japan - see also Koyo Precision Co Ltd](#)

208. [Hong Kong X'tals Ltd. \(HKC\), member of the Kolinker Group, Hong Kong](#)
209. [Hooray Electronics Co Ltd, Hong Kong](#)
210. [Hosonic Electronic Co Ltd, Shulin City, Taipei, Taiwan - Hosonic Group](#)
211. [Huang Cheng Company Ltd / Cinetech Ind. Co Ltd, Taipei, Taiwan](#)
212. [Hubei Dongguang Electronics Co Ltd](#)
213. [Hubei Zhiyuan Electronics Co Ltd \('HZE'\) - original name Shishou Zhiyuan Quartz Crystal Co Ltd](#)
214. [Huilong electronic \(Jinhua\) Co Ltd \(HLC\), Jinhua, Zhejiang, China - 匯隆電子 \(金華\)有限公司](#)
215. [Hunan Horizon Electronics Co Ltd, Changsha, China; Resonators - Oscillators - Filters; 湖南海天电子有限公司 \(Horizon Electronics Enterprises Group\)](#)
216. [Hy-Q International \(Australia\) Pty. Ltd., Clayton, Victoria, Australia](#)
217. [Hy-Q UK \(now Precision Devices UK Ltd., PDI\), Whittlesford, Cambridge, UK](#)
218. [IKE Electronics Co Ltd \(IKE Xtal\), Anyang-city, Korea](#)
219. [Ilshin Communication Co Ltd \('ITC'\), Seoul, Korea](#)
220. [ILSI America, Inc., Reno, NV, USA](#)
221. [IMP - Piezotechnology Ltd \(Institute Mihailo Pupin\), Belgrade, Serbia](#)
222. [Impact, LLC, Temecula, CA, USA - Worldwide supplier Frequency Control Devices](#)
223. [IMTECH \('I.M.Tech'\), Seoul, Korea](#)
224. [Inficon EDC, Inc., an Inficon subsidiary](#)
225. [Inotech \(Shanghai\) Co Ltd - "the leading supplier of quartz blanks, high quality crystals, resonators, oscillators, and other frequency control components for piezo-electric, laser and optical communications applications"](#)
226. [International Crystal Manufacturing Company, Inc. \(ICM\), Oklahoma City, OK, USA - "Manufacturing quartz crystals, oscillators, precision crystals, filters, TCXOs / VCTCXOs, QCM crystals and other frequency control products.](#)
227. [International Radio \(InRad\), Aptos, CA, USA - supplier of custom quartz crystal filters for communications receivers and transceivers](#)
228. [InterQuip Electronics Co Ltd, Hong Kong - "Organized for Quality - Dedicated to Service"](#)
229. [IQD \(International Quartz Devices or Interface Quartz Devices\) aka "IQD Crystals" => C-MAC => Rakon => IQD Frequency Products](#)
230. [IQD Frequency Products, Crewkerne, UK - "Worldwide Frequency Products" - previously part of Rakon \(before Rakon part of C-MAC\)](#)
231. [Isotemp Research Inc. \(A Taitien Company\), Charlottesville, VA, USA - "...a design and manufacturing facility for precision frequency control products"](#)
232. [Isotronics Co Ltd, Kanagawa, Japan \(株式会社 アイソトロニクス\) Quartz crystal devices and related materials](#)

- 233. [ITTI \(International Timing Technologies Incorporated\) Company Ltd, Hong Kong](#)
- 234. [Jaeil Telecommunication Co Ltd, Korea \(JTC, J-Tech\)](#)
- 235. [JAN Crystals, Fort Myers, FL, USA - "Exploring and expanding the capabilities of quartz crystals"](#)
- 236. [Jauch Quartz GmbH \('HC Jauch'\), Schwenningen, Germany - "The pulse of progress"](#)
- 237. [JenJaun Quartek Corporation \('NSK'\), Taipei, Taiwan - 津統石英科技股份有限公司](#)
- 238. [Jiangmen Taichang Electronic Co Ltd](#)
- 239. [Jiangxi Tiansheng Electronic Co Ltd \(previous domain name has expired\)](#)
- 240. [Jiaxing JingKong Electronic Co Ltd](#)
- 241. [Jiayeda Electronics Co Ltd, Shenzhen sells parts manufactured by Hunan Changde Jiayeda Electronics - specializes in the production of piezoelectric ceramic frequency components and quartz crystal oscillators](#)
- 242. [Jinhua Fuhua Electronic Co Ltd](#)
- 243. [Jinhua ZhengGong Electronics Co Ltd \('ZGC'\) aka Zheng Gong Electric](#)
- 244. [Jinzheng Tech Co Ltd \('C CEL'\), Dongguan, Guangdong, China](#)
- 245. [Jiyuan Jingti](#)
- 246. [Join Mark Industrial Limited, Hong Kong - 豐里實業有限公司](#)
- 247. [Justiming Electronics Technology \(Shanghai\) Corp Ltd \(JTM'\)](#)
- 248. [JY Electronics Co Ltd, Shenzhen, China - \('J&Y'\)](#)
- 249. [K.C.C. brand courtesy of Fairply Enterprises Inc, Taiwan](#)
- 250. [Kadco Ceramics \(Easton PA\) manufacturer](#)
- 251. [Kai Yip Electronic Company \('KYC'\), Hong Kong](#)
- 252. [KDS \(Daishinku Corp.\), Hyōgo, Japan - 大真空](#)
- 253. [KDS America \(Marietta GA\) manufacturer](#)
- 254. [Keltron Crystals Ltd., Kannur, Kerala State, India](#)
- 255. [KeoSung Electronics Co., Ltd., \('KSE'\), Suwon, South Korea](#)
- 256. [Kernco, Inc., Danvers, MA, USA](#)
- 257. [King Fai International Enterprise Co Ltd \(KFI\), Hong Kong](#)
- 258. [KingSta Electronic Co Ltd, Beijing, China - 精时基](#)
- 259. [Kitami Tokyo Denpa Co., Ltd. \('TEW'\)](#)
- 260. [Klove Electronics BV., Heerhugowaard, Netherlands](#)
- 261. [Koan Dongguang Electron](#)
- 262. [KONY Precision Co Ltd \(name changed to ChungHo Elcom\), Incheon, Korea](#)
- 263. [Kookje Elec. Ind. Co Ltd former name of Bubang Techron](#)
- 264. [Korea Electronics Co Ltd \(KEC\) - no longer supplies crystals and oscillators](#)
- 265. [Korea Quartz Technology Co Ltd \(KQT\), Seoul/Daejeon, Korea](#)
- 266. [Koyo Precision Co Ltd, Koasumi, Japan \(for several years part of Hokuriku Electric Industry, HDK\)](#)
- 267. [Krish Electronics Ltd, Bhubaneswar, India - "Small is Beautiful"](#)
- 268. [KRYSTALY, Hradec Králové, a.s., Hradec Kralove, Czech Republic](#)
- 269. [KS Electronics LLC, Phoenix, AZ - "Where your dreams turn into reality"](#)

270. [KSS Kinseki \(京セラキンセキ\), a Kyocera subsidiary](#)
271. [Kunshan Atop Electronic Technology Co Ltd - 正耀电子科技有限公司](#)
272. [Kvartselektronik AB \('KVE'\), Spånga, Sweden - "Kvartselektronik AB is Scandinavia's leading supplier of Quartz components"](#)
273. [KVG Quartz Crystal Technology GmbH, Neckarbischofsheim, Germany](#)
274. [Kwang il Electronics Co., Gyeonggi-do, Korea](#)
275. [K-WELL Electronics Co Ltd, Seoul, Korea - before April 2000 known as Hyo Sung Crystal Co., Ltd. \('Hyosung' or 'HSC'\)](#)
276. [Kyocera Electronic Devices \(KED\), Kyoto, Japan](#)
277. [KYOCERA KINSEKI Corporation - formerly Kinseki Ltd - trading as American KSS Inc / AVX Corporation / Kyocera Electronic Devices 'KED' LLC](#)
278. [Kyushu Dentsu Co Ltd \(KDK\), Nagasaki, Japan - 九州電通](#)
279. [Laboratoire Piezo Electricité S.A. \(LPE\) => LPE-Telequarz \(now Vectron\)](#)
280. [Langfang CEC Dacheng electronic Co Ltd - a CEC \(China Electronic Corporation\) company](#)
281. [Lap-Tech Inc., Bowmanville, Ontario, Canada - "Focused on Frequency"](#)
282. [Le Xing Crystal Co Ltd, Fujian, China](#)
283. [Lianyungang Ji Yuan Crystal Components Co Ltd](#)
284. [Lianyungang Wenfeng Electronics Co Ltd](#)
285. [LiaoYang HongYu Crystal Co Ltd \(original name LiaoYang Crystal Components Factory\) - 鸿宇晶体](#)
286. [Liberal Industrial Limited, Hong Kong \(利圖隆工業有限公司\)](#)
287. [Linear Components, Costa Mesa, CA, USA](#)
288. [L-Tron Co Ltd, Seoul, Korea - □□□\(□\)](#)
289. [Luguang Electronic Technology Co Ltd, specializes in R&D, manufacturing, selling of various piezoelectric materials, piezoelectric frequency components, diodes, transistors, modules, digital television receivers, wireless controllers, etc.](#)
290. [M H Electronics, Rancho Cucamonga, CA, USA](#)
291. [Macrobiz Co Ltd, Lianyungang, Jiangsu, China \(joint venture of Lianyungang International Marketing Company, Lianyungang Mxtal Electronics Co Ltd and Dong-A Quartz Co Ltd\) - 'MXTAL'](#)
292. [Magic Crystal Ltd, Omsk, Russia \('MXL'\) Мэджик Кристалл - "Only Magic Technologies!"](#)
293. [Magna Frequency Components, Sawston, Cambridge, England](#)
294. [Manudax, Paris, France - sells One Light Electronics \(ChungHo-Elcom\) parts under private label MDX Kony - marketed as 'MDX Time and Frequency Control Devices'](#)
295. [Matel-Fordahl, Créteil, France - "...résonateurs, oscillateurs, filtres à Quartz, cristaux piézoélectriques"](#)
296. [Maxim/Dallas Semiconductor, Sunnyvale, CA, USA](#)
297. [McTRON Electronics Co Ltd, Anyang City, Kyongki-Do, Korea](#)
298. [MEC Quartz Crystal, Hong Kong & Dongguan City, China](#)

299. [Meiden Quartz \(Singapore\) Pte Ltd / Meiden Quartz \(Malaysia\) SDN BHD - both Meidensha Corp units were acquired by Herbert C Jauch \(HC\) in 2000](#)
300. [Meiden Tsushin Kogyo Co Ltd \(a Meidensha Corp subsidiary\) - acquired by Siward / incorporated with Siward Crystal Technology Co Ltd \(Japan\) in 2000](#)
301. [Mercury Electronics \(MEC\), Taipei, Taiwan](#)
302. [Messiah Co Ltd, Yamanashi Japan \('MES'\)](#)
303. [Meteor Plant JSC, Volzhsky, Russia \(ОАО Завод Метеор\) - subsidiary production unit is called Meteor-Kurs \(Метеор-Курс\)](#)
304. [MF Electronics \(now Valpey Fisher\)](#)
305. [Micro Crystal \(Div. of ETA SA\), Grenchen, Switzerland - "Good Vibrations"](#)
306. [Microquartz Electronics Co Ltd, Seoul, Korea](#)
307. [Microtek Corporation, Gu-Ri City, Korea](#)
308. [Millennium Components Corp - Lotron, Kaohsiung, Taiwan](#)
309. [Mita Denpa, Tokyo, Japan - 三田電波](#)
310. [MMD Components \(includes Monitor & Quartztek\), Rancho Santa Margarita, CA, USA - "Perfect Timing"](#)
311. [Momentive Performance Materials \(Albany NY and Hebron OH\) manufacturing](#)
312. [Monitor Products Company Inc. \(see MMD\)](#)
313. [Morion Inc., St.Petersburg, Russia - МОПНО](#)
314. [Motorola Component Products Division \(CPD\)](#)
315. [MTI-Milliren Technologies Inc., Newburyport, MA, USA](#)
316. [MtronPTI, Yankton, SD, USA \(merger of M-tron Industries, Inc. and Piezo Technology, Inc.\) - "...when timing matters"](#)
317. [Murata Manufacturing Co Ltd \(in partnership with Tokyo Denpa\)](#)
318. [Murata, 'Erie' name has been dropped and N.A. Crystal Oscillator Division has been closed](#)
319. [MyFrequency, Inc., Gyeonggi-do, Korea](#)
320. [N.SET, S. Korea - □□\(□\) - "All that TCXO & Electronics Technology"](#)
321. [Naka & Co., Ltd., Japan](#)
322. [Nakagawa Electronics Ltd \(NKG\), Hong Kong \(two production facilities in mainland China - one located in Zhoushan, Zhejiang, the other, in Suzhou, Jiangsu\)](#)
323. [Namtech Tai Ltd. \('NTL'\), Bangalore, India \(a 100 percent subsidiary company of Namtech Electronic Devices Limited\)](#)
324. [Nanjing Highjoint Technology Co Ltd \('HJ'\)](#)
325. [Nanjing HuaLianXing Electronic Co Ltd \('HLX'\)](#)
326. [Nanjing Panda Piezoelectricity Technology Co Ltd - 南京熊猫玉电技术有限公司](#)
327. [NDK \(Nihon Dempa Kogyo Co Ltd\), Shibuya-ku, Tokyo - 日本電波工業 - "Crystal Bridge to the Future"](#)
328. [NDKHi-rel.com, Belvidere, IL, USA](#)
329. [NEL Frequency Controls, Inc., Burlington, WI, USA \(formerly Midland-Ross/NEL\)](#)
330. [Netcom Inc., Wheeling, IL, USA](#)

331. [Networks International Corporation \(NIC\), Overland Park, KS, USA](#)
332. [New Crystal World - 宇晶电子 - Hongkong Crystal World - factory in Wuhan, sales in Hong Kong & Shenzhen, China](#)
333. [Nikko Denshi Co Ltd \('NKD'\), Fushu-City, Tokyo, Japan - 日興電子株式会社](#)
334. [Nikkoh Densan Co Ltd, Kawasaki-city, Kanagawa, Japan](#)
335. [Nippon Crystal, Inc., Duluth, GA, USA](#)
336. [Nofech Electronics Ltd., Jerusalem, Israel \(NEL\)](#)
337. [Oak Frequency Control \(OFC\) => Corning => Vectron](#)
338. [Ole Wolff \(Asia\) Ltd. \(Hong Kong SAR\)](#)
339. [Omig S.A., Warsaw, Poland](#)
340. [ON Semiconductor > Clock Oscillator Modules](#)
341. [One Light Electronics, Incheon, Korea - took over the crystal division of ChungHo Elcom \(formerly Kony Precision\) including Chinese factory Yantai-Konex \('OLE'\)](#)
342. [OnSpec Oscillators Limited, Nuneaton, Warwickshire, England - "Your Spec, OnSpec"](#)
343. [OPT Hellas SA, Athens, Greece](#)
344. [Orient Supply Instruments Ltd / Orient Supply Technology \(H.K.\) Ltd, Hong Kong - "Crystal Device Connecting the world"](#)
345. [Oscilent Corporation, Irvine, CA, USA](#)
346. [Oscillatek => Vectron](#)
347. [Oscilloquartz S.A., Neuchâtel, Switzerland, a company of the Swatch Group](#)
348. [OST, Taiwan OSTOR Corp.](#)
349. [P&Y Crystal Industrial Ltd, Shenzhen, China](#)
350. [Pascall Electronics Limited, Ryde, Isle of Wight, UK - a subsidiary of EMRISE Electronics](#)
351. [PDI \(Precision Devices Incorporated\), Middleton, WI, USA - "Precision Engineering - Unrivalled Quality"](#)
352. [Pericom Semiconductor Corp. \(SaRonix\), San Jose, CA, USA](#)
353. [Petermann-Technik GmbH, Kaufering, Germany - Special Distributor of Time & Frequency Components](#)
354. [Philips Quartz Crystal Devices \(has been sold to SaRonix, Doetinchem site now demolished\)](#)
355. [Piezo Crystal Company => Oak / Corning => Vectron](#)
356. [Piezo enterprises group, Moscow, Russia - Группа предприятий "Пьезо" - "Piezoelectric devices and materials"](#)
357. [Piezo Technology, Inc. \(PTI\) => MtronPTI](#)
358. [Piezo Tecnologia Ltda, Rio de Janeiro, Brasil - Componentes eletrônicos para controle de frequências \(Cristais osciladores, Osciladores a cristal, Filtros a cristal\)](#)
359. [PIEZOCRISTAL Cristales, Alcobendas \(Madrid\), Spain - Cristales Cuarzo, Osciladores](#)
360. [Piezoquartz, Bulgaria - Quartz Piezoelectric Devices](#)
361. [Pletronics Inc., Lynnwood, WA, USA - "Manufacturer of High Quality Crystals and Oscillators"](#)
362. [Polaros Electronics Ltd. \(PEL\), Yavne, Israel](#)

- 363. [Power Control Devices, Inc. \(PCD\), Olathe, KS, USA - includes Frequency Control Products, Inc., FCP, Inc., Bulova Electronics & American Time Products](#)
- 364. [Precise Time and Frequency, Inc. \(PTF\), Peabody, MA, USA](#)
- 365. [Programmierservice Doris Reinhold, Mettmann, Germany - is no longer...](#)
- 366. [PT. Great Microtama Electronics Indonesia \(GXC\), Surabaya Indonesia](#)
- 367. [Putian Chun Wai Quartz Crystal c/o Comways \(H.K.\) Electronics Ltd.](#)
- 368. [QMAX Electronics, Incheon, Korea](#)
- 369. [QPE - Shenzhen Quartz Crystal Co Ltd \(SZQC\)](#)
- 370. [QT Quarztechnik GmbH, Daun, Deutschland](#)
- 371. [Q-Tech Corporation, Culver City, CA, USA - "High Reliability Hybrid Crystal Oscillators"](#)
- 372. [Quartech Electronic Co Ltd, Taipei, Taiwan](#)
- 373. [QuartSLab Marketing Ltd, Sevenoaks, Kent, UK \('OSL', formerly C&C Electronics\)](#)
- 374. [Quartz Crystal Technology \('QCT'\), Heerhugowaard, Netherlands - bankrupt \("schuldsanering"\)](#)
- 375. [Quartz Frequency Technology Ltd \('QFT'\), Hsin Chu, Taiwan](#)
- 376. [Quartz Pro AB \(also www.qpro.se\), Järfälla, Sweden](#)
- 377. [Quartz Tech Co Ltd, Bucheon-City, Korea - QTC](#)
- 378. [QuartzCom AG \('QCOM'\), Bettlach, Switzerland](#)
- 379. [Quartzlock \(UK\) Ltd., Totnes, Devon, UK](#)
- 380. [QuartzMaker \('QM'\) a brand name of Altec Electronic AG, Fahrweid, Switzerland - component distributor](#)
- 381. [Quartztek Inc. acquired by MMD Components](#)
- 382. [Quarzkeramik GmbH, Stockdorf, Germany - has been bought by KVG Quartz Crystal Technology GmbH \(when they were a part of Vectron\)](#)
- 383. [Quintenz Hybridtechnik, Neuried, Germany - Hybridtechnik, Dünnschichttechnik, Dickschichttechnik, Quarzoszillatoren...](#)
- 384. [QVS Tech, Carlsbad, CA, USA - "Quality, Value, and Service"](#)
- 385. [Raditek Inc., San Jose, CA, USA](#)
- 386. [Rakon Limited, Auckland, New Zealand, Harlow & Lincoln, UK and Argenteuil, France - "Lock on To Rakon"](#)
- 387. [Raltron Electronics Corporation, Miami, FL, USA \('RAL'\) => RAMI Technology Group, Hong Kong](#)
- 388. [RAMI Technology Group, Hong Kong - Raltron distributor who bought Raltron...](#)
- 389. [Reeves-Hoffman acquired by CTS Corp. in 1997](#)
- 390. [RF Monolithics, Inc. \(RFM\) - Crystal Based Products](#)
- 391. [RFX Ltd., Livingston, West Lothian, Scotland - precision quartz oscillators](#)
- 392. [River Eletec Corp., Nirasaki, Yamanashi, Japan - リバーエレクトック - crystal devices are manufactured at Aomori River Techno Co., Ltd, established 1989](#)
- 393. [Roch Co Ltd, Shenzhen, China \(诺和有限公司 \)](#)
- 394. [Roditi \(The Roditi International Corporation Ltd.\), London, England](#)

- 395. [ROM-QUARTZ S.A., Bucharest, Romania](#)
- 396. [Roson Electronics Co Ltd, YEDT Zone, Shandong, China](#)
- 397. [RXD Technologies, L.L.C., Lenexa, KS - acquired by ECS Inc. - "Reliability, eXcellence, Dependability"](#)
- 398. [Samjoon Ind. Co Ltd, Korea](#)
- 399. [Samsung Electro-Mechanics \('SEM'\), Korea - "The Inside Edge that shapes the Future"](#)
- 400. [Sanei-crystal co ltd, Tsuruoka, Japan - サンエイクリスタル](#)
- 401. [Sanho Ostor Electronics Corp., Sanhe-city, Hebei, China](#)
- 402. [Sanshin Electric Co., Ltd \('SAE'\) サンシン電機株式会社- do they still make crystal oscillators?](#)
- 403. [SaRonix acquired by Pericom Semiconductor Corporation in 2003](#)
- 404. [SaRonix-eCera, Chung Li city, Taiwan - a wholly-owned subsidiary of Pericom Semiconductor Corp.](#)
- 405. [Sbtron, Seoul, S. Korea - □□□□□](#)
- 406. [SCTB EIPA Ltd. \(CKTB ЭлПА\), Uglich \(Yaroslavl region\), Russia - special engineering and design bureau specialized in manufacture and R&D of quartz resonant devices](#)
- 407. [SEI \(Salford Electrical Instruments\), A subsidiary of GEC => GEC Plessey Semiconductors => C-MAC => Rakon](#)
- 408. [Seiko Epson Corporation => Epson Toyocom](#)
- 409. [Seiko Instruments Inc. \(SII\), Japan](#)
- 410. [Sentry Manufacturing Company, Chickasha, OK, USA \(used to be www.sentrymfg.com\) acquired by International Crystal Manufacturing, Inc. \(ICM\)](#)
- 411. [Seoan Electronics Co Ltd, Sungnam City, KyungKi-Do, Korea - "Global Electronics Company Seoan"](#)
- 412. [Shaanxi Huajing Beichuan Electronic Technology Co Ltd - predecessor is "shaanxi bei chuan radio component factory"](#)
- 413. [Shandong Kaijing Electronics Co Ltd is a professional manufacturer of quartz crystal resonator, including hc-49u, hc-49u/S, um-1, um-5, fork tuning, clock oscillator, etc.](#)
- 414. [Shanghai Jingding Electronic Co Ltd \(JDS\)](#)
- 415. [Shanghai Jingshi Frequency Control Co Ltd \('JSFCP'\)](#)
- 416. [Shanghai Kuixi Electronics Co Ltd](#)
- 417. [Shanghai Perfect Crystal Electronics Co Ltd](#)
- 418. [Shanghai Sitron Technology Co Ltd \(domain name expired\)](#)
- 419. [Shanghai STD-Crystal Elec-Technology Co Ltd / Wuxi Zhengke Electronics Co Ltd](#)
- 420. [Shanghai Strong Industrial Corporation Ltd \('STRONG'\)](#)
- 421. [Shanghai Worldwide Quartz Crystal Co Ltd](#)
- 422. [Shanghai Xiong Ying Electronic Technology Co Ltd \('XY'\)](#)
- 423. [Shanghai YIZHEN electronic Science & Technology Development Co Ltd - 上海易圳电子科技有限公司](#)
- 424. [Shanghai Zili Piezo Crystal Unit Corporation](#)
- 425. [Shenzhen Huajingda Electronics Co Ltd \('HJD'\)](#)
- 426. [Shenzhen Ao Yu Da Electronic Co Ltd - AYD](#)
- 427. [Shenzhen Auder Electronics Co Ltd \(owned by Utech Industrial Co Ltd\)](#)
- 428. [Shenzhen Biaojing Electronics Co Ltd \(domain name expired\)](#)

429. [Shenzhen Cryscraft Technology Limited \('HWI'\) - "Cryscraft—your wisdom choice!"](#)
430. [Shenzhen Feike Electronic Co Ltd \('F&K'\) - agent](#)
431. [Shenzhen Five-Ten Technology Co Ltd](#)
432. [Shenzhen Fronter Electronics Co., Ltd. \(mainland China\)](#)
433. [Shenzhen GF Electronic Co Ltd \('GoFine', 'Go Fine', 'GF'\)](#)
434. [Shenzhen Great Electronics Co Ltd - private label & agent](#)
435. [Shenzhen Guangzhongxin Electronics Co Ltd \('GZX'\) - Gang Zhong Xin](#)
436. [Shenzhen Hongxiang Electron Factory](#)
437. [Shenzhen JinBang Electronic Co Ltd - 深圳劲邦电子晶振有限公司](#)
438. [Shenzhen Jinfengrui Electronic Co Ltd \('JFR'\)](#)
439. [Shenzhen Jing Li Tong Electronics Co Ltd](#)
440. [Shenzhen Jing Peng Yuen Electronics Co Ltd - 晶鹏源电子](#)
441. [Shenzhen Jing Yi Electronics Co Ltd \('JY'\)](#)
442. [Shenzhen JingFeng Technology Development Co Ltd \('Jing Feng Crystal'\)](#)
443. [Shenzhen JingKaiYe Technology Co Ltd](#)
444. [Shenzhen Jingke Crystals Co Ltd](#)
445. [Shenzhen Jingxi Dianzi \(JXI\)](#)
446. [Shenzhen Jingyuan Precision Frequency Device Corp. Ltd. \(SZJY\), Nanshan, Shenzhen, China - Parent Company: Tangshan Jingyuan Yufeng Electronics Co Ltd](#)
447. [Shenzhen Jixiang Electronic Co Ltd a subsidiary of Hebei Tianxiang \(Group\) Ltd - 'JX'](#)
448. [Shenzhen Kaiyuexiang Electronics Co Ltd \('KYX'\)](#)
449. [Shenzhen Kangtong Electronics Co Ltd \('K'\)](#)
450. [Shenzhen Khanate Electronics Co Ltd \('KHR'\) - out of business?](#)
451. [Shenzhen Khanate Enterprise Limited \(mainland China\)](#)
452. [Shenzhen Kingwe Technology Co Ltd](#)
453. [Shenzhen Konuaer Electronics Co Ltd \(Konua\)](#)
454. [Shenzhen Luguang Electronic Technology Co Ltd \('LGE'\), Linyi, China \(鲁光电子\) specializes in R & D, manufacturing, selling of various piezoelectric materials, piezoelectric frequency components, etc.](#)
455. [Shenzhen New Quartz Electronics Co Ltd \(formerly Shenyi Piezoelectricity Technology Co Ltd\) 'SY'](#)
456. [Shenzhen Oscilla Industrial Limited Company \('Koyo'\) - distributor](#)
457. [Shenzhen Pengfei Technological Co Ltd - 'CSPXO' \(see also \[www.cspxo.com\]\(http://www.cspxo.com\)\)](#)
458. [Shenzhen Platinum Electronics Technology Develop Co Ltd \('PETD'\) - domain name expired](#)
459. [Shenzhen Rongtai Electronic Co Ltd - subsidiary of Harbin Ssangtae Electronics Industrial Co Ltd](#)
460. [Shenzhen SCTF Electronics Co Ltd](#)
461. [Shenzhen Selectech Electronics Co Ltd - "Manufacturer of Reliable Components"](#)
462. [Shenzhen South Star Electronics Co Ltd](#)
463. [Shenzhen SunCrystal Electronics Co Ltd \('SXJ'\)](#)
464. [Shenzhen TGD Crystal Electronics Co Ltd manufacturer](#)
465. [Shenzhen Timemaker Crystal Technology Co Ltd](#)

- 466. [Shenzhen TKD Crystal Industrial Co Ltd - 深圳市泰晶实业有限公司](#)
- 467. [Shenzhen Weilichuang Electronics \('SWE '\), Shenzhen, China \(domain name expired\)](#)
- 468. [Shenzhen Wenten Electronics Co Ltd \(Wenten Shen Zhen\)](#)
- 469. [Shenzhen Xin Da Li Electronics Co Ltd](#)
- 470. [Shenzhen XingGuangHua Electronic Co Ltd \('XGH', also Star Crystal, also \[www.xghcrystal.com\]\(http://www.xghcrystal.com\)\)](#)
- 471. [Shenzhen Yuechen Electronics science & technology Co Ltd - development, manufacture and sales of 49/U 49/T 49/S UM-1 UM-5 SMD AT38 JU26 JU38 OSC VCXO TCXO OCXO MCF SCF etc](#)
- 472. [Shenzhen Zhenfeng Ind Limited Co \('ZCF'\)](#)
- 473. [Shijiazhuang Boya Electronic Sci.&Tec. Co Ltd](#)
- 474. [Shijiazhuang Yanxing Electronics Co Ltd \('YXE'\)](#)
- 475. [Shimmer Enterprise Co. Ltd. \(Taiwan\)](#)
- 476. [Shin Koln Corporation \(SKCtech.com Inc. or 'SKC'\), Taipei, Taiwan, R.O.C.](#)
- 477. [Shinsung Electronics Co Ltd, Sasang-Gu, Busan, Korea - "Specialist of Frequency Control Devices - Discretion, Creation, Challenge - Work at the Discretion, with Creative technique, spirit of Challenge to the world"](#)
- 478. [Shoulder Electronics Ltd., Wuxi, Jiangsu, China](#)
- 479. [Showa Crystal Co Ltd, Funabashi, Japan](#)
- 480. [Sichuan GuoJing Technology Co Ltd](#)
- 481. [Sichuan Xinghua Time & Frequency Co Ltd \(XHTF\) - 四川天奥星华时频技术有限公司](#)
- 482. [Siward Crystal Technology Co Ltd., Taichung, Taiwan](#)
- 483. [Siward Technology Co Ltd, Yamagata Factory + Tokyo Office - web site for Japanese market](#)
- 484. [SJK - Shenzhen Crystal Technology Industrial Co Ltd, Yantai, China \(\[q-crystal.com\]\(http://q-crystal.com\)\) - JinKeXing](#)
- 485. [Skytech Co Ltd, Ansan-Si Korea, founded as Sky Raltron Co Ltd in 1999, changed name to Skytec Electronic Co Ltd in 2000 \(sometimes spelled Sky Tech\).](#)
- 486. [SMI Inc., Saitama-Ken, Japan - "Your Quartz, Your Quality, Your Source"](#)
- 487. [SNK TECH Co Ltd, Bundanggu Seongnam-City, Korea](#)
- 488. [SNR Corporation - suspended](#)
- 489. [Sobretom Indústria e Comércio Ltda, Rio de Janeiro, Brasil \('ST'\)](#)
- 490. [SOE - Shanghai South Ocean Electron Co Ltd](#)
- 491. [Solelectron Centum Electronics Ltd \(formerly C-MAC Centum Electronics Ltd\) - FCP division now Centum-Rakon India Pvt Ltd.](#)
- 492. [Soojung Communication Co Ltd \('x-tal'\), S. Korea](#)
- 493. [Sorachi Quartz Co Ltd \('S.Q.C.'\), Akabira, Akabira-shi, Hokkaido, Japan](#)
- 494. [SPECIALTEL-LEM, Assago \(Milano\), Italy - out of business - Quarzi e Oscillatori al Quarzo](#)
- 495. [Spectrum Microwave, Inc - oscillator divisions in Auburn \(formerly Creative Electric, Inc\) and State College, PA \(formerly EMF Systems, Inc\)](#)

496. [SPK Electronics Co Ltd, Taipei, Taiwan - Manufacture/OEM as well as Sales Channel of Epson Toyocom](#)
497. [SQC Technology Ltd, Taipei City, Taiwan - a sales outlet for Siward \(?\)](#)
498. [ST telecom co ltd \('STQ'\), Chungbuk, Korea](#)
499. [Standard Crystal Corporation, El Monte, CA, USA - "Quartz Crystal Products"](#)
500. [Statek Corporation, Orange, CA - "Ultra Miniature Quartz Crystals, Oscillators and Sensors"](#)
501. [STC Components \(Quartz Crystal Division\), Harlow, UK => C-MAC => Rakon](#)
502. [STC Frequency Technology \(Pty\) Ltd, Boksburg, South Africa - the manufacturing division was closed and the importing/resale business was sold to Arrow Altech Distribution \(Pty\) Limited \('AAD'\), Johannesburg with effect from 1 Dec. 2001](#)
503. [STC Microwave Systems, formerly Signal Technology - a Crane Aerospace & Electronics company - Olektron](#)
504. [Stonebell Co., Inc., Jungheung-town, S. Korea](#)
505. [Sun Device Co Ltd, Itoigawa, Japan - SDC](#)
506. [Sunlead Co Ltd, Niigata, Japan - "Towards a global standard"](#)
507. [Sunny Electronics Corp USA](#)
508. [Sunny Electronics Corp., Chungju, Chungbuk 380-240, Korea \(Sunny EMD\) includes subsidiaries: Philippine Sunny Electronics Corp. and Sunny Electronics Yantai Corp.](#)
509. [Suntsu Frequency Control, Inc., Irvine, CA - "Improving your performance"](#)
510. [Suzhou Industrial Park Togawa Seiko Co Ltd \('TSC'\)](#)
511. [Tae Sung Technology Company \(TAE SUNG\), Hong Kong, China](#)
512. [Taidi Electric Co Ltd - 泰地电子有限公司 \('TD'\)](#)
513. [Tai-Saw Technology Co Ltd \('TST'\), Taoyuan, Taiwan](#)
514. [Taitien Electronics Co Ltd, Taipei, Taiwan \(also taitien.com\)](#)
515. [Taizhou Abel Electronic Co Ltd \('TAE'\), Taizhou, China \(also taecn.com\)](#)
516. [Taizhou Joinic Electronic Co Ltd, Taizhou, Zhejiang, China, formerly known as Taizhou JingRui / Ruijing Electronic, imports and exports via Taizhou A-CRYSTAL Electronic, specialized cylinder crystal \(tuningfork\) manufacturer, \('TJR'\)](#)
517. [TamaDevice Co Ltd \(TMD\), Kawasaki City, Japan - 多摩デバイス- a trading company specializing in crystal devices, rep for Micro Crystal & Oscilloquartz](#)
518. [Tangshan Jingyuan Yufeng Electroncis Co Ltd - 晶源电子- 'JYEG'](#)
519. [Tangshan Lida Technology Co Ltd](#)
520. [Tangshan Wanshihe Electronics Co Ltd partnering with Woo Sung Electronic and Yantai Jiacheng Electronics](#)
521. [Tech Time Ltd, Or-Aqiva, Israel - a division of Data JCE Ltd \(formerly known as Time Squared Ltd\)](#)
522. [Technical Crystal Ltd \('TIC'\), Hong Kong, China](#)
523. [Technical Link Co Ltd, Saitama-ken, Japan](#)

524. [Techtrol Cyclonetics, Inc. \(TCI\), New Cumberland, PA, USA - "The Leader In Ultra Low Noise Technology"](#)
525. [TELE FILTER tft GmbH, Teltow, Germany - acquired in 1997 by Vectron, now 'VI Teltow, Germany' \(often spelled Telefilter\)](#)
526. [Tele Quarz Group \(often spelled TeleQuarz or TeleQuartz\), Neckarbischofsheim, Germany => Corning Frequency Control => Vectron](#)
527. [Teletec Corporation, Saitama-City, Japan](#)
528. [Tellurian Technologies, Inc., Rolling Meadows, IL - "Quality Comes First"](#)
529. [Temex \(Tekelec\), Sophia-Antipolis / Pont Sainte Marie, France - "Worldwide leader for high-performance Time and Frequency solutions"](#)
530. [TES Electronic Solutions \(formerly Thales Microelectronics, Sorep\), Bruz \(Rennes\), France](#)
531. [TEW \(Tokyo Denpa Co Ltd\), Tokyo, Japan - 東京電波](#)
532. [TGS \(USA\), Inc sales outlet for Wuhan TGS Crystals Co Ltd](#)
533. [TGS Crystals Ltd / Tigers Electronics \(USA\), Inc., WuHan, China](#)
534. [Tianjin Huaguang Electronic Devices Factory](#)
535. [Tianqin \(Kunshan\) Electronic Technology Co Ltd \('TOE'\)](#)
536. [Tinsuo Technological Co Ltd, Shenzhen, Guangdong, China](#)
537. [T-Mall USA \(sales outlet for Taitien\)](#)
538. [TND Electronics Co Ltd, Tongxiang, China - 桐乡市天峰电子有限公司](#)
539. [Tohoku Crystal Company \(ToCry\), Yamagata-city, Japan](#)
540. [Tokyo Denpa Co Ltd \(TEW\), Tokyo, Japan - 東京電波](#)
541. [Tokyo Quartz Co Ltd \('T.Q.C' / 'TQC'\) - 東京クォーツ](#)
542. [Tongling Jingweite Electronics Co Ltd \(JWT\) - 晶威特电子](#)
543. [Tongling Risheng Electronics Co Ltd](#)
544. [Top Crystal \(Changzhou\) Electronic Co Ltd - 常州华宙电子有限公司 \(TCE\)](#)
545. [Top Crystal Technology Inc., Miaoli Hsien, Taiwan - 台晶晶體科技股份有限公司 \(TCI\)](#)
546. [Total Frequency Control Ltd. \(TFC\), Storrington, West Sussex, England, UK](#)
547. [Toyocom, see Epson Toyocom Corporation](#)
548. [Transcend Electronic Co., Ltd. \(mainland China\)](#)
549. [Transko Electronics, Inc., Anaheim, CA, USA](#)
550. [TROQ Electronic Co Ltd, Jinhua, Zhejiang, China](#)
551. [TruXtal a private label brand of Rapid Electronics Ltd \(a distributor from Colchester, Essex, UK\)](#)
552. [Tsurudenpa Co Ltd, Tsuru, Japan](#)
553. [TXC Corporation, Taipei, Taiwan - 台灣晶技- "Think of Frequency, Think of TXC"](#)
554. [U.S. Electronics Inc. \('USE'\), St.Louis, MO, USA](#)
555. [Ukoudenshi Co Ltd \('UKD SUISHO'\), Sayama, Japan](#)
556. [Ukrpiezo J.S.Co, Cherkassy, Ukraine](#)
557. [Uniden Electronics Products \(Shenzhen\) Co Ltd - a subsidiary of Uniden Corporation](#)
558. [Unifirst Enterprise Corp, Taipei, Taiwan - "TDX" brand](#)

559. [Union Plus Technology Co Ltd formerly known as Technology Quatek Corp, Chungho City, Taipei, Taiwan \('TQ' or 'TQC'\) - partners with Yantai Technology Quartz Co Ltd - "A professional manufacturer of X'TAL and quartz Oscillator"](#)
560. [United States Crystal Corp. \(US Crystal or USCC\) - acquired by EDC in 2002](#)
561. [Universal Technologies Group \(UTG\), Las Vegas, NV, USA - aka World Technologies, Ltd. \(WTL\) - factories located in Japan, Korea, and China.](#)
562. [Valpey Fisher Corporation \('VPF'\), Hopkinton, MA, USA](#)
563. [Vanlong Technology Co Ltd \(VTC\)](#)
564. [Vectron International, Inc.](#)
565. [VIC-DAWN \(brand name KTS\), Taipei, Taiwan](#)
566. [Vishay Dale](#)
567. [VITE \(Vectron International Technology Express\)](#)
568. [Voltronics Frequency Control Products Inc.](#)
569. [Waysun Electronics Ltd - 炜昇科技开发公司 - ceased to exist](#)
570. [WDL, Shenzhen, China](#)
571. [Webel Crystals Limited \('WCL'\), India - stopped production in April 2001](#)
572. [Wenzel Associates, Inc., Austin, TX, USA](#)
573. [West Crystal Company Ltd, Kelowna, BC, Canada](#)
574. [Wintron Technology Inc., Shenzhen, China - Innovation beyond Imagination](#)
575. [Wisdom Technology Co Ltd, ShangHai, China](#)
576. [WIT Technology Co Ltd, Shenzhen, China](#)
577. [Wo Sai Electronics Co Ltd, Nanjing, China - 南京沃赛电子有限公司 \('WS'\)](#)
578. [Wolfgang Knap GmbH & Co KG, Vienna, Austria - wholesale \(distributor, sole agent and importer\) of quartz crystals, crystal oscillators and -filters](#)
579. [Worldbond Piezo-electric Corp., Richmond, Canada \('WB'\)](#)
580. [Wuhan Hi-Trusty Electronics Co Ltd \(also hi-trusty.com\)](#)
581. [Wuhan Jingke Information Industry Co Ltd](#)
582. [Wuhan Suncom Technolgy Co Ltd, Wuhan, China](#)
583. [Wuxi Beiduo Electronic element Co Ltd c/o Beiduo Electronic \(Hong Kong\) Ltd](#)
584. [Wuxi Kai Yu Electronic Factory](#)
585. [Wuxi Xunda Electron Co Ltd - 无锡迅达电子有限公司 - \('XD'\)](#)
586. [XECO Inc., Cedar City, UT, USA - Inverted Mesa and High Frequency Crystal Manufacturer](#)
587. [Xi'an Wudee Electronic Co Ltd \('WDE'\), Xian, China](#)
588. [Xiamen Frequency-Tech Electronics Company Ltd - XMFT](#)
589. [Xiamen Zhicheng Diangong Chailiao Co., Ltd. \(mainland China\)](#)
590. [Xianyang Liyade Electronics Co Ltd](#)
591. [Xsis Electronics Inc., Shawnee, KS, USA](#)
592. [Xtal Technologies Ltd. \(incorporates the Crystal and Coil Manufacturing Operation of Ericsson-GE\), Lynchburg, VA, USA - no longer exists](#)
593. [Yakumo INS Co Ltd, Toyama-city, Japan - design, manufacture and sale of SMD type Crystal devices](#)

594. [Yamanashi Denpa Co Ltd, Kofu-city, Yamanashi, Japan \('YD'\)](#)
595. [Yantai Chungho Electronics Co Ltd \(Yantai Konex Electronics\),
Yantai, China - Chinese partner of Chungho Elcom \('KONY'\), Korea](#)
596. [Yantai Cn Electronics Co Ltd](#)
597. [Yantai Dynamic Electronics Co Ltd. Previously known as
Shengli Electronics Co Ltd](#)
598. [Yantai ETDZ Kesheng Electric Co Ltd \('KSH'\)](#)
599. [Yantai ETDZ Taichang Electronic Co Ltd \('T'\)](#)
600. [Yantai Huafeng Crystal Co Ltd](#)
601. [Yantai K&K Crystal co Ltd \(KK\)](#)
602. [Yantai Kanghong Electronic Co Ltd \('KHE'\)](#)
603. [Yantai Kexin](#)
604. [Yantai Kingwell Co Ltd \(Ytkingwell\)](#)
605. [Yantai NEAN Develops Co Ltd](#)
606. [YIC \(Yuechung International Corp.\) - 裕中企業股份有限公司 - Hsi-
Chih, Taipei Hsien, Taiwan](#)
607. [Yoketan, Taichung, Taiwan \(Yoketant or YOKE\)](#)
608. [Yueqing Xinjing Electronic Co Ltd](#)
609. [Yunike Technologies Inc. \(YNK\), Beijing, China - formerly
Keysida](#)
610. [ZGC Electronic Co Ltd, Guangzhou](#)
611. [Zhaoqing Kay Quartz Crystal Technology Co Ltd -
肇慶安基石英晶体科技有限公司](#)
612. [Zhe Jiang Yu Yao Wan Quan Industry & Commerce Company](#)
613. [ZheJiang East Crystal Electronic Co Ltd \('ECEC'\), Jinhua,
Zhejiang, China](#)
614. [Zhejiang Jiakang Electronics Co Ltd, Jiaxing, China - sells via
Jiakang Ceratronics, Hongkong](#)
615. [Zhejiang Materials Development General Company](#)
616. [Zhenjiang Gangnan Electronics Co Ltd - expert in manufacturing
quartz crystal blanks.](#)
617. [Zhoushan Golden Way Electronics Co Ltd](#)
618. [Zhoushan Runda Electronic Co Ltd](#)
619. [Zhuhai DongJingDa Electronics Technology Co Ltd \('DONG
JING DA'\)](#)
620. [Zhuhai Sigma Electronics Limited](#)
621. [Zibo Carry-Leid Electronics Co Ltd - 淄博凱瑞力特电子有限公司](#)
622. [Zibo China-xtal Electronics Co Ltd, a trading \(import/export\)
company](#)
623. [Zibo Daxiang Electronics Co Ltd](#)
624. [Zibo Fengjing \('FJ'\)](#)
625. [Zibo Fengyan Electronical Component Co Ltd \(also Fengyuan
Electronic\)](#)
626. [Zibo Fijing Electronics Co Ltd \('JQL'\)](#)
627. [Zibo Jinli - inactive](#)
628. [Zibo YuFeng Industrial Co Ltd, subsidiaries include Zibo
ChuanBei Crystal Material Factory \(synthetic quartz\), Zibo Yuchi &
ShanDong Yufeng & YanTai Yuchi Electronics \(leaded crystals\),
Yufeng Raltron Electronics \(SMD 5032\) - Yu Feng](#)
629. [Декo-Кварц](#)